



Novel Luminescent Peptide Conjugates for Assessing Protein and other Biomolecules Location and Function

A thesis submitted to Dublin City University for the award of PhD.

By

Lorraine Blackmore, B.Sc. (Hons)

School of Chemical Sciences,
Dublin City University,
Glasnevin,
Dublin 9.

January 2013

Supervisors:

Prof. Tia Keyes (DCU)/Dr. Marc Devocelle (RCSI)

Declaration

I hereby certify that this material, which I now submit for assessment on the programme of study leading to the award of PhD. is entirely my own work, that I have exercised reasonable care to ensure that the work is original, and does not to the best of my knowledge breach any law of copyright, and has not been taken from the work of others save and to the extent that such work has been cited and acknowledged within the text of my work.

Signed: _____

ID No.: _____

Date: _____

Acknowledgments

First and foremost, I would like to extend my sincerest gratitude to my supervisor's Dr. Marc Devocelle and Prof. Tia Keyes for their advice, time, help and encouragement throughout the duration of the project. I am indebted to them for giving me the opportunity to work on such an excellent project. I would also like to extend my gratitude to Prof. Robert Forster for his advice over the past few years. To the NBIPI for providing the all important financial assistance throughout my research and the staff of the NBIPI for their assistance throughout the project. This work was supported through the National Biophotonics and Imaging Platform, Ireland, and funded by the Irish Government's Programme for Research in Third Level Institutions, Cycle 4, Ireland's EU Structural Funds Programmes 2007 – 2013 and is based upon work supported by the Science Foundation Ireland under Grant No. [10/IN.1/B3025] Science Foundation Ireland.

Special thanks to my Dublin City University colleagues, Lynda, Ciaran, Kellie for their friendship and materials. Matthias, Elena, Zoe, Shane, Jamie, Aaron for their time spent giving advice and for all their help in the lab, continued friendship and good memories. Big thanks to Róisín for all the cell work. They all have provided great companionship and made my work environment really enjoyable. I would also like to extend my thanks to all of the post-grads, postdocs and technical staff in the department past and present in Dublin City University.

I would like to thank all the members of staff and post graduates of the Pharmaceutical and Medicinal Chemistry Department in the RCSI for their help and friendship. The members of the RCSI research group, David, Sarah and Aoife, for all their help and discussion when called upon over the years. Stephane who gave me a world of wisdom on peptide synthesis, it was really appreciated. James, Suzanne, Alan, Graeme, Christine and Emmet who not only gave me lots of help and support with the project but also made my postgraduate experience so enjoyable, good friends. I would like to thank Adam Coburn, University College Dublin for High-Resolution mass spectrum and Suzanne Donnelly, RCSI, for elemental analysis. Special thanks to the girls from home, the RCSI basketball crew, the larger DCU and RCSI family as a whole for the great friendship and to Paul who was always there for me with endless support.

Finally, I would like to give my biggest thanks to my Dad, Mam, Olga and Bob, for their endless encouragement. You have been a rock of support for me throughout the years. Thank you for everything.

This thesis is dedicated to my parents.

Table of Contents

<i>Declaration.....</i>	<i>ii</i>
<i>Acknowledgments.....</i>	<i>iii</i>
<i>Abstract.....</i>	<i>x</i>
<i>List of Acronyms/Symbols/Complexes.....</i>	<i>xii</i>
<i>Amino Acid List.....</i>	<i>xiv</i>
<i>Glossary of Structures.....</i>	<i>xvi</i>

Chapter 1: Introduction	1
1.1 Cell Imaging.....	2
1.2 Novel Luminescent Chromophores for Living Cells	3
1.3 Introduction to Photoactive Supramolecular Chemistry	4
1.3.1 The Photoactive component.....	6
1.4 Luminescent Metal Complexes in Cell Imaging.....	9
1.4.1 Ruthenium (II) Polypyridal Probes	10
1.5 Delivery Vectors	12
1.5.1 Liposome	13
1.5.2 Dendrimers.....	14
1.5.3 Viral Vectors.....	15
1.5.4 Solid Lipid Nanoparticles	16
1.5.5 Cell Penetrating Peptides	16
1.5.5.1 Mechanism of uptake.....	17
1.6 Cell Penetrating peptides delivery of imaging agents.....	19
1.7 Probe Peptide Conjugates of Metal Complexes.....	20
1.8 Targeting (homing) Peptides.....	25
1.8.1 Targeting DNA	32
1.8.1.1 Reactive Oxygen Species.....	33
1.9 Apoptosis	35
1.9.1 Caspase	36
1.9.2 Role of B-cell lymphoma-2 (Bcl-2) proteins	38
1.9.3 BH-3 only proteins.....	40

1.9.4 BH3 interacting death agonist (BID)	40
1.9.5 Synthetic Peptides and Organic molecules as probes for the investigation of the structure and function of members of the Bcl-2 family- Targeted therapy.....	41
1.9.6 BID peptides	42
1.9.7 ABT-263	43
1.10 Aims of Project	46
<i>References</i>	48

Chapter 2: Experimental Methods and Instrumentation..... 57

2.0 Peptide Synthesis	60
2.1 Resins for solid phase synthesis	60
2.2 Protecting groups	60
2.3 Coupling Methods.....	62
2.4 Microwave assisted peptide synthesis.....	62
2.5 Instrumentation and Reagents	63
2.5.1 Reagents and Solvents	63
2.5.2 Microwave Synthesis	63
2.5.3 Nuclear Magnetic Resonance (NMR) Spectroscopy	63
2.5.4 Thin Layer Chromatography.....	63
2.5.5 Mass Spectrometry Analysis.....	64
2.5.5.1 Matrix Assisted Laser Desorption Ionisation-time of flight	64
2.5.5.2 Electrospray ionization (ESI).....	64
2.5.6 Elemental Analysis	64
2.5.7 Absorption Spectroscopy	64
2.5.8 Fluorescence Spectroscopy	64
2.5.9 Lifetime Measurements	65
2.5.10 Freeze Drier	65
2.5.11 Confocal Fluorescence Microscopy.....	65
2.5.12 Cell Culture.....	66
2.5.13 Cellular Uptake of Complexes.....	66
2.5.14 Cytotoxicity Assay.....	67
2.6 Peptide Synthesis	67
2.6.1 Automatic Peptide Synthesis	67
2.6.2 Manual Coupling	67
2.6.3 Microwave Coupling	68
2.6.4 Manual Deprotection	68
2.6.5 Microwave Deprotection	69

2.6.6 Cleavage.....	69
2.6.7 HPLC Analysis of Peptides	70
2.6.8 HPLC Purification of Peptides.....	70
References.....	71

Chapter 3: Luminescent Chromophores for Cellular Imaging 72

3.1 Introduction.....	73
3.2 Experimental Details for the Synthesis of targeting peptides-dye conjugates	74
3.2.1 Preparation of Ru(dpp) ₂ PIC-βAla-NF-κB (-VQRKRQKLMP-NH ₂) conjugate.....	74
3.2.2 Preparation of Ru(bpy) ₂ PIC-βAla-NF-κB (-VQRKRQKLMP-NH ₂) conjugate.....	75
3.2.3 Preparation of Ru(dpp) ₂ PIC-Ahx-NF-κB (-VQRKRQKLMP-NH ₂) conjugate.....	77
3.2.4 Preparation of Ru(bpy) ₂ PIC-Ahx-NF-κB (-VQRKRQKLMP-NH ₂) conjugate.....	79
3.2.5 Preparation of Ru(dpp) ₂ PIC-Ahx- Sv-40 (-PKKKRKV-NH ₂) conjugate.....	80
3.2.6 Preparation of Ru(bpy) ₂ PIC-Ahx- Sv-40 (-PKKKRKV-NH ₂) conjugate.....	81
3.3 Results and Discussion.....	82
3.4 Photophysical Characterisation of Peptide-Chromophore Conjugates	86
3.4.1 Absorbance	87
3.4.2 Emission.....	89
3.5 Cellular Uptake of Chromophores-Peptide Conjugates	89
3.6 Cytotoxicity.....	96
3.7 Conclusions.....	98
References.....	101

Chapter 4: Preparation and Characterisation of overlapping peptides of BH3

Interacting Domain Death Agonist (BID) 102

4.1 Introduction.....	103
4.2 Experimental Details for the synthesis of BID peptides	104
4.2.1 Preparation of biotinylated BID 01-20	104
4.2.2 Preparation of biotinylated BID 18-36	105
4.2.3 Preparation of biotinylated BID 29-48	106
4.2.4 Preparation of biotinylated BID 46-64	106
4.2.5 Preparation of biotinylated BID 62-82	107
4.2.6 Preparation of biotinylated BID 78-101	108
4.2.7 Preparation of biotinylated BID 97-117	108
4.2.8 Preparation of biotinylated BID 116-137.....	109
4.2.9 Preparation of biotinylated BID 137-157.....	109
4.2.10 Preparation of biotinylated BID 155-177.....	110

4.2.11 Preparation of biotinylated BID 175-195.....	110
4.2.12 Preparation of BID 137-157 conjugated to Ru (dppz) ₂ PIC	101
4.2.13 Preparation of BID 155-177 conjugated to Ru (dppz) ₂ PIC	112
4.3 Results and Discussion.....	113
4.3.1 Synthesis	113
4.3.2 Coupling Reagents	115
4.3.3 Resin	117
4.3.4 Aspartimide Formation	118
4.3.5 Selecting BID sequences for studies with oxygen-sensitive probes	119
4.3.6 [Ru(dppz) ₂ PIC]ClO ₄ conjugation	121
4.3.7 Method of Synthesis of Ruthenium polypyridyl BID peptide conjugates	121
4.3.8 Oxidation of Methionine.....	123
4.3.9 Results from chromophore conjugation.....	124
4.3.10 Preliminary Cell Imaging Studies	126
4.4 Conclusion	128
References.....	130
Chapter 5: Targeting Mitochondria with Luminescent Chromophores.....	133
5.1 Introduction.....	131
5.2 Experimental Details for the Synthesis of targeting peptides-dye conjugates	136
5.2.1 Preparation of Ru(dpp) ₂ PIC-Magainin 2 conjugate	136
5.2.2 Preparation of Ru(bpy) ₂ PIC-Magainin 2 conjugate.....	138
5.3 Results and Discussion.....	139
5.4 Photophysical Characterisation of the Peptide-Chromophore Conjugates	141
5.4.1 Absorbance	141
5.4.2 Emission.....	142
5.5 Cellular Uptake of Chromophores-Peptide Conjugates.....	144
5.6 Cytotoxicity.....	145
5.7 Conclusion	146
References.....	148
Chapter 6: Small molecule Inhibitors of Bcl-2 family proteins.....	149
6.1 Introduction.....	150
6.1.2 Protein interactions between the Bcl-2 family proteins	151
6.2 ABT 737 and 263.....	152
6.3 Synthetic Route 1 of ABT 737.....	154
6.3.1 Preparation of N-benzyloxycarbonyl-D-aspartic acid anhydride	154

6.3.2 Preparation of (R)-benzyl (5-oxotetrahydrofuran-3-yl)carbamate.....	154
6.3.3 Preparation of (R)-benzyl (4-(dimethylamino)-1-hydroxy-4-oxobutan-2-yl)carbamate.....	155
6.4. Synthetic Route 2 of ABT 737.....	156
6.4.1 Preparation of 4-fluoro-3-nitrobenzene-1-sulfonyl chloride.....	156
6.4.2 Preparation of 4-fluoro-3-nitrobenzenesulfonamide.....	156
6.5 Synthetic Route 3 of ABT 737.....	157
6.5.1 Preparation of ethyl 4-(piperazin-1-yl)benzoate	157
6.5.2 Preparation of ethyl 4-(4-(2-bromobenzyl)piperazin-1-yl)benzoate.....	158
6.5.3 Preparation of ethyl 4-(4-((4'-chlorobiphenyl -2-yl)methyl)piperazin-1-yl)benzoate.....	159
6.5.4 Preparation of 4-(4-((4'-chloro-[1,1'-biphenyl]-2-yl)methyl)piperazin-1-yl)benzoic acid.....	160
6.6 Synthetic procedures of ABT 263.....	160
6.6.1 Preparation of ((R)-benzyl (1-hydroxy-4-morpholino-4-oxobutan-2-yl)carbamate.....	160
6.6.2 Preparation of 1-bromo-4,4dimethylcyclohex-1-ene-carbaldehyde	161
6.6.3 Preparation of ethyl 4-(4-((2-bromo-5,5-dimethylcyclohex-1-en-1-yl)methyl)piperazin-1-yl)benzoate	162
6.7 Results and Discussion.....	165
6.7.1 ABT 263	165
6.7.1.1 Route 1 ABT 263.....	165
6.7.1.2 Route 3 ABT 263	168
6.7.2 ABT 737	170
6.7.2.1 Route 1 ABT 737.....	171
6.7.2.2 Route 2 ABT 737.....	172
6.7.2.3 Route 3 ABT 737.....	173
6.8 Photophysical Results	174
6.9 Cytotoxicity.....	176
6.10 Conclusions.....	177
References.....	179
Chapter 7: Conclusions and Future Work	181
7.0 Conclusions and Future Work.....	182
Appendix: NMR, HPLC and Mass Spectrometry Results	I-XXXV
Publications and Posters.....	XXXVI

Abstract

Luminescent dye molecules capable of passive cell delivery may be used as molecular probes in cellular and tissue imaging. Inorganic transition metal complexes have been under extensive investigation for many years in supramolecular assemblies in application ranging from sensing to photovoltaics. This is due to their favourable photophysical and redox properties including absorbance and emission in the visible region of the spectrum, large stokes shifts, long lifetimes, intense luminescence, good photostability and useful photosensitising properties for photodynamic therapy. However, their application in cell imaging can be limited by their inability to cross the cell membrane. Recent work by our group has shown that the cellular uptake of ruthenium complexes can be promoted through their conjugation to a cell penetrating peptide. Peptides combined to Ru(II) provide unique opportunities for imaging dynamic processes in living cells avoiding limitations associated with fixation.

This thesis continues this work by reporting on the synthesis, characterisation and identification of novel ruthenium complex-peptide bioconjugates suitable for applications in cellular imaging and the investigation of their sub-cellular targeting and localisation. Some preliminary studies of their application in cell imaging are also presented.

Chapter 1 introduces metal complexes previously used in cellular imaging and how the conjugation of these transition metal complexes to targeting biomolecules has led to successful applications in medical diagnostics, photodynamic therapy, cellular imaging and pharmaceutical drug delivery. Chapter 2 outlines the general details of the experimental methods used. In chapter 3, the synthesis of 6 novel dye conjugates is detailed, of which 4 were shown to transport efficiently across the cellular membrane of CHO cells and locate throughout the cell's organelles. The spectral (absorption and emission) and photophysical (fluorescence lifetime) properties of these metal-ligand peptide complexes are also described. The complex exhibits long-lived, intense and oxygen-sensitive luminescence which is relatively unchanged in the conjugates from the parent dyes. Preliminary results on their application in cell imaging are also presented which demonstrate excellent nuclear permeability and nuclear localisation which depends on the hydrophobicity of the metal centre.

Chapter 4 details the preparation of the BID protein, a pro-apoptotic member of the BCL-2 family, as a number of overlapping peptides. The aim of this work was to identify a functional region of the parent protein. Two BID sequences were selected for conjugation to probes for localisation and function studies. Along with the BID sequences, another BCL-2 family member was investigated.

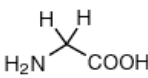
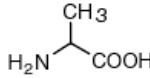
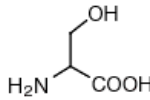
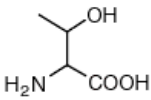
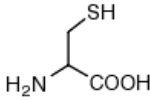
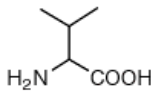
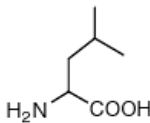
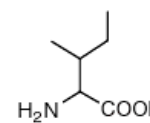
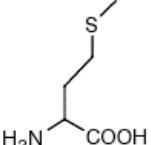
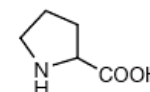
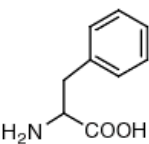
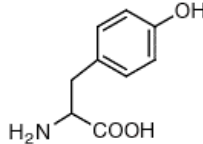
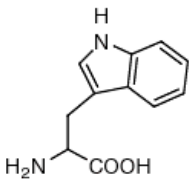
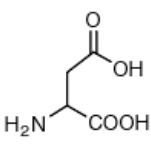
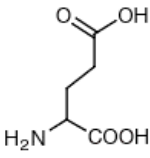
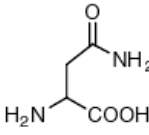
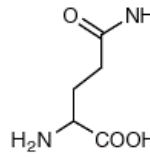
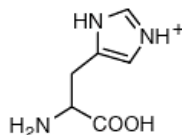
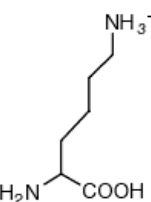
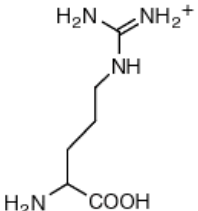
Chapter 6 describes the synthesis and characterisation of 2 peptide-metal dye conjugates targeting the mitochondria. Photophysical and cellular localisation and cytotoxic properties of these metal-ligand peptide complexes are described. Finally, the synthetic route to an organic mimic molecule of BAD, another pro-apoptotic protein, was also explored as described in Chapter 5. It consists of a convergent synthesis involving 3 separate synthetic sequences containing overall 14 reaction steps. Two key synthons were synthesised and examined for photophysical and cytotoxicity properties.

List of Acronyms/Symbols/Complexes

Ac	Acetyl
ACN	Acetonitrile
Arg8	Octaarginine
Boc	<i>tert</i> -butoxycarbonyl
bpy	2,2'-Bipyridyl
Cbz, Z	Benzyloxycarbonyl
CHO cells	Chinese Hamster Ovary cells
CPPs	Cell Penetrating Peptides
CT	Charge Transfer
COSY	CORrelated SpectroscopY
DCM	Dichloromethane
DEPT	Distorsionless Enhancement by Polarisation Transfer
DIEA	<i>N,N</i> -Diisopropylethylamine
DMF	<i>N,N</i> -Dimethylformamide
DMSO	Dimethylsulfoxide
EDT	1,2-Ethanedithiol
eq.	Molar equivalents
ESI	Electrospray Ionisation
ESMS	Electro Spray Mass Spectrometry
Fmoc	9-Fluorenylmethyloxycarbonyl
HATU	2-(1H-7-Azabenzotriazol-1-yl)-1,1,3,3-tetramethyl-uronium-hexafluorophosphate
HBTU	2-(1H-Benzotriazole-1-yl)-1,1,3,3-tetramethyl-uronium-hexafluorophosphate
HOBt	Hydroxybenzotriazole
HOMO	Highest Occupied Molecular Orbital
LC	Ligand Centred
LUMO	Lowest Unoccupied Molecular Orbital
MLCT	Metal to Ligand Charge Transfer
MC	Metal Centred
λ	Wavelength
(m, μ) g	(milli, micro) gram
(m, μ) L	(milli, micro) litre
(m, μ) mol	(milli, micro) mole
(m, μ) M	(milli, micro) molar

MALDI	Matrix Assisted Laser desorption Ionisation
MBHA	4-Methylbenzhydrylamine Hydrochloride
MeOH	Methanol
MS	Mass Spectrometry
NLS	Nuclear Localisation Signal
nm	nano meter
NMP	<i>N</i> -Methyl-2-pyrrolidone
NMR	Nuclear magnetic resonance
Pbf	2,2,4,6,7-Pentamethyldihydrobenzofuran-5-sulfonyl
PBS	Phosphate Buffer Saline
ppm	Part per million
PyBOP®	Benzotriazole-1-yloxy-tris-pyrrolidino-phosphonium hexafluorophosphate
Rink Amide	4-[(2,4-Dimethoxyphenyl)(Fmoc-amino) methyl]phenoxyacetic acid resin
ROS	Reactive Oxygen Species
SPPS	Solid Phase Peptide Synthesis
<i>t</i>Bu	<i>t</i> -Butyl
TCSPC	Time Correlated Single Photon Counting
THF	Tetrahydrofuran
TFA	Trifluoroacetic Acid
TIS	Triisopropylsilane
TLC	Thin Layer Chromatography
Trt	Trityl
UV	Ultra-Violet

Amino Acid List

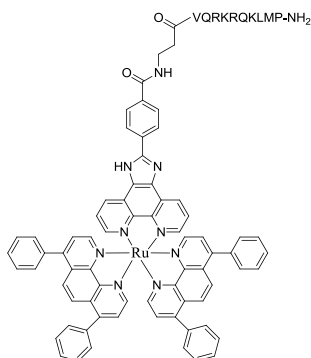
Small		Nucleophilic											
	Glycine (Gly, G) MW: 57.05		Alanine (Ala, A) MW: 71.09		Serine (Ser, S) MW: 87.08, pK _a ~ 16		Threonine (Thr, T) MW: 101.11, pK _a ~ 16		Cysteine (Cys, C) MW: 103.15, pK _a = 8.35				
Hydrophobic			Valine (Val, V) MW: 99.14		Leucine (Leu, L) MW: 113.16		Isoleucine (Ile, I) MW: 113.16		Methionine (Met, M) MW: 131.19		Proline (Pro, P) MW: 97.12		
Aromatic			Phenylalanine (Phe, F) MW: 147.18		Tyrosine (Tyr, Y) MW: 163.18		Tryptophan (Trp, W) MW: 186.21	Acidic			Aspartic Acid (Asp, D) MW: 115.09, pK _a = 3.9		Glutamic Acid (Glu, E) MW: 129.12, pK _a = 4.07
Amide			Asparagine (Asn, N) MW: 114.11		Glutamine (Gln, Q) MW: 128.14	Basic			Histidine (His, H) MW: 137.14, pK _a = 6.04		Lysine (Lys, K) MW: 128.17, pK _a = 10.79		Arginine (Arg, R) MW: 156.19, pK _a = 12.48

Fmoc-Tyr(tBu)-OH	Y	Fmoc-His(trt)-OH	H
Fmoc-Val-OH	V	Fmoc-Ile-OH	I
Fmoc-Ala-OH	A	Fmoc-Leu-OH	L
Fmoc-Arg(Pbf)-OH	R	Fmoc-Lys(Boc)-OH	K
Fmoc-Asn(trt)-OH	N	Fmoc-Met-OH	M
Fmoc-Asp(OtBu)-OH	D	Fmoc-Phe-OH	F
Fmoc-Cys(Trt)-OH	C	Fmoc-Pro-OH	P
Fmoc-Glu(OtBu)-OH	E	Fmoc-Ser(tBu)-OH	S
Fmoc-Gln(trt)-OH	Q	Fmoc-Thr(tBu)-OH	T
Fmoc-Gly-OH	G	Fmoc-Trp(Boc)-OH	W

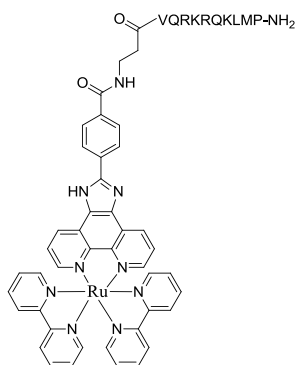
Standard Amino acids used during synthesis

Glossary of Structures

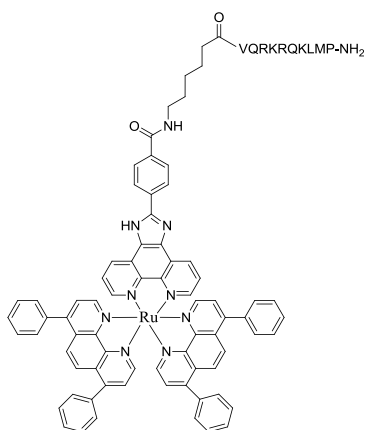
- Ru (dpp)₂PIC- βAla- NF-κB (-VQRKRQKLMP-NH₂)



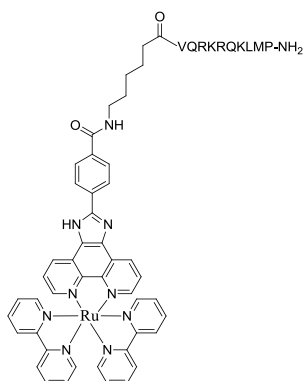
- Ru(bpy)₂PIC-βAla-NF-κB (-VQRKRQKLMP-NH₂)



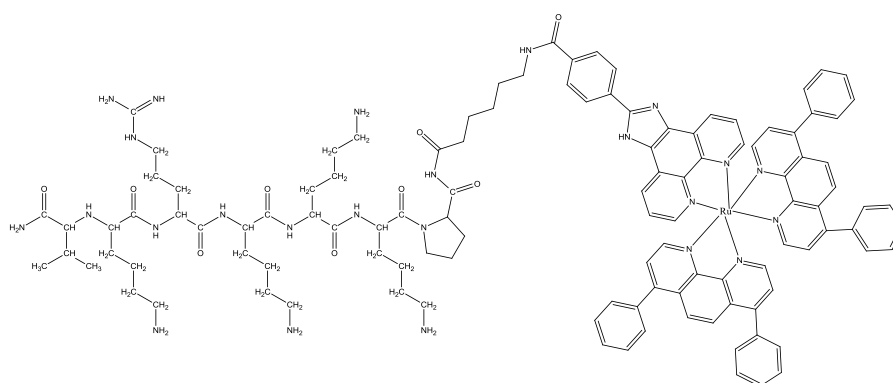
- Ru(dpp)₂PIC-Ahx-NF-κB (-VQRKRQKLMP-NH₂)



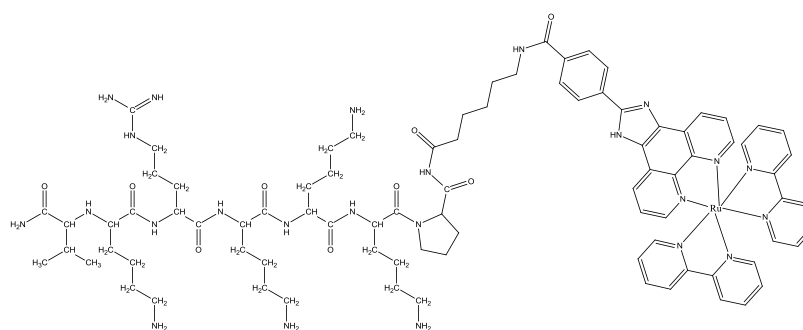
- Ru(bpy)₂PIC-Ahx-NF-κB (-VQRKRQKLMP-NH₂)



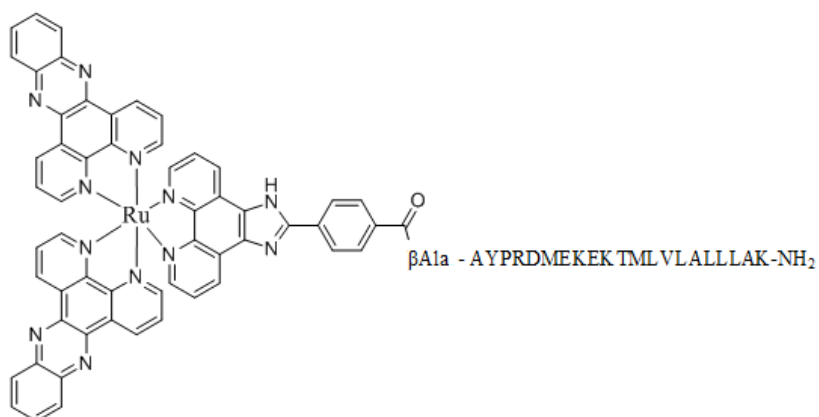
- Ru(dpp)₂PIC-Ahx-Sv-40 (-PKKKRKV-NH₂)



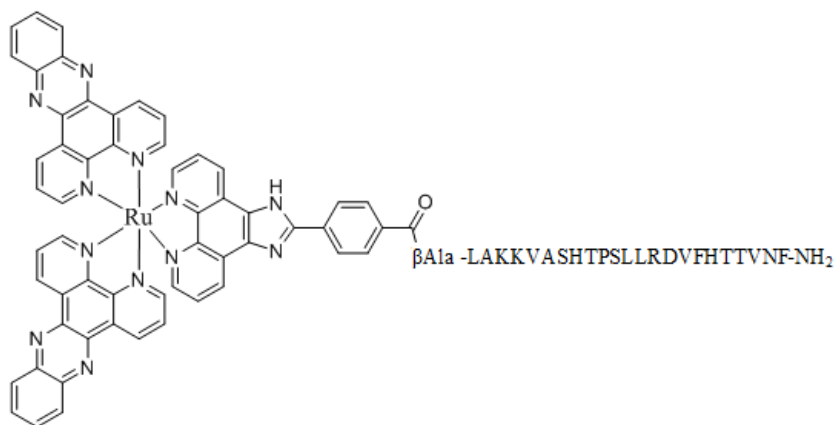
- Ru(bpy)₂PIC-Ahx-Sv-40 (-PKKKRKV-NH₂)



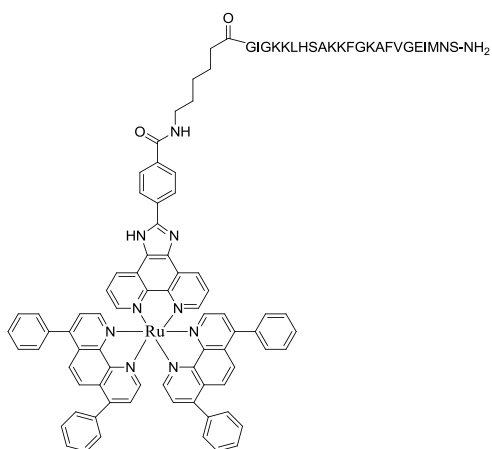
- BID 137-157 - Ru (dppz)₂PIC



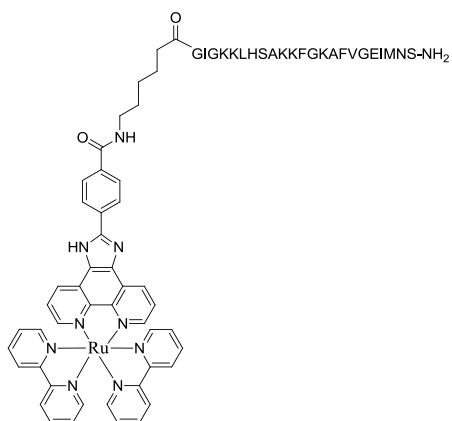
- BID 155-177 - Ru (dppz)₂PIC



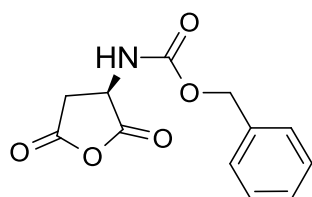
- Ru(dpp)₂PIC- Magainin 2 (Ahx-GIGKKLHSAKKFGKAFVGEIMNS-NH₂)



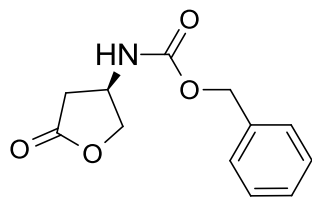
- Ru(bpy)₂PIC- Magainin 2 (Ahx-GIGKKLHSAKKFGKAFVGEIMNS-NH₂)



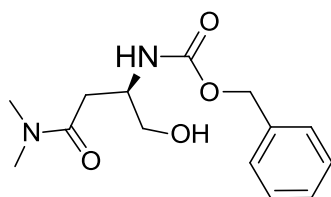
- N-benzyloxycarbonyl-D-aspartic acid anhydride



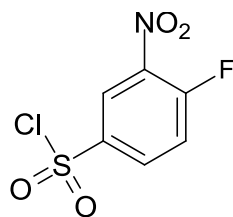
- (R)-benzyl (5-oxotetrahydrofuran-3-yl)carbamate



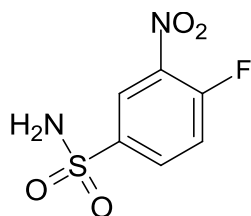
- (R)-benzyl (4-(dimethylamino)-1-hydroxy-4-oxobutan-2-yl)carbamate



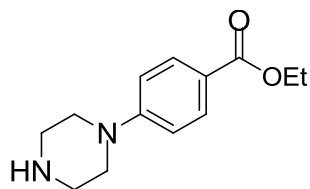
- 4-fluoro-3-nitrobenzene-1-sulfonyl chloride



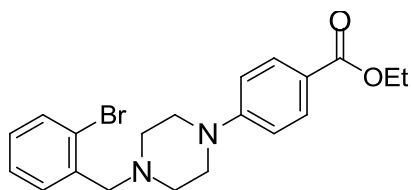
- 4-fluoro-3-nitrobenzenesulfonamide



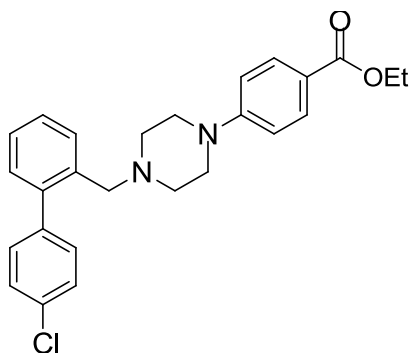
- ethyl 4-(piperazin-1-yl)benzoate



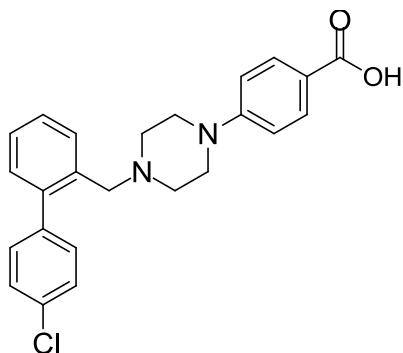
- ethyl 4-(4-(2-bromobenzyl)piperazin-1-yl)benzoate



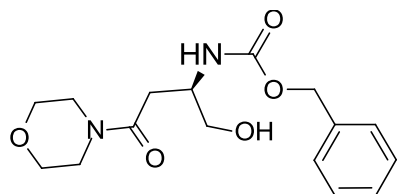
- 4-(4-((4'-chlorobiphenyl-2-yl)methyl)piperazin-1-yl)benzoate



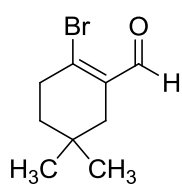
- 4-(4-((4'-chloro-[1,1'-biphenyl]-2-yl)methyl)piperazin-1-yl)benzoic acid



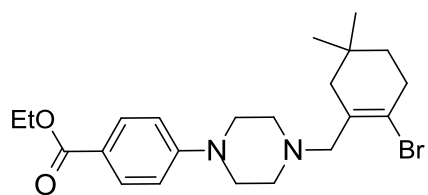
- (R)-benzyl (1-hydroxy-4-morpholino-4-oxobutan-2-yl)carbamate



- 1-bromo-4,4-dimethylcyclohex-1-ene-carbaldehyde



- ethyl 4-(4-((2-bromo-5,5-dimethylcyclohex-1-en-1-yl)methyl)piperazin-1-yl)benzoate



Chapter 1: Introduction

1.1 Luminescent Cell Imaging

Cell imaging is an important tool in molecular biology research used widely for the investigation of biochemical processes in cells. Luminescent cell imaging provides an insight into how biological systems function at the sub-cellular level and into cell signalling events. This can be achieved by targeting chromophores using peptides to the sub-cellular level and monitoring with confocal microscopy.

Thirty years ago, optical microscopy may have been seen as stationary technology. One limitation has been the difficulty in imaging in three dimensions. This is not the case today, where vast improvements are continuing to take place in cameras, lasers, software and probes. These advances in imaging have contributed to cell and microbiology research and continue to do so. One of the main techniques used today in such imaging is confocal laser scanning microscopy. The concept of the confocal microscope was patented in 1961 by Minsky^[1] and since then the instrument has been produced and developed, surviving challenges from alternative technologies and contributing to countless scientific papers.^[2] Confocal microscopy overcame the limitations associated with conventional wide field fluorescence microscopy by eliminating out of focus contributions to the image and has the ability to create three dimensional images and to observe deep within cells.^[3]

In geometry the term confocal means having the same foci and for optics, that, two lenses are arranged to focus on the same point. The key feature of confocal microscopy is the use of pinholes as a filtering technique to eliminate out of focus light as seen in Figure 1.1. Light inside the plane of focus is reflected into a pinhole whereas light outside the focus is scattered at different angles onto an opaque block, therefore the pin holes only allow the light from the plane of focus to reach the detector. This results in excellent clarity and resolution, and three dimensional images can be created from optical slices taken at successive planes of focus.^[4] The combination of digital image collection, three-dimensional image building and rapid image formation make the confocal microscope a powerful and widely applied analytical tool.

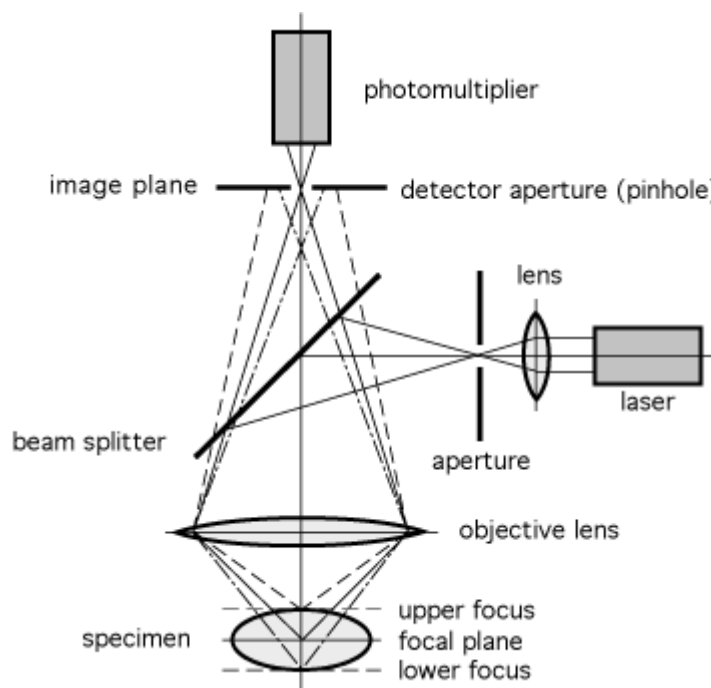


Figure 1.1 Schematic diagram illustrating the components present in a confocal microscope.^[5]

1.2 Novel Luminescent Chromophores for Living Cells

As research in cell biology has advanced from merely structural characterisation of cells towards understanding of dynamic processes, fixed cell fluorescent techniques have been eclipsed by new methodologies appropriate for application in live cell imaging. There are a large variety of fluorescent labels and probes commercially available for the study of living cells^[6]. Selection of the suitable probes can be a complicated task, due to the wide array of prospective imaging agents and several variables that can influence the utility of these fluorescent materials for imaging. Progress in the field of optical imaging is becoming more and more dependent on the development of novel imaging probes.^[7] An appreciation as to how probes are designed and operate can help researchers to make informed choice about probes to examine and solve technical problems, as well as inspiring the development of new probes and new applications. The wide array of imaging agents has been influenced by the combination of fluorophores with materials such as peptides, polymers and metals. These combined materials have also considerably enhanced the performance of numerous optical imaging systems.^[8, 9]

Traditionally, the most widely used probes in cellular imaging are fluorescent organic molecules based on, polycyclic aromatic dyes and chromophores. The short

luminescence lifetimes of such species, typically < 10ns, limits their environmental sensitivity, *e.g.*, towards molecular oxygen and their application in fluorescent lifetime imaging (FLIM).^[10] Another key disadvantage is their tendency to photobleach which can lead to unreliable and irreproducible results.

As outlined by Johnson a fluorescent probe for live cell imaging must address the following criteria: Delivery, Targeting, Detectability and Fluorescence Response.^[11] The probe must be delivered in a way that minimise damage to the physiological and structural integrity of the cell. Also the ideal technique of delivery would be straightforward, economical, rapid, reproducible; applicable to a diverse cell types and capable of uniform loading. Probes with lipophilic structural characteristics can usually be introduced to a cell by adding some of the probe to the extracellular medium. This can then enter the cell by diffusion. More polar probes require further techniques to enable delivery within a cell; these include bulk loading or microinjection. Detailed comparison of loading techniques have been published previously and discussed at length.^[12, 13]

1.3 Introduction to Photoactive Supramolecular Chemistry

In this thesis we take a supramolecular approach to target cell delivery by preparing compounds of the type A-L-B, where A is the photoactive Ru centre, L is the bridging linker and B is the peptide or targeting agent. Supramolecular component may be defined as a “complex system made up of molecular components with definite individual properties”.^[14] These components retain their individual characteristics which are what distinguishes them from a “large molecule“. The original supramolecular studies were typically not covalent but the concept has expanded to include a wide range of studies of general type A-L-B as shown in Figure 1.2.^[15]

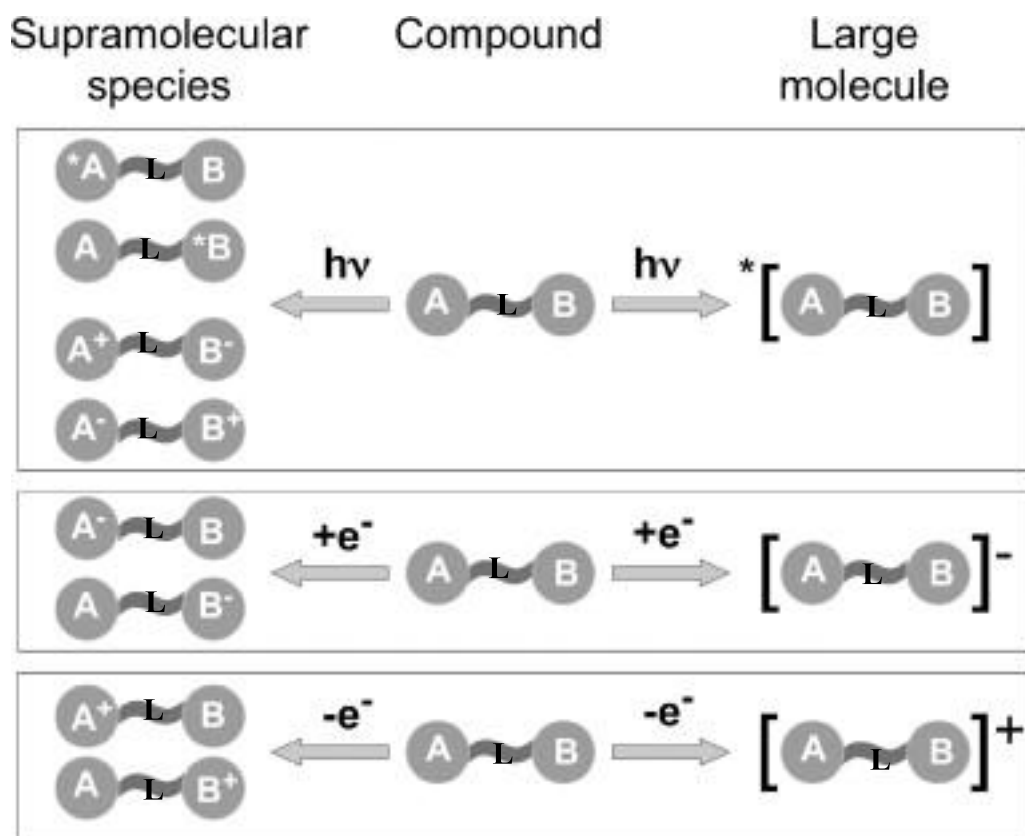


Figure 1.2 Photochemical and electrochemical criteria used to classify a complex chemical species as a supramolecule or as a large molecule.^[15]

In the system A-L-B of Figure 1.2, if light excitation of a molecule results in the excited states that are substantially localised on one of the two components A or B, or causes an electron transfer from one to the other (or vice versa), it is defined as a supramolecule as seen on the left. Distinguished from when the excited states are substantially delocalized on the complete system, the species can be better considered as a large molecule as seen on the right of Figure 1.2. Analogous arguments can be applied to changing the redox states of the system.

We take a supramolecule approach to designing targeted metal complex imaging probes in this thesis where our systems can be thought of as A-L-B dyads. The photoactive components (A) consist of, ruthenium (II) polypyridyl coordination compounds, a bridging unit (L) acts in the present case as an aliphatic and hopefully, electronically benign linker of variable length. The linker connects A to the second components (B), consisting of the transmembrane transport/targeting peptide or organic units. In the resulting A-L-B dyad assemblies both components; maintain their original properties, i.e. photophysical

characteristics and peptide localisation properties but combined form novel and valuable targeted probes, a true characteristic of a supramolecular assembly.

1.3.1 The Photoactive component

A molecular chromophore can be irradiated with UV or visible electromagnetic radiation leading to the promotion of an electron from a lower energy state to a higher energy state, resulting in the formation of an excited state with a discrete lifetime. The energy of the excited state can be dissipated by radiative or non radiative decay. Luminescence is a radiative process by which the electron returns to the ground state with the emission of a photon and if it occurs between states of the same multiplicity it is labelled fluorescence (Figure 1.3).

If the electron experiences a change of spin state, i.e. convert from a singlet ground to triplet excited state, or less commonly, vice versa, according to the selection rules spin change is forbidden. As a result, the energy can become trapped in the triplet state in the former example. Typically triplet states are long lived and return slowly to the ground state via non radiative intersystem crossing or a radiative process called phosphorescence (Figure 1.3). In terms of applications of supramolecular assemblies, emission of radiation by luminescence is important in sensing and signalling because triplet excited states have strong reactivity with molecular oxygen which, relatively unusually is itself a triplet in the ground state. In addition, the long lived nature of triplet states often leaves sufficient time for increased exposure, to diffusive quenchers.

Figure 1.3 shows a Jablonski diagram that is a partial energy diagram that represents the energy of photoluminescent molecule in its different energy states. The lowest and darkest horizontal line represents the lowest vibrational level in each electronic state of the molecule which is the singlet state labelled as S_0 .

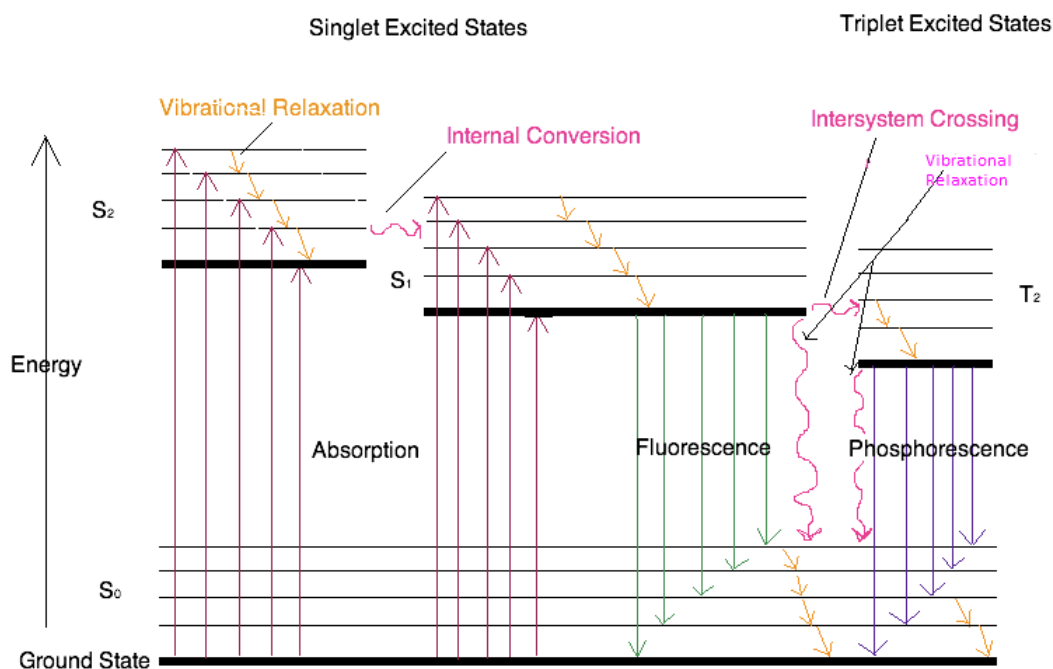


Figure 1.3 Energy scheme to show the difference between fluorescence and phosphorescence.^[16]

The upper lines in Figure 1.3 represent the energy state of the three excited electronic states: S_1 and S_2 represent the electronic singlet state (left) and T_1 represents the first electronic triplet state (right). The energy of the triplet state is always lower than the energy of the corresponding singlet state.

Absorption (red lines in Figure 1.3) leads to electronic promotion from the ground singlet electronic state (S_0) to various vibrational levels within the singlet excited vibrational states. Deactivation of the excited state by fluorescence and phosphorescence involve an emission of a photon radiation as shown by the straight arrow in Figure 1.3. The curled arrows in Figure 1.3 are deactivation processes without the use of radiation.

If inter-system crossing or internal conversion occur, i.e. non-radiative transition to a new electronic state, this is followed by vibrational relaxation and possibly radiative deactivation through fluorescence or phosphorescence. Intersystem crossing is a process where there is a crossover between electronic states of different multiplicity as demonstrated in the singlet state to a triplet state (S_1 to T_1) on Figure 1.3. The probability of intersystem crossing is enhanced if molecule contains heavy nuclei, such as a ruthenium complex, through a process known as spin orbit coupling. The distinction between fluorescence and phosphorescence lies with a change in the spin quantum number between the initial state and

the final state. The emission is defined as fluorescence when the transition spin is allowed, the spin quantum numbers are the same and $\Delta S = 0$. If there is any change in spin quantum number $\Delta S \neq 0$ then the emission is defined as phosphorescence. Throughout this thesis the terms fluorescence and phosphorescence will be referred to as a general luminescence, as in ruthenium complex the distinction is somewhat blurred due to heavy atom effect.

For supramolecular assemblies the photoactive components can be transition metal complexes. In the case of a mononuclear transition metal complexes, molecular orbitals (MO) can be tuned by modifying the individual ligands and complex orbitals leading to significant synthetic control over the optical and photophysical properties of the complexes. The individual orbitals are labelled M or L depending on whether they are mainly metal or ligand centred. A scheme of octahedral metal complex orbitals is shown in Figure 1.4. From this orbital diagram the four types of optical transition of metal complexes can be identified. The metal orbitals are shown on the left of Figure 1.4 where as the ligand orbitals are shown on the right and the molecular orbitals are centered. Absorbance bands are usually assigned to electronic transitions which can be regarded as metal centred (MC) transitions, ligand centered (LC) transitions or charge transfer (CT). The lowest energy excitation is metal centred (MC) transitions (d-d transitions), provide that all the d orbitals are not filled. Usually the metal's d orbitals are partially filled and depend on the oxidation state of the metal. These arise from the localised orbitals on the metal centre and are usually very weak.^[17] Next in order of energy is the charge transfer transitions where metal to ligand (MLCT), also known as $d-\pi^*$, and ligand to metal charge transfer (LMCT) known as $\pi-d$ are the most investigated. Finally in order of energy is ligand to ligand charge transfer (LC) as seen in Figure 1.4, for example $\pi-\pi^*$ in a bipyridine ligand^[17]. In general, in a metal complexes' ground energy state the σ^L and π^L ligand orbitals are full. Other anti-bonding σ^{*L} and π^{*L} ligand orbitals are usually empty.

Once light energy is absorbed the population of these orbitals change. Metal centred (MC) transitions (or d-d transitions) involves a rearrangement of the metal d-electrons from the t_{2g} to e_g sets such transitions are LaPorte forbidden in octahedral complexes becoming more allowed as the geometry deviates from this symmetry. The energy of dd transitions varies, but depends on the ligand field splitting which is influenced by the σ -donor and π -acceptor ability of the coordinating ligands. Interligand charge transfer transitions are basically ligand centred transitions (LC) analogous to those occurring in organic molecules, they are of much higher energy than dd or CT transitions and generally occur when chromophoric ligands are coordinated to the metal centre (Figure 1.4).

Charge transfer transitions are typically responsible for the strong colour of many coordination compounds. These are typically allowed transitions with high extinction coefficients, MLCT is particularly common since it involves promotion of an electron from a metal based highest occupied molecular orbital (HOMO), t_{2g} in an octahedral field, to the lowest unoccupied molecular orbital (LUMO) based on the ligand.^[18] All of these excited energy states may have singlet or triplet multiplicity.

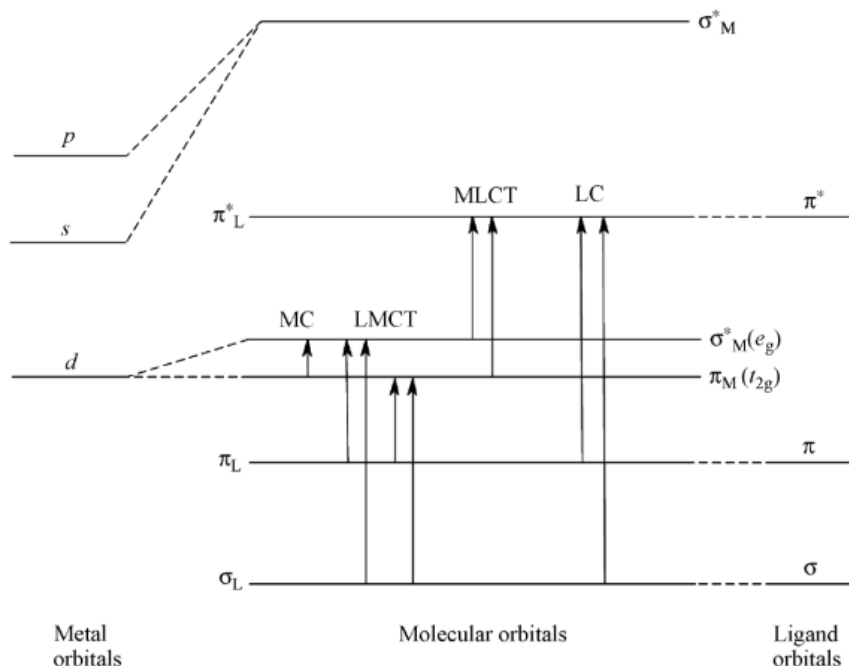


Figure 1.4 Energy level diagram of a transition metal complex showing the various types of electronic transitions.^[14]

1.4 Luminescent Metal Complexes in Cell Imaging

Lanthanide luminescent probes^[19, 20] and organometallic complexes are emerging as viable alternatives to organic dyes as fluorescent probes.^[21-23] This is because they are not very prone to photobleaching and possess long-lived excited states. In addition they tend to display large Stokes shifts. The Stokes shift is the difference between positions of the band maxima of the absorption and emission spectra of the same electronic transition. Large Stokes shifts will reduce artifacts in imaging due to the amount of self-quenching possible at high dye concentrations. Luminescent metal complexes are increasingly desirable applicants for cellular imaging as they can also be designed for low toxicity, good cellular uptake and targeted intercellular localisation.^[21, 24]

In recent decades, much attention has been focused on organometallic complexes of various heavy metals, including Ru,^[25-27] Os,^[25] Ir^[24, 28] and Pt^[29] for their potential use as phosphorescent materials across a range of applications. Applications in biological imaging has come relatively late for these materials but the focus has been with the d⁶ transition metal complexes, such as Re^I^[30] Ru^{II}^[31] and Ir^{III}^[24] in particular polypyridal complexes. As part of a continuing effort toward the development of organometallic materials exhibiting desired properties, our group are focusing on ruthenium based probes.

1.4.1 Ruthenium (II) Polypyridal Probes

Ruthenium (II) has extensive coordination chemistry. Derivatives of polypyridine, in particular bipyridine, are widely used due to their potential for luminescence the most well known being the luminescent tris-(bipyridine) ruthenium(II) dichloride with the formula [Ru(bpy)₃]Cl₂.^[31] In particular, these Ru(II) polypyridine complexes are the class of transition metal complexes which have been most extensively studied from a photochemical viewpoint. The reason for such great interest in these Ru complexes comes from an exclusive combination of chemical stability, excited-state reactivity, luminescence emission, redox properties and excited-state lifetime. Ruthenium polypyridine complexes are indeed good visible light absorbers, feature relatively intense and long-lived luminescence and can undergo reversible redox processes in both the ground and excited states.^[13, 32] Although relatively few reports exist on their application in cell imaging, examples of ruthenium polypyridyl complexes applied to cell imaging are increasing.^[33-35]

Many of the photophysical and redox characteristics of [Ru(bpy)₃]²⁺ have been detailed extensively in the literature^[13, 36-38] and it may be used as a example to explain similar processes occurring in other ruthenium (II) polypyridyl complexes discussed in this thesis. Figure 1.5 shows the typical absorbance and emission profile for the [Ru(bpy)₃]²⁺ complex in acetonitrile solution.^[39] The UV-vis spectrum of [Ru(bpy)₃]²⁺ is dominated by a spin allowed ¹MLCT transition from the ruthenium (dπ (t_{2g}) orbital) to a bipyridyl ligand (π*) orbital at 451 nm, a further MLCT transition at a higher energy at 241 nm as seen in Figure 1.5.^[39] The MLCT transition leads to an excited triplet MLCT state that can be explained by the spin-orbit coupling of the d⁶ metal centres, leading to large stokes shifts. Spin-orbit coupling involves mixing of both the singlet and triplet excited energy states of the molecule. However, the lowest lying energy state responsible for emission remains largely triplet in nature. The efficiency of intersystem crossing

following light absorption is known to be close to unity for ruthenium (II) polypyridyl complexes.^[40] The strong absorbance at 286 nm is ascribed to LC (π - π^*) electronic transitions within the bipyridyl ligands orbitals.^[13]

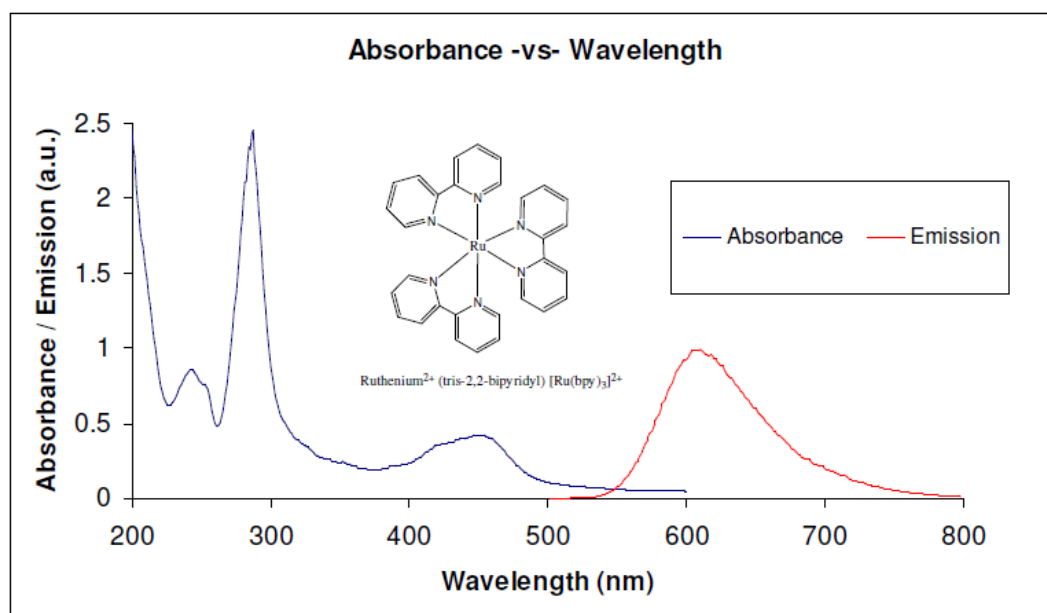


Figure 1.5: Absorbance and normalised emission spectra (excited at 451 nm, slit widths: 5 nm – normalised to 1 arbitrary unit) of 20×10^{-6} M [Ru(bpy)₃]²⁺ in acetonitrile solution.^[39]

The optical transitions of ruthenium polypyridyl complexes may be tuned with the addition of certain electron withdrawing or donating ligands, which influence the ligand field splitting of the complex, in other words the relative energies of the t_{2g} and e_g states. One may therefore tune the wavelength of the lowest excited state transition by manipulating the ligands.^[38] There are two approaches to shift the $d\pi$ - π^* bands band to longer wavelengths of the spectrum one may add electron withdrawing groups to the polypyridyl ligands of ruthenium in an effort to lower their π^* energy level. Another technique is to introduce an electron donating ligand to stabilise the positive hole at the metal centre following MLCT.^[41]

One of the most common ligands in supramolecular chemistry is the bidentate chelate 2,2-bipyridine (bpy Figure 1.6.1).^[14] This is the first member of a series of polypyridyl ligands used in our supramolecular chemistry assembly. Other members include 1,10-diphenylphenanthroline (dpp Figure 1.6.2) and dipyrldophenazine (dppz Figure 1.6.3)

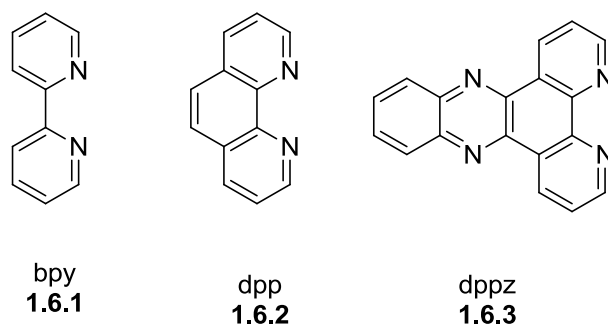


Figure 1.6 Polypyridal ligands used in supramolecular chemistry

Bipyridine ligands are good σ -donor ligands as the lone pair of electrons on the nitrogen is able to form a σ -bond with the unoccupied orbital of the metal ion centre. d-orbitals of a metal can overlap with an unoccupied π^* orbital of the acceptor ligands. The σ -donor bonding increases the electron density on the metal ion; its ability to form a π bond with the ligand is enhanced resulting in back bonding. Also the diimine moiety, $-\text{N}=\text{C}-\text{C}=\text{N}-$ of bpy supports a delocalisation of the electrons around the ring. This produces greater π acceptor strength.

The long standing barrier to the utilization of ruthenium (II) complexes in the context of cell imaging has been that these complexes do not passively diffuse across the cell membrane.^[42] One way to overcome this limitation is to attach the fluorophore to biological targeting molecules that are capable of cell penetration.

1.5 Delivery Vectors

The key problem of application of metal complexes in therapeutic and imaging effectiveness lies in the cellular delivery of therapeutic and imaging agents. The plasma membrane forms an impermeable barrier for large hydrophilic therapeutic agents and probes. The need to develop efficient strategies for cellular uptake is driven by the cell impermeable nature of these agents. Numerous strategies have been developed to facilitate the import of these agents and nucleic acids into cells, among these are viral vectors^[43, 44], cationic lipids^[45], polymers^[46] and cell penetrating peptides (CPPs).^[47, 48]

Several useful delivery vectors have emerged in recent years, including liposomes, viral vectors, dendrimers, polymer-based nanoparticles and peptides. In our supramolecular assembly approach A-L-B the delivery vector is the B unit linked to the photoactive agent.

Drugs and imaging agents with intercellular targets or receptors are required to cross the cell membrane. The ideal cellular transporter would be low cost, non-toxic, and could transport any cargo across the cellular membrane.^[49]

1.5.1 Liposome

Lipid amphiphilic compounds are a broad class of organic molecules than contain a hydrophilic head group and a hydrophobic chain region. A liposome is a vesicle composed of a lipid bilayer. The liposome can be used as a medium for administration of nutrients and pharmaceutical drugs. Liposomes are fabricated from reasonably bio-compatible and biodegradable material.^[50] They consist of aqueous volume captured by one or more bilayers of natural and/or synthetic lipids. Drugs or imaging agents with a wide array of lipophilicities can be encapsulated in liposomes, either in the bilayer itself or in the aqueous volume (Figure 1.7). Also as seen in Figure 1.7, ligands are on the outside of the liposome to target receptors within the cell.

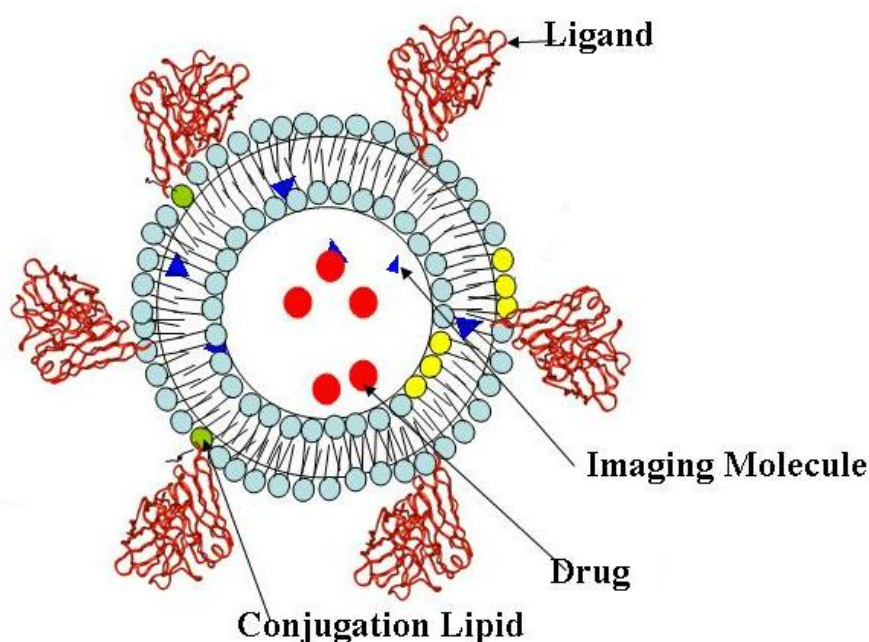


Figure 1.7 Scheme of Liposome formed by phospholipids in an aqueous solution.^[51]

Liposomes can be used to increase cytosolic delivery of certain drugs. The potential of liposomes to enable internalization and pharmacological activity of cell-impermeable drugs has been documented long ago for drugs such as methotrexate-gamma-aspartate^[52] and

N-(phosphonacetyl)-L-aspartic acid (PALA) ^[53], that were referred to as “liposome-dependent drugs.”^[54]

A recent study from the Gabizon laboratory in Israel with zoledronic acid, another cell-impermeable drug and a potent inhibitor of farnesyl-pyrophosphate synthase, has indicated that folate liposomal targeting of zoledronic acid results in a major increase of drug uptake and in a »100-fold increase of *in vitro* cytotoxicity when compared to the free drug.^[55] They also constructed studies using pegylated liposome doxorubicin (PLD) and results clearly showed that PLD was superior to free doxorubicin in all tumour models studied.^[54]

Liposomes have been investigated as carriers of various materials however there are limitations associated with them. Some of the problems limiting the manufacture and development of liposomes have been stability issues, batch-to-batch reproducibility, sterilization methods, low drug entrapment, particle size control, amongst others.^[50]

1.5.2 Dendrimers

Dendrimers are repetitively branched molecules organised around an inner core. A dendrimer adopts a spherical three-dimensional structure. Applications of dendrimers typically involve conjugating other chemical species to their surface that can function as detecting agents, such as affinity ligands, targeting components, radioligands, imaging agents, or pharmaceutically active compounds. One dendrimer molecule has hundreds of probable sites to couple to an active species. The range of chemical structures making up the class of dendrimer makes it extremely difficult to generalise on their application in delivery.

A significant example of architecturally-optimized dendritic drug delivery was reported by Fréchet and Szoka where an asymmetric doxorubicin-functionalized bow-tie dendrimer was prepared by PEGylation of one side of a 2,2-bis(hydroxymethyl)propionic acid dendrimer and conjugation of the drug via an acyl hydrazone linkage to the other side resulting in 8–10 wt.% doxorubicin content overall (Figure 1.8). These gave a 9 fold increase in tumour uptake in comparison to doxorubicin alone.^[56] In comparison to other delivery techniques dendrimers are in their infancy.

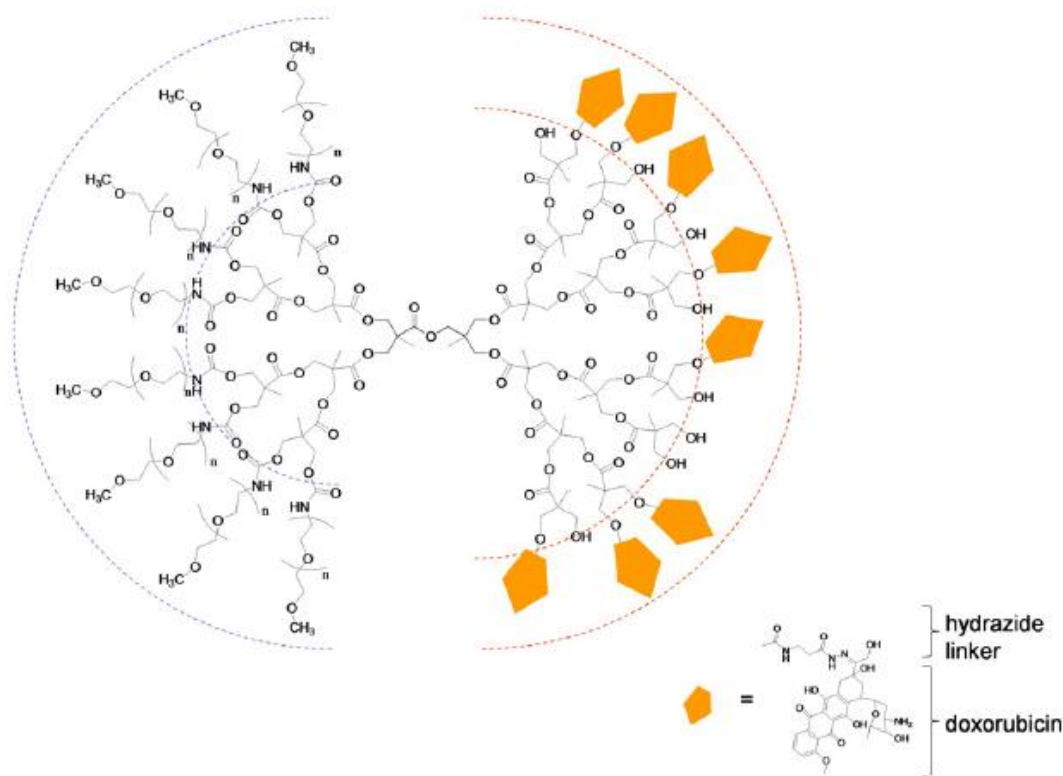


Figure 1.8 Doxorubicin functionalised bow tie dendrimer.^[57]

1.5.3 Viral Vectors

Viral vectors are a means generally used by molecular biologists to deliver genetic material into cells. Viruses have developed specific molecular mechanisms to efficiently transport their genomes inside the cells they infect. Delivery of genes by a virus is termed transduction. This machinery was first utilised in the 1970s by Paul Berg used with a tailored SV40 virus containing DNA from the bacteriophage lambda to infect monkey kidney cells maintained in culture.^[58]

Synthetic or modified viruses can carry the therapeutic gene inside their capsid until it reaches the intended target. Viral vectors are occasionally created from pathogenic viruses. While they are modified in such a way as to minimize the risk of handling them, this is still seen as a limitation. Some viruses are also genetically unstable and can quickly rearrange their genomes. This unfavourable predictability and reproducibility of the work performed using a viral vector is a key limitation in their application.^[59]

1.5.4 Solid Lipid Nanoparticles

Solid Lipid Nanoparticles (SLN) are another type of colloidal carrier system. They possess a solid lipid core matrix that can solubilise lipophilic molecules as seen in Figure 1.9. The ability to incorporate drugs into nanocarriers offers a new prototype in drug delivery that could hold great promise for attaining the bioavailability enhancement along with controlled and site specific drug delivery. It has been proposed that SLNs combine numerous advantages over the other colloidal carriers *i.e.* incorporation of lipophilic and hydrophilic drugs feasible, no biotoxicity of the carrier, avoidance of organic solvents, possibility of controlled drug release and targeting, increased drug stability and no problems with respect to large scale production.^[60] SLN can also be exploited for different administration routes. Like dendrimers, SLN are relatively young drug systems with trends increasing.^[61] Tumour targeting has been achieved with SLNs loaded with drugs like camptothecin.^[62]

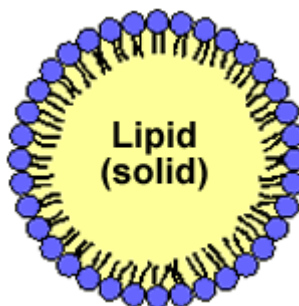


Figure 1.9 Generic structure of solid lipid nanoparticle (SLN)^[63]

1.5.5 Cell Penetrating Peptides

Cell-Penetrating Peptides (CPPs), are short peptides (≤ 40 amino acids), with the capability to enter the interior of almost any cell. The method of penetration remains controversial, but there is abundant evidence that they may involve several mechanisms, including direct translocation across the plasma membrane and endocytosis. They have the outstanding property of carrying into the cells a wide variety of covalently and non-covalently conjugated cargoes. Therefore they are extremely attractive candidates to transport therapeutic agents, imaging agents amongst others to the interior of cells. Evidently CPPs have potential as universal delivery agents. Furthermore, their capability to preserve the biological activity of their therapeutic cargoes makes the CPP delivery approach truly desirable. One of the earliest interest was the Tat peptide, derived from the HIV Tat trans-

activation protein.^[64] It was first revealed that the full-length protein crossed the plasma membrane and investigations led to the identification of small fragments that could efficiently enter cells.^[65, 66] These findings, along with those identifying other peptides with membrane crossing activities^[67], assisted in the development of cell-penetrating peptides (CPPs) as a class of molecular transporters. For this thesis and our supramolecular assembly, CPPs were chosen as our delivery system.

CPP are often positively charged sequences of amino acids.^[68] Compared with other systems, CPPs have numerous advantages due to the capability of simple modification, allowing them to target different sub-cellular domains and/ or transport various types of cargoes. The main feature of CPPs is their capability to penetrate the cell at low concentrations and without causing any significant membrane damage.^[48] Also they are capable of internally localising biologically active agents and probes with high efficiency and low toxicity into a cell.^[69]

Until recently, extracellular or externally located membrane receptors have been the target of peptide-based imaging probes. This limitation occurred mainly due to charge and size concerns associated with conventional probes which therefore do not allow for the passive uptake into cells. Charged compounds are inhibited from passing into the cells by the dielectric constant of the lipid bilayer of the plasma membrane.^[70, 71] A few cationic peptides have been shown to have a distinctive capability to cross the cytoplasmic membrane of cells and subsequently have been used as delivery agents for a variety of biopolymers and small molecules.^[47, 72, 73] Peptide-based imaging agents offer high molecular target specificity and a great degree of flexibility in their design and ease of synthesis.

1.5.5.1 Mechanism of uptake

Many different short peptide sequences have been identified that are able to transport diverse types of cargo molecules. Acquiring information about common trends governing CPP uptake, such as the effects of peptide length, chemical properties and size, has significant implications for designing CPPs. With facts regarding how certain properties favour one mechanism of uptake over another, designing new peptides with a required uptake mechanism is important to their application.^[49] Several investigations have been performed to clarify how CPPs gain access to the interior of cells. A variety of uptake

mechanisms appear to be operative in different systems and, in some cases, the mechanism is cell-type or cargo-specific. It appears that CPPs can be classified according to three main entry mechanisms: translocation through the formation of a transitory structure, direct penetration in the membrane and endocytosis-mediated entry as seen in Figure 1.10.

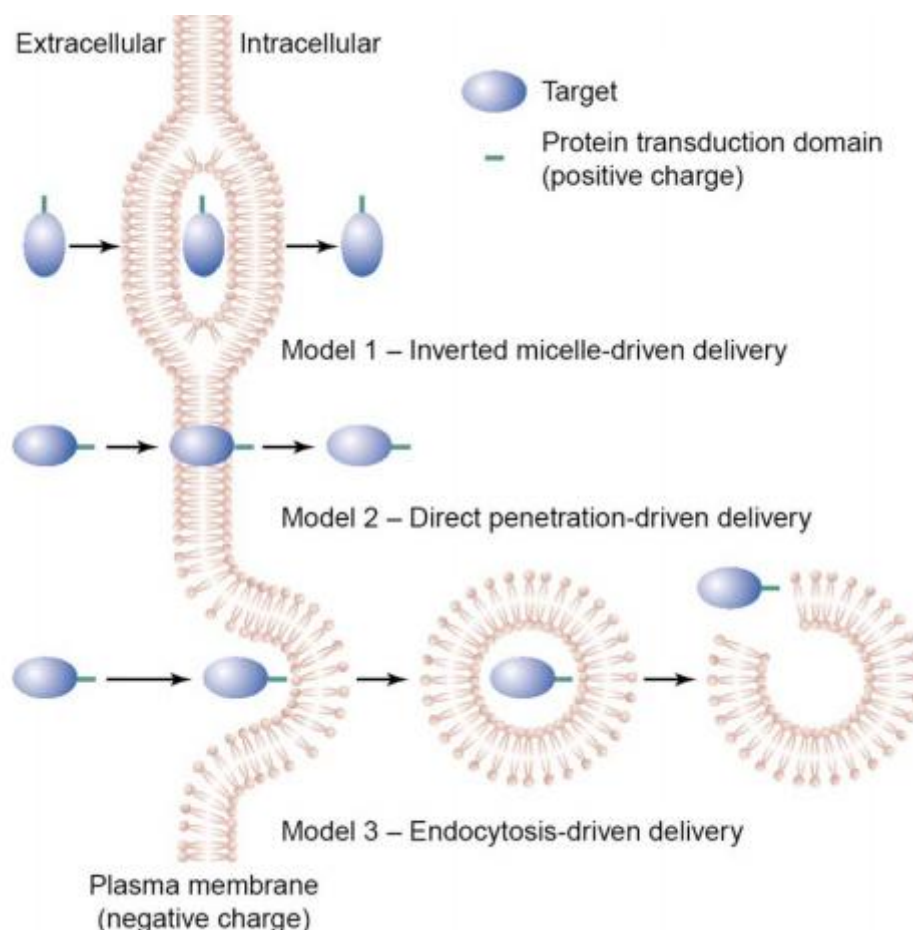


Figure 1.10 Proposed mechanisms of cellular delivery of cargoes mediated by cell penetrating peptides (CPPs). Model 1 represents a mechanism that is assumed to occur through the formation of an inverted micelle. Model 2 suggests direct penetration of the plasma membrane.

Both mechanisms were considered to occur via rapid, energy- and receptor-independent pathways. However, more recent observations imply that the uptake of a majority of CPPs and cargo-conjugated CPPs results from endocytosis by which small quantities of the conjugates are released via an unknown mechanism (Model 3).^[74]

In the early stages of investigation into the mechanism of entry of CPP's, direct permeabilization was evident, (Figure 1.10, Model 2). This was found to be an energy-independent mechanism. Numerous experiments were conducted in conditions of reduced

ATP concentration and low temperatures, which failed to inhibit internalization of Tat^[75] and pAntp^[76], and therefore supported a non-endocytic uptake mechanism.

In 1996, researchers proposed the inverted micelle model (Figure 1.10, Model 1) to explain the penetration of the bilayer in terms of receptor-, energy-, and endocytosis-independence.^[74] Inverted micelles are aggregates of colloidal surfactants within the cell membrane with a hydrophilic cavity present within the two bilayers and a hydrophobic environment of the phospholipid tails. The structure of the inverted micelles permits the peptide to remain in a hydrophilic environment during translocation. This micellar phase in the membrane is temporary, and the CPP is subsequently released, directly into the cytosol and independent of any vesicular body, as the micelle passes to the cytosolic side of the bilayer.^[48]

Endocytosis is the process of cellular ingestion by which the plasma membrane folds inward to bring substances into the cell (Figure 1.10, Model 3). During this process cells absorb by engulfing the material from the outside of the cell within their cell membrane. Evidence for this process accumulated from 2002 and although it is considered that each CPP expresses its own preferred mechanism of uptake^[74], this evidence has yet to be disproved.^[48]

1.6 Cell Penetrating peptides delivery of imaging agents

The capacity to picture internal features and physiological structures of living organisms and monitor cellular functions *in vivo* is vital for understanding, diagnosing and treating disease. Non-invasive biomedical imaging methods such as fluorescence imaging and magnetic resonance imaging (MRI) have been developed for *in vivo* applications such as directly visualising diseased tissue during surgical procedures or following the dynamics of the immune cells in living animals.^[49] The plasma membrane forms an impermeable barrier for large hydrophilic imaging agents and probes and CPPs have proven useful in this field as delivery vehicles (Figure 1.11).

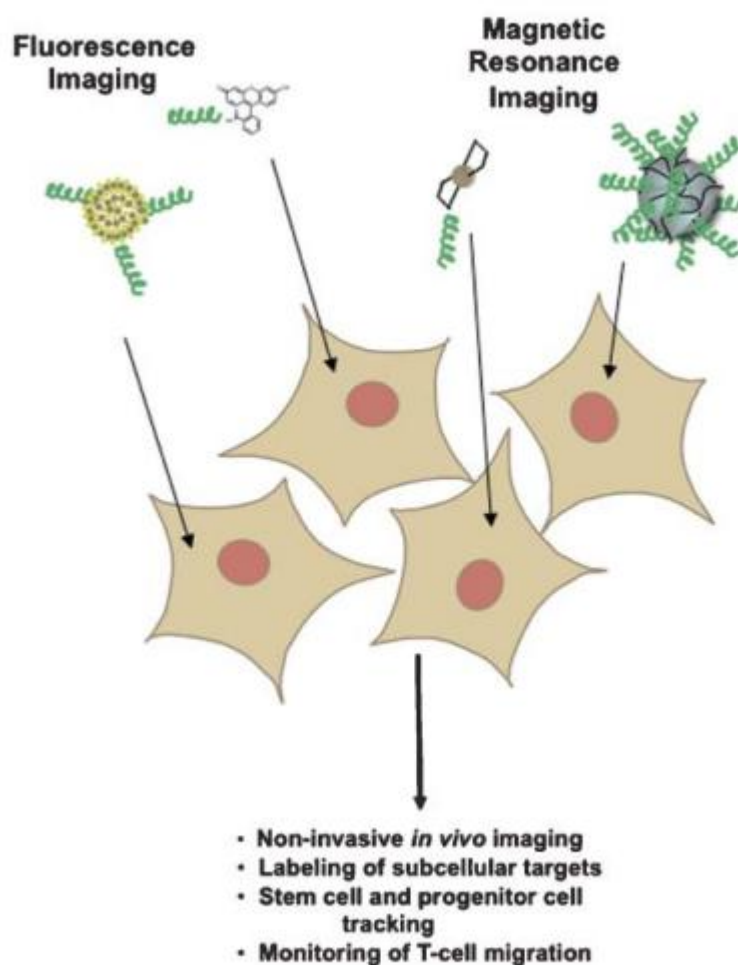


Figure 1.11 CPP (shown as green helices) mediated delivery of imaging agents.^[49]

1.7 Probe Peptide Conjugates of Metal Complexes

The long standing barrier to the utilization of ruthenium (II) complexes in the context of cell imaging has been that these complexes do not passively diffuse across the cell membrane.^[42] Therefore, in the few examples where they have been applied to imaging the cells, they must be permeabilised by electroporation, detergent or treated with some other transfection agent.^[10, 77] This typically damages the cells or causes its biochemistry to change.

Because targeted delivery of peptide agents to intracellular compartments can enable a wide range of novel applications in medicinal imaging, a peptide conjugate with good imaging properties, while capable of permeating the plasma membrane is highly desirable. Recent work by our group has reported that polyarginine labelled ruthenium complexes efficiently and rapidly transport across the cell membrane into the cytoplasm.^[35, 78] Such chromophores provide unique opportunities for imaging dynamic processes in living cells avoiding limitations associated with fixation.

Neugebauer *et al* were the first to report the synthesis of two novel ruthenium polypeptide conjugates for the purpose of cellular imaging, as illustrated in Figure 1.12.

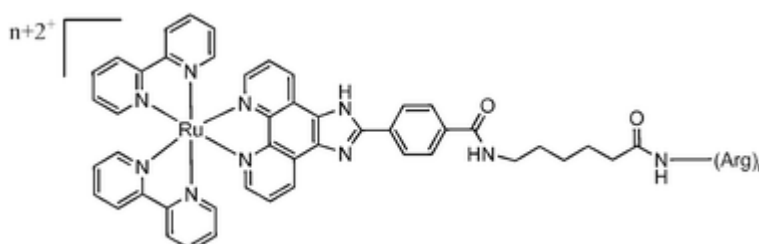


Figure 1.12 Structure of the first ruthenium (II) conjugate suitable for cellular imaging. (n=5 or 8).^[78]

The highlight of these results was the capacity of the octarginine dye-conjugate $[\text{Ru}(\text{bpy})_2(\text{picCOOH})\text{Arg}_8]^{10+}$ to passively transport across the cell membrane of SP2 myeloma cells without the need to use organic solvents. In contrast, the parent dye (without peptide) and shorter pentarginine conjugate showed no evidence of distribution across the cell membrane. This suggested that the length of the cell penetrating peptide was important in its transmembrane capabilities. Diffusion of the parent ruthenium complex across the membrane could be achieved using the detergent Triton, DMSO or ethanol to permeabilise the cell. The migration of the octarginine dye-peptide in absence of permeabilization was established completely after 10-15 minutes at room temperature, in a temperature-dependent and by an irreversible process. SP2 myeloma cells in a buffered solution were exposed to 3.5×10^{-5} M of $[\text{Ru}(\text{bpy})_2(\text{picCOOH})\text{Arg}_8]^{10+}$ which led to bright luminescence within the cells cytoplasm after only 2 minutes as shown in Figure 1.13. Over the next 10 minutes the dye-peptide continued to distribute throughout the cell in various concentrations across the cellular plasma in a non-selective manner.

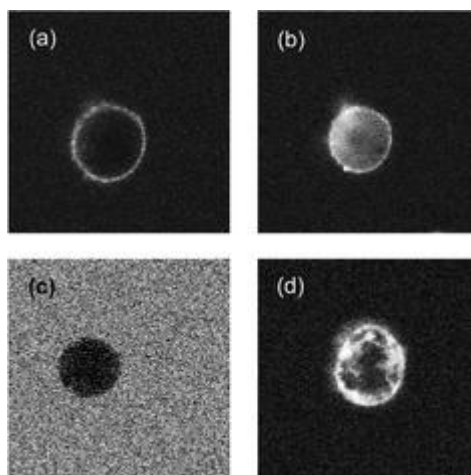


Figure 1.13 Luminescent images of SP2 myeloma cells incubated with $[\text{Ru}(\text{bpy})_2(\text{picCOOH})\text{Arg}_8]^{10+}$ after (a) 3 min and (b) 5 min. (c) Myeloma cell incubated with the parent complex $[\text{Ru}(\text{bpy})_2(\text{picCOOH})]^{2+}$ ($3.5 \times 10^{-5} \text{ M}$ in PBS) for 26 min and (d) for 5 min after permeabilizing the cell with Triton (1% v/v).^[79]

In an attempt to assess the distribution of the dye-peptide across SP2 myeloma cell organelles, Neugebauer *et al.*^[78] counterstained the cells with a cell permeable localising dye. 3,3'-Dihexyloxacarbocyanine iodide $[\text{DiOC6}(3)]$ was used to selectively stain the mitochondria and at higher concentrations the membrane structures within the cell including lysosomes and endoplasmic reticulum. Analysis of both $[\text{Ru}(\text{bpy})_2(\text{picCOOH})\text{Arg}_8]^{10+}$ and $[\text{DiOC6}(3)]$ in SP2 cells using confocal fluorescence microscopy showed that their luminescence did not coincide and therefore it may be concluded that the ruthenium dye-peptide does not distribute strongly within the mitochondria or endoplasmic reticulum of SP2 cells.

In a more recent paper by the group^[35] a $[\text{Ru}(\text{dppz})_2(\text{picCOOH})\text{Arg}_8]^{10+}$ complex (Figure 1.14) is utilized with the intention of multimodal cellular imaging. As this dye demonstrates a 'molecular switching effect' only the dye molecules shielded by and associated with membrane structures emit phosphorescence and therefore, cannot be used to assess the true distribution of the dye in the cell. Nevertheless, resonance Raman mapping does not rely on the emission of the dye and is employed here for the first time as a complementary technique to assess the localisation of the parent dye and dye-conjugate.

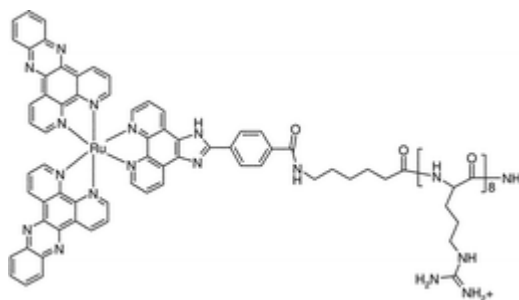


Figure 1.14 Chemical structure of $[\text{Ru}(\text{dppz})_2(\text{picCOOH})\text{Arg}_8]^{10+}$.^[35]

Figure 1.15 illustrates the plot intensity of these ruthenium (II) vibrational modes and therefore the dye concentration within the cell. It is observed that the parent dye remains in the outer cell membrane (Figure 1.15, image B1), while, the dye peptide diffuses across the cell membrane (Figure 1.15, image A1) and is distributed throughout the entire cell.

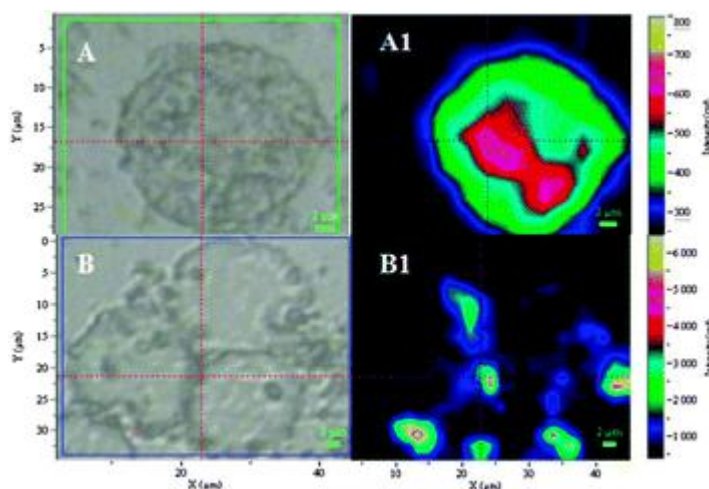


Figure 1.15 Resonance Raman intensity map of live myeloma cells after incubation with $[\text{Ru}(\text{dppz})_2(\text{picCOOH})\text{Arg}_8]^{10+}$ (A1) and free parent dye (B1) after excitation at 458 nm. A and B represents the brightfield images of the cells in PBS.^[35]

Another group, the Barton group have demonstrated the potential of using a cell penetrating peptide to facilitate entry of a ruthenium dye peptide into HeLa cells. They used ruthenium complexes as probes to study the chemical and physical properties of DNA and the biological implications of those properties. Their results showed that the parent complex $[\text{Ru}(\text{phen})(\text{bpy})(\text{dppz})]^{2+}$ showed no transport across a cellular membrane prior to conjugation to the octaarginine peptide. Interestingly, the uptake of a labelled peptide conjugate ruthenium-Arg₈-fluorescein is far greater at lower concentrations when compared to the ruthenium-Arg₈ conjugate alone.^[80] It is thought that the greater lipophilicity of the conjugate containing the fluorescein moiety increases the interaction of the labelled conjugate with the cellular membrane.

The Barton group then went on to use short peptides to target the nucleus, in particular DNA. They studied $[\text{Ru}(\text{phen})(\text{bpy})(\text{dppz})]^{2+}$ conjugated to a peptide, RrRK, of reduced length and net positive charge.^[81] This peptide efficiently targeted the organic fluorophore thiazole orange to the nucleus.^[82] They found that RrRK conjugation increases cellular uptake as compared to analogous unconjugated complexes, and that, above a threshold concentration of 30 μM , this peptide targets the ruthenium complex to the nucleus as shown in Figure 1.16.

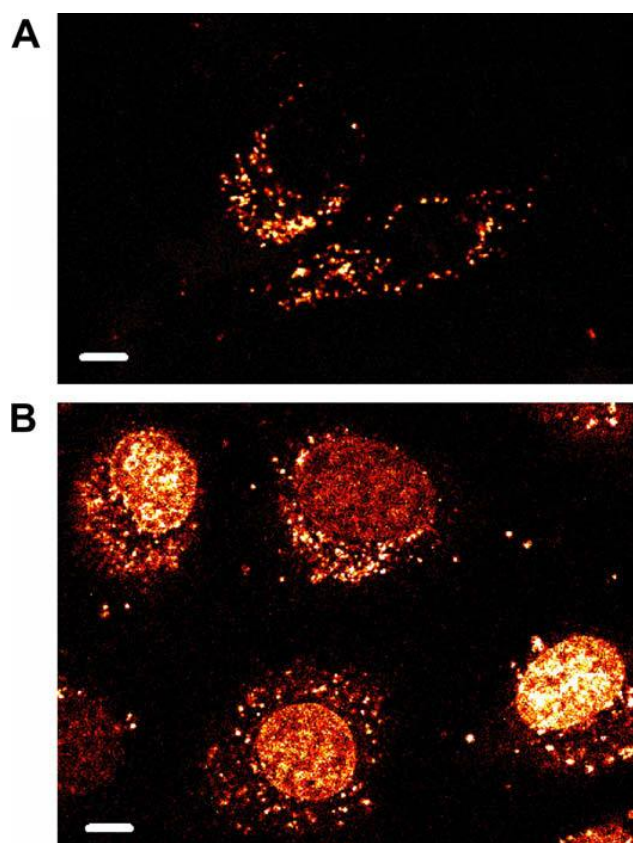


Figure 1.16 Subcellular distribution of Ru–RrRK in serum-free medium. HeLa were incubated with (A) 20 or (B) 40 μM Ru–RrRK in for 2 h. At 20 μM in medium without serum, most cells show only punctuate cytoplasmic staining, while at 40 μM , the majority of cells exhibit additional nuclear labelling. Scale bars are 10 μm .^[81]

1.8 Targeting (homing) Peptides

To achieve an effective local concentration at a disease site by systematic drug administration one must use a high concentration of the drug. This can be problematic because it may result in nonspecific toxic side-effects. In the 19th century, German scientist Paul Ehrlich brought about the concept of targeting drugs to specific sites of the disease, ‘the magic bullet’ concept and this remains the goal of pharmaceutical scientists worldwide. ^[83]

In addition to assisting transport across the plasma membrane, applications of CPPs aimed at specific organelles can be envisioned. The capacity to target specific organelles generates opportunities to study biological processes at the subcellular level and to deliver therapeutics to targets within cellular compartments. Currently, the nucleus and the mitochondria have been successfully targeted with CPPs. The nucleus, the location of DNA, is an attractive target and the essential destination for agents used in gene therapy. ^[84] The mitochondrion is a particularly appealing organelle for drug therapy given its role in the pathology of cancer, neurodegenerative diseases, and others where reactive oxygen species are linked with disease progression. ^[85, 86] Kelley and co-workers have completed comparative studies on nuclear and mitochondria targeting peptide conjugates. Two peptide conjugates with specific cellular localization profiles were developed to separately address oxidative stress occurring in the nuclei and mitochondria of living HeLa cells (Figure 1.17). ^[82] Colocalisation studies confirmed the localisation profiles obtained. Their results indicated that different molecular charges of TO-FrFK and TO-RrRK were responsible for the distinct localisation profiles, where TO is thiazoleorange (TO), a chromophore that produces singlet oxygen (¹O₂) upon exposure to visible light. It is also noteworthy that both their compounds cross the plasma membrane with efficiencies that approach what has been previously observed for CPPs.

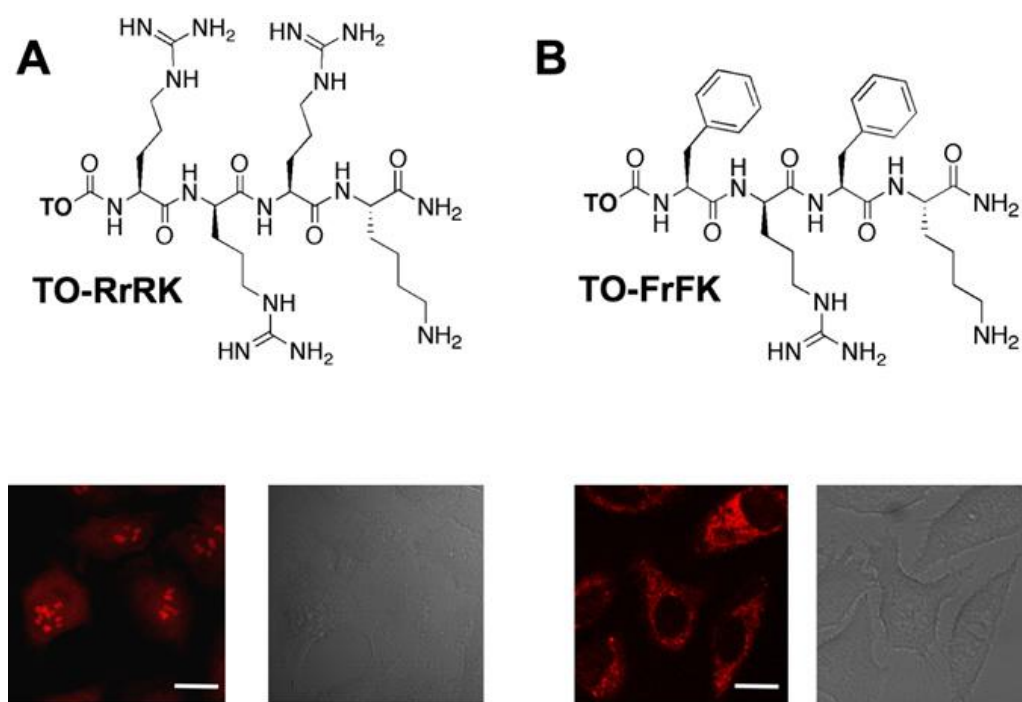


Figure 1.17 (A) Structure and fluorescence confocal microscopy images for TO-RrRK demonstrating localization of this compound within the nuclei of living, unfixed HeLa cells. Fluorescence image (left) is shown alongside corresponding DIC image (right). (B) Structure and fluorescence confocal microscopy images for TO-FrFK demonstrating localization of this compound within the mitochondria of living, unfixed HeLa cells. Fluorescence image (left) is shown alongside corresponding DIC image (right). The scale bars represent 10 μm .^[82]

Thus far the work done by our group has been with the cell penetrating peptide Arg₈. This peptide sequence is capable of penetrating the cell membrane but do not localise preferentially in specific sub-cellular compartments. Although some cell penetrating peptides have entered clinical trials^[87], some weaknesses are still encountered, in particular due to the lack of specificity of unmodified CPPs toward targets.^[47, 73, 88] Further localisation of these imaging agents within the cell will be useful in the study of mechanism(s) leading to membrane translocation and can also be useful in targeted therapy. This requires understanding of the interactions of these carrier peptides with the membrane components and the structural consequences of these interactions. These studies can then provide an insight into the ability of peptides to act as drug carriers. Several peptide sequences capable of permeating the plasma membrane of cells with various cargos have been reported.^[47] These include a group of peptides called nuclear localisation signals (NLS) that can be targeted within the cell to the nucleus.

NLS peptides, particularly the NLS from simian virus 40 (SV40) large T antigen, have been used in several studies to drive uptake of DNA for non-viral gene therapy.^[84] Most studies have focused on the capability of the NLS sequences to drive localization of some exogenous DNA into the nucleus. Some studies use transfection agents or microinjection to assist with uptake efficiency and others exploits the cell-penetrating properties of the NLS peptides driving translocation in unaided uptake.^[49] Nuclear localisation signals are mainly short cationic peptides that interact with receptors at the nucleus. These peptides can be exploited to introduce linked cargo into the cell and ultimately its nucleus.^[73]

In the case of this thesis the NLS were used to target the novel chromophores to the nucleus. The first NLS chosen for our supramolecular assembly was the first NLS to be discovered from the SV40 large T antigen.^[89] It is imported into the nucleus by its interaction with importin α .^[90] The NLS sequence of SV40 is PKKKRKV.

The second sequence chosen for supramolecular assembly with the chromophores was a sequence derived from NF- κ B. This peptide is derived from a transcription factor. Transcription is an important regulatory event in the pathway leading to gene expression. NF- κ B has been the subject of intense study as it is implicated as a key mediator of a wide variety of cellular inflammatory responses.^[91] Although NF- κ B activation has also been linked to the development of cancer, a cationic sequence limited to the protein transduction domain and mediating nuclear membrane translocation was employed.^[92] These sequences have the added advantage of directing the attached molecule to the nucleus, which is the site of action for numerous chemotherapy agents. NF- κ B has been investigated for entry into various cancer cell lines. Its labelled version demonstrated rapid accumulation within cells and therefore shown the ability of this sequence to import linked cargo.^[73]

Ragin and co workers investigated a series of NLS sequence peptides (Figure 1.18, Table 1) for entry into different cancer cell lines by flow cytometry and confocal microscopy, which included SV-40 and NF- κ B conjugated to fluorescein.^[73] All NLS peptides demonstrated rapid accumulation within cells when added to the media of MCF-7 (breast carcinoma) cells, as shown by flow cytometry in Figure 1.18A. To determine if cellular uptake of the NLS peptides could be extended beyond the MCF-7 cell line, four other cancerous cell types (KB, nasopharyngeal; HT29, colon; MIAPACA2, pancreatic; PC3, prostate) were evaluated. Cellular fluorescence was observed with all cell lines, demonstrating their broad capacity for cellular uptake (Figure 1.18 B).

Table 1. Fluorescent Nuclear Localization Signal Sequences Used for Cellular Uptake Experiments	
Fluorescent Peptides	Sequence
FI-NF- κ B	FI-VQRKRQKLMP-NH ₂
FI-TFIIE- β	FI-SKKKKTKV-NH ₂
FI-OCT-6	FI-GRKKKKRT-NH ₂
FI-TCF1- α	FI-GKKKKKKREKL-NH ₂
FI-SV40	FI-PKKKKRKV-NH ₂
FI-HATF3	FI-ERKKRRRE-NH ₂
FI-C.e. SDC3	FI-FKKFRKF-NH ₂

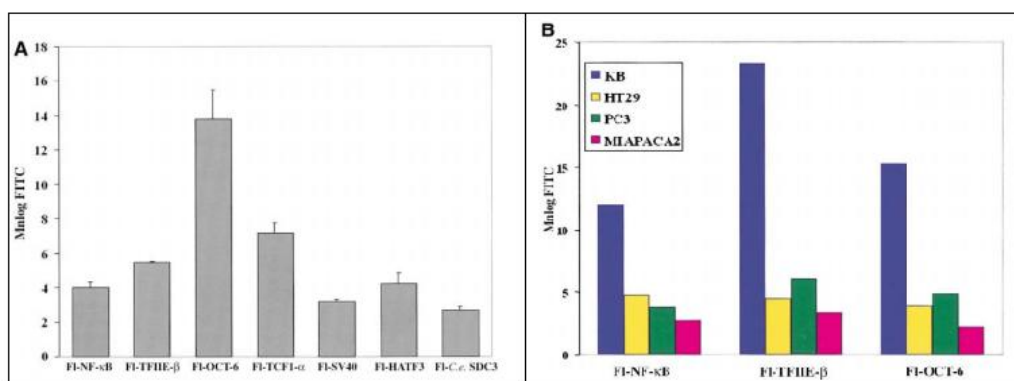


Figure 1.18 Table 1 Fluorescent nuclear localisation signal sequences used for cellular uptake experiments. (A) Uptake of fluorescently labelled NLS sequences (50 μ M) with the MCF-7 (breast carcinoma) cell line after 4 hr as measured by flow cytometry. (B) Uptake of the fluorescently labelled NLS sequences FI-NF- κ B, FI-TFIIE- β , and FI-Oct-6 (50 μ M) with four other cancerous cell types—KB (nasopharyngeal), HT29 (colon), MIAPACA2 (pancreatic), and PC3 (prostate)—after 4 hr as measured by flow cytometry.^[73]

The cellular location of a subset of the NLS peptides FI-NF- κ B, FI-Oct-6, and FI-TFIIE- β , was evaluated by confocal microscopy, where FI is fluorescein and the peptide sequences of NF- κ B, Oct-6, and TFIIE- β are given in Figure 1.18. FI-NF- κ B was distributed in both the cytosol and the nucleus, showing greatest accumulation observed within nucleoli, whereas the other two sequences were located almost exclusively in the cytoplasm. FI-Oct-6,

and Fl-TFIIE- β are highly cationic and they may tightly associate with negatively charged membrane lipids, preventing their release into the cytoplasm and subsequent routing to the nucleus. However, the NF- κ B NLS sequence is able to escape from, or is never within, a similar endosomal compartment, possibly pointing to a unique mode of cellular uptake for NF- κ B.

Ragain *et al* also exploited the membrane-translocating property of the NLS of NF- κ B to deliver covalently linked cargoes across the plasma membrane of MCF-7 cells. A fluorescein labelled, 10-mer oligonucleotide (5'-GCCTCTAGCT-3) derived from the Kras oncogene was covalently linked to the NLS of NF- κ B via a disulfide linkage. Without the attached NLS sequence, the oligonucleotide demonstrated no tendency to enter MCF-7 cells (Figure 1.19 B2), whereas cellular uptake of the Fl-DNA-NF- κ B conjugate was observed and found to increase with increasing concentration of the conjugate as shown by flow cytometry analysis (Figure 1.19). Confocal microscopy images established the presence of the oligonucleotide within the cells, and revealed that the conjugate had accumulated in the cytoplasm (Figure 1.19 B4). The NF- κ B sequence was also assessed for transduction of the protein lysozyme. Flow cytometry analysis revealed a 25-fold increase in cellular uptake of lysozyme when conjugated to the NF- κ B NLS sequence.

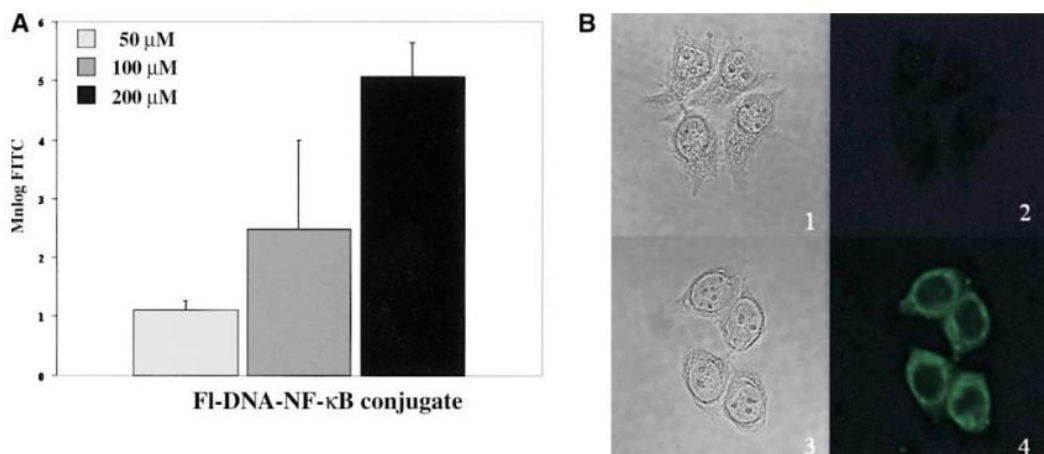


Figure 1.19 Cellular Uptake of the Fl-DNA-NF- κ B Conjugate with MCF-7 Cells

(A) Cellular uptake as a function of concentration of the Fl-DNA-NF- κ B conjugate with MCF-7 cells. (B) Cellular localization was determined by confocal microscopy: (1) transmitted light image and (2) fluorescence image for cells treated with Fl-DNA (50 μ M) for 4 hr; (3) transmitted light image and (4) fluorescence image for cells treated with Fl-DNA-NF- κ B (50 μ M) for 4 hr.^[73]

Another important membrane enclosed organelle of a eukaryotic cell is the mitochondria. Certain disease are caused by mutations in mitochondrial DNA^[93] and it also has been reported that the mitochondria are key regulators of programmed cell death by apoptosis.^[94] There are multiple diseases including cancer, diabetes, some cardiovascular and neurodegenerative diseases that have a considerable mitochondrial element. The design and development of drugs specifically targeting mitochondria is consequently on the increase.^[95]

Antimicrobial peptides (AMPs) are short cationic peptides that are strongly membrane active. Some of these AMP can penetrate a cell without permanent damage of the membrane.^[96] This feature has made them attractive as transport vectors in the context of drug delivery and imaging agents. One such peptide is a well studied Magainin 2 (MG2), isolated from the skin of the African clawed frog *Xenopus laevis*.^[97] MG2 has been shown to accumulate fluorescent cargo probes in the mitochondria and nuclei.^[98] We used this peptide for our supramolecular assembly to target mitochondria organelle. The distinct membrane-permeabilizing processes of magainin 2 in bacterial and mammalian cells were visualized and characterized in detail for the first time by Matsuzaki *et al* in 2008.^[98] They wisely used unfixed cells as it has been noted that this process significantly alters the intracellular distribution of cationic peptides.^[99] Similarly the results presented in this thesis are on live cells.

Matsuzaki *et al* successfully permeabilised bacteria membranes with Magainin 2 attached to a fluorescent marker, TAMRA, a rhodamine based fluorophore Figure 1.20 (B). They also had Calcein, another fluorescent complex, present, however without the peptide present this did not penetrate the bacteria. When the peptide formed a pore in the bacteria membrane the Calcein entered also.

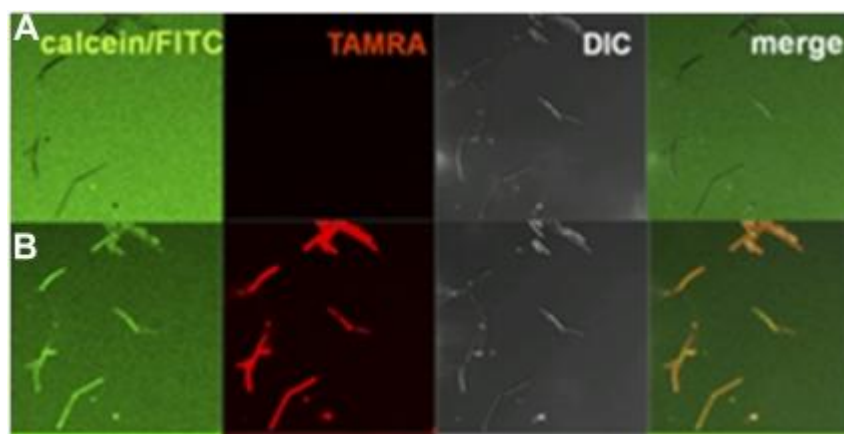


Figure 1.20 Permeabilization of membranes by Magainin 2 in *B. megaterium*. Cells in calcein solution before (A) and 68–70 s after (B) addition of Magainin 2-TAMRA at a final concentration of 10 μM (9.8/0.2 μM).^[98]

The permeabilization of plasma membranes of CHO-K1 cells by Magainin 2 was also examined, based on fluorescent molecules. Again before the addition of peptide, calcein was excluded from the cells (Figure 1.21(A)). The Magainin 2-TAMRA peptide also induced the influx of calcein through mammalian membranes. They also noted that the Magainin 2 peptide induced membrane budding during the process of membrane permeabilization, as shown by arrows in Figure 1.21.

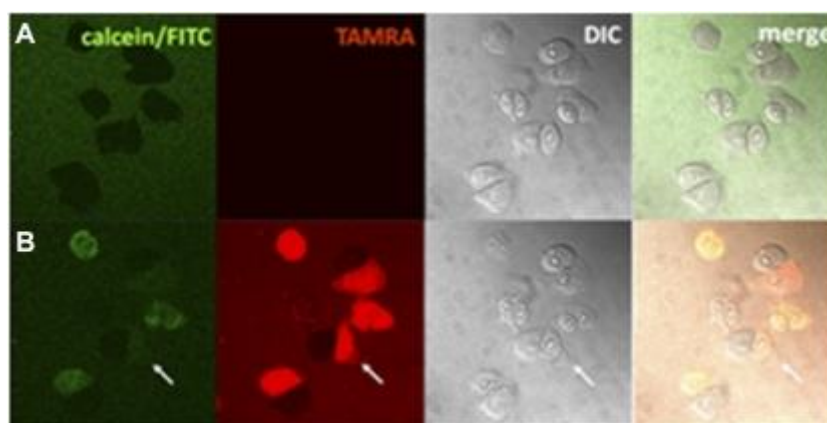


Figure 1.21 Permeabilization of membranes by Magainin-2 in CHO-K₁ cells. Cells (105 cells/mL, 63 \times) in calcein solution before (A) and 68–70 s after (B) addition of Magainin-2-TAMRA at a final concentration of 10 μM (9.8/0.2 μM). (B) Arrow indicates membrane budding.^[98]

Matsuzaki *et al* then investigated the localisation of the Magainin-2 peptide within mammalian cells. To determine the intracellular localization of the peptide, cells labelled with the mitochondria marker Mitotracker Green FM were treated with the TAMRA-

labelled peptide. The peptide was colocalized with the mitochondria marker (Figure 1.22). The TAMRA fluorescence was also observed in nuclei. Thus, the internalized peptide mainly accumulated in mitochondria and nuclei.

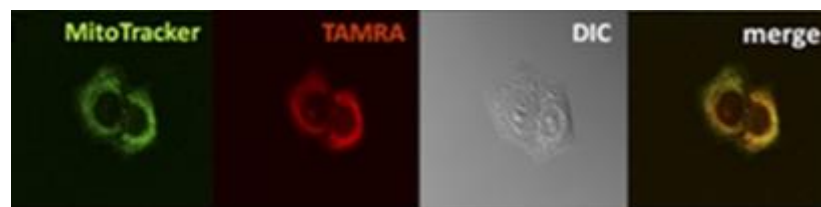


Figure 1.22 Permeabilization of membranes by Magainin-2 in CHO-K₁ cells. Cells with MitoTracker Green FM staining 70 s after addition of Magainin-2-TAMRA at a final concentration of 10 μ M (9.8/0.2 μ M). From left to right: MitoTracker, TAMRA, DIC, and merged images.^[98]

1.8.1 Targeting DNA

In the last few decades, coordination complexes based on d⁶ metal centres and polypyridyl ligand architectures been developed as structure- and site-specific reversible DNA binding agents.^[100] The focus of this research is on ruthenium(II) centres due to their appealing photophysical properties. The attention has turned to the use of these complexes in biological contexts and numerous applications ranging from imaging to therapeutics are coming to light with the increase in understanding of the cellular uptake and cellular localisation of such systems. Ruthenium(II) polypyridyl complexes and DNA have been investigated heavily from structural probes to cellular imaging and therapeutics.^[100]

DNA, or deoxyribonucleic acid, is the hereditary material in all known living organisms. Most DNA is located in the cell nucleus (nuclear DNA), but a small amount of DNA can also be found in the mitochondria (mitochondrial DNA or mtDNA). The information in DNA is stored as a code made up of four chemical bases: adenine (A), guanine (G), cytosine (C), and thymine (T). DNA bases pair up with each other, A with T and C with G, to form units called base pairs. Each base is also attached by a glycosidic bond to a sugar molecule. The sugar molecule is attached to a phosphate molecule by a phosphodiester bond. Together, a base, sugar, and phosphate are called a nucleotide. Nucleotides are arranged in two long polymers that form a double helix.

Nuclear DNA (nDNA) exists as chromatin during non-replicative stages of the cell cycle and is compacted into combined structures known as chromosomes during cell division. DNA is highly compacted and wound up around bead-like proteins called histones during both states. DNA can be damaged by either normal metabolic processes inside the cell or environmental factors. DNA can repair itself through a set of processes by which the cell identifies and corrects damage to DNA molecules.

DNA damage can be subdivided into two main types, endogenous damage and exogenous damage. Endogenous damage can occur from normal metabolic pathways by-products such as reactive oxygen species. Exogenous damage occurs from an external source such as radiation, ultraviolet, X- and gamma-rays, toxins and viruses.

DNA damage plays a major role in mutagenesis, carcinogenesis and ageing. A detailed understanding of the types and frequency of endogenous DNA damage can be considered crucial for an understanding of the interaction of exogenous agents and influences with endogenous processes in the stimulation of cancer and other diseases.^[101] Endogenous DNA damage occurs at a high occurrence compared with exogenous damage. The types of damage produced by normal cellular processes are related to those caused by some environmental agents.^[102] The frequency of cancer and other diseases might be significantly reduced if an approach could be developed leading to a decrease in endogenous DNA damage and endogenous mutations. Endogenous DNA damage occurs via numerous reactive oxygen species and products generated as a consequence of endogenous reactive chemicals and chemical DNA instability.

1.8.1.1 Reactive Oxygen Species

Reactive oxygen species (ROS) are chemically reactive molecules containing oxygen. ROS are highly reactive due to the presence of unpaired valence shell electrons. ROS are generated in our body by various systems involving both endogenous and environmental factors as seen in Figure 1.23.

During times of environmental stress (*e.g.*, UV or heat exposure), ROS levels can increase dramatically. This may result in significant damage to cell structures, adversely alter lipids, proteins and DNA and have been implicated in aging and a number of human

diseases.^[103] Damage caused to DNA, can result in mutagenesis and carcinogenesis. Cumulatively, this is known as oxidative stress.

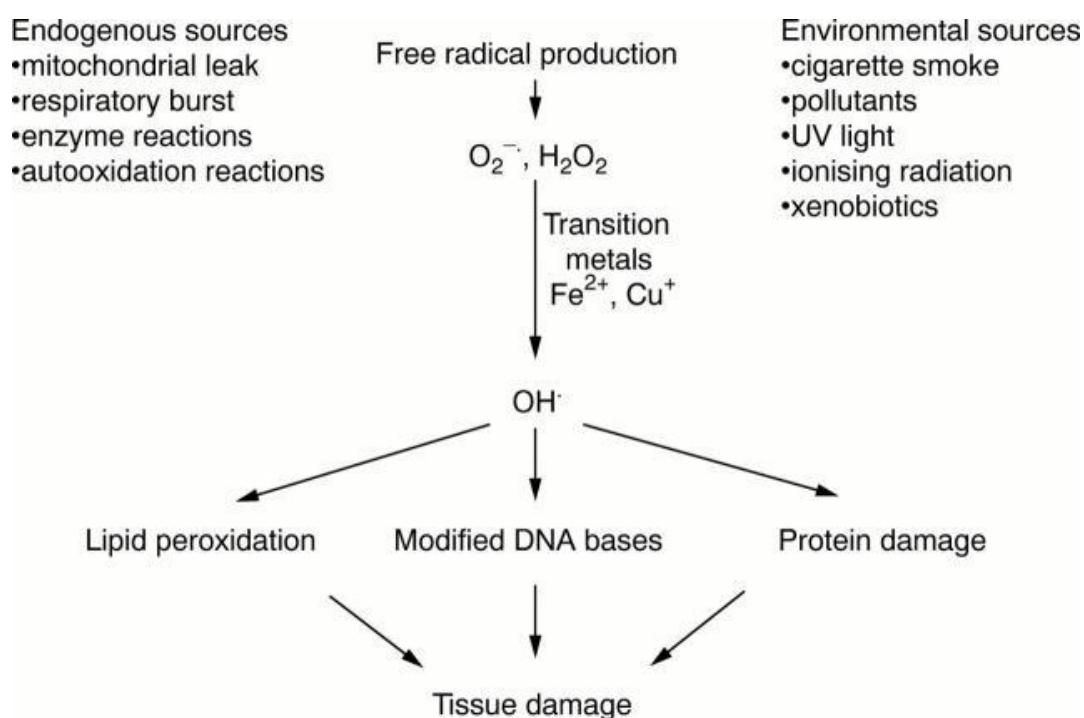


Figure 1.23 Major sources of free radicals in the body and the consequences of free radical damage.^[103]

Oxidative stress is caused by an imbalance between the production of reactive oxygen species (ROS) and a biological system's capability to readily detoxify the reactive intermediates or to repair the consequential damage. Oxidative stress, arising as a result of an imbalance between free radical production and antioxidant defences, is associated with damage to a wide range of molecular species including lipids, proteins, and cellular macromolecules such as nucleic acids and proteins.^[104]

The initial players in the defence against the destructive effects of ROS are a variety of antioxidants. Upon oxidative stress the ratio of oxidants to antioxidants rises. One of the most dramatic consequences of oxidative stress is the development of DNA lesions, which might result in genomic instability and can lead to various diseases.^[105-107] The cellular response to oxidative damage involves numerous processes, such as DNA repair, cell cycle arrest and apoptosis, while irreversible mutations contribute to oncogenesis.^[108]

Cellular DNA is constantly in danger of oxidation from a host of sources.^[101, 102, 107] Reactive oxygen species (ROS) constantly attack DNA. One of the best-characterized

oxidative DNA lesions is 7,8-dihydro-8-oxoguanine (8-oxo-G). Many human diseases, such as cancer and neurodegenerative disorders, have been correlated with oxidative DNA damage.^[105]

It is essential to use a wide diversity of chemical and biological tools to advance our understanding of the chemical mechanisms underlying oxidative damage as well as the biological factors affecting the frequency, detection and repair of such damage. Optical probes for cellular imaging are important in understanding the structure and function of biological systems. Transition metal complexes have enormous potential as diagnostic and therapeutic agents. Ruthenium complexes are known to show environmental sensitivity. Their photophysical properties can exhibit a light switch effect, making them highly luminescent in hydrophobic surroundings such as inside stacks of DNA bases or lipid membrane bilayers, whereas in aqueous solutions the emission is strongly quenched.^[109, 110]

Their characteristic photophysical properties as outlined previously, including long lived excited metal to ligand charge transfer state and red emission wavelengths, make them ideal candidates for cellular imaging using confocal microscopy. Recently, the DNA binding properties of mono- and binuclear ruthenium complexes have been heavily investigated.^[109-112] In this thesis we target our ruthenium complexes to specific organelles with the aim to increase the understanding of the cellular uptake and cellular localisation of such systems.

1.9 Apoptosis

Cells die in reaction to a range of stimuli and they do so in a controlled, regulated fashion. These stimuli may originate either extracellularly or intracellularly. Necrosis, caused by external stimuli, occurs following a cell's encounter with harmful events such as hypoxia, toxins, and bacterial or viral infection. Resulting damage ultimately causes the cell to swell and lyse, or rupture. Some extracellular signals, such as toxins,^[113] must cross the plasma membrane to effect a response.

Intracellular apoptotic signalling can also occur in response to a stress from within the cell. Apoptosis is a normal cellular process and is essential for the proper development and maintenance of the organism; it is also often called programmed cell death.^[114] The apoptotic pathway is triggered that leads to the destruction of the cell by a characteristic set of reactions that require energy. The cascade of events that causes apoptosis is controlled

genetically by the cell, does not cause swelling, and completely removes the cell from the tissue or the body. Unique transformations occur in the cell once it has received precise signals instructing it to undergo apoptosis. The end result of apoptosis is cell death without inflammation of the surrounding tissue. Flawed apoptotic processes have been implicated in a widespread array of diseases. Excessive apoptosis causes atrophy, whereas an inadequate amount results in uncontrolled cell proliferation, such as cancer.

Apoptosis is necessary for the elimination of cells deemed a threat, for example cells infected with viruses such as AIDS, cells with DNA damage and cancerous cells. Abnormal regulation of apoptosis has been implicated in a number of human diseases including cancer, autoimmune diseases, viral infections, neurodegenerative diseases, AIDS and cardiovascular diseases.^[115] Apoptotic failure has been associated with cancer's resistance towards chemo- or radio-therapy.^[116] There has been recent discovery of molecular pathways that govern apoptosis and clinical studies now focus on connections among apoptosis, disease, and new therapeutic modalities. These have driven the design of peptides that in some cases can function as simplified versions of their parent pro- or anti-apoptotic proteins.^[117] These molecules are contributing to a better understanding of the activity and regulation of apoptotic proteins and setting the scene for the discovery of effective drugs to combat important diseases related to apoptosis.

1.9.1 Caspase

Since the idea of apoptosis was established in 1972^[114], research efforts have led to the recognition of hundreds of genes that control the initiation, execution and regulation of apoptosis. A family of proteins known as caspases are typically activated in the early stages of apoptosis. Caspases are the essential component of the apoptotic process and they irreversibly commit a cell to die. These proteins break down or cleave key cellular components that are required for normal cellular function.^[114] Three major pathways of apoptosis, associated with caspase activation, have been identified in mammals (Figure 1.24): the extrinsic or death receptor pathway, the intrinsic or apoptosome pathway and the cytotoxic lymphocyte-initiated granzyme B pathway.^[118]

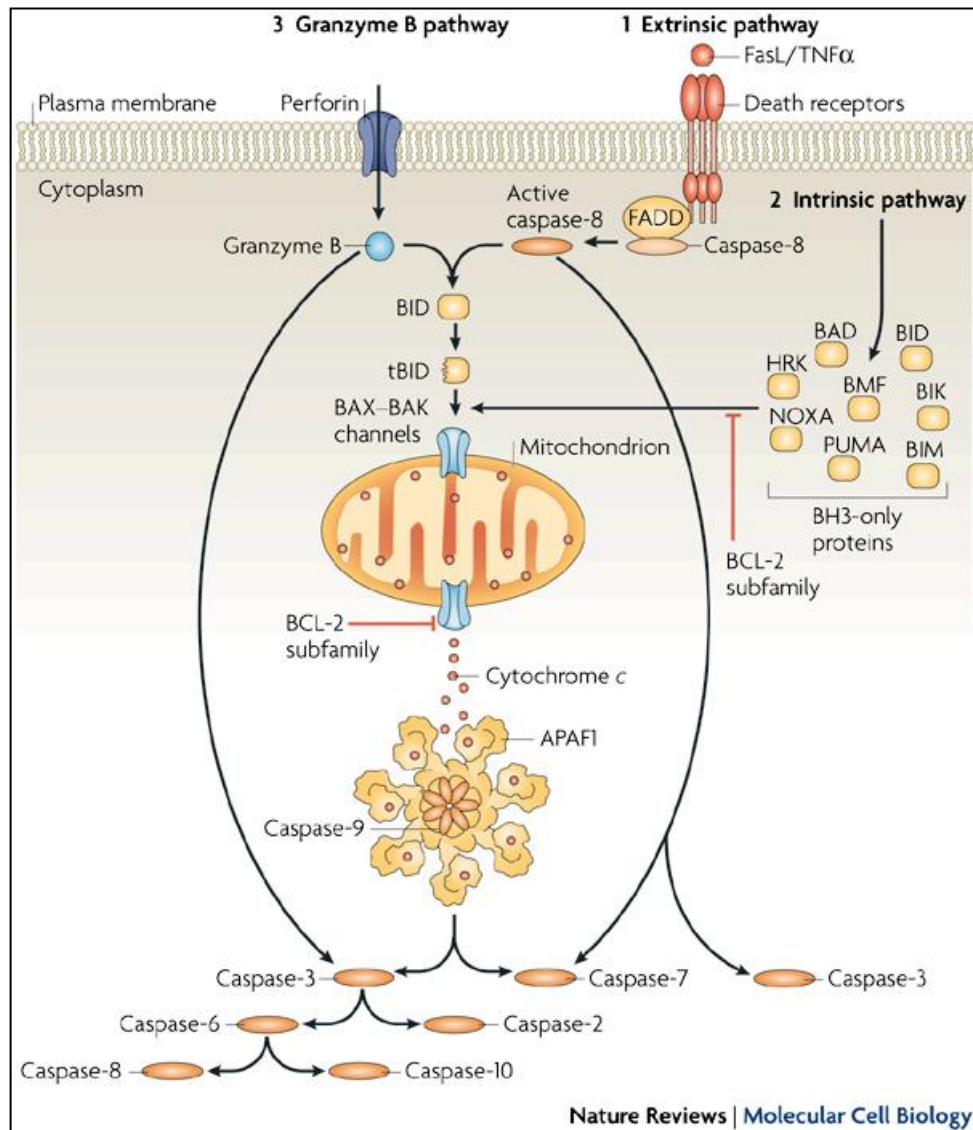


Figure 1.24 Caspase activation pathways. 1. The extrinsic or death receptor pathway, 2. The intrinsic or apoptosome pathway. 3. The cytotoxic lymphocyte-initiated granzyme B pathway^[118]

The intrinsic pathway is triggered in response to a broad range of death stimuli that are generated from within the cell, such as DNA damage. The inactivation of this pathway is normally regarded as a trademark of cancer.^[119] The intrinsic pathway is mediated by mitochondria, and, in reply to apoptotic stimuli, numerous proteins are released from the intermembrane space of mitochondria into the cytoplasm.^[120] One such protein and possibly the most fascinating one of these pro-apoptotic proteins is cytochrome c, which binds to and activates the protein APAF1 in the cytoplasm, eventually leading to a cascade of caspase activation.^[121] The extrinsic pathway is initiated by the binding of an extracellular death ligand to its cell-surface death receptor. The extrinsic pathway can crosstalk to the intrinsic

pathway through the caspase- 8-mediated cleavage of BID (a BH3-ONLY member of the Bcl-2 family of proteins) which then triggers the release of mitochondrial proteins.^[122, 123]

1.9.2 Role of B-cell lymphoma-2 (Bcl-2) proteins

The Bcl-2 family of proteins is involved in the response to apoptosis through their ability to regulate mitochondrial cytochrome c release. Bcl-2 proteins regulate the extrinsic and intrinsic pathway of apoptosis which converge at the mitochondria (Figure 1.24).^[124] The Bcl-2 family comprises of both anti- and pro-apoptotic molecules and these are broken down into 3 sub-families based on their homology domains and function (Figure 1.25).

The pro-apoptotic BAX-like subfamily share sequence homology at BH1, BH2 and BH3 but lacks BH4 domains and promotes apoptosis by forming pores at the mitochondrial outer membrane. When these members are activated the change from monomers to oligomers and these then disrupt the integrity of the outer mitochondrial membrane, a process called mitochondrial outer membrane permibilisation (MOMP), realising components such as cytochrome c, initiating apoptosis.

The BH3-only sub-family of proteins, all of which are pro-apoptotic, contains structurally diverse members that only display homology within the BH3 domain. ^[118, 125, 126] These proteins can sense cell damage and interact with pro-apoptotic members such as Bax/Bak causing them to oligomerise. The BH3-only proteins are either absent or inactive in a normal cell not undergoing stress. These proteins are involved in both the sensing and activation stages of apoptosis.

The anti-apoptotic sub-family comprises proteins such as Bcl-2, Bcl-xL and Bcl-w, which share sequence homology particularly within four regions, BH1 through BH4 (Figure 1.25).^[126] Most members of this subfamily also contain transmembrane domains (TM) and are therefore typically associated with cell membranes. These work by inhibiting the effects of the BH-3 only proteins after apoptosis is initiated as well as inhibiting the oligomerisation of activated pro-apoptotic members.

Abnormal gene expression of some Bcl-2 family members that inhibits cell death contributes to the resistance of tumour cells to conventional therapies by interfering with a large variety of apoptotic stimuli, including chemotherapeutic agents.^[127-130] Recent studies have shown that the functional blockade of Bcl-2 or Bcl-X_L restored the apoptotic process in

tumour cells^[131] and also reduced the resistance to chemo- and radiotherapies that some tumours possessed.^[132, 133]

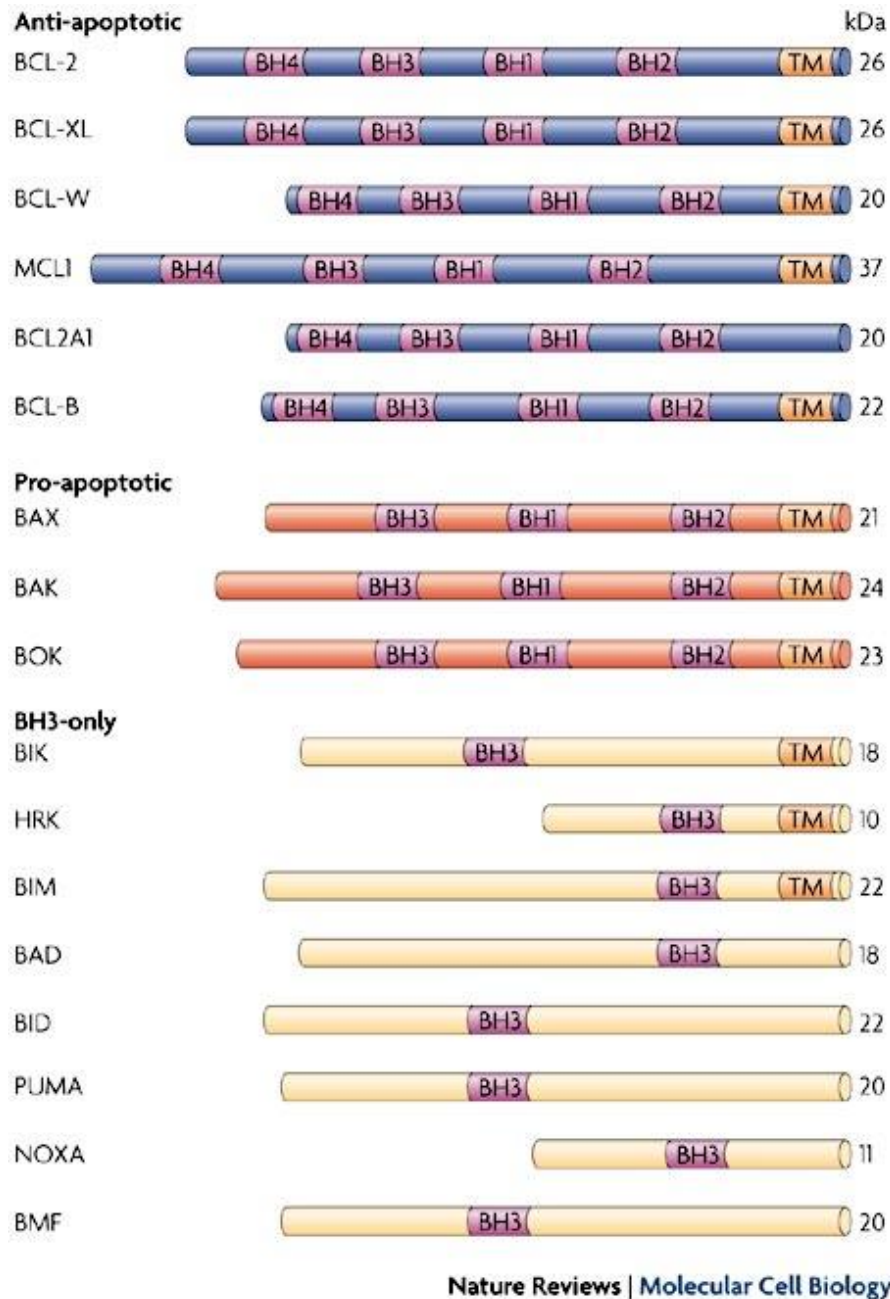


Figure 1.25 The Bcl-2 family comprises of anti- and pro-apoptotic molecules and are broken down into 3 sub-families based on their homology and function.^[118]

1.9.3 BH-3 only proteins

The mammalian BH3-only protein family currently comprises eight members (BID, BAD, BIM, BIK, BMF, NOXA, PUMA and HRK), all of which have pro-apoptotic activity when over-expressed (Figure1.26).^[118] Apart from the BH3 homology domain, these proteins share little sequence similarity and are regulated in distinct ways. BH3 proteins use their BH3 domain to interact with other proteins when exerting their pro-apoptotic activity and because of this, the BH3 proteins are thought to be death ligands and their targets can be categorised as death receptors.^[134]

1	2	3	4	5	6	7	8	9	10	11	12	13	14	15	16	17	18	19	20	21	22	23	24	25	26		
h1								h2				h3				h4									Targets		
D	M	R	P	E	I	W	I	A	Q	E	L	R	R	I	G	D	E	F	N	A	Y	Y	A	R	R	BIM	Promiscuous
E	E	Q	W	A	R	E	I	G	A	Q	L	R	R	M	A	D	D	L	N	A	Q	Y	E	R	R	PUMA	
H	R	A	E	V	Q	I	A	R	K	L	Q	C	I	A	D	Q	F	H	R	L	H	T	Q		mBMF	BCL-2, BCL-X _L , BCL-w	
N	L	W	A	A	Q	R	Y	G	R	E	L	R	R	M	S	D	E	F	V	D	S	F	K	K	G	BAD	
M	E	G	S	D	A	L	A	L	R	L	A	C	I	G	D	E	M	D	V	S	L	R	A	P	BIK	BCL-X _L , BCL-w, A1	
R	S	S	A	A	Q	L	T	A	A	R	L	K	A	I	G	D	E	L	H	Q	R	T	M	W	R	HRK	
Q	E	D	I	I	R	N	I	A	R	H	L	A	Q	V	G	D	S	M	D	R	S	I	P	P	G	BID	
P	A	E	L	E	V	E	C	A	T	Q	L	R	R	F	G	D	K	L	N	F	R	Q	K	L	L	NOXA	MCL1, A1
P	A	E	L	E	V	E	C	A	T	Q	L	R	R	I	G	D	E	L	N	F	R	Q	K	L	L	NOXA m3	not BCL-2
D	M	R	P	E	I	W	I	A	Q	E	A	R	R	I	G	D	E	A	N	A	Y	Y	A	R	R	BIM2A	MCL1

Nature Reviews | Drug Discovery

Nature Reviews | Drug Discovery

Figure1.26 BH3 domain sequences of BH3 only proteins and their pro-survival protein binding targets.^[135]

1.9.4 BH3 interacting death agonist (BID)

The BID protein is a pro-apoptotic member of the Bcl-2 family that contains only the BH3 homology domain (Figure1.27). BID is found in the cytosol of cell and at membrane locations. BID can stimulate apoptosis by activating BAX to trigger mitochondrial apoptosis.^[136] Activated BAX polymerises and induces permeabilization of the outer mitochondrial membrane, enabling released mitochondrial factors to activate

caspases, which in turn irreversibly implement the death program.^[137] The amino acid sequence of BID is shown in Figure 1.27.

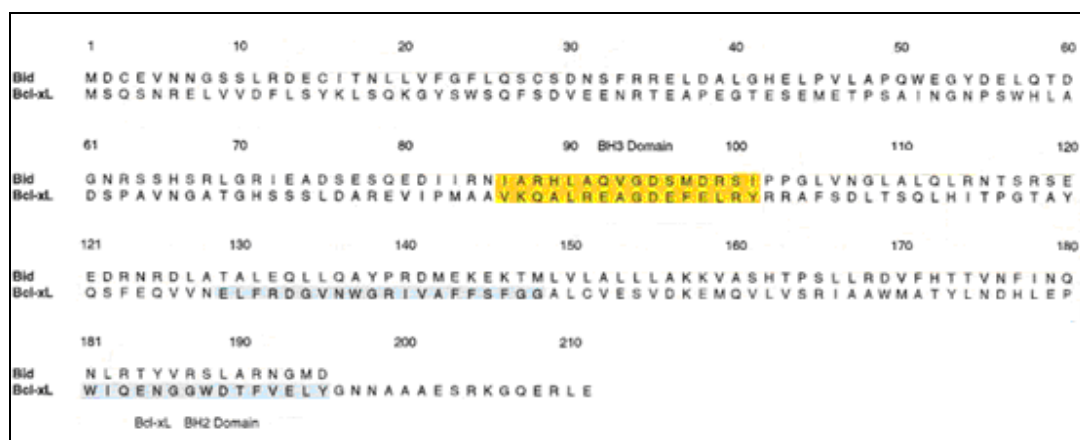


Figure 1.27 Amino acid sequences of BID and BCL-X_L Aligned at the BH3 Domains (Shaded in Yellow)^[138]

1.9.5 Synthetic Peptides and Organic molecules as probes for the investigation of the structure and function of members of the Bcl-2 family- Targeted therapy

The different domains found in the sequence of Bcl2 proteins have inspired the design and synthesis of a number of small organic molecules and active peptides.^[135, 139] Cell permeable synthetic peptides and small organic molecules targeted to a precise Bcl-2 family member can be utilised to control and modulate the function of that particular protein (Figure 1.28). They are also the preferred leads for development of tumour selective anti cancer drugs, one reason being, that patient tailored cancer cell directed therapeutic approaches offer the potential to have fewer side effects.^[140, 141]

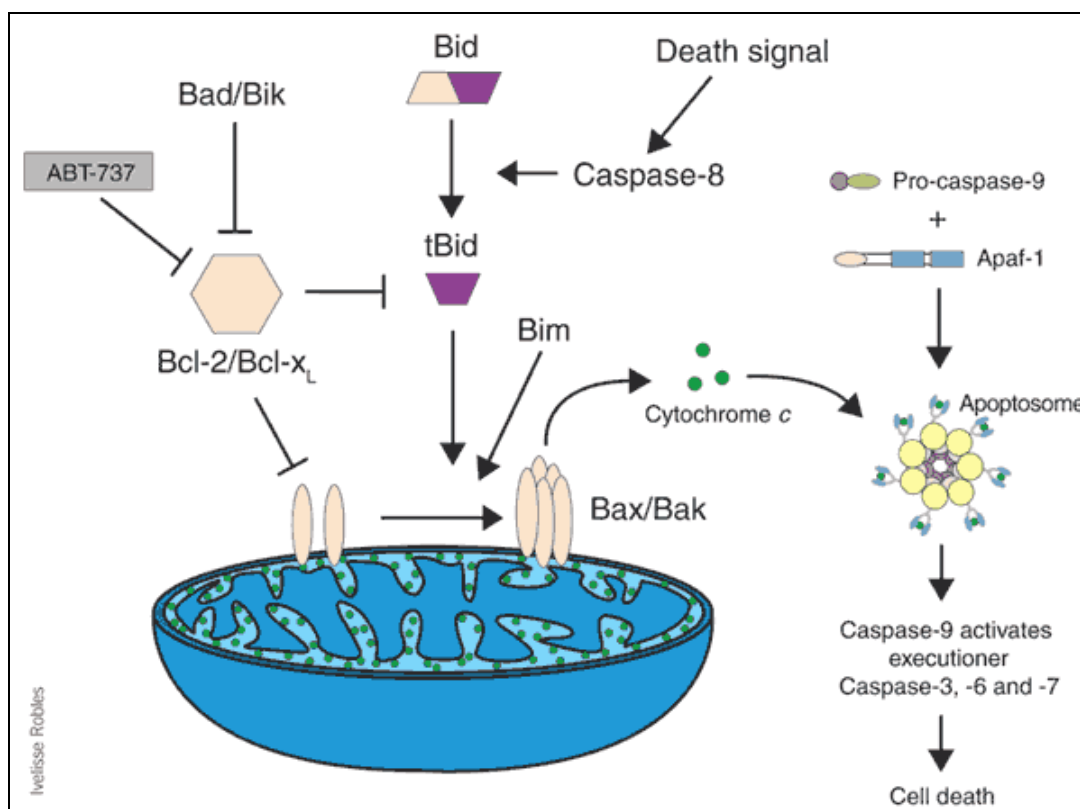


Figure 1.28 Cell permeable synthetic peptides (BID) and small organic molecules (ABT-737) targeted to a precise Bcl-2 family member can be utilised to control and modulate the function of that particular protein and lead to cell death.^[142]

1.9.6 BID peptides

One approach for studying and controlling the function of Bcl-2 family proteins is the use of synthetic peptides derived from the functional domains of pro-apoptotic and anti-apoptotic Bcl-2 members. In comparison with full-length proteins that may contain other domains, these peptides offer simplified models for functional and structural studies *in vitro* or in cell free systems.^[139, 143] This is a means of testing and identifying the functional sequences in BID, which may lead to therapeutic targets. Modification with cell permeable moieties would allow these peptides to be exploited to investigate mechanisms of Bcl-2 function in living cells.^[139, 144]

In this thesis, small fragments (overlapping peptides) of the BID protein will be synthesized to investigate the structure and function of this protein. These studies will include labelling of the peptide sequences with novel fluorescent probes, both metal complexes and by biotinylation as part of supramolecular assembly. As metal complexes can

photochemically generate active O₂ species, these peptide-label conjugates will also have the potential to promote apoptosis in tumour cells and may be implemented in the development of anticancer drugs.

Biotinylation is the procedure of covalently attaching biotin to a protein, nucleic acid or other molecule. Biotinylation is unlikely to disturb the natural function of the molecule due to the small size of biotin (MW = 244.31). Biotin binds to streptavidin and avidin with an extremely high affinity, fast on-rate, and high specificity, and these interactions are exploited in many areas of biotechnology to isolate biotinylated molecules of interest. Biotin-binding to streptavidin and avidin is resistant to extremes of heat, pH and proteolysis, making capture of biotinylated molecules possible in a wide variety of environments. Biotin binding proteins have the capacity to bind up to four biotin molecules, as shown in Figure 1.29, making this interaction ideal for both purification and detection strategies. For this thesis the BID sequence peptides were biotinylated to be used in protein binding studies.

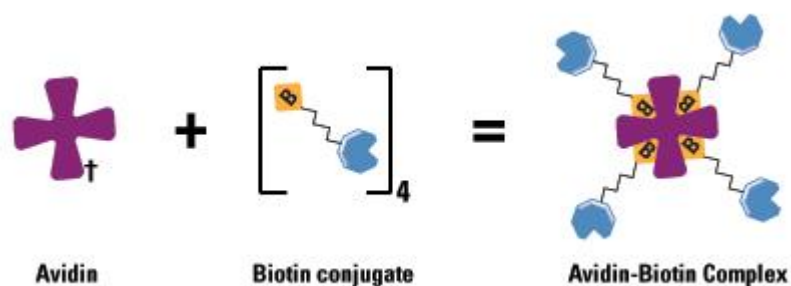


Figure 1.29 Schematic of the avidin-biotin interaction.^[145]

1.9.7 ABT-263

Small organic molecules can be used toward the investigation of the role of Bcl-2 in regulating apoptosis. These molecules offer advantages over peptide-based drugs in that they can easily be adapted for optimal stability, cell permeability, solubility and activity. Such low molecular weight compounds usually have high membrane permeability and thus can be used to study and control intracellular apoptotic signalling pathways. Such small organic molecules can either be discovered by random screening procedures or from natural products libraries or designed by computational methods that target certain functional sites of the Bcl-2 family. The three-dimensional structures of Bcl-X_L and more recently Bcl-2, as determined by X-ray crystallography and/ or NMR spectroscopy, provides the structural basis for the prediction of new inhibitors of these anti-apoptotic proteins.^{[146] [147]}

These X-ray crystallography and NMR spectroscopy studies have resulted in the identification of natural products which induce apoptosis in cells over-expressing Bcl-2 or Bcl-X_L.^[148, 149] Also by using these techniques other small molecule inhibitors such as HA14-1^[150] and the BH3I^[151] class of compounds, have been identified.

By means of structure activity relationships studies (SAR), performed by nuclear magnetic resonance spectroscopy (NMR), ligands were found that had high binding affinities for the hydrophobic groove of Bcl-X_L.^[152] From further studies of these lead compounds, a small organic molecule, ABT-737, was developed (Figure 1.30).^[153] This was shown to have a high affinity to Bcl-2 and Bcl-X_L, however ABT-737 fails the classified rules of drug likeness when it comes to molecular mass, number of hetero-atoms, functional groups and rotational bonds.^[154, 155]

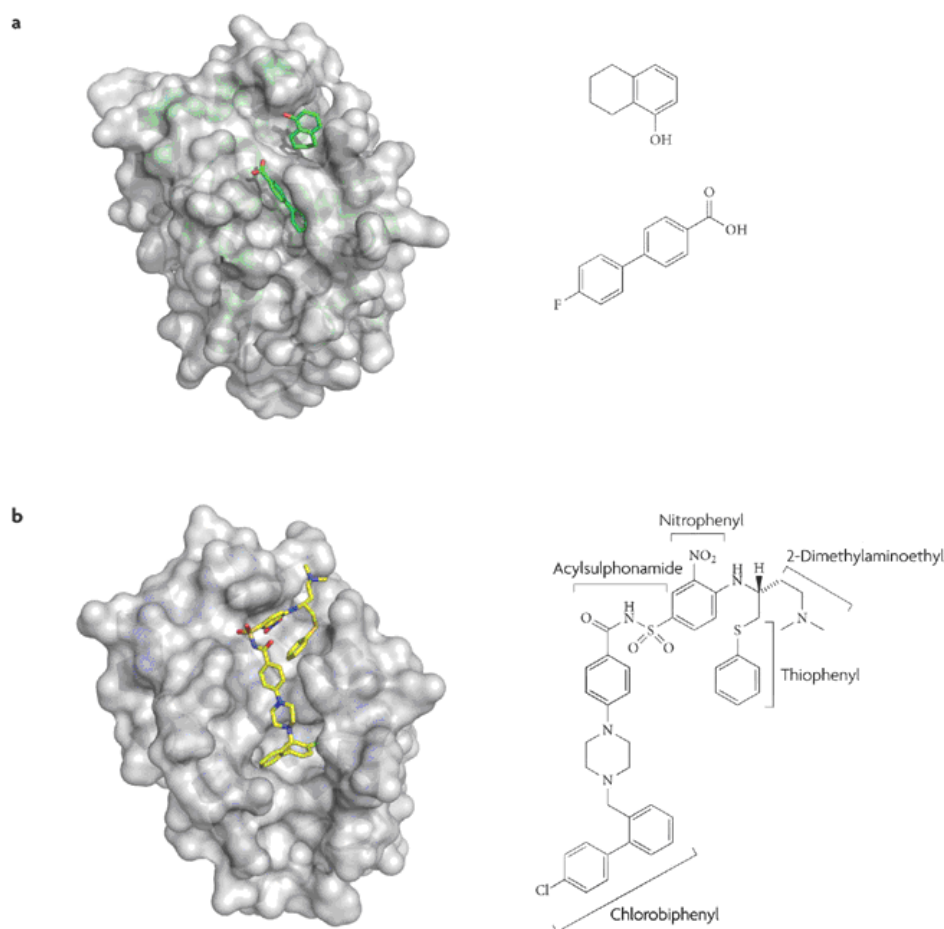


Figure 1.30 (a) Structure of BCL-X_L bound to fragments discovered by nuclear magnetic resonance. (b) BCL-X_L bound to ABT-737.^[135]

Major differences are observed in both potency and selectivity of the various small molecule Bcl-2 inhibitors for the different anti-apoptotic Bcl-2 proteins.^[150, 151, 153, 156-162] By far the most potent small molecule inhibitors described to date are the BAD-like BH3 mimetics, ABT-737 and its orally available analogue, ABT-263.^[163] These bind with very high affinity to Bcl-2, Bcl-X_L and Bcl-w but with much lower affinity to Mcl-1 or Bcl2A1.^[161, 164] The majority of detailed mechanistic studies on Bcl-2 inhibitors have been carried out using ABT-737.^[165] The development of an orally bioavailable Bcl-2 inhibitor, such as ABT-263, with the ability to inhibit specifically BH3-Bcl-2 protein-protein interactions at low nanomolar concentrations, potentially marks a significant development in cancer therapy.

Modifications to ABT-737 led to the discovery of ABT-263. ABT-263 retains its potency for Bcl-2 and BCL-X_L and its oral availability properties made it a clinical candidate. The binding capabilities of ABT-263 is reminiscent of the BH-3 only protein BAD. ABT-263 has had positive results as an active agent in cell based assays.^[161]

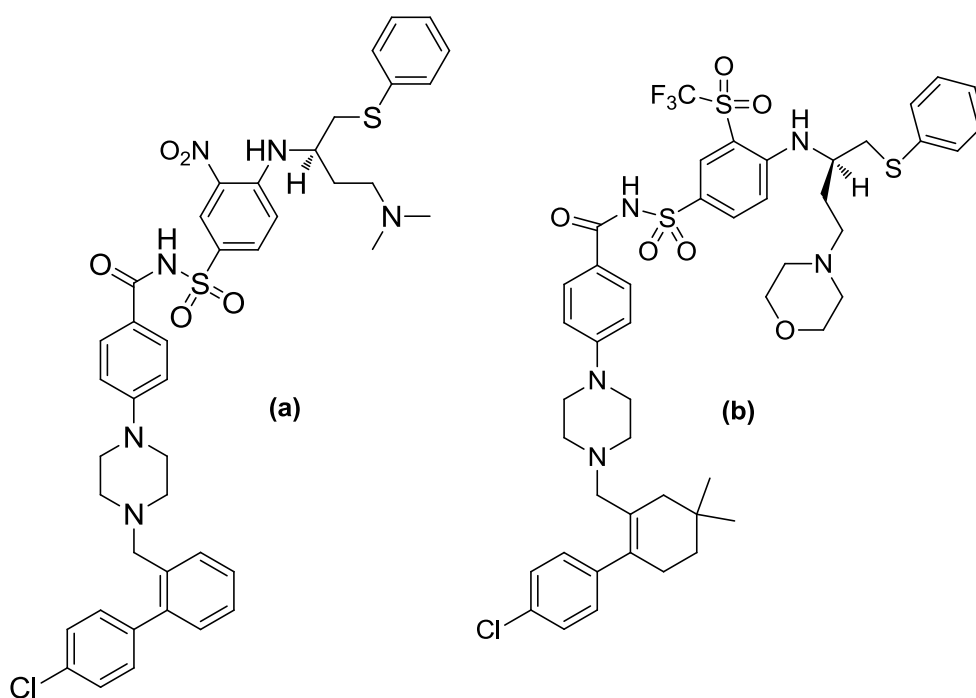


Figure 1.31 Structures of (a) ABT-737 and (b) ABT-263

With regards to this thesis, ABT-737 and ABT-263 (Figure 1.31) can be used as probes complementing the peptide-based probes developed to investigate apoptotic pathways.

1.10 Aims of the Project

Over the past number of years research into the potential applications of photoactive supramolecular assemblies has extended to many areas including very recently therapeutics and diagnostics. The use of these assemblies in live cell imaging is enabled by optical imaging methods such as of confocal microscopy and fluorescent chromophores. Inorganic chromophores have many advantages over their organic counterparts and are looking increasingly viable as alternative molecular probes. Not only do they have good photophysical features such as long lived, polarised luminescence, good photostability, they also have the capacity to make their photophysical properties dependent on their environment.

However in the past their weakness was their lack of uptake by the cell, but in recent times this has been overcome with cell penetrating peptides. As part of this research we looked at Ru (II) Chromophores and their conjugation to targeting peptides. Localisation of these chromophores can be used for diagnostic and therapeutic effects. A series of water soluble ruthenium (II) polypyridyl-peptide conjugates were synthesised and their spectroscopic and photophysical properties fully characterised and compared. Most of the assemblies detailed in this thesis are established by the supramolecular dyad system of A-L-B, where the features or applications of the assembly outweigh that of the individual components.

Successful conjugation of metal luminophores to peptides has been accomplished before by our group^[35, 39]; however, their specific localisation using targeting peptides is yet to be reported. It was anticipated that the use of localising peptides would further enhance the applications of the chromophores compared to existing transition metal-polypeptide conjugates which tend to localise in the cytoplasm. In Chapters 3 and 6, conjugation of ruthenium (II) to biomolecules builds upon previously reported work by our group and facilitates the analysis of biological samples through targeted localisation within a cell, but most crucially without damaging the cell membrane in the process. The production of reactive oxygen species following absorption of light energy by the transition metal luminophores may also induce cell apoptosis and could potentially make these a powerful

diagnostic agents photo-therapeutic tools. We investigated conjugation of both nuclear and mitochondria targeting assemblies.

Numerous reports highlight attempts to create targeted therapy for cancer treatment. Directed therapy blocks the growth of cancer cells by interfering with specific targeted molecules needed for carcinogenesis and tumour growth, rather than by simply interfering with rapidly dividing cells (*e.g.* traditional chemotherapy). Targeted cancer therapies are attractive as they may be more effective than current treatments and have less side-effects. The first step in targeted therapy is to identify and understand the protein-protein interactions within cells. By understanding the apoptotic pathway to induce cell death would be an attractive strategy in developing targeted therapy.

For this research we selected BH3 domain death agonist BID, a pro-apoptotic member of the Bcl2 family. BID can be fragmented into overlapping sequences of peptides for the investigation of the localisation and function properties of the parent protein by supramolecular assemblies. Conjugated to biotin allows for protein binding studies and conjugation to a Ru(II) chromophore could be used for cellular imaging.

The Abbott molecule ABT 737 is a small molecule designed to react with anti-apoptotic members. By attaching a chromophore to this molecule its cellular uptake and localisation can be investigated. This is in keeping with the general focus of research in constructing photoactive supramolecular assemblies based on biomolecules for applications in areas ranging from diagnostics to therapeutics.

One of the main aims of this thesis is to apply suitable luminophores to demonstrate how their conjugation to cell membrane transporters enables their applications in cellular imaging. Furthermore, the inherent properties of the dyes may then be exploited to determine characteristics such as pH and oxygen levels within cellular structures. This thesis presents an insight into the production of supramolecular assemblies from its individual subunit synthesis to their collective functional applications. It also gives an idea of the work presently being undertaken across a range of disciplines and will add to the understanding of the basic principles on which these luminophores may be exploited for their potential uses in photoactive supramolecular assemblies, diagnostics and therapeutics.

References

- [1] Minsky, M., (1961) Microscopy apparatus, United States Patent 3013467.
- [2] Amos, W. B.; White, J. G., *Biology of the cell / under the auspices of the European Cell Biology Organization*, (2003) **95**, 335.
- [3] van der Voort, H. T. M.; Brakenhoff, G. J.; Baarslag, M. W., *Journal of Microscopy*, (1989) **153**, 123.
- [4] Fung, D. C.; Theriot, J. A., *Curr Opin Microbiol*, (1998) **1**, 346.
- [5] Forster, R. J. K., T.E. Vos In, J.G., *Interfacial Supramolecular Assemblies*, Wiley: (2003).
- [6] LifeTechnologiesCorporation, Molecular Probes, In (2012).
- [7] Lee, S.; Park, K.; Kim, K.; Choi, K.; Kwon, I. C., *Chemical Communications*, (2008), 4250.
- [8] Ghoroghchian, P. P.; Therien, M. J.; Hammer, D. A., *Wiley Interdiscip Rev Nanomed Nanobiotechnol*, (2009) **1**, 156.
- [9] Tung, C. H., *Biopolymers*, (2004) **76**, 391.
- [10] Zhong, W., Urayama, P. and Mycek, M.A., *Journal of Physics D: Applied Physics*, (2003) **36**, 1689.
- [11] Johnson, I., *The Histochemical Journal*, (1998) **30**, 123.
- [12] Paul L, M.; Yu-Li Wang, D. L. T. a. K. W. J., (1988) Chapter 10 Incorporation of Macromolecules into Living Cells, in *Methods in Cell Biology*, Academic Press Vol. Volume 29, 153.
- [13] Juris, A.; Balzani, V.; Barigelletti, F.; Campagna, S.; Belser, P.; von Zelewsky, A., *Coordination Chemistry Reviews*, (1988) **84**, 85.
- [14] Steed, J. W.; Atwood, J. L., Molecular Devices, In *Supramolecular Chemistry*, John Wiley & Sons, Ltd: (2009); pp 707.
- [15] Balzani, V.; Bergamini, G.; Ceroni, P., *Coordination Chemistry Reviews*, (2008) **252**, 2456.
- [16] The Regents of the University of California, D., Electronic Spectroscopy: Theory, In (2011).
- [17] Suppan, P., Chapter 4 The Chemistry of Excited Molecules, In *Chemistry and Light*, The Royal Society of Chemistry: (1994); pp 87.
- [18] Steed, J. W.; Atwood, J. L., Supramolecular Polymers, Gels and Fibres, In *Supramolecular Chemistry*, John Wiley & Sons, Ltd: (2009); pp 861.
- [19] Deiters, E.; Song, B.; Chauvin, A. S.; Vandevyver, C. D.; Gumy, F.; Bunzli, J. C., *Chemistry*, (2009) **15**, 885.

- [20] Bunzli, J. C., *Acc Chem Res*, (2006) **39**, 53.
- [21] Pandya, S.; Yu, J.; Parker, D., *Dalton Trans*, (2006), 2757.
- [22] Keefe, M. H.; Benkstein, K. D.; Hupp, J. T., *Coordination Chemistry Reviews*, (2000) **205**, 201.
- [23] Otsuki, J.; Akasaka, T.; Araki, K., *Coordination Chemistry Reviews*, (2008) **252**, 32.
- [24] Yu, M.; Zhao, Q.; Shi, L.; Li, F.; Zhou, Z.; Yang, H.; Yi, T.; Huang, C., *Chem Commun (Camb)*, (2008), 2115.
- [25] Bernhard, S.; Barron, J. A.; Houston, P. L.; Abruna, H. D.; Ruglovksy, J. L.; Gao, X.; Malliaras, G. G., *J Am Chem Soc*, (2002) **124**, 13624.
- [26] Buda, M.; Kalyuzhny, G.; Bard, A. J., *J Am Chem Soc*, (2002) **124**, 6090.
- [27] Payne, S. J.; Fiore, G. L.; Fraser, C. L.; Demas, J. N., *Analytical chemistry*, (2010) **82**, 917.
- [28] Hsu, N. M.; Li, C. Y.; Yang, C. M.; Lin, T. S.; Hu, B. H.; Tingare, Y. S.; Chang, W. C.; Srivastava, G. K.; Li, W. R., *J Comb Chem*, (2009) **11**, 943.
- [29] Brooks, J.; Babayan, Y.; Lamansky, S.; Djurovich, P. I.; Tsyba, I.; Bau, R.; Thompson, M. E., *Inorg Chem*, (2002) **41**, 3055.
- [30] Mullice, L. A.; Pope, S. J. A., *Dalton Transactions*, (2010) **39**, 5908.
- [31] Lo, K. K.; Lee, T. K.; Lau, J. S.; Poon, W. L.; Cheng, S. H., *Inorg Chem*, (2008) **47**, 200.
- [32] Balzani, V.; Juris, A., *Coordination Chemistry Reviews*, (2001) **211**, 97.
- [33] Zhang, K. Y.; Lo, K. K., *Inorg Chem*, (2009) **48**, 6011.
- [34] Haas, K. L.; Franz, K. J., *Chem Rev*, (2009) **109**, 4921.
- [35] Cosgrave, L.; Devocelle, M.; Forster, R. J.; Keyes, T. E., *Chem Commun (Camb)*, (2010) **46**, 103.
- [36] Steed, J. W.; Atwood, J. L., *The Supramolecular Chemistry of Life*, In *Supramolecular Chemistry*, John Wiley & Sons, Ltd: (2009); pp 49.
- [37] Dixon, I. M.; Lebon, E.; Sutra, P.; Igau, A., *Chemical Society Reviews*, (2009) **38**, 1621.
- [38] Balzani, V.; Campagna, S.; Campagna, S.; Puntoriero, F.; Nastasi, F.; Bergamini, G.; Balzani, V., *Photochemistry and Photophysics of Coordination Compounds: Ruthenium*, In *Photochemistry and Photophysics of Coordination Compounds I*, Springer Berlin Heidelberg: (2007); Vol. 280, pp 117.
- [39] Dolan, C., Dublin City University Dublin, (2011), p 382.
- [40] Durham, B.; Caspar, J. V.; Nagle, J. K.; Meyer, T. J., *Journal of the American Chemical Society*, (1982) **104**, 4803.

- [41] Adeloye, A. O. O., T.O.; Adebayo, A.I.; Ajibade, P.A., *Int. J. Mol. Sci.*, (2012) **13**, 3511.
- [42] Terpetschnig, E.; Dattelbaum, J. D.; Szmecinski, H.; Lakowicz, J. R., *Analytical Biochemistry*, (1997) **251**, 241.
- [43] Hu, W.-S.; Pathak, V. K., *Pharmacological Review*, (2000) **52**, 493.
- [44] Waehler, R.; Russell, S. J.; Curiel, D. T., *Nat Rev Genet*, (2007) **8**, 573.
- [45] Chesnoy, S.; Huang, L., *Annual Review of Biophysics and Biomolecular Structure*, (2000) **29**, 27.
- [46] Zaric, V.; Weltin, D.; Erbacher, P.; Remy, J.-S.; Behr, J.-P.; Stephan, D., *The Journal of Gene Medicine*, (2004) **6**, 176.
- [47] Deshayes, S.; Morris, M. C.; Divita, G.; Heitz, F., *Cellular and Molecular Life Sciences*, (2005) **62**, 1839.
- [48] Sebbage, V., *Bioscience Horizon*, (2009) **2**, 64.
- [49] Stewart, K. M.; Horton, K. L.; Kelley, S. O., *Organic & Biomolecular Chemistry*, (2008) **6**, 2242.
- [50] Sharma, A.; Sharma, U. S., *International Journal of Pharmaceutics*, (1997) **154**, 123.
- [51] National Institute of Cancer, Centre of Cancer Research (2012) Liposomes [online], available : <http://ccr.cancer.gov/staff/gallery.aspx?profileid=6797> [accessed 15 December 2012]
- [52] Matthey, K. K.; Heath, T. D.; Papahadjopoulos, D., *Cancer Research*, (1984) **44**, 1880.
- [53] Kim JS, H. T., *Arch Pharm Res.*, (2000) **23**, 167.
- [54] Gabizon, A.; Tzemach, D.; Gorin, J.; Mak, L.; Amitay, Y.; Shmeeda, H.; Zalipsky, S., *Cancer Chemotherapy and Pharmacology*, (2012) **66**, 43.
- [55] Shmeeda, H.; Amitay, Y.; Gorin, J.; Tzemach, D.; Mak, L.; Ogorka, J.; Kumar, S.; Zhang, J. A.; Gabizon, A., *Journal of Controlled Release*, (2010) **146**, 76.
- [56] Lee, C. C.; Gillies, E. R.; Fox, M. E.; Guillaudeu, S. J.; Frachet, J. M. J.; Dy, E. E.; Szoka, F. C., *Proceedings of the National Academy of Science*, (2006) **103**, 16649.
- [57] Wolinsky, J. B.; Grinstaff, M. W., *Advanced Drug Delivery Reviews*, (2008) **60**, 1037.
- [58] Goff, S. P.; Berg, P., *Cell*, (1976) **9**, 695.
- [59] Thomas, C. E.; Ehrhardt, A.; Kay, M. A., *Nat Rev Genet*, (2003) **4**, 346.
- [60] Muller, R. H.; Mader, K.; Gohla, S., *European Journal of Pharmaceutics and Biopharmaceutics*, (2000) **50**, 161.

- [61] Mukherjee S, R. S., Thakur R S *Indian Journal of Pharmaceutical Sciences*, (2009) **71**, 349.
- [62] Yang, S. C.; Lu, L. F.; Cai, Y.; Zhu, J. B.; Liang, B. W.; Yang, C. Z., *Journal of Controlled Release*, (1999) **59**, 299.
- [63] A to Z Nanotechnology, Lipid Nanoparticles Used in Skin Care Cosmetics - Processes and Associated Benefits, (2012), available: <http://www.azonano.com/article.aspxArticleID=1245> [accessed 15 December 2012] .
- [64] Hauber, J., Perkins, A., Heimer, E.P., and Cullen, B.R., *Proc Natl Acad Sci U S A*, (1987) **84**, 6364.
- [65] Frankel, A. D.; Pabo, C. O., *Cell*, (1988) **55**, 1189.
- [66] Green, M.; Loewenstein, P. M., *Cell*, (1988) **55**, 1179.
- [67] Joliot, A.; Prochiantz, A., *Nat Cell Biol*, (2004) **6**, 189.
- [68] Madani, F.; Lindberg, S.; Langel, I.; Futaki, S.; Grslund, A., *Journal of Biophysics*, (2011)
- [69] Jarver, P.; Langel, U., *Biochimica et Biophysica Acta (BBA) - Biomembranes*, (2006) **1758**, 260.
- [70] Flewelling, R. F.; Hubbell, W. L., *Biophysical journal*, (1986) **49**, 541.
- [71] Liu, S.; Edwards, D. S., *Chemical Reviews*, (1999) **99**, 2235.
- [72] Mitchell, D. J.; Steinman, L.; Kim, D. T.; Fathman, C. G.; Rothbard, J. B., *The Journal of Peptide Research*, (2000) **56**, 318.
- [73] Ragin, A. D.; Morgan, R. A.; Chmielewski, J., *Chem Biol*, (2002) **9**, 943.
- [74] Trehin, R.; Merkle, H. P., *European Journal of Pharmaceutics and Biopharmaceutics*, (2004) **58**, 209.
- [75] Lebleu, B., Vives E., Brodin P., *J Biol Chem*, (1997) **272**, 16010.
- [76] Derossi, D.; Joliot, A. H.; Chassaing, G.; Prochiantz, A., *The Journal of Biological Chemistry*, (1994) **269**, 10444.
- [77] Jurek W, D., *Journal of Photochemistry and Photobiology B: Biology*, (2001) **65**, 136.
- [78] Neugebauer, U.; Pellegrin, Y.; Devocelle, M.; Forster, R. J.; Signac, W.; Moran, N.; Keyes, T. E., *Chemical Communications*, (2008), 5307.
- [79] Neugebauer, U.; Pellegrin, Y.; Devocelle, M.; Forster, R. J.; Signac, W.; Moran, N.; Keyes, T. E., *Chem Commun (Camb)*, (2008), 5307.
- [80] Puckett, C. A.; Barton, J. K., *Journal of the American Chemical Society*, (2009) **131**, 8738.
- [81] Puckett, C. A.; Barton, J. K., *Bioorganic & Medicinal Chemistry*, (2010) **18**, 3564.

- [82] Mahon, K. P.; Potocky, T. B.; Blair, D.; Roy, M. D.; Stewart, K. M.; Chiles, T. C.; Kelley, S. O., *Chemistry Biology*, (2007) **14**, 923.
- [83] Strebhardt, K.; Ullrich, A., *Nat Rev Cancer*, (2008) **8**, 473.
- [84] Cartier, R., Reszka R., *Gene Therapy*, (2002) **9**, 157.
- [85] Dickinson, B. C.; Srikun, D.; Chang, C. J., *Current Opinion in Chemical Biology*, (2010) **14**, 50.
- [86] Murphy, M. P.; Smith, R. A. J., *Advanced Drug Delivery Reviews*, (2000) **41**, 235.
- [87] Milletti, F., *Drug Discovery Today*, (2012) **17**, 850.
- [88] Shen, H.-M.; Tergaonkar, V., *Apoptosis*, (2009) **14**, 348.
- [89] Kalderon, D.; Roberts, B. L.; Richardson, W. D.; Smith, A. E., *Cell*, (1984) **39**, 499.
- [90] Fontes, M. R. M.; Teh, T.; Kobe, B., *Journal of Molecular Biology*, (2000) **297**, 1183.
- [91] Chen, L. F. G., W.C., *Nat Rev Mol Cell Biol*, (2004) **5**, 392.
- [92] Garg, A.; Aggarwal, B., *Leukemia*, (2002) **16**,
- [93] Wallace, D. C.; Singh, G.; Lott, M. T.; Hodge, J. A.; Schurr, T. G.; Lezza, A. M.; Elsas, L. J.; Nikoskelainen, E. K., *Science*, (1988) **242**, 1427.
- [94] Liu, X.; Kim, C. N.; Yang, J.; Jemmerson, R.; Wang, X., *Cell*, (1996) **86**, 147.
- [95] Armstrong, J. S., *British Journal of Pharmacology*, (2007) **151**, 1154.
- [96] Splith, K.; Neundorf, I., *European Biophysics Journal*, (2011) **40**, 387.
- [97] Zasloff, M., *Proc Natl Acad Sci U S A*, (1987) **84**, 5449.
- [98] Imura, Y.; Choda, N.; Matsuzaki, K., *Biophysical journal*, (2008) **95**, 5757.
- [99] Lundberg, M.; Johansson, M., *Biochem Biophys Res Commun*, (2002) **291**, 367.
- [100] Gill, M. R.; Thomas, J. A., *Chemical Society Reviews*, (2011) **41**, 3179.
- [101] De Bont, R.; van Larebeke, N., *Mutagenesis*, (2004) **19**, 169.
- [102] Jackson, A. L.; Loeb, L. A., *Mutation Research/Fundamental and Molecular Mechanisms of Mutagenesis*, (2001) **477**, 7.
- [103] Young, I. S.; Woodside, J. V., *Journal of clinical pathology*, (2001) **54**, 176.
- [104] McCord, J. M., *The American journal of medicine*, (2000) **108**, 652.
- [105] van Loon, B.; Markkanen, E.; Hubscher, U., *DNA Repair*, (2010) **9**, 604.

- [106] Maynard, S.; Schurman, S. H.; Harboe, C.; de Souza-Pinto, N. C.; Bohr, V. A., *Carcinogenesis*, (2009) **30**, 2.
- [107] Valko, M.; Rhodes, C. J.; Moncol, J.; Izakovic, M.; Mazur, M., *Chemico-Biological Interactions*, (2006) **160**, 1.
- [108] Khanna, K. K.; Jackson, S. P., *Nat Genet*, (2001) **27**, 247.
- [109] Friedman, A. E.; Chambron, J. C.; Sauvage, J. P.; Turro, N. J.; Barton, J. K., *Journal of the American Chemical Society*, (1990) **112**, 4960.
- [110] Matson, M.; Svensson, F. R.; Norden, B.; Lincoln, P., *The Journal of Physical Chemistry B*, (2011) **115**, 1706.
- [111] Ardhammar, M.; Lincoln, P.; Nordan, B., *The Journal of Physical Chemistry B*, (2001) **105**, 11363.
- [112] Svensson, F. R.; Abrahamsson, M.; Stroimberg, N.; Ewing, A. G.; Lincoln, P., *The Journal of Physical Chemistry Letters*, (2012) **2**, 397.
- [113] Popov, S. G.; Villasmil, R.; Bernardi, J.; Grene, E.; Cardwell, J.; Wu, A.; Alibek, D.; Bailey, C.; Alibek, K., *Biochemical and Biophysical Research Communications*, (2002) **293**, 349.
- [114] Kerr, J. F.; Wyllie, A. H.; Currie, A. R., *Br J Cancer*, (1972) **26**, 239.
- [115] Thompson, C. B., Apoptosis in the pathogenesis and treatment of disease, In (1995); Vol. 267, pp 1456.
- [116] Mendoza, F. J., Espino, P. S., Cann, K. L., Bristow, N., McCrea, K. and Los, M., *Arch Immunol Ther Exp*, (2005) **53**, 47.
- [117] Salgado, J.; García-Sáez, A. J.; Malet, G.; Mingarro, I.; Pérez-Payá, E., *Journal of Peptide Science*, (2002) **8**, 543.
- [118] Taylor, R. C.; Cullen, S. P.; Martin, S. J., *Nat Rev Mol Cell Biol*, (2008) **9**, 231.
- [119] Hanahan, D.; Weinberg, R. A., *Cell*, (2000) **100**, 57.
- [120] Wang, X., *Genes and Development*, (2001) **15**, 2922.
- [121] Li, P.; Nijhawan, D.; Budihardjo, I.; Srinivasula, S. M.; Ahmad, M.; Alnemri, E. S.; Wang, X., *Cell*, (1997) **91**, 479.
- [122] Luo, X.; Budihardjo, I.; Zou, H.; Slaughter, C.; Wang, X., *Cell*, (1998) **94**, 481.
- [123] Li, H.; Zhu, H.; Xu, C.-j.; Yuan, J., *Cell*, (1998) **94**, 491.
- [124] Kutuk, O.; Basaga, H., *Apoptosis*, (2006) **11**, 1661.
- [125] Salgado, J.; Garcia-Saez, A. J.; Malet, G.; Mingarro, I.; Perez-Paya, E., *J Pept Sci*, (2002) **8**, 543.
- [126] Tsujimoto, Y., *Genes to Cells*, (1998) **3**, 697.

- [127] Lotem, J.; Sachs, L., *Cell Growth Differ*, (1993) **4**, 41.
- [128] Miyashita, T.; Reed, J. C., *Blood*, (1993) **81**, 151.
- [129] Reed, J. C.; Miyashita, T.; Takayama, S.; Wang, H. G.; Sato, T.; Krajewski, S.; Aime-Sempe, C.; Bodrug, S.; Kitada, S.; Hanada, M., *J Cell Biochem*, (1996) **60**, 23.
- [130] Walton, M. I.; Whysong, D.; O'Connor, P. M.; Hockenbery, D.; Korsmeyer, S. J.; Kohn, K. W., *Cancer Research*, (1993) **53**, 1853.
- [131] Webb, A.; Cunningham, D.; Cotter, F.; Clarke, P. A.; di Stefano, F.; Ross, P.; Corbo, M.; Dziewanowska, Z., *Lancet*, (1997) **349**, 1137.
- [132] Piche, A.; Grim, J.; Rancourt, C.; Gomez-Navarro, J.; Reed, J. C.; Curiel, D. T., *Cancer Research*, (1998) **58**, 2134.
- [133] Jansen, B.; Schlagbauer-Wadl, H.; Brown, B. D.; Bryan, R. N.; van Elsas, A.; Muller, M.; Wolff, K.; Eichler, H. G.; Pehamberger, H., *Nature medicine*, (1998) **4**, 232.
- [134] Tsujimoto, Y., *Genes Cells*, (1998) **3**, 697.
- [135] Lessene, G.; Czabotar, P. E.; Colman, P. M., *Nat Rev Drug Discov*, (2008) **7**, 989.
- [136] Wang, K.; Yin, X. M.; Chao, D. T.; Milliman, C. L.; Korsmeyer, S. J., *Genes Dev*, (1996) **10**, 2859.
- [137] Walensky, L. D.; Pitter, K.; Morash, J.; Oh, K. J.; Barbuto, S.; Fisher, J.; Smith, E.; Verdine, G. L.; Korsmeyer, S. J., *Mol Cell*, (2006) **24**, 199.
- [138] Chou, J. J.; Li, H.; Salvesen, G. S.; Yuan, J.; Wagner, G., *Cell*, (1999) **96**, 615.
- [139] Liu, D.; Huang, Z., *Apoptosis*, (2001) **6**, 453.
- [140] Mendoza, F. J.; Espino, P. S.; Cann, K. L.; Bristow, N.; McCrea, K.; Los, M., *Arch Immunol Ther Exp (Warsz)*, (2005) **53**, 47.
- [141] Johar, D.; Roth, J. C.; Bay, G. H.; Walker, J. N.; Krocak, T. J.; Los, M., *Rocz Akad Med Bialymst*, (2004) **49**, 31.
- [142] Wagner, G., *Nat Chem Biol*, (2005) **1**, 8.
- [143] Shangary, S.; Johnson, D. E., *Biochemistry*, (2002) **41**, 9485.
- [144] Huang, Z., *Oncogene*, (2000) **19**, 6627.
- [145] Thermo Scientific, (2012) Avidin-Biotin Interactions, [online], available: <http://www.piercenet.com/browse.cfm?fldID=4A957146-5056-8A76-4E97-81995432210B> [accessed 15 December 2012]
- [146] Petros, A. M.; Medek, A.; Nettesheim, D. G.; Kim, D. H.; Yoon, H. S.; Swift, K.; Matayoshi, E. D.; Oltersdorf, T.; Fesik, S. W., *Proc Natl Acad Sci U S A*, (2001) **98**, 3012.
- [147] Muchmore, S. W.; Sattler, M.; Liang, H.; Meadows, R. P.; Harlan, J. E.; Yoon, H. S.; Nettesheim, D.; Chang, B. S.; Thompson, C. B.; Wong, S. L.; Ng, S. L.; Fesik, S. W., *Nature*, (1996) **381**, 335.

- [148] Nakashima, T.; Miura, M.; Hara, M., *Cancer Res*, (2000) **60**, 1229.
- [149] Tokutake, N.; Miyoshi, H.; Satoh, T.; Hatano, T.; Iwamura, H., *Biochim Biophys Acta*, (1994) **1185**, 271.
- [150] Wang, G.; Nikolovska-Coleska, Z.; Yang, C. Y.; Wang, R.; Tang, G.; Guo, J.; Shangary, S.; Qiu, S.; Gao, W.; Yang, D.; Meagher, J.; Stuckey, J.; Krajewski, K.; Jiang, S.; Roller, P. P.; Abaan, H. O.; Tomita, Y.; Wang, S., *J Med Chem*, (2006) **49**, 6139.
- [151] Degterev, A.; Lugovskoy, A.; Cardone, M.; Mulley, B.; Wagner, G.; Mitchison, T.; Yuan, J., *Nat Cell Biol*, (2001) **3**, 173.
- [152] Petros, A. M.; Dinges, J.; Augeri, D. J.; Baumeister, S. A.; Betebenner, D. A.; Bures, M. G.; Elmore, S. W.; Hajduk, P. J.; Joseph, M. K.; Landis, S. K.; Nettesheim, D. G.; Rosenberg, S. H.; Shen, W.; Thomas, S.; Wang, X.; Zanze, I.; Zhang, H.; Fesik, S. W., *J Med Chem*, (2006) **49**, 656.
- [153] Oltersdorf, T.; Elmore, S. W.; Shoemaker, A. R.; Armstrong, R. C.; Augeri, D. J.; Belli, B. A.; Bruncko, M.; Deckwerth, T. L.; Dinges, J.; Hajduk, P. J.; Joseph, M. K.; Kitada, S.; Korsmeyer, S. J.; Kunzer, A. R.; Letai, A.; Li, C.; Mitten, M. J.; Nettesheim, D. G.; Ng, S.; Nimmer, P. M.; O'Connor, J. M.; Oleksijew, A.; Petros, A. M.; Reed, J. C.; Shen, W.; Tahir, S. K.; Thompson, C. B.; Tomaselli, K. J.; Wang, B.; Wendt, M. D.; Zhang, H.; Fesik, S. W.; Rosenberg, S. H., *Nature*, (2005) **435**, 677.
- [154] Veber, D. F.; Johnson, S. R.; Cheng, H. Y.; Smith, B. R.; Ward, K. W.; Kopple, K. D., *J Med Chem*, (2002) **45**, 2615.
- [155] Lipinski, C. A.; Lombardo, F.; Dominy, B. W.; Feeney, P. J., *Adv Drug Deliv Rev*, (2001) **46**, 3.
- [156] Chan, S. L.; Lee, M. C.; Tan, K. O.; Yang, L. K.; Lee, A. S.; Flotow, H.; Fu, N. Y.; Butler, M. S.; Soejarto, D. D.; Buss, A. D.; Yu, V. C., *J Biol Chem*, (2003) **278**, 20453.
- [157] Becattini, B.; Kitada, S.; Leone, M.; Monosov, E.; Chandler, S.; Zhai, D.; Kipps, T. J.; Reed, J. C.; Pellecchia, M., *Chem Biol*, (2004) **11**, 389.
- [158] Kitada, S.; Leone, M.; Sareth, S.; Zhai, D.; Reed, J. C.; Pellecchia, M., *J Med Chem*, (2003) **46**, 4259.
- [159] Mohammad, R.; Giri, A.; Goustin, A. S., *Recent Pat Anticancer Drug Discov*, (2008) **3**, 20.
- [160] Nguyen, M.; Marcellus, R. C.; Roulston, A.; Watson, M.; Serfass, L.; Murthy Madiraju, S. R.; Goulet, D.; Viallet, J.; Belec, L.; Billot, X.; Acoca, S.; Purisima, E.; Wiegman, A.; Cluse, L.; Johnstone, R. W.; Beauparlant, P.; Shore, G. C., *Proc Natl Acad Sci U S A*, (2007) **104**, 19512.
- [161] Tse, C.; Shoemaker, A. R.; Adickes, J.; Anderson, M. G.; Chen, J.; Jin, S.; Johnson, E. F.; Marsh, K. C.; Mitten, M. J.; Nimmer, P.; Roberts, L.; Tahir, S. K.; Xiao, Y.; Yang, X.; Zhang, H.; Fesik, S.; Rosenberg, S. H.; Elmore, S. W., *Cancer Res*, (2008) **68**, 3421.
- [162] Tang, G.; Yang, C. Y.; Nikolovska-Coleska, Z.; Guo, J.; Qiu, S.; Wang, R.; Gao, W.; Wang, G.; Stuckey, J.; Krajewski, K.; Jiang, S.; Roller, P. P.; Wang, S., *J Med Chem*, (2007) **50**, 1723.

- [163] Zhang, L.; Ming, L.; Yu, J., *Drug Resist Updat*, (2007) **10**, 207.
- [164] Zhai, D.; Jin, C.; Satterthwait, A. C.; Reed, J. C., *Cell Death Differ*, (2006) **13**, 1419.
- [165] Vogler, M.; Dinsdale, D.; Dyer, M. J.; Cohen, G. M., *Cell Death Differ*, (2009) **16**, 360.

Chapter 2:

Experimental Methods and Instrumentation

2.0 Peptide Synthesis

Peptides are synthesized by coupling the carboxyl group of one amino acid or C-terminus of a peptide chain to the amino group of another amino acid or N-terminus of a peptide chain. Protecting groups for either the α -amino or α -carboxyl group and for functional side-chains are generally required due to the risk of side-reactions. Historically, a liquid phase approach has been used in peptide synthesis, but this has been replaced by the solid phase technique. The latter is now the preferred method for the synthesis of peptides, both for small scale (research) and large scale (manufacturing) synthesis.

Solid Phase Peptide Synthesis (SPPS) was pioneered by Robert Bruce Merrifield.^[1] Small insoluble solid polymer beads known as resin are modified with functional units on which peptide chains can be immobilised and elongated. The polymer remains insoluble but is solvated, allowing the reaction of the resin-bound amino acid / peptide with other reagents dissolved in the solution. The peptide will stay covalently bonded to the resin until cleaved from it by a reagent such as anhydrous hydrogen fluoride or trifluoroacetic acid. The peptide is retained on the solid-phase during a filtration process, allowing liquid-phase reagents and by-products of synthesis to be rinsed away. This is illustrated in Figure 2. 1 where alpha-amino acid group is deprotected before coupling the next amino acid.

The general principle of SPPS is one of recurring cycles of coupling-wash-deprotection-wash. The free N-terminal amine of the resin is coupled to a single N-protected amino acid unit. This unit is then deprotected, revealing a new N-terminal amine to which another amino acid may be connected. The advantage of the SPPS partially lies in the ability of removing excess reagent by wash cycles after each reaction, with the growing peptide remaining covalently attached to the insoluble resin.

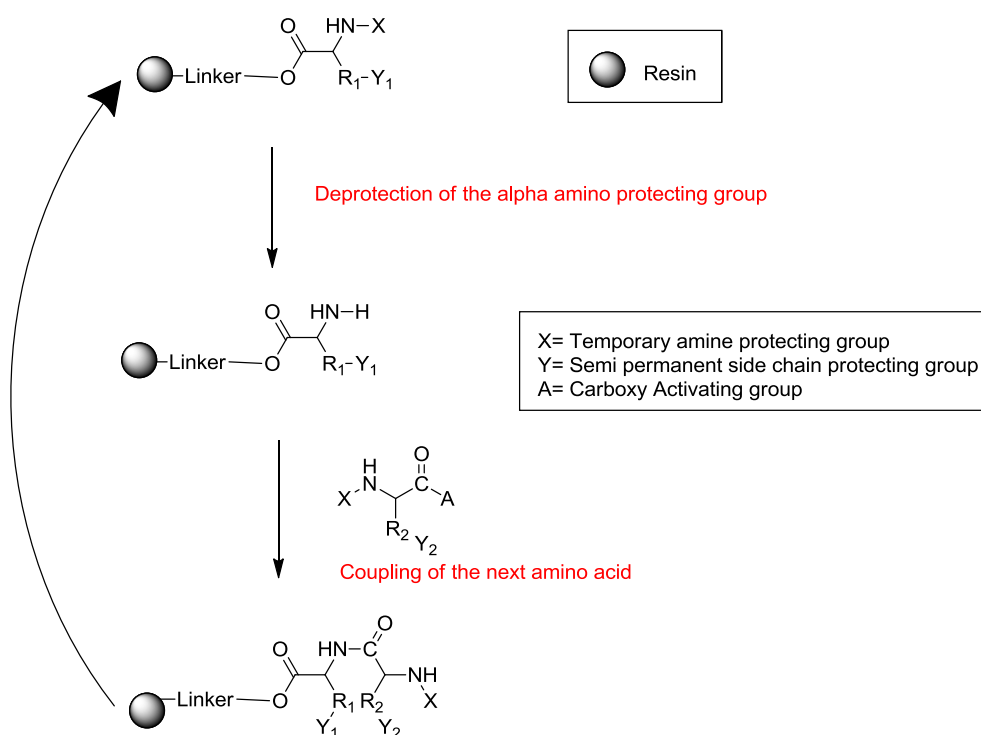
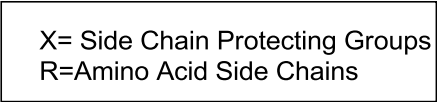


Figure 2. 1 General Scheme of SPPS

There are two commonly used strategies of SPPS, Fmoc and Boc, depending on the temporary protection used for the α -amino group (X in Figure 2. 1). For this thesis the Fmoc/*t*-Bu strategy was applied. The Fmoc strategy was applied for the following reasons; the repetitive TFA acidolysis required for Boc group deprotection may lead to alteration of sensitive peptide bonds as well as acid catalysed side-reactions. In the Fmoc strategy, the growing peptide chain is exposed to mild base conditions during Fmoc-group deprotection and TFA is only required for the final cleavage. In Figure 2. 2 the general orthogonal temporary and semi-permanent protections and cleavage strategy for Fmoc/*t*-Bu strategy is shown, where the side-chain deprotection of *t*-butyl-based groups and final cleavage from the resin is completed by acidic treatment (TFA) while the Fmoc group is removed by basic treatment (piperidine). In contrast the Boc strategy cleavage requires the use of highly corrosive HF and specialised laboratory apparatus that was not available. An automated peptide synthesizer was available and was used in conjunction with manual synthesis.



acids are purchased with these protecting groups prior to synthesis and then selectively removed during specific steps of peptide synthesis.

The N-terminal protecting group used throughout this thesis is Fmoc. Cleavage of the Fmoc requires ~20% piperidine in DMF or NMP as shown in the scheme of Figure 2. 3. Because the liberated dibenzofulvene group is a chromophore, deprotection of Fmoc can be monitored by UV absorbance of the runoff, a strategy which is employed in automated synthesizers. Amino acids are added in excess to guarantee complete coupling during each synthesis step, and without N-terminal protection, polymerization of unprotected amino acids would occur, resulting in low peptide yield or synthetic failure.

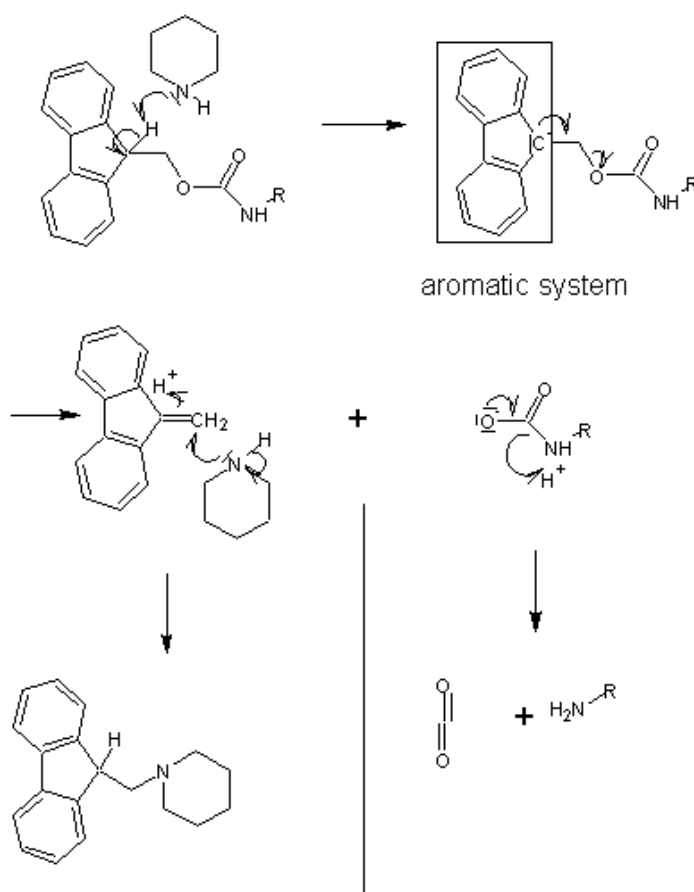


Figure 2. 3 Fmoc Cleavage

Amino acid side-chains are a diverse range of functional groups and are potential sites of non-specific reactivity during peptide synthesis. Therefore various protecting groups are necessary that are usually based on the benzyl (Bzl) or *tert*-butyl (*t*-Bu) group. Side-chain protecting groups are semi-permanent protecting groups, because they can endure the multiple cycles of chemical treatment during synthesis and are only removed during

treatment with strong acids after peptide synthesis is completed. This occurs during the cleavage step.

2.3 Coupling Methods

For the peptide bond formation, the carboxyl group of the N-protected amino acid requires activation for reaction with the amino group of another amino acid or of a peptide chain. *In situ* activating agents are widely accepted because they are easy to use, give fast reactions and are generally free of side-reactions. For this thesis, the coupling reagents used were phosphonium or uronium agents. In the presence of a tertiary base they convert protected amino acids into a variety of activated species.

2.4 Microwave assisted peptide synthesis

Since the first reports of microwave heating in the laboratory, more than 3500 articles have been published in this fast moving and exciting field. However, there have been only very few reports on the use of microwave irradiation in combination with solid phase peptide synthesis. In 1991, Wang et al. described the use of microwave irradiation to increase coupling efficiency and reduce reaction time in SPPS.^[2] Several groups have since reported the synthesis of difficult peptide sequences using this technique, showing better results in term of yields and purities.^[3] In peptide synthesis, microwave irradiation has been used to complete long peptide sequences in high yields. It has also shown low degrees of racemisation and reduced aspartimide formation.^[4] The technique uses microwave irradiation and cooling simultaneously to keep the overall bulk temperature of the solution low, while allowing for maximum microwave energy input. Aggregation, a process of β -sheet formation between resin-bound protected peptides which compromises the reactions required for sequence elongation, is lessened by microwave energy allowing for the possibility of longer peptide sequences assembly.

2.5 Instrumentation and Reagents

2.5.1 Reagents and Solvents

Material and reagents were of reagent grade purchased from commercial suppliers and were used without purification unless otherwise stated. Protected amino acids, HBTU, PyBOP and Rink-amide MBHA resin were obtained from Novabiochem (Merck Biosciences). HOBt was purchased from Iris Biotech GmbH. Synthesizer filters (in-line and reactor) and solvents (DCM, NMP) were obtained from Applied Biosystems. Other reagents and solvents were supplied by Sigma- Aldrich.

2.5.2 Microwave Synthesis

Microwave experiments were performed in a Biotage Initiator microwave equipped with pressure vessels and temperature and pressure controls.

2.5.3 Nuclear Magnetic Resonance (NMR) Spectroscopy

^1H NMR spectra were determined at 400MHz with a BRUKER NMR spectrometer. The chemical shift values are expressed in δ values (parts per million). Coupling constants (J) are in Hertz and are corrected to the nearest 0.5 Hz. Multiplicities are reported as follows: s, singlet, d, doublet, dd, double doublet, t, triplet, q quartet, m, multiplet and br broad. ^1H NMR spectral assignments are supported by ^{13}C - ^1H COSY. Samples were prepared in CDCl_3 (referenced to 7.26ppm for ^1H and 77.0 for ^{13}C) and DMSO-d_6 (referenced to 2.50ppm for ^1H and 40.45 for ^{13}C) All NMR spectra were processed and analysed using Topspin NMR software.

2.5.4 Thin Layer Chromatography

Thin layer chromatography (TLC) was performed on glass silica gel (Merck, 250 μm thickness) plates. These were then immersed in a beaker containing mobile phase of interest and analysed under UV light (254 and 365 nm).

2.5.5 Mass Spectrometry Analysis

2.5.5.1 Matrix Assisted Laser Desorption Ionisation-time of flight

The mass spectrometry analyses were performed on a LaserToF by Matrix Assisted Laser Desorption Ionisation-time of flight (MALDI-TOF). α -cyano-4-hydroxy cinnamic acid matrix, dissolved in 1:1 H₂O containing 0.1% TFA : CH₃CN containing 0.1% TFA, at a concentration of 10mg/ml, was used. Two microliters of 1:1 solution of peptide to matrix were applied to the MALDI plate.

2.5.5.2 Electrospray ionization (ESI)

Mass spectrometry experiments were carried out using a Bruker Esquire LC_00050 electron spray interface (ESI) with a positive ion polarity. Samples were dissolved in HPLC grade methanol/ acetonitrile or de-ionised water.

2.5.6 Elemental Analysis

Elemental analyses were carried out on an CE440 Elemental Analyser at the School of Pharmacy in RCSI. (*Conducted by Senior Technician, Ms. Suzanne Donnelly*).

2.5.7 Absorption Spectroscopy

UV-Vis spectra were recorded on a Varian Cary 50 spectrophotometer. Samples were analysed in a quartz cuvette with a path length of 1 cm with a spectral range of 200-800 nm unless otherwise stated. The background was corrected for the absorption of the buffer prior to every measurement and was performed at room temperature.

2.5.8 Fluorescence Spectroscopy

Emission spectra were recorded on a Varian Cary Eclipse fluorescence spectrophotometer with an excitation slit width of 5 nm and an emission slit width of 5 nm unless otherwise stated. All experiments were performed using a 1 cm path length quartz

cuvette. The background was corrected for blank solvent fluorescence prior to each measurement and was performed at room temperature.

2.5.9 Lifetime Measurements

Luminescent lifetimes were obtained using a Picoquant Fluotime 100 TCSPC (Time Correlated Single Photon Counting) system exciting at 450 nm and using a 510 nm narrow band pass dielectric filter for ruthenium complexes. 5,000 counts were collected for each lifetime measurement and all measurements were performed in triplicate using Nanoharp software to confirm results. Typical pulse rates of the excitation source were $1 \times 10^5 \text{ s}^{-1}$ with typical pulse widths of 300 ps. Degassed samples were degassed with nitrogen for 20 minutes prior to analysis.

The calculation of the luminescent lifetimes was performed by fitting an exponential decay function to each decay plot to extract the lifetime information using FluoFit software. Due to the inherently long lifetimes of inorganic complexes all data were fitted to mono exponential decay functions to the baseline of the decay curve using tail-fit with an x2 value of between 0.9-1.1.

2.5.10 Freeze Drier

The freeze drier used was an EC Modulyo system. Prior to placement on the freeze drier, all samples were dissolved or dispersed in deionised water and fully frozen in liquid nitrogen. The samples were then left on the freeze drier overnight.

2.5.11 Confocal Fluorescence Microscopy

Confocal fluorescence microscopy is an imaging technique that performs a point-by-point image construction by focusing a point of light sequentially across a specimen to eliminate out of focus light in samples that are thicker than the focal plane as outlined in chapter 1. Luminescent images were recorded using with a Zeiss LSM510 Meta confocal microscope using a 63x oil immersion objective lens (NA 1.4). The 458 nm argon ion laser excitation was used for ruthenium samples. The luminescence from ruthenium was collected using 560 nm long pass filters. *(Conducted by Research Engineer, Dr. Roisin Moriarty)*

2.5.12 Cell Culture

Chinese hamster ovarian (CHO) (CHO-K1, ATCC no. CCL-61) were purchased from ATCC Cell Biology Collection (UK). The adherent cell line CHO were grown in DMEM/Hams F-12 supplemented with 10% foetal calf serum (Biosera) at 37 °C with 5% CO₂. Cells were harvested or split when they reached 90% confluency for CHO cells.

The SK-N-AS and Kelly neuroblastoma cell line were a kind gift from Prof. Ray Stallings. *(Conducted by Dr. Roisin Moriarty, Research Engineer, DCU)*

2.5.13 Cellular Uptake of Complexes

In order to assess and compare the ability of the compounds to transport across the cell membrane, CHO cells were cultured on 35 mm glass bottom culture dishes. CHO cells were harvested after trypsinisation (0.25% trypsin for 5 mins at 37 °C) and seeded at 8×10^4 cells in 2 ml media. Cells were grown for 24 hours before imaging. For confocal measurements the growth medium was removed by washing with PBS buffer (pH 7.4) and dye-peptide (40 µM final concentration) in PBS (pH 7.4, with MgCl₂ and CaCl₂) was added.

The cell lines used throughout this thesis are CHO cell line and Kelly neuroblastoma cell line. Chinese hamster ovary (CHO) cells are epithelial cells which grow as an adherent monolayer in culture in many academic research laboratories. Furthermore, they are the most widely used mammalian cells for transfection, expression and protein production.

The Kelly neuroblastoma cell line is predominantly neuroblastic and therefore a good model of neuroblastoma. The SK-N-AS neuroblastoma cell line is derived from a female patient with neuroblastoma from the metastasis of the bone marrow. *(Conducted by research engineer, Dr. Roisin Moriarty)*

2.5.14 Cytotoxicity Assay

Cells were seeded in a 96-well plate in 100 μ l of media for 24 hours at 37 °C with 5% CO₂ before addition of compounds. CHO cells at 1×10^4 cells per well. 10 μ l of resazurin reagents (PromoKine) were added and incubated for 7 hours for resazurin at 37 °C. The resazurin converted to resorufin in viable cells was detected at absorbance 570 nm with background subtracted at 600 nm. Absorbance readings were performed using a Tecan 96-well plate reader. All cytotoxicity experiments are reported in terms of % cytotoxicity, e.g. 100% cytotoxicity = 100% of cells non-viable and carried out in triplicate ($n=3 \pm$ SD). (Conducted by research engineer, Dr. Roisin Moriarty)

2.6 Peptide Synthesis

2.6.1 Automatic Peptide Synthesis

Syntheses were carried out by automated Standard Solid Phase Peptide Synthesis (SPPS), performed on an Applied Biosystem ABI 433A Synthesizer (Warrington, UK). 1 mmol (10 fold molar excess) quantities of each protected amino acids were used. The amine group on the resin is Fmoc protected initially but is available for amino acid coupling at the start of the synthesis, as a result of piperidine (20% in NMP) deprotection. The peptide was elongated from the C-terminus (amide functional group) to the N-terminus (amino group). The sequence was assembled with monitoring of the Fmoc deprotection by UV absorption at 301nm.

2.6.2 Manual Coupling

Manual peptide synthesis is used to elongate difficult sequences and to reduce the quantities of valuable reagents required for the labelling of peptides. The resin was placed into a 5ml syringe fitted with a Teflon filter and a stopcock. The resin was swelled for 1 hour in NMP. Coupling reagents HBTU and HOBt, or PyBOP, and HOBt were used in 4.5 molar equivalents to the resin. The molecule to be coupled is used in 4.5 molar equivalents to the resin and DIEA is used in 10 molar equivalents. The coupling reagents and the protected amino acid are dissolved in 4ml of DMF and then DIEA is added. The solution is then added to the syringe and placed on the shaker for 4 hours. The resin is filtered and then washed consecutively twice with NMP and then a third time with DCM (3 x 5 ml aliquots for each

solvent, with 2 minutes agitation). An aliquot of the resin was then analysed to confirm that the coupling was complete using the qualitative Kaiser test. The Kaiser test is a colorimetric test for the presence of a primary N-terminal amino group on the peptide. It is based on the reaction of ninhydrin with amino groups to form an adduct characterised by a blue colour. Therefore, an incomplete coupling cycle will lead to a positive Kaiser test, confirmed by the development of a blue colour, while complete coupling will produce a negative (yellow/clear) coloured test.

2.6.3 Microwave Coupling

The microwave synthesizer (Biotage Initiator 2.5) was used to couple amino acids in a difficult sequence. This technique is used when other coupling techniques have been exhausted. The resin is swelled for 1 hour in NMP prior to using the microwave synthesizer. Coupling reagents HBTU and HOBt, or PyBOP and HOBt are used together in 5 molar equivalents to the resin. The protected amino acid is used in 5 molar equivalents to the resin and DIEA is used in 10 molar equivalents. The coupling reagents and the protected amino acid are dissolved in 4ml of NMP and then DIEA is added. The resin is placed in the microwave vial 2-5ml with the corresponding stirrer. The coupling reagents are then added to the vial and the vial is then sealed. The vial is placed in the port in the synthesizer using the correct adapter for the vial size used.

Coupling reactions took place for 5 minutes at 50°C with pre-stirring for 30 seconds and with fix hold time on. Absorption level was set to high as NMP was the solvent used.

2.6.4 Manual Deprotection

Manual deprotection was used after manual coupling to remove the Fmoc group. If the resin is not already swelled, then it should be swelled for 1 hour in DMF before deprotection. Manual deprotection took place in the syringe fitted with the filter. 20% piperidine in DMF (v/v) is added to the syringe and placed on the shaker for 10-15 minutes. The syringe is then drained and 20% piperidine in DMF (v/v) is added again and shaken for a further 10 minutes. This step is repeated and monitored by a positive Kaiser test as described above.

2.6.5 Microwave deprotection

The microwave synthesizer (Biotage Initiator 2.5) was used to deprotect the Fmoc group when vortexing at room temperature had been attempted without success for the deprotection reaction. The resin and the stirring bar is added to a 2-5ml vial and placed in the synthesizer port.

Deprotection reactions took place for 2 minutes at 50°C with pre-stirring for 30 seconds; fix hold time on and absorption were set to high.

2.6.6 Cleavage

The cleavage procedure was used to remove the peptide from the resin and deprotect the amino acid side-chains once assembly of the sequence is complete. The resin (188mg, substitution 0.53mmol/g) was placed in a test tube with a magnetic stirrer and the cleavage cocktail was added. A cleavage cocktail consisting of 4 ml of trifluoroacetic acid (TFA 80%) was used, while scavenging of the cationic species formed from the protecting groups was achieved by using the following reagents – 250 µl of water (5%), 250 µl of triisopropylsilane (TIS or TIPS, 5%), 250 µl of thioanisole (TA, 5%), 250 µl of 1,2-ethanedithiol (EDT, 5%). The cleavage cocktail is made up freshly in a separate centrifuge tube and added altogether to the test tube. The mixture is let stir for 2 hours with an additional half an hour for each arginine residue present in the sequence (with a maximum of 4 hours).

After stirring the solution was filtered into a plastic centrifuge tube using a teflon tube fitted with a filter. To the centrifuge tube, diethyl ether (~10ml) is added (to precipitate the peptide). The centrifuge tube can then be placed in the freezer for 5-10 minutes to aid the precipitation process. The product is centrifuged for five minutes at 2.8×10^3 rpm. The acidic liquid was drained off and disposed of carefully. The peptide was then washed twice using 15 ml of ether each time before being air dried for 1hr. The product was lyophilised overnight using a Thermo Electron Corporation, Modulyop-230 Freeze Dryer.

2.6.7 HPLC Analysis of Peptides

Chromatographic analyses were carried out on a Varian HPLC Chromatography Workstation using Gemini (C-18) reverse-phase chromatography column obtained from Phenomenex. The Gemini C 18 (250mm x 2.5 mm) was used at $1\text{ml}\cdot\text{min}^{-1}$ with linear gradient programs. UV was monitored at 214nm unless otherwise indicated and for dye-peptide conjugates at dual wavelength of 214nm and 452nm. Solvent A consisted of H_2O containing 0.1% TFA and solvent B of CH_3CN containing 0.1% TFA. The gradient ran over 30 min going from 5% to 65% of buffer A.

2.6.8 HPLC Purification of Peptides

Reverse Phase Purifications were carried out on a PerSeptive Biosystems BioCAD SPRINT using a semi preparative column Gemini (C-18) reverse-phase chromatography column obtained from Phenomenex. The Gemini C 18 (250mm x 10 mm) column was used at $4\text{ml}\cdot\text{min}^{-1}$ with linear gradient programs. UV was monitored at 214nm unless other wise indicated and for dye-peptide conjugates at dual wavelength of 214nm and 452nm. Solvents were degassed using Helium for 20 minutes. Solvent A consisted of H_2O containing 0.1% TFA and solvent B of CH_3CN containing 0.1% TFA. The gradient ran over 30 min going from 5% to 65% of buffer A.

References

- [1] Merrifield, R. B., *Journal of the American Chemical Society*, (1963) **85**, 2149.
- [2] Chen, S. T.; Chiou, S. H.; Wang, K. T., *Journal of Chinese Chemical Society*, (1991) **38**, 85.
- [3] Bacsa, B.; Desai, B.; Dibo, G.; Kappe, C. O., *J Pept Sci*, (2006) **12**, 633.
- [4] Palasek, S. A.; Cox, Z. J.; Collins, J. M., *J Pept Sci*, (2007) **13**, 143.

Chapter 3:

Luminescent Chromophores for

Cellular Imaging

3.1 Introduction

A major barrier to the application of inorganic chromophores in cell imaging to date has been the inability of such materials to passively diffuse across a cell membrane without membrane permeabilisation. The comparatively low cationic charge associated with many of these metal complexes means that they are unable to successfully use the cell's membrane potential as means for cellular entry. Reported methods for permeabilisation include electroporation, the use of organic solvents and detergents; all of them potentially affect the cell viability.^[1]

However, research published by our group ^[2, 3] established that conjugation of a metal complex to a CPP can assist in the efficient translocation of the luminescent probe across mammalian cell membranes without destroying the lipid bilayer and without the need for permeabilisation. Additionally, once inside the cytoplasm, the environmentally sensitive photophysics and spectroscopic properties of the dye-peptide may be exploited to report on the intracellular environment. Chapter 1 reviewed examples where localising peptides have been used for the internalisation of inorganic luminophores into cellular structures for live cellular imaging and the processes by which these biomolecules are uptaken by the cell.

The aim of this chapter was first the synthesis of a range of peptide-probe conjugates and then to evaluate their application in delivery of the Ru centre to the nucleus. The environmentally sensitive ruthenium polypyridyl peptide conjugates, were investigated as a membrane permeable, oxygen sensitive, probe in myeloma cells, and the labelling of the peptide sequences preferentially localising to the nucleus was also investigated.

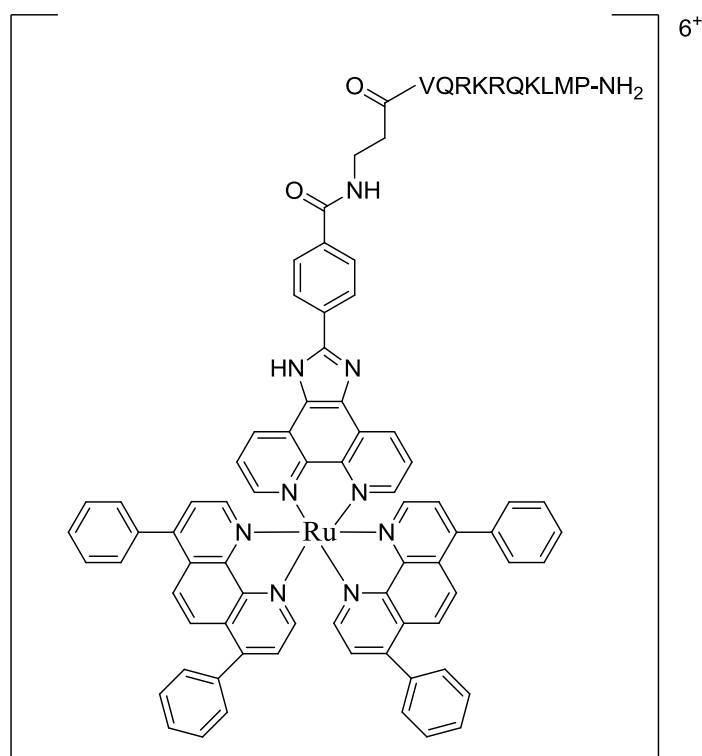
This chapter details the synthesis of ruthenium (II) inorganic metal luminophores conjugated to nuclear localisation peptides and the preliminary studies on cell imaging. As discussed in Chapter 1, metallo dye-peptide conjugates hold significant potential for use as molecular probes in multimodal cellular imaging. Due to their large Stokes shifts, photostability, long aqueous lifetimes and pH / oxygen sensitivity, these conjugates can label cells / sub-cellular structures. As outlined in Chapter 1, the interaction of Ru chromophores with DNA needs to be targeted to the nucleus if used for a therapeutic context. This may prove very valuable as they can sensitize photodamage to DNA and can have potential therapeutic use if delivered to the nucleus of, for example, cancer cells. Additionally, the intrinsic photophysical properties of these metal complexes, with their triplet excited states allowing for the generation of singlet oxygen and other reactive oxygen species may lead to

induced apoptosis in cells, thus, making these dye-peptides potentially valuable in the area of photodynamic therapy.

The supramolecular assemblies synthesized were prepared in a similar way to previously reported methods developed by Cosgrave *et al.* [3] The precursor Ru(II) polypyridal complexes were supplied by Ciaran Dolan and Kellie Adamson (Dublin City University). The peptide N-terminally modified with a β -alanine spacer was then prepared by Merrifield's Solid Phase Peptide Synthesis.[4] The novel complex [Ru(dpp)₂PIC]ClO₄ is based on the related ruthenium complex [Ru(bpy)₂(pic)]²⁺ where pic is 2-(4-carboxyphenyl)imidazo[4,5-f][1,10]phenanthroline, bpy is 2,2-bipyridine, dpp is 4,7-diphenyl-1,10-phenanthroline. Conjugation to the peptide occurs through the aromatic carboxyl group. The coupling reaction was performed on the side-chain protected resin-bound peptide.

3.2 Experimental Details for the Synthesis of targeting peptides-dye conjugates

3.2.1 Preparation of Ru (dpp)₂PIC- β Ala- NF- κ B (-VQRKRQKLMP-NH₂) conjugate.



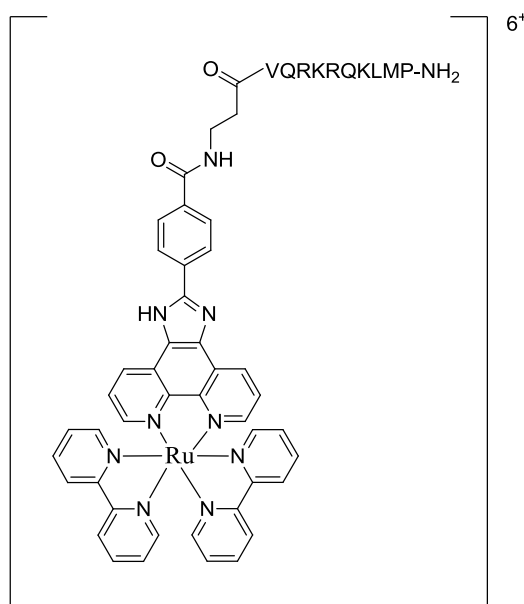
Synthesis of β Ala- NF- κ B (- β Ala -VQRKRQKLMP-NH₂) took place on an automated synthesizer by standard SPPS using 0.1mmol of Rink Amide Resin (substitution 0.7mmol/g). Manual coupling of [Ru(dpp)₂PIC]ClO₄ (supplied by DCU) took place by solid phase synthesis using PyBOP/HOBt (3eq) / DIEA (6eq) coupling chemistry overnight. The peptide was cleaved by standard methods and then purified as usual by RP-HPLC. Fractions collected by semi-preparative HPLC were analysed by mass spectrometry and analytical HPLC.

Purity 97% (Appendix Figure 1).

MALDI-MS 2440.46 [M+1]⁺ calculated for C₁₂₆H₁₅₀N₃₀O₁₄RuS 2439.95 (Appendix Figure 2).

Experiment Number: LB-3-05

3.2.2 Preparation of Ru(bpy)₂PIC- β Ala-NF- κ B (-VQRKRQKLMP-NH₂) conjugate.

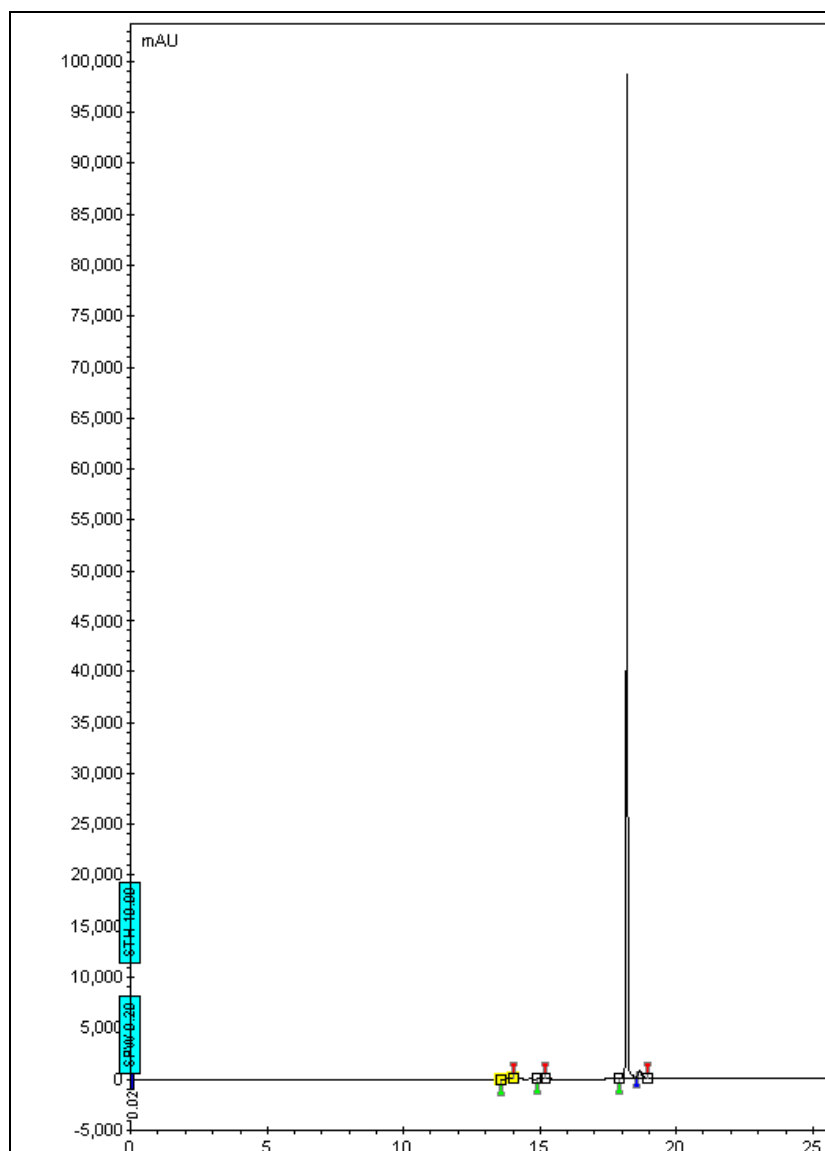


The β Ala-NF- κ B (β Ala -VQRKRQKLMP-NH₂) peptide was assembled using 0.1mmol of Rink Amide Resin (substitution 0.7mmol/g) on the automated synthesizer as previously described. Manual coupling of [Ru(bpy)₂PIC] ClO₄ (supplied by DCU) to the resin-bound peptide took place overnight using PyBOP/HOBt (3eq) / DIEA (6eq) coupling chemistry. The peptide was cleaved by standard methods and then purified as usual by RP-HPLC. Fractions collected by semi-preparative HPLC were analysed by mass spectrometry and analytical HPLC.

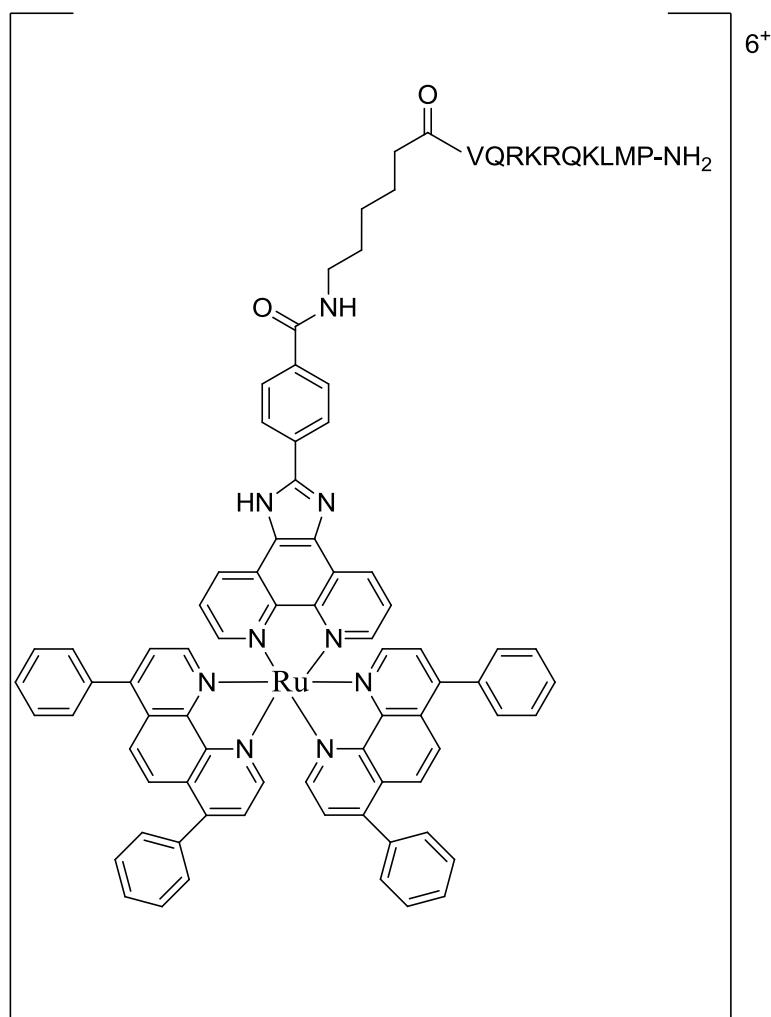
Purity 98% (Figure 3.1).

$m/z=1044.64$ (100%, $[M + 2 H]^{2+}$) calculated for C₉₈H₁₃₄N₃₀O₁₄RuS 2088.95 (Appendix Figure 3).

Experiment Number: LB-1-05



3.2.3 Preparation of $Ru(dpp)_2PIC-Ahx-NF-\kappa B$ (-VQRKRQKLMP-NH₂) conjugate.



The peptide NF- κ B (Ahx-VQRKRQKLMP-NH₂) was assembled using 0.1mmol of Rink Amide Resin (substitution 0.7mmol/g) by automated synthesis as previously described. Manual coupling of [Ru(dpp)₂PIC]ClO₄ (supplied by DCU) took place on the resin using PyBOP/HOBt (3eq) / DIEA (6eq) coupling chemistry with overnight shaking. The peptide was cleaved by standard methods and then purified as usual by RP-HPLC. Fractions collected by semi-preparative HPLC were analysed by mass spectrometry and analytical HPLC.

Purity 96% (Appendix Figure 4)

HRMS m/z: found 833.70[M + 3H]³⁺, calculated for C₁₂₉H₁₅₆N₃₀O₁₄RuS 2493.94 (Figure 3. 2).

Experiment Number: LB-2-72

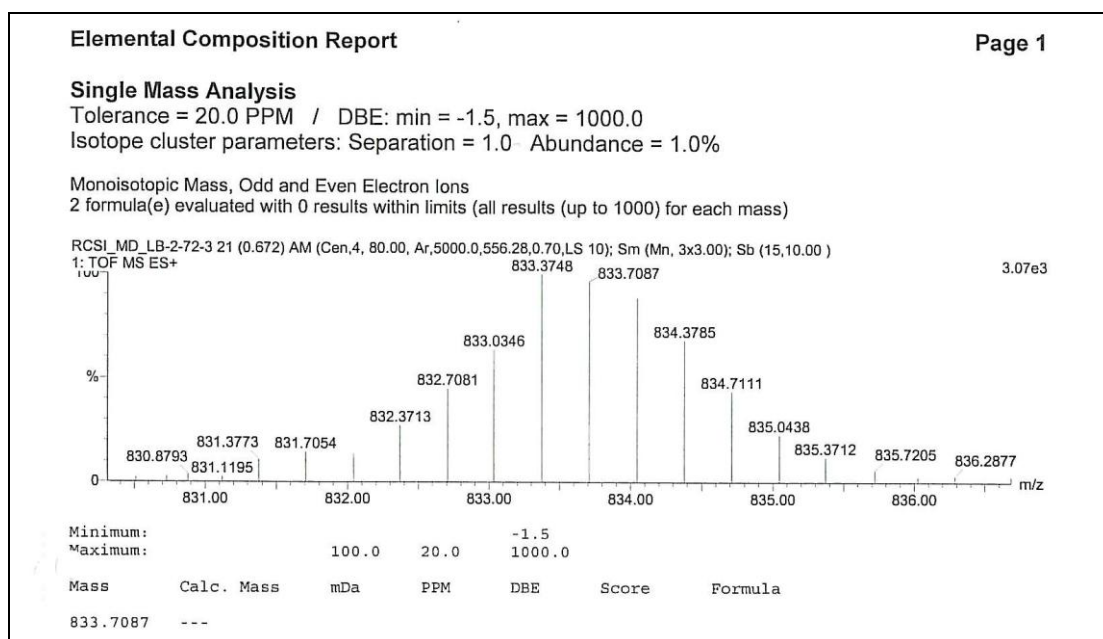
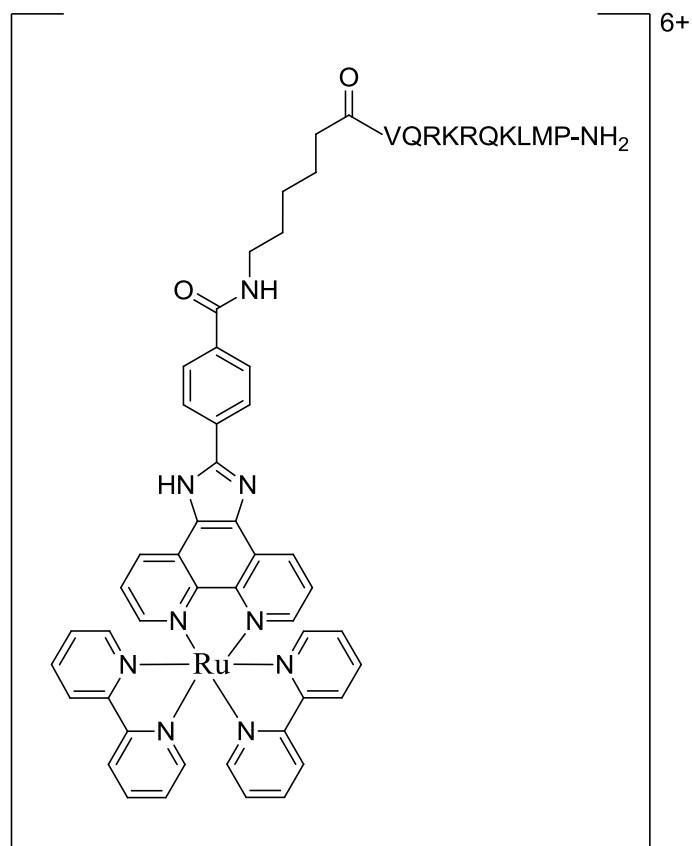


Figure 3. 2: Mass Spectra of the [Ru(dpp)₂PIC] ClO₄.NF-κB (Ahx-VQRKRQKLMP-NH₂) conjugate

3.2.4 Preparation of $Ru(bpy)_2PIC-Ahx-NF-\kappa B$ (-VQRKRQKLMP-NH₂) conjugate.



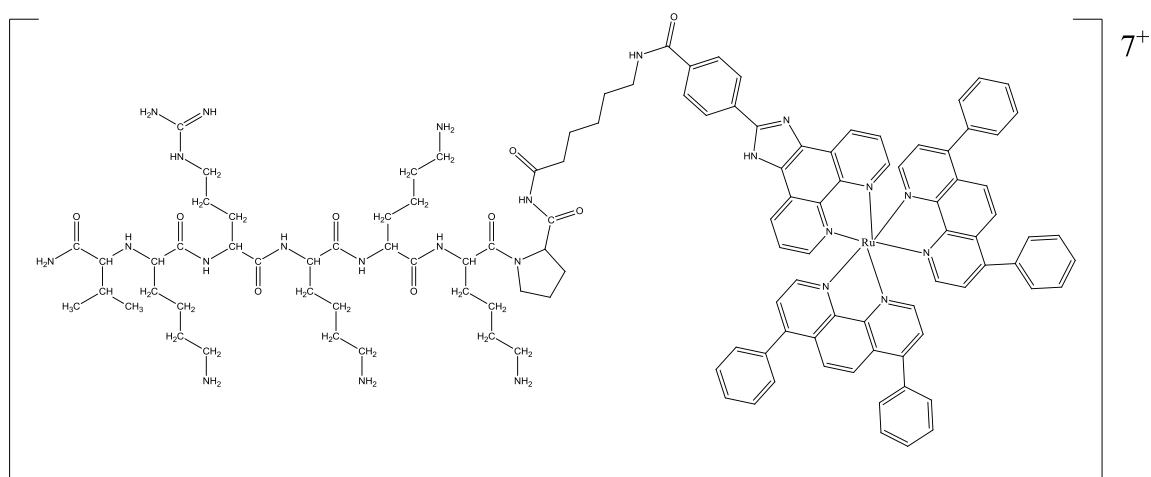
The peptide β Ala NF- κ B (β Ala -VQRKRQKLMP-NH₂) was assembled using 0.1mmol of Rink Amide Resin (substitution 0.7mmol/g) on an automated synthesizer as previously described. Manual coupling of $[Ru(bpy)_2PIC]ClO_4$ (supplied by DCU) took place by solid phase synthesis, using PyBOP/HOBt (3eq) / DIEA (6eq) coupling chemistry with overnight shaking. The peptide was cleaved by standard methods and then purified as usual by RP-HPLC. Fractions collected by semi-preparative HPLC were analysed by mass spectrometry and analytical HPLC.

Purity 85% (Appendix Figure 5)

MALDI-MS 2130.99 $[M+1]^+$ calculated for $C_{101}H_{140}N_{30}O_{14}RuS$ 2129.714 (Appendix Figure 6).

Experiment Number: LB-2-71

3.2.5 Preparation of $Ru(dpp)_2PIC$ –Ahx- Sv-40 (-PKKKRKV-NH₂) conjugate.



The Ahx- Sv-40 (Ahx -PKKKRKV-NH₂) peptide was assembled from a Rink Amide Resin (0.1 mmol scale, substitution 0.7mmol/g) by automated synthesis as previously described. Manual coupling of $[Ru(dpp)_2PIC]ClO_4$ (supplied by DCU) to the resin-bound peptide using PyBOP/HOBt (3eq) / DIEA (6eq) coupling chemistry was performed by overnight reaction. The peptide was cleaved by standard methods and then purified as usual by RP-HPLC. Fractions collected by semi-preparative HPLC were analysed by mass spectrometry and analytical HPLC.

Purity 89% (Appendix Figure 7)

HRMS m/z : found 1041.48 $[M + 2H]^{2+}$, calculated for $C_{114}H_{132}N_{24}O_9Ru$ 2083.96 (Figure 3. 3).

Experiment Number: LB-2-83

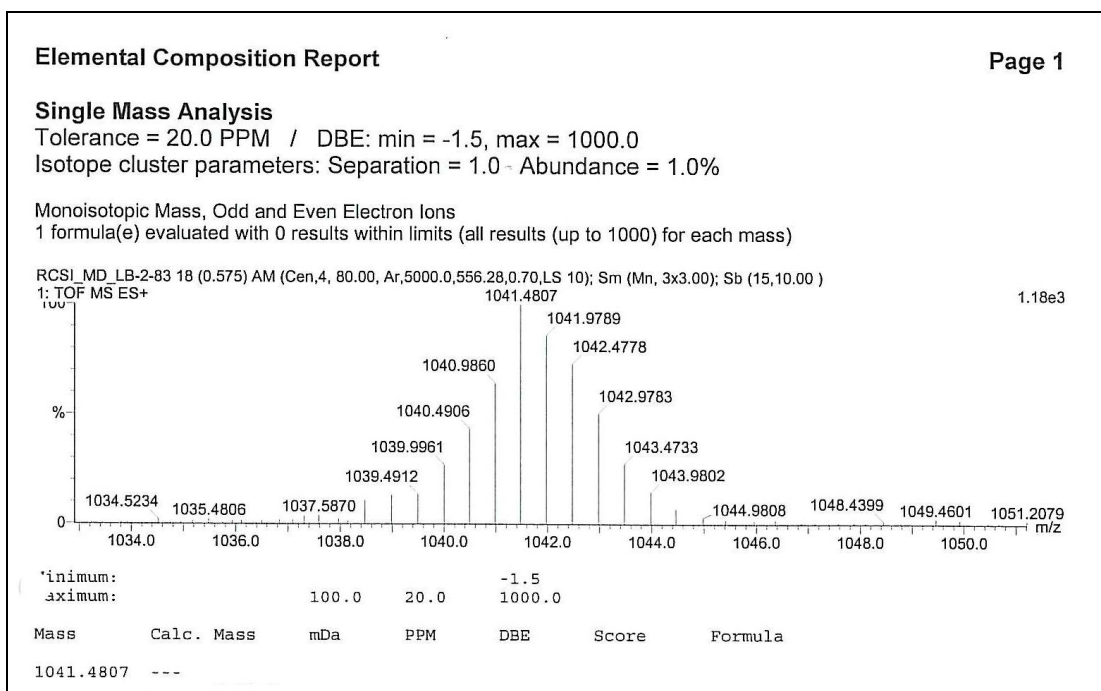
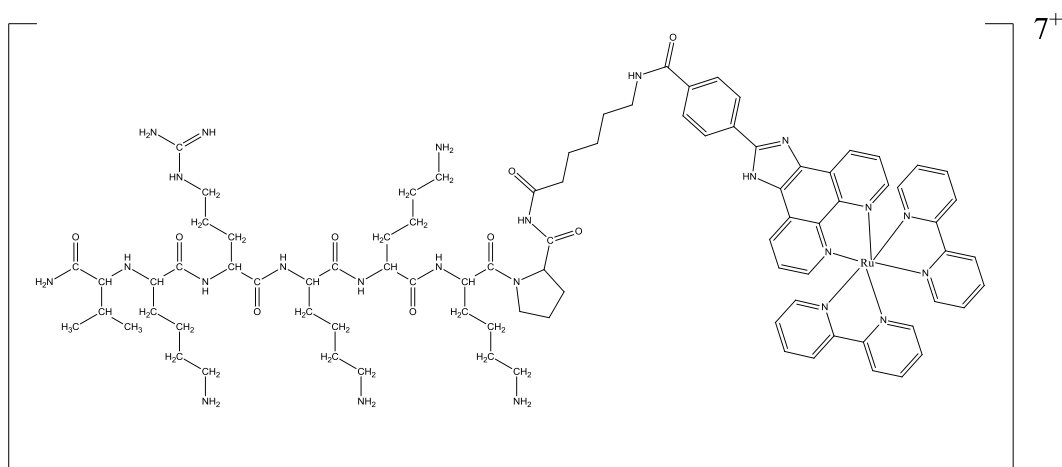


Figure 3. 3: Mass Spectra of Ru(dpp)₂PIC–Ahx-Sv-40 (-PKKKRKV-NH₂) conjugate

3.2.6 Preparation of Ru(bpy)₂PIC–Ahx-Sv-40 (-PKKKRKV-NH₂) conjugate.



The Ahx-Sv-40 (Ahx -PKKKRKV-NH₂) peptide was assembled using 0.1mmol of Rink Amide Resin (substitution 0.7mmol/g) and took place on the AB 433A synthesizer as previously described. Manual coupling of [Ru(bpy)₂PIC]ClO₄ (supplied by DCU) took place on the resin using PyBOP/HOBt (3eq) / DIEA (6eq) coupling chemistry with overnight shaking. The peptide was cleaved by standard methods and then purified as usual by RP-HPLC. Fractions collected by semi-preparative HPLC were analysed by mass spectrometry and analytical HPLC.

Purity 96% (Figure 3. 4)

HRMS m/z: found 865.422 $[M + 2H]^{2+}$, calculated for $C_{86}H_{116}N_{24}O_{94}Ru$ 1730.84 (Appendix Figure 8).

Experiment Number: LB-2-82

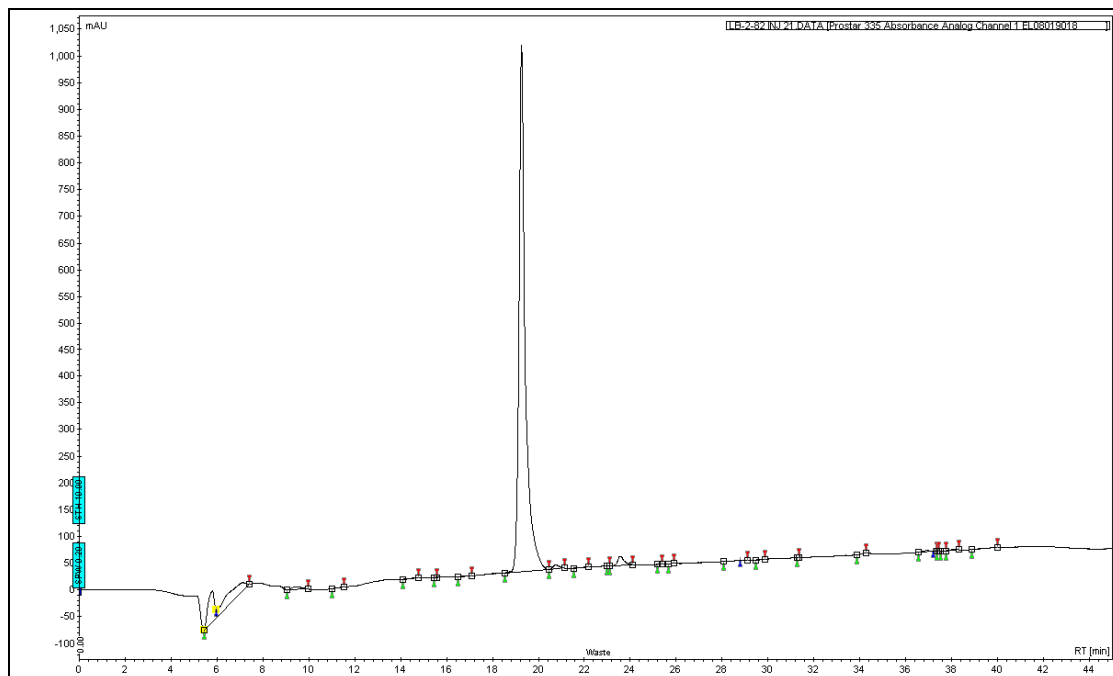


Figure 3. 4 Purity of Ru (bpy)₂ PIC –Ahx- Sv-40 (-PKKKRKV-NH₂) conjugate

3.3 Results and Discussion

Synthesis

Six novel Ru II polypyridyl peptide conjugates were synthesised by standard SPPS. Rink amide MBHA resin, a common cross-linked polystyrene support for the synthesis of peptide amides was chosen for several reasons. NLS sequences do not require a C-terminal carboxyl group and can be prepared as peptide amides. The latter are more conveniently synthesised than peptide acids and are moreover more resistant to proteolytic degradation mediated by exopeptidases. The peptide was elongated from the C-terminus to the N-terminus, as traditionally performed in solid phase synthesis to prevent racemisation and was therefore modified at its N-terminus with the ruthenium label. Assembly of the peptide sequence and elongation with a (2 or 5 carbon) linker was performed by automated synthesis, with final N-terminal deprotection. The resin-bound peptide was then transferred

to a fritted funnel for manual coupling of the Ru (II) polypyridyl complex. The latter contained a PIC ligand which had a carboxy functional group, allowing therefore its conjugation to the peptide through a stable amide bond. The conjugation of the chromophore to the peptide was performed by solid phase synthesis as shown in

Figure 3. 5. PyBOP was chosen as the coupling reagent over HBTU as previous in-house labelling studies had shown the superiority of the phosphonium reagent over the uronium reagent for the amidation of peptides with a chromophore. Due to the limited amount of Ru (II) complexes available, only 3 equivalents of the Ru (II) complexes to the resin were used in comparison to the 10 equivalents of each amino acid used by the synthesizer.

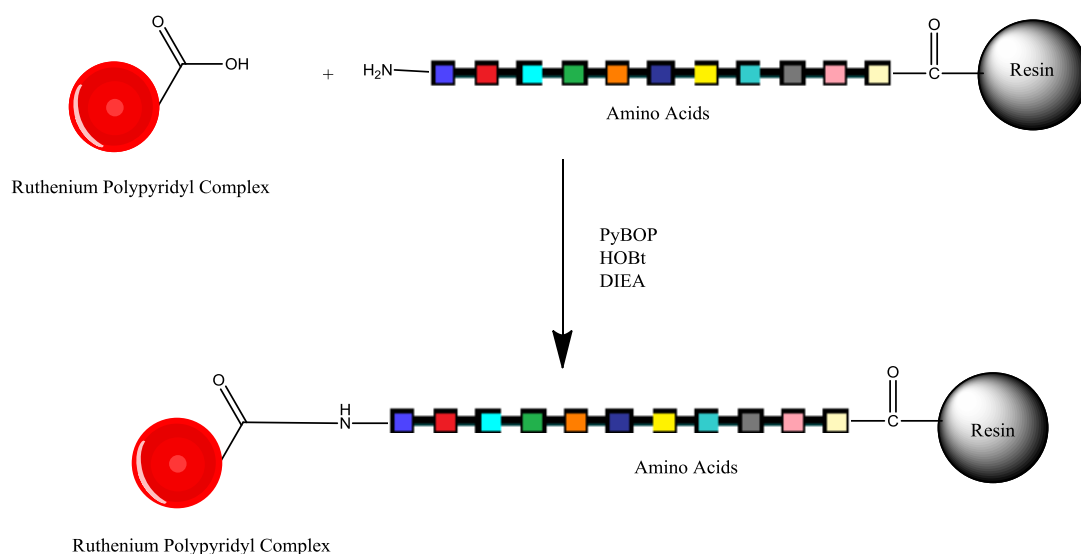


Figure 3. 5 Schematic of Ru (II) polypyridyl complex conjugation to a peptide

Cleavage of the Ru (II) polypyridyl peptide conjugates from the resin took place by treatment with TFA in the presence of scavengers. High concentrations of TFA are used for Rink Amide resins. Optimum cleavage conditions are very much dependent on the individual amino acid residues present in the peptide sequence, the side-chain protecting groups and the type of linker attached to the resin. Small scale cleavages, between 30-50mg of resin were carried out to determine the optimum cleavage conditions and to assess the integrity of the conjugate by mass spectrometry. TFA/TIS/Water/TA/EDT (80:5:5:5:5) was generally used as the cleavage cocktail. The benzhydryl linkage of the Rink Amide resin is acid sensitive and can be broken, resulting in coloured bi-products which are not easily removed from the product by simple washes. This can be overcome by using silane scavengers such as triisopropylsilane (TIS). Methionine, cysteine and tryptophan are

extremely susceptible to alkylation by cations produced during the cleavage process. Reaction of these amino acids with *t*-butyl cations results in modification of the product peptide. By adding scavengers to the cleavage mixture these side-reactions can be largely suppressed. The most commonly used scavenger is EDT. It is an extremely good scavenger of *t*-butyl cations; it assists in the removal of the trityl protecting group from cysteine and can be effective in preventing the acid-catalysed oxidation of methionine and cysteine residues. Thioanisole (TA) can also help with suppressing acid-catalysed oxidation of methionine. The oxidation of methionine can also be minimized by carrying out the reaction cleavage under nitrogen; this procedure was used for peptides containing a methionine residue. The cleavage times varied from 2-4 hours depending on the number of arginine residues in the sequence. The Pbf group used to protect the guanidino group of arginine requires extended deprotection times. Therefore if the sequence contained no Arg residues, the cleavage times were 2 hours and increased by 30 mins for every Arg residue with a maximum cleavage time of 4 hours. After this time the TFA could potentially break down the peptide chain. The polypyridyl peptide conjugate was precipitated by addition of diethyl ether and then lyophilised before purification.

Semi-preparative HPLC on a reverse phase polymeric support was used to achieve purities of the metal complex metal conjugates >85%. The selection of the stationary phase for the column was guided by the length of the peptide and the hydrophobicity of its conjugate. In the case of the Ru (II) polypyridal peptide conjugates, C₁₈ packings were suitable. A water/ACN gradient with TFA as the acidic ion pairing reagent was used. Monitoring was performed using UV-VIS detector at wavelengths of 214nm for the amide bond and 452nm for the Ru (II) polypyridal complex. The pure Ru (II) polypyridal peptide conjugates were then re-lyophilized and stored in the freezer until use. The Ru (II) polypyridal peptide conjugates were characterised by mass spectroscopy. The isotopic distribution of Ru is shown in the mass spectrums in Figure 3.2 and Figure 3.3.

The NF- κ B sequence, VQRKRQKLMP, was chosen first as this had shown ability to import conjugated fluorescein to the nucleus in previous reports.^[5, 6] However, this peptide was prone to oxidation as seen in Figure 3. 6. A minor signal at 2090.6522 represents the non-oxidised peptide whereas the larger signal at 2105.447 represent the oxidised peptide with an increased mass of 16. It is likely that this oxidation occurred at the methionine (M) residue in the sequence, either during a post-synthetic (cleavage and/or purification) step. Methionine oxidation is discussed further in Chapter 4. This NF- κ B conjugate was synthesised again with the cleavage taking place under nitrogen and with careful purification. The non-oxidised peptide was successfully isolated under these conditions and

used for testing. This led us to seek out an NLS sequence that did not have a residue prone to oxidation, such as methionine or cysteine, and with the SV-40 sequence was therefore selected. The synthesis and purification of the SV-40 peptide and its conjugates led to no difficulties.

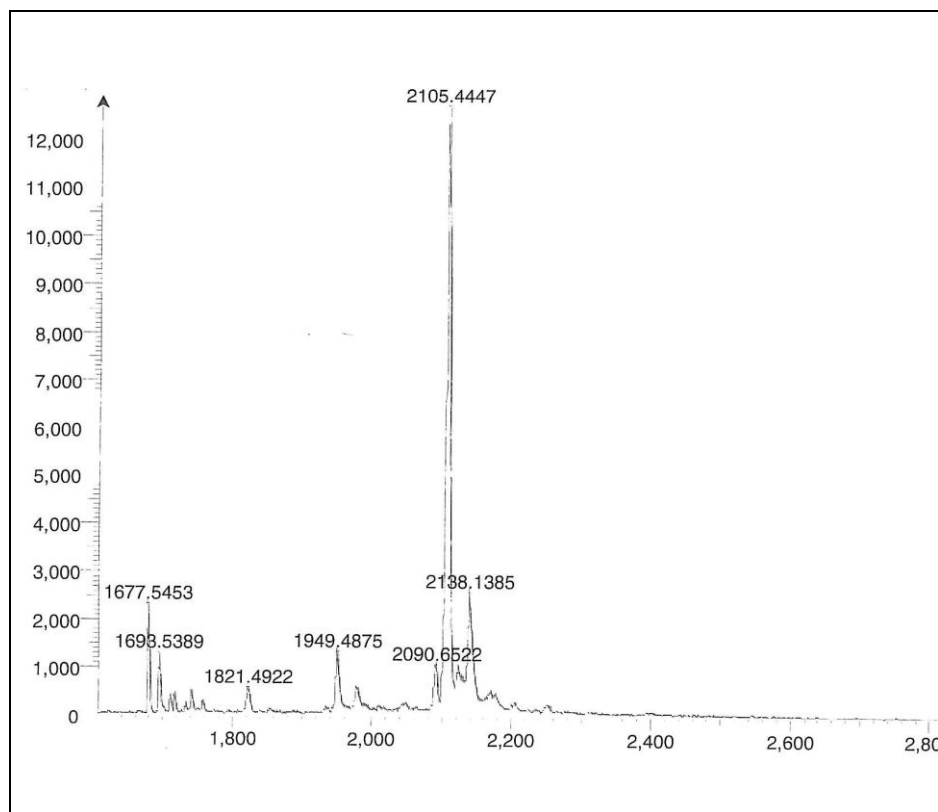


Figure 3. 6 MALDI-TOF of NF-κB (βAla-VQRKRQKLMP-NH₂) [Ru (bpy)₂ PIC] ClO₄ conjugate using α-cyano-4-hydroxycinnamic acid matrix.

Mass spectrometry and HPLC analysis were used routinely to confirm the purity of the chromophore peptide conjugates. The ruthenium (II) polypyridyl chromophores used were conjugated through a single reactive carboxyl group on the hetero ligand with the amino functionality on the protected peptide while on the resin. As a consequence of the selective coupling reactivity they normally do not contain isomers or other competing functional groups that may in turn lower the synthetic yields.

Mass spectra of the chromophore-peptide conjugates are reported in Section 3.2 and the Appendix. The purity of these conjugates was confirmed by HPLC analysis, their chromatograms showing a single peak. Their retention times, obtained under HPLC conditions as set out in the Chapter 2, are reported in Table 3.1. It is noted that the more

hydrophobic $[\text{Ru}(\text{dpp})_2\text{PIC}]^{2+}$ polypyridyl peptide conjugates have longer retention times than the $[\text{Ru}(\text{bpy})_2\text{PIC}]^{2+}$ polypyridyl peptide conjugates as expected by RP-HPLC. As seen in Table 3.1 the retention times of $\text{Ru}(\text{dpp})_2\text{PIC}$ polypyridyl peptide conjugates are approximately 30 minutes whereas the $\text{Ru}(\text{bpy})_2\text{PIC}$ polypyridyl peptide conjugates are approximately 19 minutes. On a reverse phase C18 column the more hydrophobic conjugates would have a stronger affinity for the hydrophobic stationary phase and remain on the column for longer until the gradient has a high enough concentration of the organic solvent to elute the molecule.

The integrity of these supramolecular assemblies was investigated with 2 different bridging linkers. There was no significant difference in photophysical or localising properties of the conjugates, between β -Ala, the 2 carbon linker or 6-amino-hexanoic acid, the 5 carbon linker, consistent with supramolecular linkers which do not influence extra electronic communication between A and B. Conjugation of the ruthenium (II) dye to the peptide did not cause any significant alterations to the wavelength of absorbance and emission of the conjugate when compared to the parent chromophores. There was an increase of the absorbance between 250-300nm due to the peptide conjugation system.

Table 3.1 Synthesised peptide-linker-chromophores with % purities and retention times

Experiment number	Peptide	Linker	Chromophore	Retention Time	% Purity	Experimental Mass (Da)
LB-2-71	NF- κ B	Ahx	$[\text{Ru}(\text{bpy})_2\text{PIC}]\text{ClO}_4$	19.8	83	2130.99
LB-2-72	NF- κ B	Ahx	$[\text{Ru}(\text{dpp})_2\text{PIC}]\text{ClO}_4$	29.2	96	2497.11
LB-2-82	SV-40	Ahx	$[\text{Ru}(\text{bpy})_2\text{PIC}]\text{ClO}_4$	18.4	96	1728.84
LB-2-83	SV-40	Ahx	$[\text{Ru}(\text{dpp})_2\text{PIC}]\text{ClO}_4$	29.1	89	2082.96
LB-1-05	NF- κ B	β -Ala	$[\text{Ru}(\text{bpy})_2\text{PIC}]\text{ClO}_4$	18.1	98	2089.28
LB-3-05	NF- κ B	β -Ala	$[\text{Ru}(\text{dpp})_2\text{PIC}]\text{ClO}_4$	32.1	97	2440.46

3.4 Photophysical Characterisation of Peptide-Chromophore Conjugates

The spectroscopic and photophysical data of all ruthenium complexes synthesised are presented in Table 3.2. The UV-VIS wavelengths in Table 3.2 are for the MLCT and the emission is the phosphorescence when excited at this wavelength. The luminescent decays

are monoexponential kinetics, recorded in aqueous solution at room temperature. The deaerated samples were bubbled with nitrogen for ~20 minutes before lifetime measurements were recorded. The deaerated lifetimes are longer than the aerated, and also noted is that the $[\text{Ru}(\text{dpp})_2\text{PIC}]^{2+}$ polypyridyl peptide conjugates lifetimes are longer than those for $[\text{Ru}(\text{bpy})_2\text{PIC}]^{2+}$ polypyridyl peptide conjugates. This is due to the collision quenching of the triplet MLCT interaction with the triplet oxygen state. $[\text{Ru}(\text{bpy})_2\text{PIC}]\text{ClO}_4$ is less rigid than $[\text{Ru}(\text{dpp})_2\text{PIC}]\text{ClO}_4$ making it less oxygen sensitive and therefore with a shorter lifetime than $[\text{Ru}(\text{dpp})_2\text{PIC}]\text{ClO}_4$. The increase in lifetime in absence of oxygen is also indication of the triplet MLCT character of the emission.^[7]

Table 3.2 The spectroscopic and photophysical data of all ruthenium complexes synthesised

Peptide	Linker	Dye	UV-VIS (nm)	Emission (nm)	Lifetimes Deaerated (μs)	Lifetimes Aerated (μs)
NF- κB	Hex-acid	$[\text{Ru}(\text{bpy})_2\text{PIC}]\text{ClO}_4$	455	607	0.89 ± 0.02	0.47 ± 0.03
NF- κB	Hex-acid	$[\text{Ru}(\text{dpp})_2\text{PIC}]\text{ClO}_4$	456	613	3.63 ± 0.04	0.73 ± 0.02
SV-40	Hex-acid	$[\text{Ru}(\text{bpy})_2\text{PIC}]\text{ClO}_4$	458	608	0.81 ± 0.03	0.70 ± 0.04
SV-40	Hex-acid	$[\text{Ru}(\text{dpp})_2\text{PIC}]\text{ClO}_4$	457	618	5.33 ± 0.02	0.24 ± 0.03
NF- κB	β -Ala	$[\text{Ru}(\text{bpy})_2\text{PIC}]\text{ClO}_4$	462	607	0.94 ± 0.02	0.80 ± 0.03
NF- κB	β -Ala	$[\text{Ru}(\text{dpp})_2\text{PIC}]\text{ClO}_4$	460	614	3.72 ± 0.04	0.49 ± 0.02
Parent	-	$[\text{Ru}(\text{bpy})_2\text{PIC}]\text{ClO}_4$	455	606	1.02 ± 0.02	0.16 ± 0.03
Parent	-	$[\text{Ru}(\text{dpp})_2\text{PIC}]\text{ClO}_4$	466	614	2.40 ± 0.03	0.20 ± 0.04

3.4.1 Absorbance

Below in Figure 3. 7, the overlaid UV-VIS absorbance spectra are shown for the ruthenium (II) polypyridal peptide conjugates synthesised. The electronic spectra of all six complexes are distinguished by a ruthenium π to ligand π^* MLCT transition at ~460 nm (individual values shown in Table 3.2). There is also evidence of a further MLCT transition within the $[\text{Ru}(\text{bpy})_2\text{PIC}]\text{ClO}_4$ conjugates at approximately 245nm. The strong absorbance band at approximately 285 nm may be assigned to π - π^* transitions within the polypyridal ligands, whereas the shoulder at approximately 330 nm is attributed to the π - π^* transitions of the carboxy-phenylphenatroline ligands containing the two ionisable protons on the imidazole ring. The carbon spacers have little effect on the absorbance spectra of the complex. There is an increase in the absorbance of the conjugates compared to the parent

complexes between 270-300nm due to the conjugation in the peptide. The absorbance profile of these conjugates are almost identical to those of their parent complexes $[\text{Ru}(\text{bpy})_2\text{PIC}]\text{ClO}_4$ and $[\text{Ru}(\text{dpp})_2\text{PIC}]\text{ClO}_4$ indicating little electronic contribution induced by the peptide or the linker.

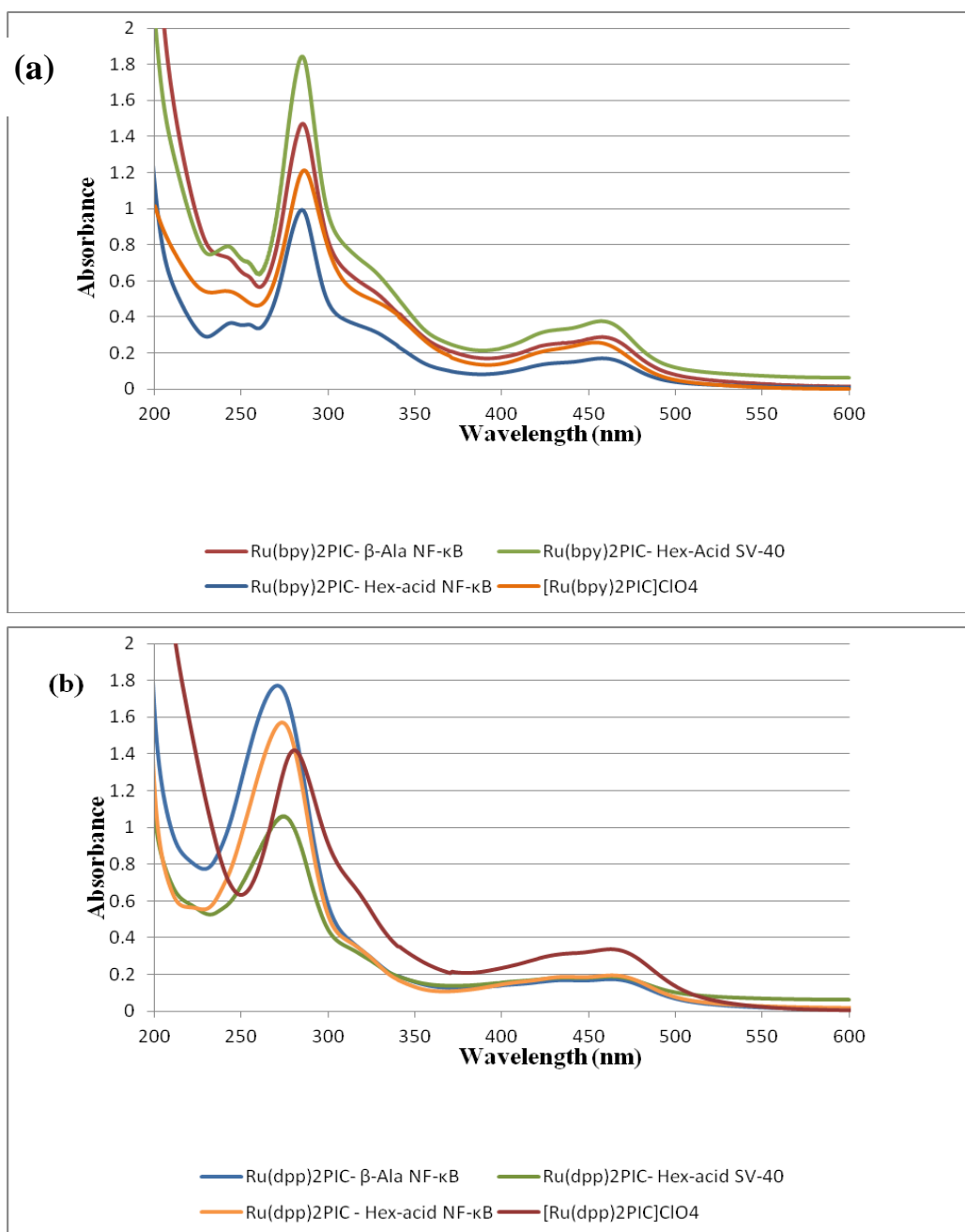


Figure 3. 7 Overlaid absorbance of the synthesised chromophore-peptide conjugates and parent complexes in water (a) $[\text{Ru}(\text{bpy})_2\text{PIC}]\text{ClO}_4$ parent complex and corresponding chromophore-peptide conjugates (b) $[\text{Ru}(\text{dpp})_2\text{PIC}]\text{ClO}_4$ parent complex and corresponding chromophore-peptide conjugates.

3.4.2 Emission

The emission spectra of the conjugates are shown in Figure 3.8. Ru(bpy)₂PIC polypyridyl peptide conjugates exhibits a maximum emission at approximately 608 nm when excited into the MLCT absorbance bands outlined in Table 3.2 which is consistent with the emission of the parent complex [Ru(bpy)₂PIC]ClO₄. Ru(dpp)₂PIC polypyridyl peptide conjugates exhibits a maximum emission at approximately 615 nm, also consistent with the [Ru(dpp)₂PIC]ClO₄ polypyridyl parent complex. All emission decays follow monoexponential kinetics with a lifetime in aerated samples being shorter than in degassed solutions. The length of the linker has no apparent effect on the lifetimes of the polypyridyl peptide conjugates. The lifetimes are comparable to those of the parent complexes.

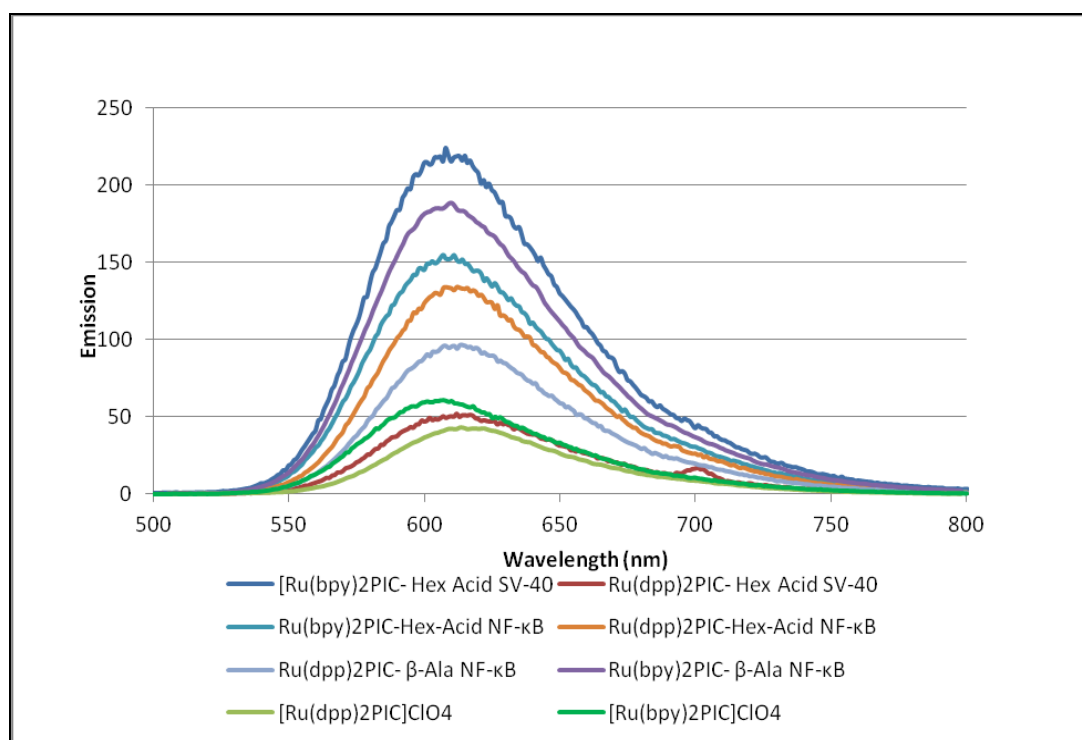


Figure 3.8 Overlaid emission of the synthesised chromophore-peptide conjugates and parent complexes in water.

3.5 Cellular Uptake of Chromophores-Peptide Conjugates

A key objective in preparing the complex conjugates was their targeting and membrane transport in mammalian cells. Their incubation with cells was therefore examined. In order to assess and compare the ability of the compounds to transport across the cell membrane of CHO cells, the latter were cultured separately on 35 mm glass bottom

culture dishes. CHO cells were seeded at 5×10^5 cells in 2 ml media and were grown for 24 hours before imaging. Incubation of the ruthenium complexes (40 μ M) was at 37 °C overnight following its addition to the cells. Images were acquired using a Zeiss LSM510 Confocal microscope, with a 63x oil immersion lens and a 458nm laser line for Ru. Cell imaging and cytotoxicity experiments presented throughout this chapter were performed by Dr. Róisín Moriarty. These were performed with co-localisation studies to confirm nuclear penetration and localisation.

Figure 3.9 shows evidence of $[\text{Ru}(\text{bpy})_2\text{PIC}]^{2+}$ chromophore being cargoed into the cell by the NF- κ B peptide and most importantly under goes strong evidence of transported to the nucleus. It shows the luminescent cross-section of the $\text{Ru}(\text{bpy})_2\text{PIC}-\beta\text{Ala-VQRKRQKLMP-NH}_2$ peptide (red) and nuclear stain DAPI (blue) in live CHO cells after overnight incubation at 37°C in PBS buffer. DAPI or 4',6-diamidino-2-phenylindole is a fluorescent stain that binds strongly to A-T rich regions in DNA. It is used extensively in fluorescence microscopy as a nuclear stain.

Influence of the counter ligand

Figure 3.9 shows a merged image of $[\text{Ru}(\text{bpy})_2 \text{PIC}-\beta\text{Ala-NF}\kappa\text{B}]^{6+}$, DAPI; the backscatter reflection is shown on the bottom right and the yellow line represents the fluorescence intensity profile in the graph on the left, generated using ImageJ image analysis software. DAPI alone is shown on the top left with $[\text{Ru}(\text{bpy})_2 \text{PIC}-\beta\text{Ala-NF}\kappa\text{B}]^{6+}$ shown alone on the top right. DAPI (300nM) was added for 30 mins at 37 °C and excited by the 375nm laser line. This image shows clear nuclear staining with $[\text{Ru}(\text{bpy})_2 \text{PIC}-\beta\text{Ala-NF}\kappa\text{B}]^{6+}$ conjugate, as confirmed by co-localisation and profile matching with the nuclear stain DAPI within the cell. Overall the images of $[\text{Ru}(\text{bpy})_2 \text{PIC}-\beta\text{Ala-NF}\kappa\text{B}]^{6+}$ show clear localisation in the nucleus confirmed by co-staining and fluorescent intensity profile.

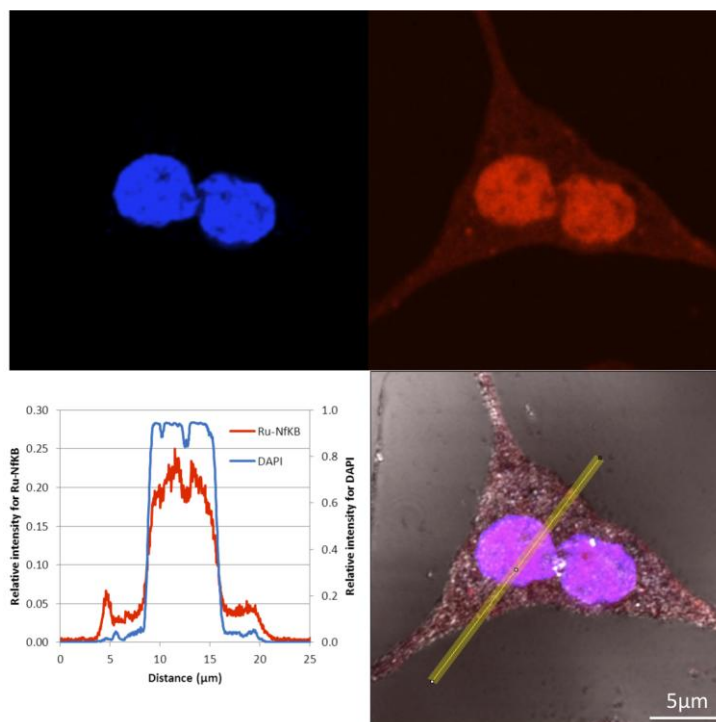


Figure 3.9 A merged image ($\text{Ru}(\text{bpy})_2\text{PIC}-\beta\text{Ala-VQRKRQKLMP-NH}_2$) 10^{-6} M, DAPI; $\lambda_{\text{ex}} = 458$ nm in PBS Buffer (Images collected by Dr. Róisín Moriarty)

Figure 3.10 shows $[\text{Ru}(\text{dpp})_2\text{PIC}]^{2+}$ crosses the cellular membrane when conjugated to NF- κ B peptide and again it is transported to the nucleus. It shows the luminescent cross-section of the $[\text{Ru}(\text{dpp})_2\text{PIC}-\beta\text{Ala-NF}\kappa\text{B}]^{6+}$ conjugate in live CHO cells. Whereas the probe does penetrate the nucleus, the dye intensity is comparable in the cytoplasm and the nucleus, it is not deemed therefore to specifically localise in the nucleus. There is evidence for localisation of the dpp probe in the cell membrane.

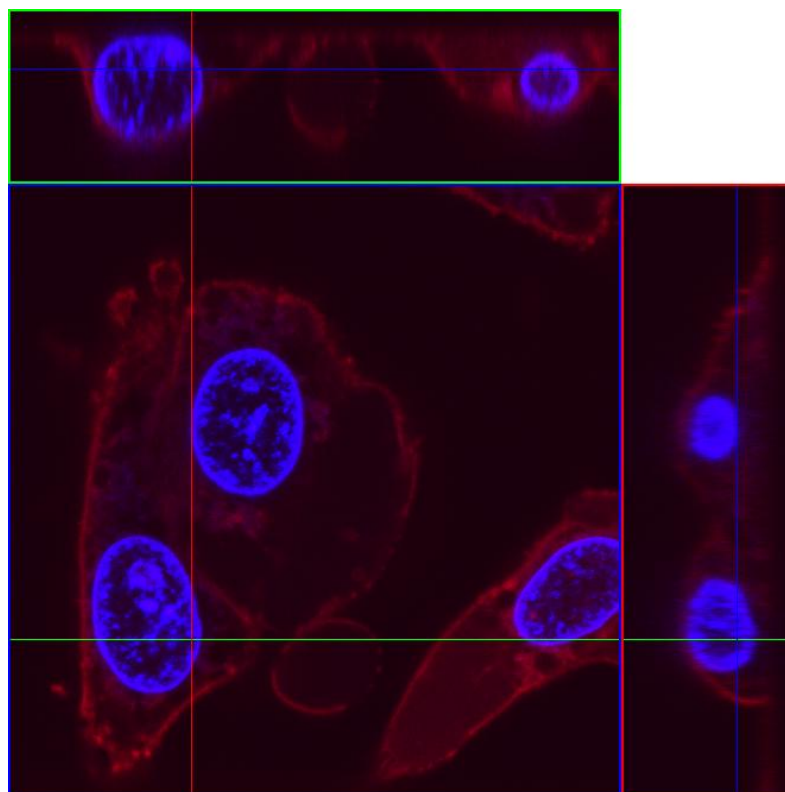


Figure 3.10 Luminescent confocal image ($\lambda_{ex} = 458 \text{ nm}$) showing luminescent cross-section of a live CHO cell incubated with NF- κ B ($\text{Ru(dpp)}_2\text{PIC-}\beta\text{Ala-VQRKRQKLMP-NH}_2$) 10^{-6} M) for 90 minutes at 37°C in PBS buffer. (Images collected by Dr. Róisín Moriarty)

The vesicles observed in the CHO cells after 90 minutes (Figure 3.10) are an indication of cell death discussed in Section 3.7. The $[\text{Ru(dpp)}_2\text{PIC-}\beta\text{Ala-NF}\kappa\text{B}]^{6+}$ exhibits high cytotoxicity in comparison to the $\text{Ru(bpy)}_2\text{PIC-}$ peptide conjugates which does not display any signs of vesicle formation in CHO cells after several hours incubation.

Figure 3.11 shows a merged image of $[\text{Ru(dpp)}_2\text{PIC-}\beta\text{Ala-NF}\kappa\text{B}]^{6+}$ (red) alone and a merged image of $[\text{Ru(dpp)}_2\text{PIC-}\beta\text{Ala-NF}\kappa\text{B}]^{6+}$ and DAPI; the backscatter reflection is on the bottom right and the yellow line represents the fluorescence intensity profile in the graph on the left, generated using ImageJ image analysis software. This image shows clear nuclear staining with $[\text{Ru(dpp)}_2\text{PIC-}\beta\text{Ala-NF}\kappa\text{B}]^{6+}$ complex as confirmed by co-localisation and profile matching with the nuclear stain DAPI within the cell.

The image also illustrates the pre-concentration of the dye inside a small spherical area within the nucleus that is likely to be the nucleolus which is particularly brightly luminescent. The nucleolus is a non-membrane bound structure composed of proteins and nucleic acids found within the nucleus of cells. Ribosomal RNA (rRNA) is transcribed and assembled within the nucleolus. Malfunction of nucleoli can be the cause for several human

diseases.^[8, 9] DAPI is not seen concentrated in this region of the cell in Figure 3.11 and this is supported by the relative intensity profile of DAPI and $[\text{Ru}(\text{dpp})_2 \text{ PIC-}\beta\text{Ala-NF}\kappa\text{B}]^{6+}$. DAPI targets DNA which is not found in the nucleolus. Further imaging is required to confirm this.

Overall the images of $[\text{Ru}(\text{dpp})_2 \text{ PIC-}\beta\text{Ala-NF}\kappa\text{B}]^{6+}$ show clear penetration of the complex in the nucleus confirmed by co-staining and fluorescent intensity profile. However compared to the corresponding $[\text{Ru}(\text{bpy})_2 \text{ PIC-}\beta\text{Ala-NF}\kappa\text{B}]^{6+}$, $[\text{Ru}(\text{dpp})_2 \text{ PIC-}\beta\text{Ala-NF}\kappa\text{B}]^{6+}$ does not only localise inside the nucleus, but tends to co-localise at the membrane. This is due to $[\text{Ru}(\text{dpp})_2 \text{ PIC-}\beta\text{Ala-NF}\kappa\text{B}]^{6+}$ hydrophobicity, arising from the dpp ligand. In addition $[\text{Ru}(\text{dpp})_2 \text{ PIC-}\beta\text{Ala-NF}\kappa\text{B}]^{6+}$, again, exhibits vesicle formation associated with its higher cytotoxicity

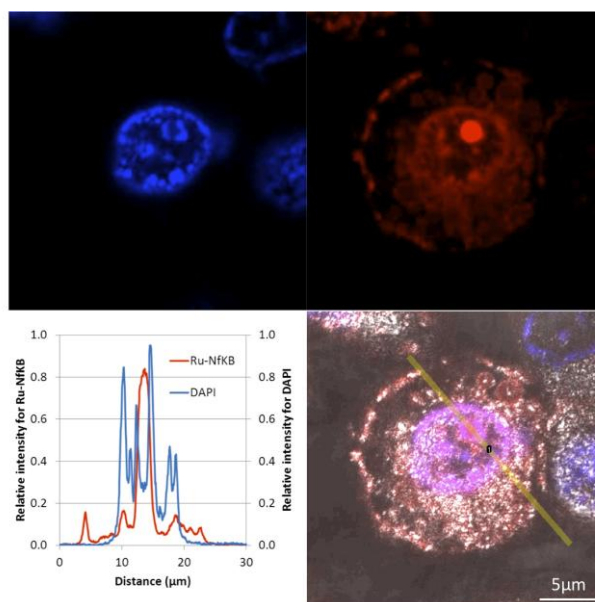


Figure 3.11 A merged image NF- κ B ($[\text{Ru}(\text{dpp})_2 \text{ PIC-}\beta\text{Ala-VQRKRQKLMP-NH}_2] 10^{-6} \text{ M}$), DAPI; the backscatter reflection is on the bottom right and the yellow line represents the fluorescence intensity profile in the graph on the left generated using ImageJ image analysis software $\lambda_{\text{ex}} = 458 \text{ nm}$ in PBS in buffer. (Images collected by Dr. Róisín Moriarty)

Influence of the Linker

Figure 3.12 shows the confocal images of CHO cells with evidence of $[\text{Ru}(\text{bpy})_2\text{PIC}]^{2+}$ chromophore being cargoed into the cell by the NF- κB peptide and transported to the nucleus with a 6-amino-hexanoic acid (Ahx) linker. Figure 3.12(a) shows a cluster of cells with an area within the cell being targeted by the Ru(II) polypyridyl peptide conjugate. Figure 3.12 (b) & (c) are focused on two cells, showing the targeted organelle within each cell which is believed to be the nucleus. These results are very similar to those of $[\text{Ru}(\text{bpy})_2\text{PIC}-\beta\text{Ala}-\text{NF}\kappa\text{B}]^{6+}$, indicating the linker has little effect on the uptake properties of the peptide. This indicates these components are good for supramolecular chemistry and suggesting that the length of the linker is benign. Figure 3.13 supports this statement for the $[\text{Ru}(\text{dpp})_2\text{PIC}]^{2+}$ chromophore as the NF- κB peptide with an amino-hexanoic acid (Ahx) linker gives similar results to those of $[\text{Ru}(\text{dpp})_2\text{PIC}-\beta\text{Ala}-\text{NF}\kappa\text{B}]^{6+}$, that contains the 2 carbon linker.

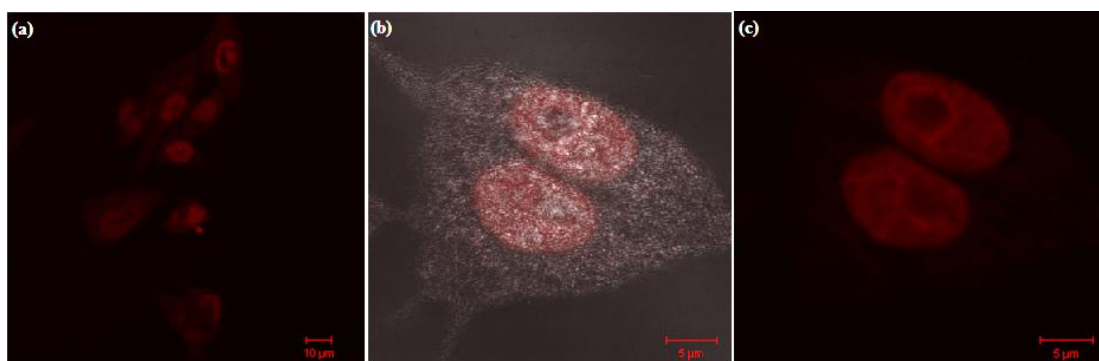


Figure 3.12 Luminescent confocal images ($\lambda_{\text{ex}} = 458\text{nm}$) of live CHO cells incubated with NF- κB ($[\text{Ru}(\text{bpy})_2\text{PIC}-\text{Ahx}-\text{VQRKRQKLMP}-\text{NH}_2] 10^{-6}\text{ M}$) overnight at 37°C with 5% CO_2 in PBS buffer. (Images collected by Dr. Róisín Moriarty)

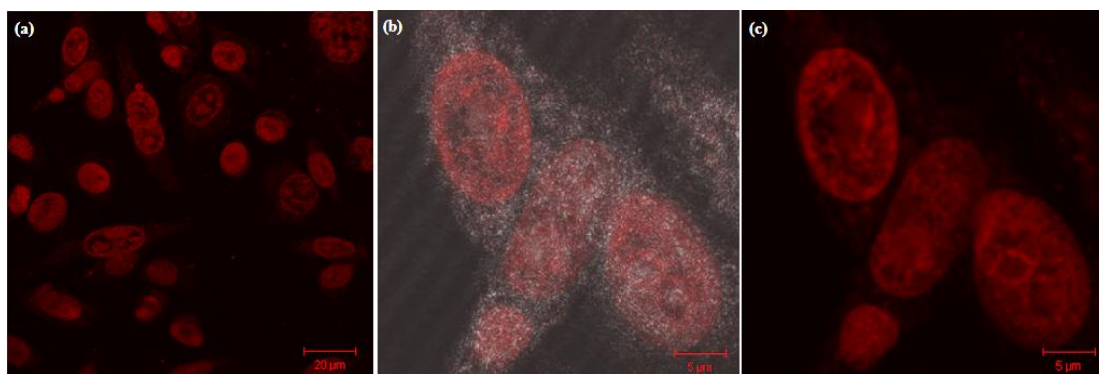


Figure 3.13 Luminescent confocal images ($\lambda_{\text{ex}} = 458\text{nm}$) of live CHO cells incubated with NF- κ B ($\text{Ru(dpp)}_2\text{PIC-Ahx-VQRKRQKLMP-NH}_2$) 10^{-6} M overnight at 37°C with 5% CO_2 in PBS in buffer. (Images courtesy of Dr. Róisín Moriarty)

SV-40 as another NLS

The next peptide to be investigated for its localisation properties was SV-40, another well known nuclear localising peptide as described in Chapter 1, section 1.8. 6-Amino-hexanoic acid was chosen as the linker. This peptide was not as successful as the NF- κ B in term of cellular uptake of the conjugated complex. The $\text{Ru(bpy)}_2\text{PIC-Ahx-SV40}$ peptide conjugate did not cross the cell membrane under the incubation conditions used for NF- κ B. There was no evidence of dye within the cells. It may be necessary for the SV40 peptide to be conjugated to a CPP to cross the cell membrane when conjugated to a cargo, at least in the case of a ruthenium bpy complex. Surprisingly, the corresponding $\text{Ru(dpp)}_2\text{PIC-Ahx-SV40}$ did cross the cell membrane as seen in Figure 3.14. However, there was no specific localisation to the nucleus. We believe the $[\text{Ru(dpp)}_2\text{PIC}]^{2+}$ disrupts the integrity of the cell membrane and therefore gains entry, eventually inducing cell death. This is supported by the cytotoxic results in section 3.7, collected by Dr. Róisín Moriarty. There are many examples of hydrophobic compounds used to induce cell death in the literature.^[10-12] There is a concentrated area within a cell organelle as seen in Figure 3.14, again this may be the nucleolus as seen previously with $\text{Ru(dpp)}_2\text{PIC}$ polypyridyl peptide conjugates. Ragin *et al* showed slightly less uptake of their SV-40 fluorescently labelled conjugate than that of their corresponding NF- κ B fluorescently labelled conjugate by flow cytometry, which is consistent with our findings that the SV-40 peptide did not show as good uptake as the NF- κ B peptide. Also Ragin *et al* found for two other NLS sequences Fl-Oct-6, and Fl-TFIIE- β (Fl-fluorescein) which are highly cationic, more cationic than Fl-NF- κ B, did not localise to the nucleus. It was suggested that Fl-Oct-6, and Fl-TFIIE- β may tightly associate with negatively charged membrane lipids, preventing their release into the cytoplasm and subsequent routing to the nucleus.^[15] As our $\text{Ru(dpp)}_2\text{PIC-Ahx-SV40}$ conjugates are more

cationic than our Ru(dpp)₂PIC-Ahx- NF-κB analogues, this also may be the reason why they did not reach the nucleus.

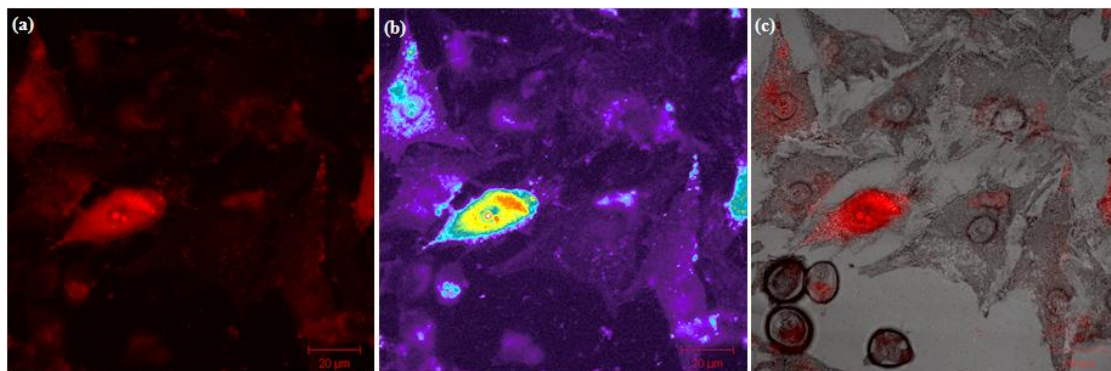


Figure 3.14 Luminescent confocal images ($\lambda_{\text{ex}} = 458\text{nm}$) of live CHO cells incubated with SV-40 (Ru(dpp)₂PIC- Ahx- PKKKRKV -NH₂) 10⁻⁶ M) overnight at 37°C with 5% CO₂. (a) Luminescent confocal image (b) Rainbow image (c) backscatter (Images collected by Dr. Róisín Moriarty)

3.6 Cytotoxicity

Resazurin is a colorimetric assay performed in cytotoxicity studies. Resazurin (7-hydroxy-3H-phenoxazin-3-one-10-oxide) is a non-fluorescent blue coloured dye. It is used mainly as an oxidation-reduction indicator in cell viability assays for bacteria and mammalian cells. As shown in Figure 3.15 upon reduction of the dye to form resorufin (red in colour) the dye is brightly fluorescent. The resazurin assay is based on the ability of viable, active cells to reduce resazurin to resorufin and dihydroresorufin, and can be readily applied to live cell cultures. This redox conversion is intracellular and is facilitated by mitochondrial, microsomal and cytosolic oxidoreductases. The rate of dye reduction is directly proportional to the amount of viable cells present in a given assay.^[13] An advantage of the resazurin assay over other cell viability assays include its low toxicity to living cells allowing for the study of cells over longer time periods.

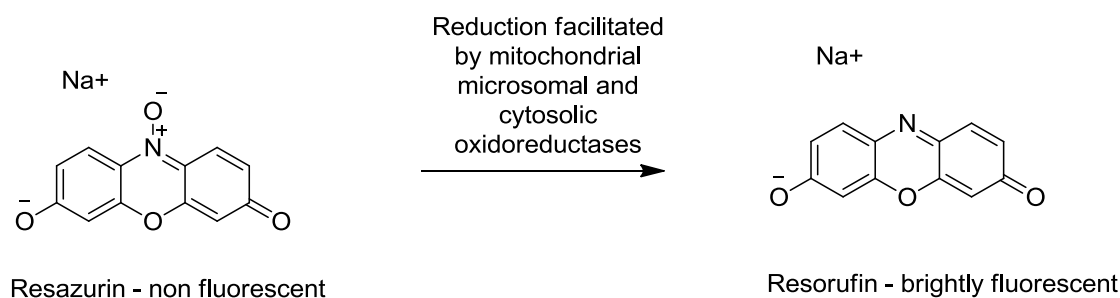
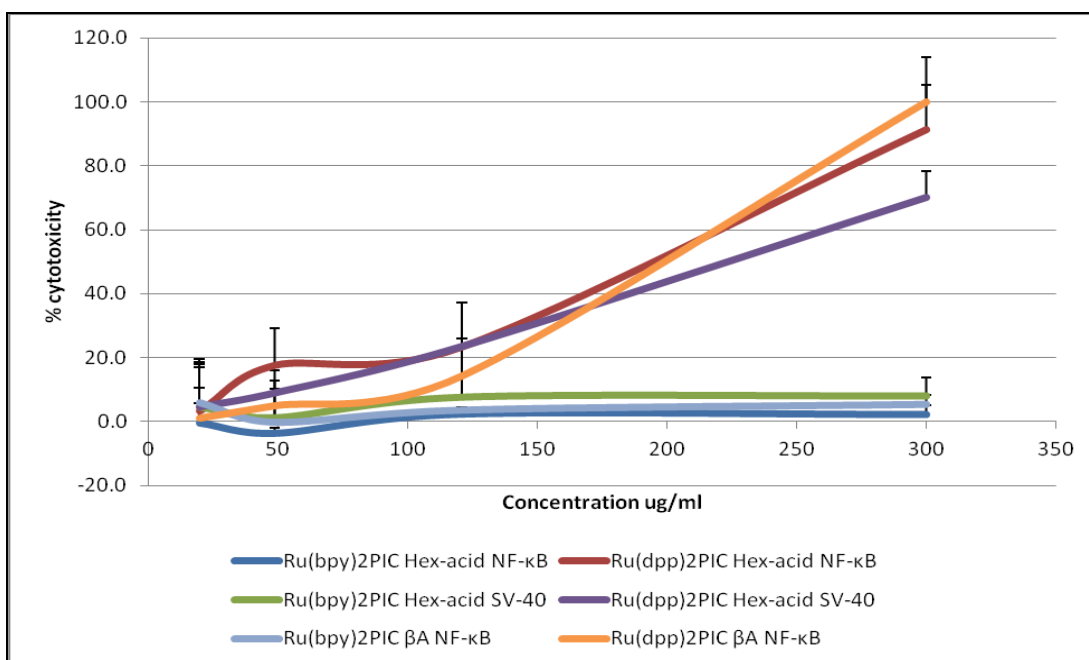


Figure 3. 15 Schematic diagram illustrating the conversion of resazurin to resorufin following reduction by active cell enzymes.

Given the evidence of vesicle formation following incubation with the $[\text{Ru}(\text{dpp})_2\text{PIC}]^{2+}$ peptide conjugates, it is important to assess the potential toxic effects of the chromophore peptide conjugates on the cell line selected. The effect of these complexes on the viability of the cells was tested using the resazurin cytotoxicity assay (also known as the alamar blue assay) which is explained in detail above and in Figure 3. 15. As seen in Figure 3. 16 which is a plot of the percentage cytotoxicity against concentration ($\mu\text{g}/\text{ml}$), it is evident from the results that the $[\text{Ru}(\text{dpp})_2\text{PIC}]^{2+}$ peptide conjugates exhibits a toxic effect on the cells well above that of the $[\text{Ru}(\text{bpy})_2\text{PIC}]^{2+}$ peptide conjugates. The $[\text{Ru}(\text{dpp})_2\text{PIC}]^{2+}$ peptide conjugates show cytotoxicity greater than 60% at 300 $\mu\text{g}/\text{ml}$, whereas the $[\text{Ru}(\text{bpy})_2\text{PIC}]^{2+}$ peptide conjugates at the same concentration shown less than 10% cytotoxicity.

The $[\text{Ru}(\text{dpp})_2\text{PIC}]^{2+}$ peptide conjugates induces cellular toxicity (in CHO cells) at concentrations above 10 μM when incubated overnight at 37°C. The most likely origin of this cytotoxicity is due to the more hydrophobic structure of $[\text{Ru}(\text{dpp})_2\text{PIC}]^{2+}$ compared to $[\text{Ru}(\text{bpy})_2\text{PIC}]^{2+}$. The $[\text{Ru}(\text{bpy})_2\text{PIC}]^{2+}$ does not induce significant cytotoxicity up to doses of 150 μM , as previously shown by our group. $\text{Ru}(\text{bpy})_2\text{PIC}$ -peptide conjugates did not induce cytotoxicity in CHO cells, this is consistent with $\text{Ru}(\text{bpy})_2\text{PIC}$ -octaarginine which also induced no cytotoxicity up to 140 μM . Furthermore the parent complexes of each conjugate act in a similarly toxic or non-toxic fashion to the chromophore peptide conjugates indicating that the toxicity is not due to the peptide moiety. Further cytotoxicity testing is ongoing and will give us insightful relationships with apoptosis vs necrosis pathways. The relatively low cytotoxicity of the $[\text{Ru}(\text{bpy})_2\text{PIC}]^{2+}$ complex further supports its value for use as a molecular probe for multimodal imaging purposes, where as the $[\text{Ru}(\text{dpp})_2\text{PIC}]^{2+}$ complex is less likely to valid as a probe but further investigated as a therapeutic agent.



**Figure 3. 16 Cytotoxicity assay with CHO cells treated with Chromophore-peptide conjugates
(Data collected by Dr. Róisín Moriarty)**

3.7 Conclusions

Chapter 3 detailed the preparation, purification and characterisation of nuclear localisation peptides, NF-κB and SV-40, and their conjugation to ruthenium (II) polypyridyl chromophores using techniques of solid phase peptide synthesis. The effect of the linker between the metal complex and the peptide was also investigated with β-alanine, a 2 carbon linker and 6-amino-hexanoic acid, a 5 carbon linker when the nuclear localisation signal peptide is NF-κB. The synthesis of the chromophore-peptides proceeded with good yields. Their purification induced minor complications in some cases with oxidation of methionine residues but was overcome by performing the cleavage under nitrogen and purifications under controlled conditions. Purifications took place on a C18 column on HPLC with purities > 85%. The hydrophobicity of the $[\text{Ru}(\text{dpp})_2\text{PIC}]^{2+}$ peptide conjugates was reflected in the longer retention times of these complexes compared to the $[\text{Ru}(\text{bpy})_2\text{PIC}]^{2+}$ peptide conjugates as expected for this HPLC system. Characterisation was conducted using MALDI-TOF and High Resolution Mass Spectroscopy and all values conformed very well to expected values.

The photophysics of the conjugates were similar to those of the parent chromophores. The wavelength of the MLCT of all the Ru(II) polypyridyl peptide conjugates was $\sim 458\text{nm}$. The emission wavelength of the $[\text{Ru}(\text{dpp})_2\text{PIC}]^{2+}$ peptide conjugates was centred at 615nm and $[\text{Ru}(\text{bpy})_2\text{PIC}]^{2+}$ peptide conjugates was centred at 607nm . The lifetimes for the $[\text{Ru}(\text{dpp})_2\text{PIC}]^{2+}$ peptide conjugates were longer than the corresponding $[\text{Ru}(\text{bpy})_2\text{PIC}]^{2+}$ peptide conjugates and the de-aerated lifetimes were longer for all Ru(II) polypyridyl peptide conjugates than the aerated samples.

Prior to peptide conjugation, neither parent complex was capable of sufficient transport across the cell membrane of CHO cells. However once both Ru(II) chromophores were coupled to the NF- κ B sequence, the complex conjugates underwent diffusion across the cell membrane of CHO cells and their uptake were not affected by the length of the linker. For NF- κ B this led to the localisation of the dyes within the cells' nucleus. Confocal fluorescence microscopy was used to determine the distribution of the dyes throughout the cells. Co-staining with a nuclear stain and fluorescent profiling confirmed nuclear localisation.

The $[\text{Ru}(\text{bpy})_2\text{PIC-SV-40}]$ conjugate did not exhibit efficient transport across the membrane. This indicates that SV-40 is not a good carrier for such complexes. However it still may be a nuclear localising peptide and further studies would be required, such as attaching a CPP or permeabilising the cells. Its corresponding $[\text{Ru}(\text{dpp})_2\text{PIC-SV-40}]$ did penetrate the cell membrane however we believe that this occurred through its disruption of the membrane, eventually leading to cell death. This is supported by the preliminary cytotoxicity studies which showed the $[\text{Ru}(\text{dpp})_2\text{PIC}]^{2+}$ peptide conjugates have higher cytotoxicity than the corresponding $[\text{Ru}(\text{bpy})_2\text{PIC}]^{2+}$ peptide conjugates.

The $[\text{Ru}(\text{bpy})_2\text{PIC}]^{2+}$ peptide conjugates show promise as imaging agents. They also exhibit efficient nuclear localisation and low cytotoxicity. The $[\text{Ru}(\text{dpp})_2\text{PIC}]^{2+}$ peptide conjugates do not appear to be as useful as imaging agents as the $[\text{Ru}(\text{bpy})_2\text{PIC}]$ polypyridyl peptide conjugates due to their higher toxicity. The $[\text{Ru}(\text{dpp})_2\text{PIC}]^{2+}$ peptide conjugates also remain mainly associated with the cell membrane. This suggests that the toxic nature of the dye occurs through its interference with the cell membrane. The ability of its conjugates to impart nuclear localization is affected by the nature of the cargo, with larger and more positively charged ruthenium complex being more difficult to direct than smaller ones. The $[\text{Ru}(\text{dpp})_2\text{PIC}]^{2+}$ peptide conjugates may be useful in therapeutics if their effects on the cell membrane could be alleviated and if their accumulation in the nucleus result in the apoptosis of cancer cells. The specific localisation of the $[\text{Ru}(\text{dpp})_2\text{PIC}]^{2+}$ requires further

investigation as it appears to be concentrated within the nucleus. NF- κ B proved to be a highly efficient NLS and was independent of its cargo. SV-40 was inefficient as a universal carrier peptide. The work would also need to be completed on a range of cell lines.

References

- [1] Jamur, M. C.; Oliver, C., *Methods Mol Biol*, (2010) **588**, 63.
- [2] Neugebauer, U.; Pellegrin, Y.; Devocelle, M.; Forster, R. J.; Signac, W.; Moran, N.; Keyes, T. E., *Chem Commun (Camb)*, (2008), 5307.
- [3] Cosgrave, L.; Devocelle, M.; Forster, R. J.; Keyes, T. E., *Chem Commun (Camb)*, (2010) **46**, 103.
- [4] Merrifield, R. B., *Journal of the American Chemical Society*, (1963) **85**, 2149.
- [5] Ragin, A. D.; Morgan, R. A.; Chmielewski, J., *Chemistry & Biology*, (2002) **9**, 943.
- [6] Ragin, A. D.; Chmielewski, J., *The Journal of Peptide Research*, (2004) **63**, 155.
- [7] Neugebauer, U.; Pellegrin, Y.; Devocelle, M.; Forster, R. J.; Signac, W.; Moran, N.; Keyes, T. E., *Chemical Communications*, (2008), 5307.
- [8] Pietrzak, M.; Rempala, G.; Nelson, P. T.; Zheng, J.-J.; Hetman, M., *PLoS ONE*, (2011) **6**, e22585.
- [9] Pyper, J. M.; Clements, J. E.; Zink, M. C., *J Virol*, (1998) **72**, 7697.
- [10] Munoz, M. A.; Pacheco, A.; Becker, M. I.; Silva, E.; Ebensperger, R.; Garcia, A. M.; De Ioannes, A. E.; Edwards, A. M., *J Photochem Photobiol B*, (2011) **103**, 57.
- [11] Araki, M.; Maeda, M.; Motojima, K., *Eur J Pharmacol*, (2012) **674**, 95.
- [12] Yui, S.; Kanamoto, R.; Saeki, T., *Nutr Cancer*, (2009) **61**, 374.
- [13] Anoopkumar-Dukie, S.; Carey, J. B.; Conere, T.; O'Sullivan, E.; van Pelt, F. N.; Allshire, A., *British Journal of Radiology*, (2005) **78**, 945.

Chapter 4:

**Preparation and Characterisation of
overlapping peptides of BH3
Interacting Domain Death Agonist
(BID)**

4.1 Introduction

Different from other pro-apoptotic Bcl-2 family members, BH3 interacting domain death agonist (BID) has evolved unique functions both in apoptosis signalling^[1, 2] and in the control of cell cycle progression.^[3, 4] BID is a 22-kDa pro-apoptotic member of the Bcl-2 family containing only the BH3 domain. BID protein usually exists in an inactive form in the cytoplasm and is inhibited by Bcl-2, but upon cleavage by activated caspase-8, truncated Bid (tBid) translocates to the mitochondria.^[5, 6] In response to apoptotic signalling, BID interacts with another pro-apoptotic protein (Bax), leading activated Bax and/or Bak to form pores that disrupt mitochondrial membrane integrity. These events precede the activation of two distinct apoptotic pathways: caspase-dependent and caspase-independent cell death pathways.^[7] This results in the release of cytochrome c^[8] and other pro-apoptotic factors from the mitochondria, often referred to as mitochondrial outer membrane permeabilization, leading to activation of caspases and ultimately causing cell death.^[9, 10] The translocation of apoptosis-inducing factor (AIF) from the mitochondria to the nucleus triggers the caspase-independent cell death pathway. At the nucleus DNA fragmentation and apoptosis occurs by an unknown, caspase-independent mechanism.^[11, 12] Therefore BID is a key factor in apoptosis as shown in Chapter 1.

For this work peptides from the BID protein were selected as targets. The long term objective of this study was to identify if any peptide sequence fulfilled the BID function outside of the protein. They were prepared for study by the group Prof. Jochen Prehn in the Department of Physiology and Medical Physics at the Royal College of Surgeons in Ireland. The protein sequence is shown in Figure 4. 1. Studies have shown that the interaction of BH3 peptides derived from BAD with Bcl-XL depend dramatically on the length of the peptide. Results show that the 25 residue long BH3 (BAD) forms additional interactions with Bcl-XL compared with the 16-mer BH3 (Bak) peptide.^[6] It has also been shown that the length of the peptide affects its helix propensity.^[13] Therefore in preparing overlapping peptides, the sequence of the protein was broken down into peptides of around 20-25 amino acids long, depending on the anticipated difficulty of synthesis of the sequence (Table 4. 1). The cysteine (C) residues were replaced with serine (S) to avoid disulphide bridge formation and oxidation.

MDCEVNGSSLRDECITNLLVFGFLQSCSDNSFRRELDALGHELPVLAPQWEGYDELQTD GNRSSHSRLGRIEADSESQEDIIRNIARHLAQVGDSMDRSIPPGLVNGLALQLRNTSRSE EDRNRDLATALEQLLQAYPRDMEKEKTMLVLALLAKKVASHTPSLLRDVFHTTVNFINQ NLRTYVRSRLARNGMD
--

Figure 4. 1 BH3-interacting domain death agonist amino acid sequence.^[14]

Table 4. 1 Overlapping sequences of truncated BID that was synthesized

BID 1-20	MDSEVNNGSSLRDESITNLL
BID 18-36	TNLLVFGFLQSSSDNSFRR
BID 29-48	SDNSFRRELDALGHELPVLA
BID 46-64	VLAPQWEGYDELQTDGNRS
BID 62-82	NRSSHSRLGRIEADSESQEDI
BID 78-101	SQEDIIRNIARHLAQVGDSMDRSI
BID 97-117	MDRSIPPGLVNGLALQLRNTS
BID 116-137	TSRSEEDRNRDLATALEQLLQA
BID 137-157	AYPRDMEKEKTMLVLALLAK
BID 155-177	LAKKVASHTPSLLRDVFHTTVNF
BID 175-195	VNFINQNLRTYVRSLARNGMD

4.2 Experimental Details for the synthesis of BID peptides

4.2.1 Preparation of biotinylated BID 01-20



Synthesis of biotinylated BID 01-20 took place on the ABI 433A synthesizer by standard SPPS as far as V¹⁷, from a Nova Peg Rink Amide Resin (scale 0.25mmol, substitution 0.5mmol/g). Fmoc-Ser(*t*Bu)-OH, Fmoc-Gly-OH, Fmoc-Asn(Trt)-OH, Fmoc-Val-OH, Fmoc-Glu(*O**t*Bu)-OH, Fmoc-Asp(*O**t*Bu)-OH, Fmoc-Met-OH and Fmoc- β Ala-OH

were then manually assembled by HATU (5eq) / DIEA (10eq) coupling chemistry. The synthesis was monitored by the qualitative Kaiser test and double coupling procedures applied when required. The coupling times were 3 hrs. Usual conditions of manual Fmoc deprotection and washes were performed as outlined in Chapter 2. Manually coupling of biotin took place using PyBOP/HOBt (3eq) / DIEA (6eq) coupling chemistry. The peptide was finally cleaved by standard methods and then purified by RP-HPLC. Fractions were collected by semi-preparative HPLC, C18 column with gradient H₂O:ACN mobile phase and were analysed by mass spectrometry.

MALDI-MS 2489.54 [M+1]⁺ calculated for C₁₀₁H₁₇₀N₃₀O₄₀S₂ 2490.766 (Appendix Figure 9)
Purity: 83% (Appendix Figure 10)

4.2.2 Preparation of biotinylated BID 18-36



The biotinylated BID 18-36 peptide was assembled as far as G²³ on the synthesizer, 0.25mmol of Rink Amide MBHA Resin (substitution 0.7mmol/g) was used. Fmoc-Phe-OH, Fmoc-Val-OH, Fmoc-Leu-OH, Fmoc-Asn(Trt)-OH, Fmoc-Thr(tBu)-OH and Fmoc-βAla-OH were manually assembled by HBTU/HOBt (5eq) / DIEA (10eq) coupling chemistry. The synthesis was followed by Kaiser test and double coupling procedures applied when required. The coupling times were 3hrs. Usual conditions of manual Fmoc deprotection and washes were performed as outlined in Chapter 2. Manually coupling of biotin took place using PyBOP/HOBt (3eq) / DIEA (6eq) coupling chemistry. The peptide is cleaved by normal methods and then purified as usual by RP-HPLC. Fractions were collected by semi-preparative HPLC, C18 column with gradient H₂O:ACN mobile phase and were analysed by mass spectrometry.

MALDI-MS 2486.1 [M+1]⁺ calculated for C₁₁₉H₁₉₂N₃₈O₃₆S₂ 2484.833 (Appendix Figure 11).

Purity: 72%(Appendix Figure 12)

4.2.3 Preparation of biotinylated BID 29-48



Synthesis of biotinylated BID 29-48 took place on the ABI 433A synthesizer by standard SPPS as far as A³⁹, 0.1mmol of PEG Fmoc Rink Amide (substitution 0.5mmol/g) was used. Fmoc-Asp(OtBu)-OH, Fmoc-Leu-OH, Fmoc-Glu(OtBu)-OH, Fmoc-Arg(Pbf)-OH, Fmoc-Phe-OH, Fmoc-Ser(tBu)-OH, Fmoc-Asn(trt)-OH and Fmoc- β Ala-OH were manually assembled by HBTU/HOBt (5eq) / DIEA (10eq) coupling chemistry. The synthesis was followed by Kaiser Test and double coupling procedures applied when required. The coupling times were 3hrs. Usual conditions of manual Fmoc deprotection and washes were performed as outlined in Chapter 2. Manually coupling of biotin took place using PyBOP/HOBt (3eq) / DIEA (6eq) coupling chemistry. The peptide is cleaved by normal methods and then purified as usual by RP-HPLC. Fractions were collected by semi-preparative HPLC, C18 column with gradient H₂O:ACN mobile phase and were analysed by mass spectrometry.

MALDI-MS 2535.30 [M+1]⁺ calculated for C₁₁₀H₁₇₇N₃₃O₃₅S 2535.88 (Appendix Figure 13).
Purity: 74 % (Appendix Figure 14)

4.2.4 Preparation of biotinylated BID 46-64



Synthesis of biotinylated BID 46-64 took place on the ABI 433A synthesizer by standard SPPS as far as G⁶¹; 0.1mmol of Nova Peg Rink Amide Resin (substitution 0.5mmol/g) was used. Fmoc-Asp(OMpe)-OH (D⁶⁰), Fmoc-Thr(tBu)-OH, Fmoc-Gln(trt)-OH, Fmoc-Leu-OH, Fmoc-Glu(OtBu)-OH, Fmoc-Asp(OtBu)-OH, Fmoc-Tyr(tBu)-OH, Fmoc-Gly-OH, Fmoc-Trp(tBu)-OH, Fmoc-Pro-OH, Fmoc-Ala-OH, Fmoc-Val-OH and Fmoc- β Ala-OH were manually assembled by HBTU/HOBt (5eq) / DIEA (10eq) coupling chemistry. The synthesis was followed by Kaiser Test and double coupling procedures applied when required. The coupling times were 3hrs. Usual conditions of manual Fmoc deprotection and washes were performed as outlined in Chapter 2. Manually coupling of biotin took place using PyBOP/HOBt (3eq) / DIEA (6eq) coupling chemistry. The peptide is cleaved by normal methods and then purified as usual by RP-HPLC. Fractions were

collected by semi-preparative HPLC, C18 column with gradient H₂O:ACN mobile phase and were analysed by mass spectrometry.

MALDI-MS 2476.1 [M+1]⁺ calculated for C₁₀₇H₁₆₂N₃₀O₃₇S₂ 2474.705 (Appendix Figure 15).

Purity: 90% (Appendix Figure 16)

4.2.5 Preparation of biotinylated BID 62-82



Synthesis of biotinylated BID 62-82 took place on the ABI 433A synthesizer by standard SPPS as far as R⁶⁸, 0.1mmol of Nova Peg Rink Amide Resin (substitution 0.5mmol/g) was used. Fmoc-Ser(tBu)-OH, Fmoc-His(trt)-OH, Fmoc-Arg(Pbf)-OH, Fmoc-Asn(trt)-OH and Fmoc-βAla-OH were manually assembled by HBTU/HOBt (5eq) / DIEA (10eq) coupling chemistry. The synthesis was followed by Kaiser test and double coupling procedures applied when required. The coupling times were 3hrs. Usual conditions of manual Fmoc deprotection and washes were performed as outlined in Chapter 2. Manually coupling of biotin took place using PyBOP/HOBt (3eq) / DIEA (6eq) coupling chemistry. The peptide is cleaved by normal methods and then purified as usual by RP-HPLC. Fractions were collected by semi-preparative HPLC, C18 column with gradient H₂O:ACN mobile phase and were analysed by mass spectrometry.

MALDI-MS 2683.79 [M+1]⁺ calculated for C₁₀₇H₁₇₂N₃₈O₄₂S 2682.882 (Appendix Figure 17).

Purity: 72% (Appendix Figure 18)

4.2.6 Preparation of biotinylated BID 78-101



Biotinylated BID 78-101 was fully assembled by automated synthesis (ABI 433A) using 0.1mmol of Nova PEG Rink Amide Resin (substitution 0.7mmol/g). All amino acids were standard, however for D⁹⁵ Fmoc-Asp (OMpe)-OH was used to prevent aspartimide formation. Manually coupling of biotin took place on the resin using PyBOP/HOBt (3eq) / DIEA (6eq) coupling chemistry. The peptide is cleaved by standard methods and the crude peptide was purified by HPLC, C18 column with gradient H₂O:ACN mobile phase and analysed by mass spectrometry.

MALDI-MS 3021.16 [M+1]⁺ calculated for C₁₂₅H₂₁₀N₄₂O₄₁S₂ 3021.44 (Appendix Figure 19).

Purity: 95% (Appendix figure 20)

4.2.7 Preparation of biotinylated BID 97-117



Synthesis of biotinylated BID 97-117 took place on the ABI 433A synthesizer by standard SPPS as far as A¹⁰⁴, 0.1mmol of Nova Peg Rink Amide Resin (substitution 0.5mmol/g) was used. Fmoc-Pro-OH, Fmoc-Ile-OH, Fmoc-Ser (tBu)-OH, Fmoc-Arg (Pbf)-OH, Fmoc-Asp (OtBu)-OH, Fmoc-Met-OH and Fmoc-βAla-OH were manually assembled by HBTU/HOBt (5eq) / DIEA (10eq) coupling chemistry. The synthesis was followed by Kaiser Test and double coupling procedures applied when required. The coupling times were 3hrs. Usual conditions of manual Fmoc deprotection and washes were performed as outlined in Chapter 2. Manually coupling of biotin took place using PyBOP/HOBt (3eq) / DIEA (6eq) coupling chemistry. The peptide is cleaved by normal methods and then purified as usual by RP-HPLC. Fractions collected by semi-preparative HPLC, C18 column with gradient H₂O:ACN mobile phase, were analysed by mass spectrometry.

MALDI-MS 2550.32 [M+1]⁺ calculated for C₁₀₉H₁₈₈N₃₄O₃₃S₂ 2549.03 (Appendix Figure 21).

Purity: 91% (Appendix Figure 22)

4.2.8 Preparation of biotinylated BID 116-137



Synthesis of biotinylated BID 116-137 took place on the ABI 433A synthesizer by standard SPPS as far as A¹²⁸, 0.1mmol of Nova Peg Rink Amide Resin (substitution 0.5mmol/g) was used. Fmoc-Leu-OH, Fmoc-Asp(OtBu)-OH, Fmoc-Arg(Pbf)-OH, Fmoc-Asn(trt)-OH, Fmoc-Glu(OtBu)-OH, Fmoc-Ser(tBu)-OH, Fmoc-Thr(tBu)-OH, and Fmoc- β Ala-OH were manually assembled by HBTU/HOBt (5eq) / DIEA (10eq) coupling chemistry. The synthesis was followed by Kaiser Test and double coupling procedures applied when required. The coupling times were 3hrs. Usual conditions of manual Fmoc deprotection and washes were performed as outlined in Chapter 2. Manually coupling of biotin took place using PyBOP/HOBt (3eq) / DIEA (6eq) coupling chemistry. The peptide is cleaved by normal methods and then purified as usual by RP-HPLC. Fractions were collected by semi-preparative HPLC, C18 column with gradient H₂O:ACN mobile phase and were analysed by mass spectrometry.

MALDI-MS 2812.44 [M-1]⁺ calculated for C₁₁₅H₁₉₆N₃₈O₄₃S 2814.42 (Appendix Figure 23)
Purity: 73 % (Appendix Figure 24)

4.2.9 Preparation of biotinylated BID 137-157



Synthesis of biotinylated BID 137-157 took place on the ABI 433A synthesizer by standard SPPS as far as K¹⁴⁶, 0.1mmol of PS PEG 600 Fmoc Rink Amide MBHA resin (substitution 0.62mmol/g) was used. Fmoc-Glu (OtBu)-OH, Fmoc-Lys (Boc)-OH, Fmoc-Met-OH, Fmoc-Asp (OtBu)-OH, Fmoc-Arg (Pbf)-OH, Fmoc-Pro-OH, Fmoc-Tyr-OH, Fmoc-Ala-OH and Fmoc- β Ala-OH were manually assembled by HBTU/HOBt (5eq) / DIEA (10eq) coupling chemistry. The synthesis was followed by Kaiser Test and double coupling procedures applied when required. The coupling times were 3hrs. E¹⁴³ was coupled by microwave activation using the same coupling chemistry and Fmoc-Glu (OtBu)-OH. Coupling reactions took place for 5 minutes at 50°C with pre-stirring for 30 seconds and with fix hold time on. Absorption level was set to high as NMP was the solvent used. Usual

conditions of manual Fmoc deprotection and washes were performed as outlined in Chapter 2. Manually coupling of biotin took place using PyBOP/HOBt (3eq) / DIEA (6eq) coupling chemistry. The peptide is cleaved by normal methods and then purified as usual by RP-HPLC, C18 column with gradient H₂O:ACN mobile phase. Fractions collected by semi-preparative HPLC were analysed by mass spectrometry.

MALDI-MS 2732.35 [M+2]⁺ calculated for C₁₂₃H₂₁₁N₃₁O₃₃S₃ 2730.41 (Appendix Figure 25).

Purity: 97.8 % (Appendix Figure 26)

4.2.10 Preparation of biotinylated BID 155-177



Synthesis of biotinylated BID 155-177 took place on the ABI 433A synthesizer by standard SPPS; 0.1mmol of Rink Amide MBHA Resin (substitution 0.7mmol/g) was used. Manual coupling of biotin took place on the resin using PyBOP/HOBt (3eq) / DIEA (6eq) coupling chemistry. The peptide is cleaved by usual methods and then purified as usual by RP-HPLC, C18 column with gradient H₂O:ACN mobile phase. Fractions collected by semi-preparative HPLC were analysed by mass spectrometry.

MALDI-MS 2878.69 [M+1]⁺ calculated for C₁₃₁H₂₀₉N₃₇O₃₄S 2878.31 (Appendix Figure 27).
Purity: 71 % (Appendix Figure 28)

4.2.11 Preparation of biotinylated BID 175-195



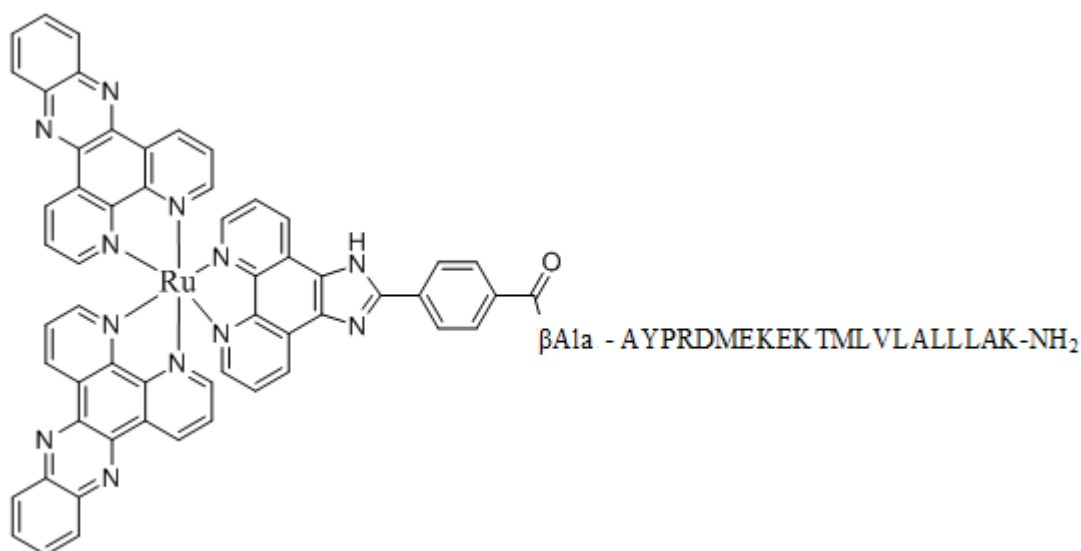
Biotinylated BID 175-195 was assembled as far as L¹⁸² on the synthesizer, 0.1mmol of preloaded (Asp) Wang Resin (substitution 0.7mmol/g) was used. Fmoc-Asn(Trt)-OH, Fmoc-Gln-OH, Fmoc-Ile-OH, Fmoc-Phe-OH, Fmoc-Val-OH and Fmoc-βAla-OH were manually assembled by HBTU/HOBt (5eq) / DIEA (10eq) coupling chemistry. The synthesis was followed by Kaiser Test and double coupling procedures applied when required. The coupling times were 3hrs. N¹⁸¹ was coupled by microwave activation using the same coupling chemistry and Fmoc-Asn (Trt)-OH. Coupling reactions took place for 5 minutes at 50°C with pre-stirring for 30 seconds and with fix hold time on. Usual conditions

of manual Fmoc deprotection and washes were performed and Fmoc deprotection of F and V took place by microwave activation as outlined in Chapter 2. Deprotection reactions took place for 2 minutes at 50°C with pre-stirring for 30 seconds; fix hold time on and absorption were set to high.

Manually coupling of biotin took place using PyBOP/HOBt (3eq) / DIEA (6eq) coupling chemistry. The peptide is cleaved by normal methods and then purified as usual by RP-HPLC. Fractions were collected by semi-preparative HPLC, C18 column with gradient H₂O:ACN mobile phase and were analysed by mass spectrometry.

MALDI-MS 2782.7 [M+2]²⁺ calculated for C₁₁₉H₁₉₂N₃₈O₃₆S₂ 2779.21 (Appendix Figure 29). Purity: 81.6 % (Appendix Figure 30)

4.2.12 Preparation of BID 137-157 conjugated to Ru (dppz)₂PIC

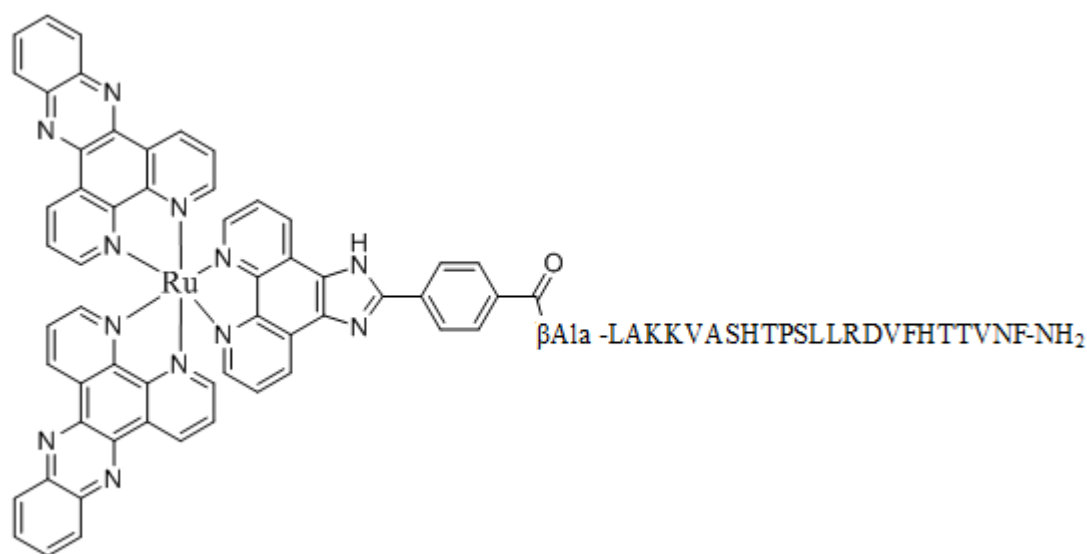


Synthesis of the peptide took place on the ABI 433A synthesizer by standard SPPS as far as K¹⁴⁶; 0.1mmol of Nova Peg Rink Amide Resin (substitution 0.62mmol/g) was used. Fmoc-Glu (OtBu)-OH, Fmoc-Lys (Boc)-OH, Fmoc-Met-OH, Fmoc-Asp (OtBu)-OH, Fmoc-Arg (Pbf)-OH, Fmoc-Pro-OH, Fmoc-Tyr-OH, Fmoc-Ala-OH and Fmoc-βAla-OH were manually assembled by HBTU/HOBt (5eq) / DIEA (10eq) coupling chemistry. The synthesis was followed by Kaiser Test and double coupling procedures applied when required. The coupling times were 3hrs. E¹⁴³ was coupled by microwave activation using

the same coupling chemistry and Fmoc-Glu (OtBu)-OH. Usual conditions of manual Fmoc deprotection and washes were performed. Manually coupling of $[\text{Ru}(\text{dppz})_2\text{PIC}]^{2+}$ took place using PyBOP (3eq) / DIEA (6eq) coupling chemistry, with $[\text{Ru}(\text{dppz})_2\text{PIC}]^{2+}$, PyBOP and DIEA allowed to react for 3 minutes before adding the peptide on resin. The peptide is cleaved by normal methods and then purified as usual by RP-HPLC. Fractions collected by semi-preparative HPLC were analysed by mass spectrometry MALDI-TOF.

MALDI-MS 3492.4609 $[\text{M}+1]^+$ calculated for $\text{C}_{169}\text{H}_{227}\text{N}_{41}\text{O}_{32}\text{SRu}$ 3492.1035 (Figure 4.9).

4.2.13 Preparation of BID 155-177 conjugated to Ru (dppz)₂PIC



Synthesis of the peptide took place on the ABI 433A synthesizer by standard SPPS; 0.1mmol of Rink Amide MBHA Resin (substitution 0.7mmol/g) was used. Manual coupling of $[\text{Ru}(\text{dppz})_2\text{PIC}]^{2+}$ took place on the resin using PyBOP/HOBt (3eq) / DIEA (6eq) coupling chemistry. The peptide is cleaved by usual methods and then purified as usual by RP-HPLC. Fractions collected by semi-preparative HPLC were analysed by mass spectrometry, MALDI-TOF.

MALDI-MS 3640.4919 $[\text{M}+1]^+$ calculated for $\text{C}_{177}\text{H}_{227}\text{N}_{47}\text{O}_{34}\text{Ru}$ 3640.0985(Appendix Figure 31).

Purity: 85% (Appendix Figure 32).

4.3 Results and Discussion

4.3.1 Synthesis

Synthesis of BID peptides was first attempted by automated standard solid phase peptide synthesis using the common amino acid precursors presented in appendix unless otherwise stated. This stepwise elongation, in which the amino acids are connected iteratively, was successful for 2 sequences, BID 155-177 and BID 78-101, the integrity of these peptides was confirmed by mass spectrometry (Appendix: Figure 31 and Figure 23 respectively). For the other BID sequences with a higher content of hydrophobic residues this method failed. This can be seen by the deprotection traces on the automated peptide synthesizer. As mentioned in Chapter 2, the peptide sequences were assembled with monitoring of the Fmoc deprotection by UV absorption at 301nm. The synthesizer removes the Fmoc and monitors the amount of dibenzofulvene-piperidine adduct form by UV as seen in Figure 4. 2. It then performs a second deprotection step of the Fmoc. The Fmoc quantity removed in the second deprotection should be less than 3.5% of the first peak. If this level is reached, the synthesiser will move on to the next amino acid and coupling step. This is seen in Figure 4. 2 for amino acids X1 to X6. However if the quantity of dibenzofulvene formed is not sufficiently low the automated synthesizer will repeat the deprotection step, up to a maximum of 5 deprotections, as shown in Figure 4. 2 for amino acids X7 to X10. After this the synthesizer will move on to the next amino acid in the sequence to be coupled regardless of the final deprotection trace. From these traces we can see where a break down occurred in the synthesis of the peptides. In the case of Figure 4. 2 this was X7 and that is where the manual coupling would begin on the second synthetic attempt.

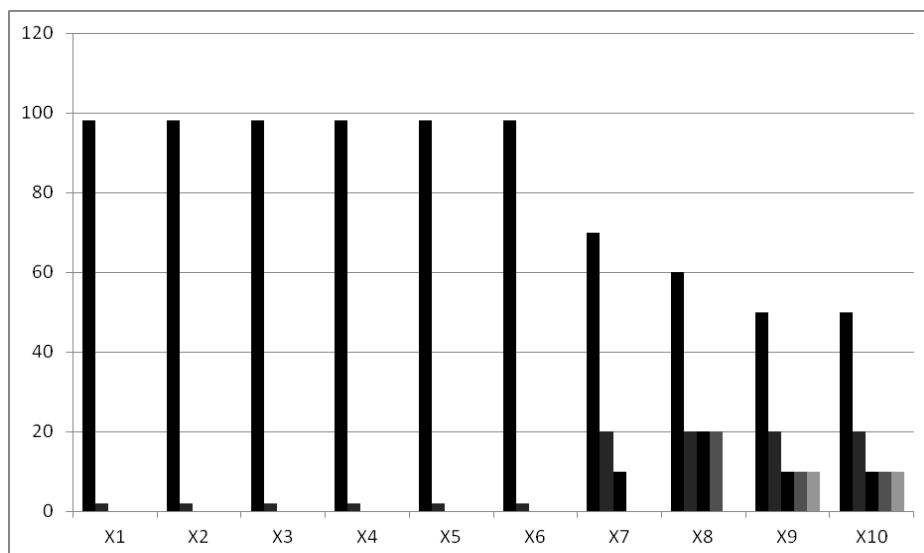


Figure 4. 2 Representation of Fmoc removal trace from an Applied Biosystem ABI 433A Synthesizer monitored by UV at 301nm. Amino acids X1-X6 have a successful deprotection trace whereas for amino acids X7-X10 the deprotection becomes sluggish with the last two amino acids receiving maximum deprotection.

As the peptide is elongated, it can form secondary structures such as β -sheets and aggregates either with other peptide chains or with the polymer support, which can result in turn in lower reaction rates. The effects can range from just a subtle slowing down to a complete failure of both deprotection and coupling reactions. The ease of assembly of a particular sequence is generally hard to predict, although peptides containing stretches of continuous hydrophobic and/or branched amino acids like Ala, Val, Ile, as well as those containing residues which can form intra-chain hydrogen bonding such as Gln, Ser and Thr are frequently difficult to make. When automated synthesis proves to be unsuitable for the assembly of difficult sequences, other methods were examined, such as manual synthesis, microwave-assisted synthesis and more efficient coupling reagents and resins.

Manual synthesis was performed when a sequence could not be fully elongated on the synthesizer. The sequence was assembled on the synthesiser up to the longest stretch of hydrophobic amino acid routinely assembled by automated synthesis and then transferred to a syringe for completion by manual synthesis as described in 2.2. This method allowed the use of longer reaction times and higher equivalents of amino acids and coupling reagents to force the reaction to completion. Both the coupling and deprotection reactions were monitored by Kaiser test, based on the formation of a blue adduct by reaction of ninhydrin (2,2-dihydroxyindane-1,3-dione) with a primary amino group.^[15] A Kaiser test is used to monitor reactions in peptide synthesis and can be performed on a resin for solid phase synthesis. A deprotected amino acid yields a positive Kaiser test indicated by the blue

coloration of the resin. Conversely, a negative Kaiser test (colourless or yellow resin) indicates the successful coupling of a N-protected amino acid or an unsuccessful deprotection of a Fmoc group.

When this elongation of the peptide sequence became difficult, as shown by mixed results from a Kaiser test, coupling and deprotection reactions were completed in the Biotage Initiator 2.5 microwave synthesizer. This was carried out for BID 175-195, residue 176 (N) and BID137-157, residue 143 (E). The parameters of the coupling reaction were based on the recommendations of the manufacturer of the microwave synthesizer. Pre-stirring between 30 seconds and 1 minute was found to improve the outcomes of the reactions. This is consistent with results reported by Coantic et al., who demonstrated the importance of maintaining stirring during Microwave-assisted Solid Phase Peptide Synthesis (MW-SPPS) on high loaded resins.^[16] Fixed hold time, which means that the time duration of the reaction did not start until the reaction temperature was reached, was also selected. Microwave coupling was successful for the amino acids that could not be coupled otherwise as outlined in Section 4.2. It was used in a similar fashion for deprotection reactions. Peptide synthesis was completed using the general methods outlined in Chapter 2.6 and the general methods outlined below.

4.3.2 Coupling Reagents

When the reactions remained unsuccessful, despite microwave activation, the resin or the coupling reagents had to be changed. Initially 2-(1H-benzotriazole-1-yl)-1, 1, 3, 3-tetramethyl-uronium-hexafluoro-phosphate (HBTU) (Figure 4. 3a) was used as the coupling reagent for both automated and manual syntheses, including microwave-assisted couplings (Figure 4. 4). The next amino acid to be added in the sequence is deprotonated by the base introduced with the coupling reagent and can then react with the latter to form an active ester as seen in Figure 4.4. This ester intermediate reacts with a polymer-bound amino deprotected residue. This is one of the most common coupling reagents that form an active hydroxybenzotriazole (HOBt) ester.

Other uronium couplings reagents, such as 2-(1H-7-azabenzotriazol-1-yl)-1,1,3,3-tetramethyl uronium hexafluorophosphate (HATU) (Figure 4. 3b), are also available that that can facilitate the reaction of the active ester, through the hypothetical formation of

hydrogen bonds between the HATU's aza group and the amino group of the incoming amino acid.^[17, 18] The coupling reagent HATU is a highly efficient coupling reagent for solid- and solution-phase peptide synthesis. In comparative studies HATU has been found to give better coupling yields with less racemisation than HBTU, TBTU, or PyBOP. HATU in the presence of a base convert carboxylic acids to the corresponding HOAt esters. Such esters are also more reactive than their HOBt counterparts owing to the lower pKa of HOAt as compared to HOBt. However owing to its cost, its use is generally only recommended for difficult and hindered couplings and the synthesis of long peptides.

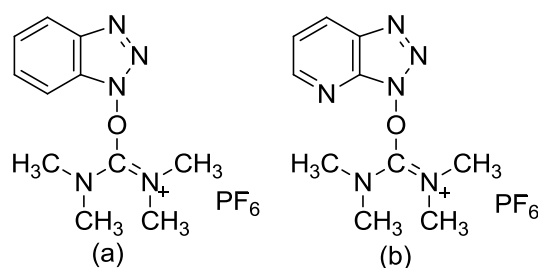


Figure 4. 3: (a) HBTU (b) HATU (uronium) coupling reagents

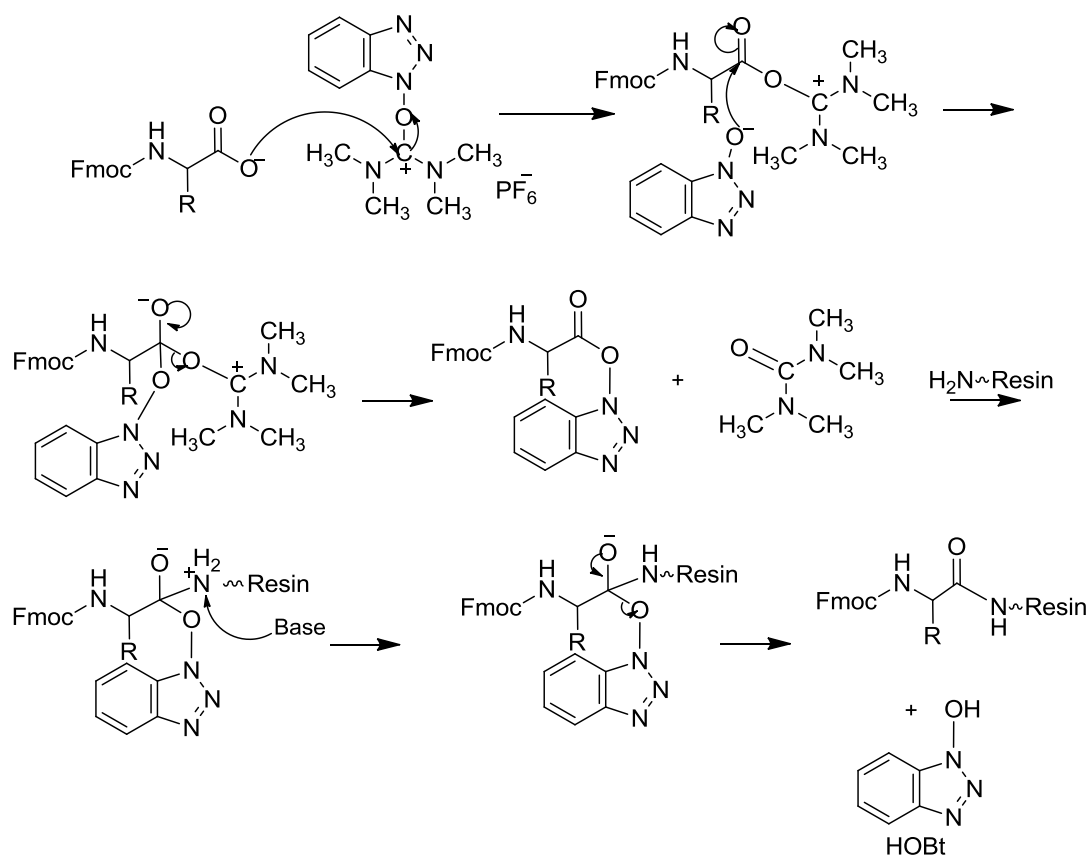


Figure 4. 4: Mechanism of HBTU/HOBt mediated coupling reaction

4.3.3 Resin

The common solid support for the synthesis of peptide amides is the Rink Amide MBHA resin. It contained a modified Rink amide linker that incorporated an acetic acid spacer that is not degraded by TFA and therefore compatible with the standard 95% TFA cleavage reaction. Rink amide MBHA resin is a polystyrene resin cross-linked with 1-2% divinylbenzene and can therefore promote aggregation of hydrophobic sequences. Nova PEG Rink Amide resin was used for these difficult sequences. Nova PEG Rink Amide resin contains the same linker but is based on PEG which provides excellent swelling, including in protic solvents, and mechanical properties to the polymeric support. Nova PEG resins have excellent chemical stability, particularly towards strong acids and bases. The amphiphilic nature of this resin makes it an excellent support for the synthesis of difficult, aggregated peptides and of long peptides.^[19] It has also been shown to increase in general the yield and purity of peptides prepared by SPPS, compared to polystyrene-based resins.^[19]

4.3.4 Aspartimide Formation

The most frequently encountered side-reaction affecting aspartic acid residues during solid phase synthesis is aspartimide formation, resulting from ring closure between the nitrogen of the amide bond and the β -carboxy side chain with loss of the ester protecting group. This problem is particularly significant in SPPS according to the Fmoc strategy, as cyclisation is promoted by bases, such as piperidine, used to remove the Fmoc group. The Asp-Gly sequence is particularly prone to aspartimide formation, which is estimated to occur to the extent of approximately 0.5% per Fmoc deprotection cycle (Figure 4. 5).^[20] The problem is most serious in long peptides, as the degree of aspartimide formation is dependent on the total exposure time to piperidine but can be reduced by using Fmoc-Asp (OMpe)-OH. By substituting OtBu for the more bulky OMpe group in the synthesis of a model Asp-Gly containing peptide, formation of aspartimide related by-products (β -branched and diastereoisomeric peptides) can be reduced considerably. This was adopted for the BID BH3 domain (78-101) which had an Asp-Gly motif near the C-terminus and therefore exposed to repetitive deprotection procedures.

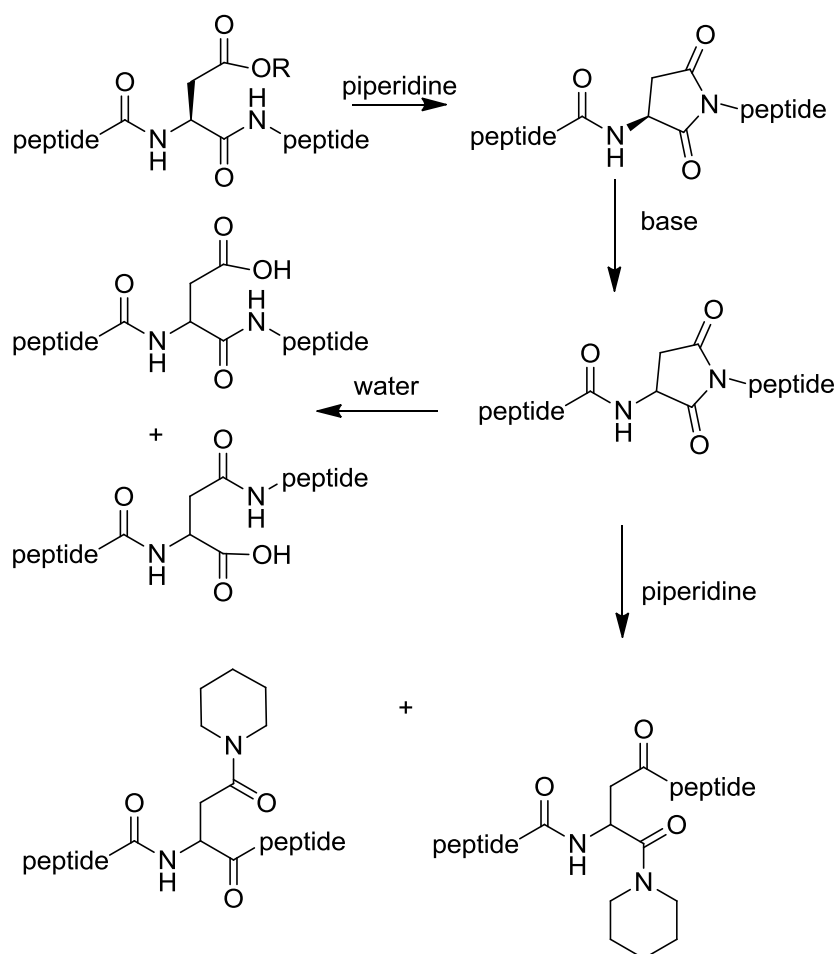


Figure 4. 5 Mechanism for aspartimide-related by-products formation

4.3.5 Selecting BID sequences for studies with oxygen-sensitive probes

Two of the BID sequences were selected for initial investigation of the chemistry required for their conjugation to a Ru (II) polypyridal probe. The two sequences chosen were BID 137-157 and BID 155-177, as they had the highest content of hydrophobic amino acids. BID 137-157 and BID 155-177 had 57% and 50% of hydrophobic residues, respectively. To ensure consistency in the linker selected for the future labelling of all the BID sequences, these least soluble sequences were chosen to determine if a hydrocarbon-based linker could be introduced between the peptide sequence and the probe, while maintaining the solubility of the conjugate in aqueous buffers. A PEG-based linker would otherwise be required to enhance this solubility.

Guidelines for hydrophobicity and solubility of peptides were taken from GenScript^[21]:

1. Peptides that are shorter than 5 residues are generally soluble in aqueous media, except where all the residues are very hydrophobic.
2. Hydrophilic peptides containing >25% charged residues and <25% hydrophobic residues also generally dissolve in aqueous media, provided that the charged residues are fairly evenly distributed throughout the sequence.
3. Hydrophobic peptides containing 50% to 75% hydrophobic residues may be insoluble or only partially soluble in aqueous solutions, even if the sequence contains 25% charged residues.
4. Very hydrophobic peptides containing 75% hydrophobic residues will generally not dissolve in aqueous solutions.

Table 4. 2 Table of BID sequences with acidic basic and hydrophobic residues identified. The % hydrophobicity is also reported. Red: acidic residues, like D and E Blue: basic residues, like R, K and H Green: hydrophobic uncharged residues, like F I L M V W A and P Black: other residues, like G S T C N Q and Y

Name	Peptide Sequence	% Hydrophobicity
BID 1-20	AMDSEVNNGSSLRDESITNLL	33.3
BID 18-36	ATNLLVFGFLQSSSDNSFRR	40.0
BID 29-48	ASDNSFRRELDALGHELPVLA	47.6
BID 46-64	AVLAPQWEGYDELQTDGNRS	35.0
BID 62-82	ANRSSHSRLGRIEADSESQEDI	23.8
BID 78-101	ASQEDIIRNIARHLAQVGDSDRSI	41.7
BID 97-117	AMDRSIPPGLVNGLALQLRNTS	50.0
BID 116-137	ATSRSEEDRNRDLATALEQLLQA	34.8
BID 137-157	AAYPREDMEKEKTMLVLALLAK	59.1
BID 155-177	ALAKKVASHTPSLLRDVFHTTVNF	50.0
BID 175-195	AVNFINQNLRTYVRSLARNGMD	40.9

4.3.6 [Ru(dppz)₂PIC]ClO₄ conjugation

As described in Chapter 1, ruthenium-based probes have many favourable photophysical properties that make them ideal as probes for cellular imaging. Another key advantage of Ru (II) complexes is the capacity to make their photophysical properties dependent on their environment. For example, the sensitivity of the excited state lifetime and hence the phosphorescent intensity to O₂ is well known for many ruthenium complexes.^[22] The probe chosen for studies with BID sequences was Ru(dppz)₂PIC. Ru-dppz has been widely investigated as a probe for nucleic acid structure.^[23] Ruthenium dipyrrophenazine (dppz) complexes were developed as luminescent probes due to their high affinity for DNA, and the “light switch effect” that makes them brightly luminescent in hydrophobic environments and virtually non-luminescent in aqueous solutions.^[24] In aqueous conditions, water quenches this excited state by hydrogen bonding with the phenazine nitrogen atoms but when the dppz is shielded from water the luminescence is activated and the complex effectively acts as if dissolved in an organic solvent.^[25]

Ruthenium (II) complexes have shown potential as luminescent probes for other interactions with biological molecules and structures, such as RNA ^[26, 27] and lipid membranes.^[28-30] Since the photoluminescence lifetime is independent of fluorophore concentration, light intensity and photo-bleaching,^[24] it is an ideal parameter to remotely monitor the local environment of the probe. Ruthenium polypyridyl complexes have been used as oxygen sensing probes,^[31-33] and their ability to monitor the microenvironment may enable probing of cellular events and biomolecular interactions. ^[34] In this study they are intended to be used to investigate the localisation and function of the BID protein. Biotinylated sequences can be used in protein arrays to identify interacting partners and consequently functional regions of the BID protein, while their ruthenium-labelled counterparts would be used to confirm the localisation of these peptides at the mitochondrial membrane, where the (predicted) interacting partners are located.

4.3.7 Method of Synthesis of Ruthenium polypyridyl BID peptide conjugates

Initially coupling took place using the HATU coupling chemistry. This caused the peptide to be capped by the coupling reagent as confirmed by an increased mass of 97 on the mass spectra (Figure 4. 6). It is likely that the steric hindrance of the large Ru complex along with the high reactivity of HATU led to the coupling reagent reacting with the peptide only and terminating the sequence by guanidination (Figure 4.7) without conjugation to the metal complex.

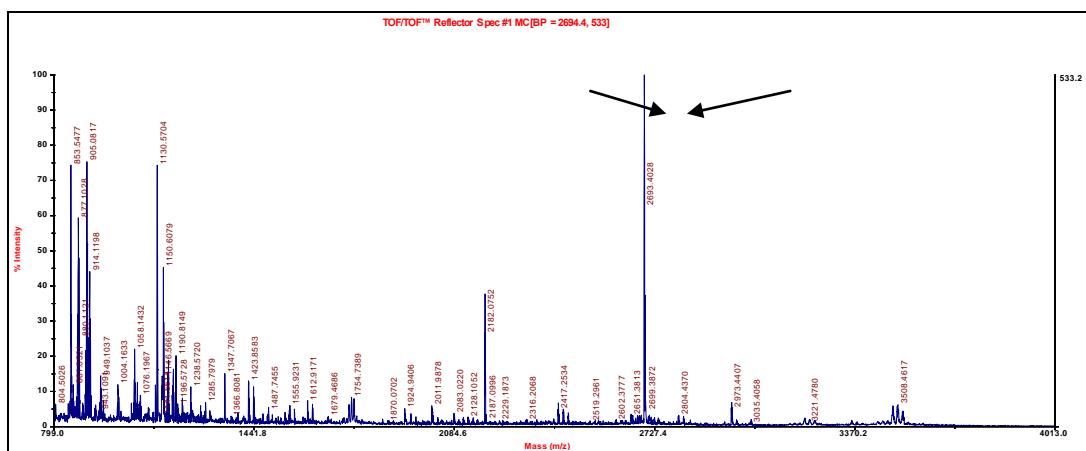


Figure 4. 6: MALDI-TOF of BID 137-157 capped by HATU coupling reagent, using α -cyano-4-hydroxycinnamic acid matrix

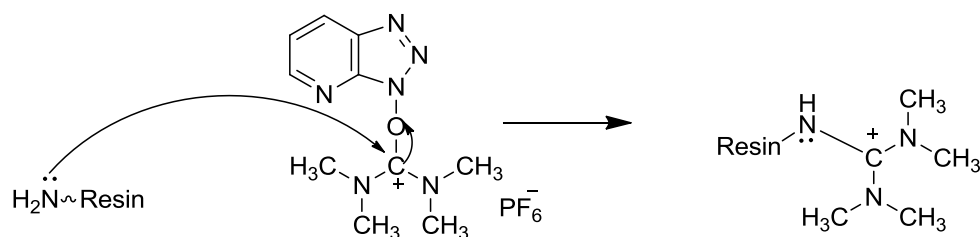


Figure 4.7 Mechanism of HATU termination

The HATU based amide coupling is mediated in two steps; activation and coupling. In the activation step HATU reacts with the deprotonated carboxylic group forming an active intermediate. In the coupling step the created intermediate reacts with the amino component to form the amide. The rate of the first step is regulated by the structural feature of the carboxylic component. In the second step the rate is regulated of characteristics of the amino group and of the coupling reagent.

During the activation of hindered carboxylic components, the aminium salts can react with the amino component, leading to a guanidine derivative, a process that terminates the peptide chain. HATU should not be used in excess because it can react with the unprotected N-terminal and block further chain elongation.

The reaction was attempted by benzotriazol-1-yl-oxytripyrrolidinophosphonium hexafluorophosphate PyBOP coupling chemistry. This resulted in a good yield of pure BID 155-177 coupled to $[\text{Ru}(\text{dppz})_2\text{PIC}]^{2+}$. The BID 137-157 peptide after conjugation to $[\text{Ru}(\text{dppz})_2\text{PIC}]^{2+}$ was poorly soluble in water and made the purification by reverse-phase chromatography more difficult resulting in a lower yield.

4.3.8 Oxidation of Methionine

Methionine, cysteine, tryptophan, tyrosine and histidine residues are vulnerable to oxidation. The oxidation of methionine to the sulfoxide form is of particular concern as it has been shown to occur in a wide variety of peptides and often reduces or eliminates biological activity.^[35] Methionine oxidation is of serious concern when proteins are used as pharmaceuticals because of the potential effects on activity and the likelihood of oxidation during processing or storage.^[36-39] It is acknowledged that side chain substitution can have profound effects on protein stability and structure. In effect oxidation can be regarded as a chemical 'mutagenesis' which substitutes the methionine side chain with methionine

sulfoxide, a larger and more polar side chain (Figure 4. 8). It can significantly disrupt protein structure and stability. ^[40]

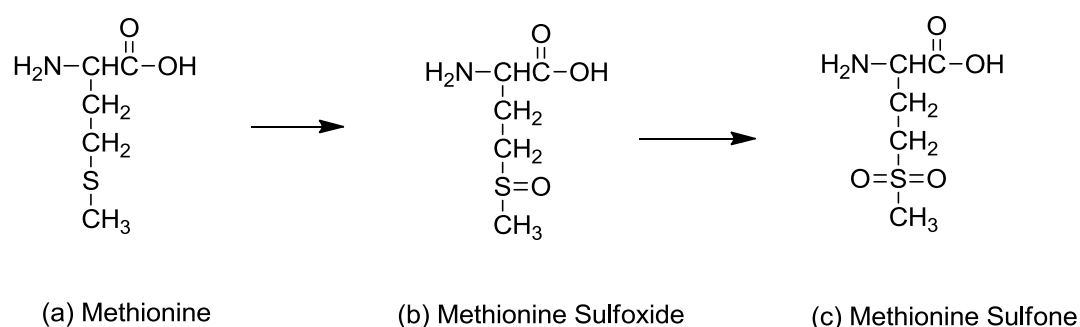


Figure 4. 8 Methionine can be oxidized to methionine sulfoxide and further to methionine sulfone.

A potential approach for protecting a protein against the effects of methionine oxidation is to substitute methionine residues with amino acids which are resistant to oxidation. Although, this may alter the properties of the peptide or protein in question. Oxidation of the methionine residues (M^{46} and M^{52}) in BID 137-157 coupled to Ru (dppz)₂PIC occurred, as shown by mass spectrometry by an increase of 16 in the mass/charge signal of the molecular ion in Figure 4.9. Figure 4.9 shows the isotopic distribution of Ru. The desired Ruthenium polypyridal peptide conjugate has a relative molecular mass of 3,493 and the corresponding signal is seen on the spectrum. The signal at $m/z = 3,509$ indicates one oxidized methionine and at 3,525 suggests the oxidation of the 2 methionines as sulfoxides or of 1 methionine as a sulfone. For future work the replacement of these residues should be considered. The most appealing alternatives for a replacement side chain resistant to oxidation are norvaline and norleucine which are isomers of valine and leucine respectively. Substitution with norvaline removes the sulphur and prevents oxidation, but reduces side chain hydrophobicity and the potential for favourable van der Waals interactions. Norleucine maintains most of the side chain hydrophobicity and steric properties of methionine, but modifies its electronic properties and could therefore potentially affect the structure and activity of the parent sequence. ^[40, 41]

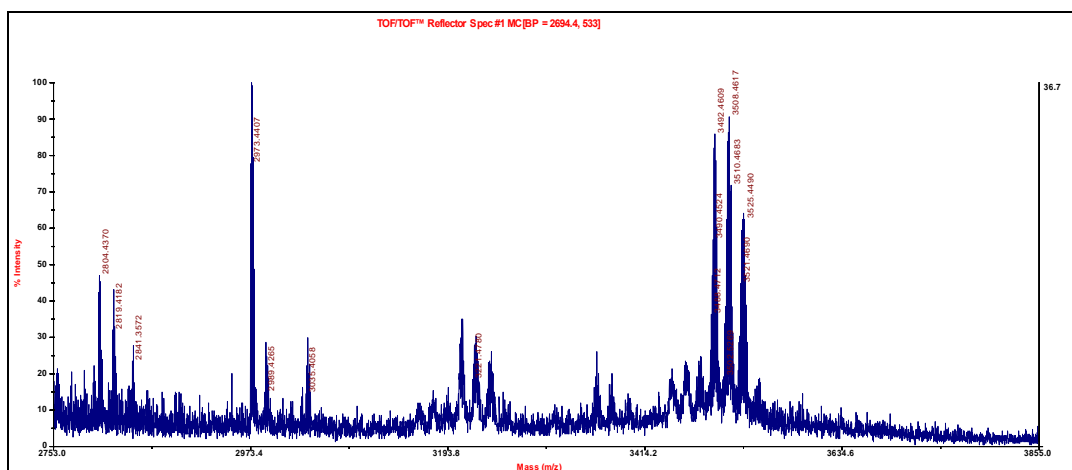


Figure 4. 9: MALDI-TOF of BID 137-157 coupled to $[\text{Ru}(\text{dppz})_2\text{PIC}]^{2+}$ using α -cyano-4-hydroxycinnamic acid matrix showing oxidation of the methionine residues.

4.3.9 Results from chromophore conjugation

BID 137-157 contained the highest quantity of hydrophobic regions out of all the BID sequences synthesized and it also contained two methionine residues. For these reasons the yields were so low that only an analytical sample was obtained for this labelled peptide. Due to time and resources constraints, the synthesis of $\text{Ru}(\text{dppz})_2\text{PIC}$ -BID 155-177 was prioritised.

The UV-VIS spectrum of $\text{Ru}(\text{dppz})_2\text{PIC}$ BID 155-177 recorded in an aqueous solution is shown in Figure 4.10. The same solution did not give an emission spectrum presumably due to the H-bond interactions between the dppz ligands and water. This confirmed that the BID peptide did not confer any protection on the Ru centre from aqueous environment. The UV-VIS spectra is distinguished by a ruthenium π to ligand π^* MLCT transition at 470 nm. The strong absorbance band at approximately 285 nm may be assigned to π - π^* transitions within the polypyridal ligands, whereas the shoulder at approximately 340 nm is attributed to the π - π^* transitions of the carboxy-phenanthroline ligands containing the two ionisable protons on the imidazole ring. The absorbance profile of this conjugate is almost identical to that of the parent complex $[\text{Ru}(\text{dppz})_2\text{PIC}]\text{ClO}_4$ seen by our group previously.

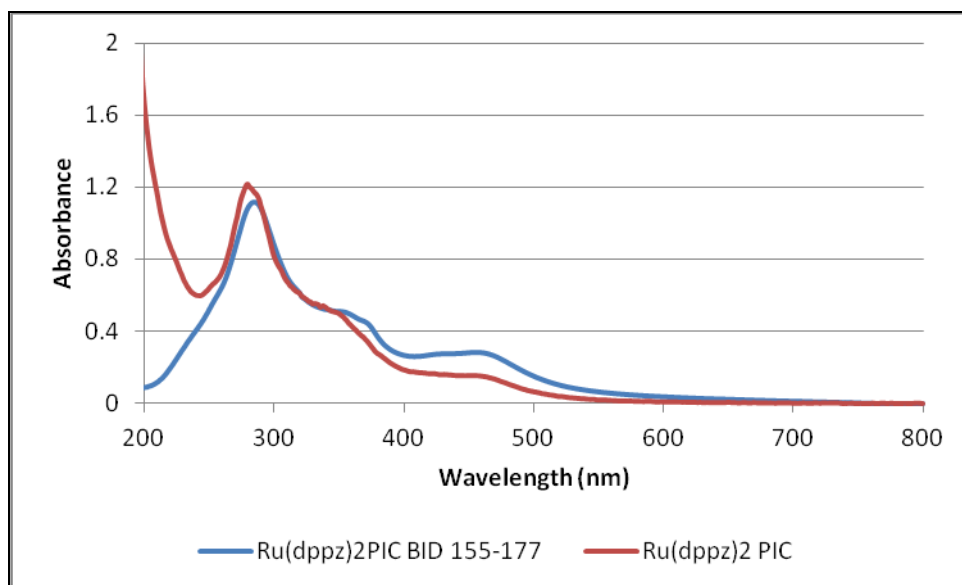


Figure 4.10 Absorbance of the synthesised $\text{Ru(dppz)}_2\text{PIC-BID 155-177}$ (aqueous solvent) chromophore-peptide conjugate and the parent complex $\text{Ru(dppz)}_2\text{PIC}$ (acetonitrile solvent)

The emission spectrum of $\text{Ru(dppz)}_2\text{PIC-BID 155-177}$ is shown Figure 4. 11. $\text{Ru(dppz)}_2\text{PIC-BID 155-177}$ exhibits a maximum emission at approximately 610 nm when excited into the MLCT absorbance band 470nm which is consistent with the emission of the parent complex $[\text{Ru(dppz)}_2\text{PIC}]\text{ClO}_4$. The emission decays follow biexponential kinetics with lifetimes for the emission decays of 0.2717 μs and 0.06795 μs . These lifetimes are comparable to those of the parent complexes $[\text{Ru(dppz)}_2\text{PIC}]\text{ClO}_4$ which also follow biexponential kinetics with lifetimes of 0.22361 μs and 0.06855 μs for the emission decays.

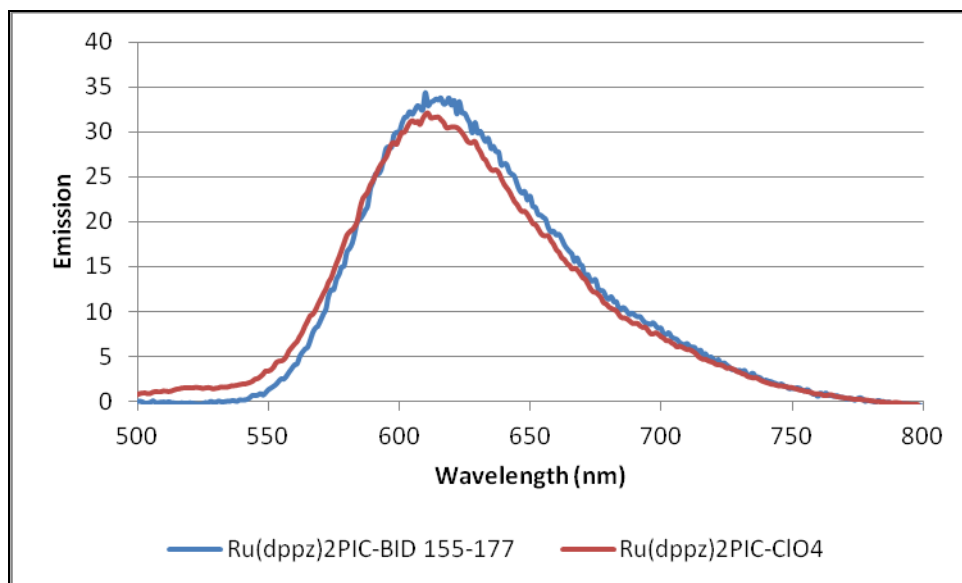


Figure 4. 11 Overlaid emission of the synthesised Ru(dppz)₂PIC-BID 155-177 and parent complex in ACN.

4.3.10 Preliminary Cell Imaging Studies

Preliminary cell imaging was conducted on Ru(dppz)₂PIC-BID 155-177 in SK-N-AS neuroblastoma cells. In order to assess the ability of the BID compounds for cell imaging, cells were cultured separately on 35 mm glass bottom culture dishes. Kelly neuroblastoma cells were seeded at 5×10^5 cells in 2 ml media and were grown for 24 hours before imaging. Addition of the ruthenium complexes (40 μ M) was performed at 37 °C and incubated overnight. Images were acquired using a Zeiss LSM510 Confocal microscope, 63x oil immersion lens, 458nm laser line for Ru.

The parent complex was used as a control and as seen from Figure 4. 12, without the peptide the parent complex, [Ru(dppz)₂PIC]ClO₄, did not penetrate the cell. Under the same conditions the Ru (dppz)₂PIC-BID 155-177 showed signs of cell penetration.

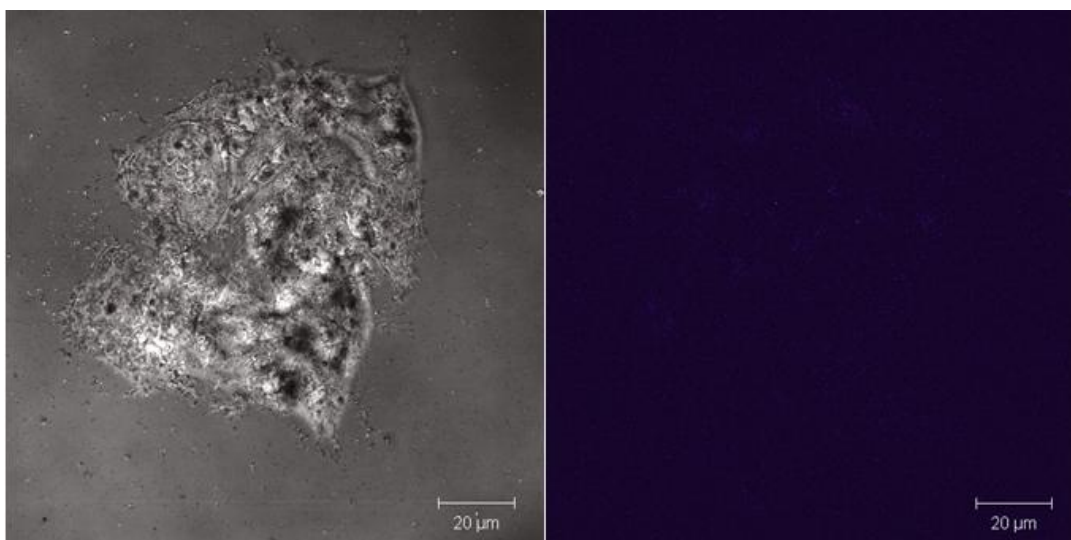


Figure 4. 12 [Ru(dppz)₂PIC]ClO₄ parent complex (200μM) in Kelly neuroblastoma cells incubated overnight. (Images collected by Dr. Róisín Moriarty)

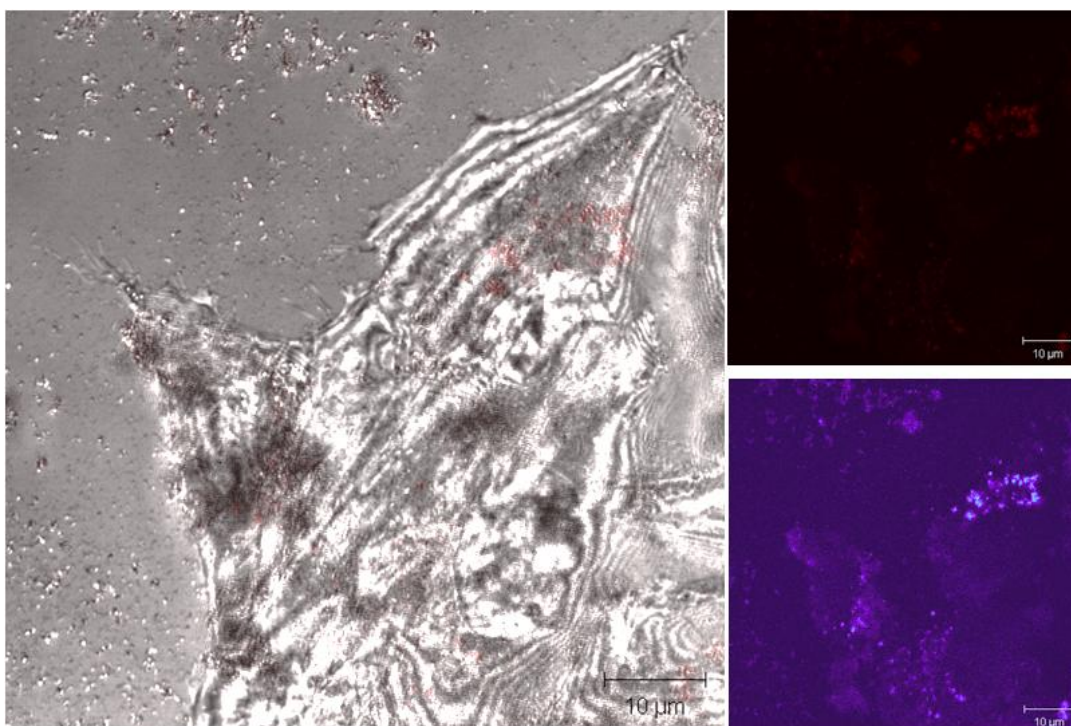


Figure 4. 13 Ru(dppz)₂PIC-BID 155-177 (200μM) in Kelly neuroblastoma cells incubated over night. (Images collected by Dr. Róisín Moriarty)

Figure 4. 14 shows the luminescent cross-section of the Ru(dppz)₂PIC-BID 155-177 peptide (red) and nuclear stain DAPI (blue) in fixed Kelly neuroblastoma cells after overnight incubation at 37°C in PBS buffer. It is evident that the Ru(dppz)₂PIC-BID 155-177 peptide does not localise in the nucleus as expected. Preliminary cytotoxicity data suggests that the Ru(dppz)₂PIC-BID 155-177 peptide (~70% toxicity at 100μM concentration) is far more toxic than the parent complex [Ru(dppz)₂PIC]ClO₄ (~10% toxicity at 100μM

concentration). Thus the imaging and preliminary cytotoxicity results provide evidences that the $\text{Ru(dppz)}_2\text{PIC-BID 155-177}$ peptide does penetrate Kelly neuroblastoma cells while the parent complex $[\text{Ru(dppz)}_2\text{PIC}]\text{ClO}_4$ which does not penetrate this cell line at all. However we cannot conclude toxicity following intracellular access or if cell penetration occurs because of toxic effects.

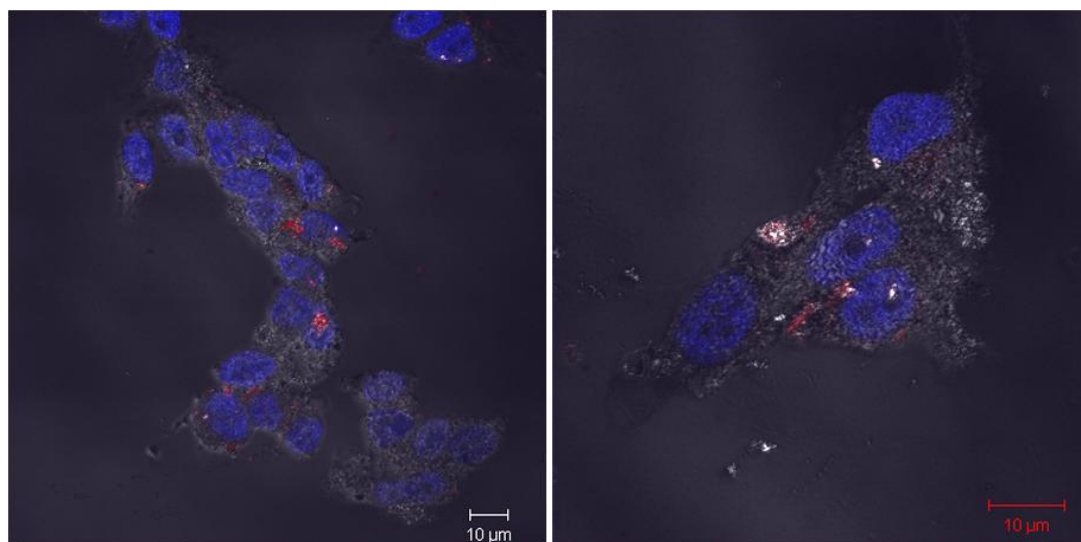


Figure 4. 14 $\text{Ru(dppz)}_2\text{-Bid}$ and DAPI in SK-N-AS fixed neuroblastoma cells. (Images collected by Dr. Róisín Moriarty)

4.10 Conclusion

This chapter described the synthesis of 11 overlapping BID peptide sequences spanning the complete protein (tBid). Most of these peptides could not be prepared by routine techniques. Only two BID sequences, BID 155-177 and BID 78-101, were successfully made by automated synthesis. The remaining 9 were partly assembled on the synthesizer and fully elongated by manual with microwave activation when required. Some sequences also required a change in the coupling chemistry and the polymeric support. Sequence assembly was carefully monitored by carrying out both a mass spectrometry analysis of the sequence resulting from the automated synthesis and a Kaiser test after each step performed manually, to ensure the integrity of the 11 BID sequences upon completion of the synthesis. Purifications took place on a C18 column on HPLC with purities > 85%. Characterisation was conducted using MALDI-TOF or High Resolution mass spectroscopy.

The 11 BID sequences were successfully coupled to biotin for protein binding studies. The latter will be conducted through an independent collaborative project. Two of the BID sequences, BID 137-157 and BID 155-177, were chosen for conjugation with $[\text{Ru}(\text{dppz})_2\text{PIC}]\text{ClO}_4$ on the basis of their high hydrophobic amino acid contents. The synthesis and purification of these proved to be more difficult than the biotin-labelled analogues, requiring a change in the coupling chemistry to overcome the low reactivity of the carboxyl group from the ruthenium complex. The latter may also promote the oxidation of sensitive residues when conjugated to a peptide sequence. The optimal conditions for $[\text{Ru}(\text{dppz})_2\text{PIC}]\text{ClO}_4$ conjugation were identified and should be successfully applied to any of the other BID sequences which would show promising results from the protein binding studies. These studies addressed in particular the choice of the linker between the label and the peptide to ensure sufficient solubility in aqueous media of the conjugates. Photophysical and imaging studies were conducted with BID 155-177 and showed that the properties of the parent complex are not significantly modified by the conjugation of the peptide sequence.

Unlike its unconjugated complex, $\text{Ru}(\text{dppz})_2\text{PIC}$ BID 155-177 underwent diffusion across the cell membrane of Kelly neuroblastoma cells, with no accumulation in the nucleus, but also showed significant toxicity which could result from its interaction with the cell membrane or uptake in the cytoplasm.

Protein binding studies with the 11 BID-Biotin peptide conjugates will be performed by the group Prof. Jochen Prehn in the Department of Physiology and Medical Physics at the Royal College of Surgeons in Ireland. Further studies with $\text{Ru}(\text{dppz})_2\text{PIC}$ -BID 155-177 by confocal microscopy, to determine its sub-cellular localisation, and by the cytotoxicity assay, to elucidate the chronology of the uptake and toxicity events are currently performed by Dr. Róisín Moriarty, research engineer, within the Prof. Tia Keyes group in Dublin City University.

References

- [1] Woo, J. S.; Jung, J. S.; Ha, N. C.; Shin, J.; Kim, K. H.; Lee, W.; Oh, B. H., *Cell Death Differ*, (2003) **10**, 1310.
- [2] McDonnell, J. M.; Fushman, D.; Milliman, C. L.; Korsmeyer, S. J.; Cowburn, D., *Cell*, (1999) **96**, 625.
- [3] Zinkel, S. S.; Hurov, K. E.; Ong, C.; Abtahi, F. M.; Gross, A.; Korsmeyer, S. J., *Cell*, (2005) **122**, 579.
- [4] Kamer, I.; Sarig, R.; Zaltsman, Y.; Niv, H.; Oberkovitz, G.; Regev, L.; Haimovich, G.; Lerenthal, Y.; Marcellus, R. C.; Gross, A., *Cell*, (2005) **122**, 593.
- [5] Breckenridge, D. G.; Stojanovic, M.; Marcellus, R. C.; Shore, G. C., *Journal of Cell Biology*, (2003) **160**, 1115.
- [6] Salgado, J.; Garcia-Saez, A. J.; Malet, G.; Mingarro, I.; Perez-Paya, E., *J Pept Sci*, (2002) **8**, 543.
- [7] Cregan, S. P.; Dawson, V. L.; Slack, R. S., *Oncogene*, (2004) **23**, 2785.
- [8] Yin, X.-M.; Wang, K.; Gross, A.; Zhao, Y.; Zinkel, S.; Klocke, B.; Roth, K. A.; Korsmeyer, S. J., *Nature*, (1999) **400**, 886.
- [9] Zou, H.; Li, Y.; Liu, X.; Wang, X., *Journal of Biological Chemistry*, (1999) **274**, 11549.
- [10] Plesnila, N.; Zinkel, S.; Le, D. A.; Amin-Hanjani, S.; Wu, Y.; Qiu, J.; Chiarugi, A.; Thomas, S. S.; Kohane, D. S.; Korsmeyer, S. J.; Moskowitz, M. A., *Proceedings of the National Academy of Science*, (2001) **98**, 15318.
- [11] Culmsee, C.; Zhu, C.; Landshamer, S.; Becattini, B.; Wagner, E.; Pellecchia, M.; Blomgren, K.; Plesnila, N., *The Journal of Neuroscience*, (2005) **25**, 10262.
- [12] Cregan, S. P.; Fortin, A.; MacLaurin, J. G.; Callaghan, S. M.; Cecconi, F.; Yu, S.-W.; Dawson, T. M.; Dawson, V. L.; Park, D. S.; Kroemer, G.; Slack, R. S., *Journal of Cell Biology*, (2002) **158**, 507.
- [13] Petros, A. M., Nettesheim, D.G. , Wang, Y., Olejniczak E.T., Meadows, R.P., Mack, J., Swift, K., Matayoshi, E.D., ; Zhang, H., Thompson, C. and Fesik S.W., *Protein Science*, (2000) **9**, 2528.
- [14] Renshaw, S. A.; Dempsey, C. E.; Barnes, F. A.; Bagstaff, S. M.; Dower, S. K.; Bingle, C. D.; Whyte, M. K., *J Biol Chem*, (2004) **279**, 2846.
- [15] Kaiser, E.; Colescott, R. L.; Bossinger, C. D.; Cook, P. I., *Analytical Biochemistry*, (1970) **34**, 595.
- [16] Coantic, S.; Subra, G.; Martinez, J., *International Journal of Peptide Research and Therapeutics*, (2008) **14**, 143.
- [17] Carpino, L. A., *Journal of the American Chemical Society*, (1993) **115**, 4397.

- [18] Albericio, F.; Bofill, J. M.; El-Faham, A.; Kates, S. A., *The Journal of Organic Chemistry*, (1998) **63**, 9678.
- [19] Garcia-Martin, F.; Quintanar-Audelo, M.; Garcia-Ramos, Y.; Cruz, L. J.; Gravel, C.; Furic, R.; Cote, S.; Tulla-Puche, J.; Albericio, F., *J Comb Chem*, (2006) **8**, 213.
- [20] Hyde, C.; Johnson, T.; Owen, D.; Quibell, M.; Sheppard, R. C., *Int J Pept Protein Res*, (1994) **43**, 431.
- [21] GenScript, https://www.genscript.com/ssl-bin/site2/peptide_calculation.cgi, In Gene Script: (2012); Vol. 2012.
- [22] Szacilowski, K.; Macyk, W.; Drzewiecka-Matuszek, A.; Brindell, M.; Stochel, G., *Chemical Reviews*, (2005) **105**, 2647.
- [23] Friedman, A. E.; Chambron, J. C.; Sauvage, J. P.; Turro, N. J.; Barton, J. K., *Journal of the American Chemical Society*, (1990) **112**, 4960.
- [24] Svensson, F. R.; Abrahamsson, M.; Stroimberg, N.; Ewing, A. G.; Lincoln, P., *The Journal of Physical Chemistry Letters*, (2012) **2**, 397.
- [25] Olson, E. J. C.; Hu, D.; Harmann, A.; Jonkman, A. M.; Arkin, M. R.; Stemp, E. D. A.; Barton, J. K.; Barbara, P. F., *Journal of the American Chemical Society*, (1997) **119**, 11458.
- [26] O'Connor, N. A.; Stevens, N.; Samaroo, D.; Solomon, M. R.; Marti, A. A.; Dyer, J.; Vishwasrao, H.; Akins, D. L.; Kandel, E. R.; Turro, N. J., *Chemical Communications*, (2009), 2640.
- [27] Xu, H.; Liang, Y.; Zhang, P.; Du, F.; Zhou, B.-R.; Wu, J.; Liu, J.-H.; Liu, Z.-G.; Ji, L.-N., *Journal of Biological Inorganic Chemistry*, (2005) **10**, 529.
- [28] Ardhammar, M.; Lincoln, P.; Nordan, B., *The Journal of Physical Chemistry B*, (2001) **105**, 11363.
- [29] Svensson, F. R.; Li, M.; Nordel•n, B.; Lincoln, P., *The Journal of Physical Chemistry B*, (2008) **112**, 10969.
- [30] Zava, O.; Zakeeruddin, S. M.; Danelon, C.; Vogel, H.; Grätzel, M.; Dyson, P. J., *ChemBioChem*, (2009) **10**, 1796.
- [31] Neugebauer, U.; Pellegrin, Y.; Devocelle, M.; Forster, R. J.; Signac, W.; Moran, N.; Keyes, T. E., *Chem Commun (Camb)*, (2008), 5307.
- [32] Dhruv Sud, W. Z., David G. Beer, Mary-Ann Mycek, *Opt. Express*, (2006) **14**, 4412.
- [33] Zhong, W., Urayama, P. and Mycek, M.A., *Journal of Physics D: Applied Physics*, (2003) **36**, 1689.
- [34] Piszczek, G., *Archives of Biochemistry and Biophysics*, (2006) **453**, 54.
- [35] Weissbach, H.; Brot, N., *Molecular Microbiology*, (1991) **5**, 1593.

- [36] Gitlin, G.; Tsarbopoulos, A.; Patel, S. T.; Sydor, W.; Pramanik, B. N.; Jacobs, S.; Westreich, L.; Mittelman, S.; Bausch, J. N., *Pharmaceutical Research*, (1996) **13**, 762.
- [37] Konz, J. O.; King, J.; Cooney, C. L., *Biotechnology Progress*, (1998) **14**, 393.
- [38] Liu, J. L.; Lu, K. V.; Eris, T.; Katta, V.; Westcott, K. R.; Narhi, L. O.; Lu, H. S., *Pharmaceutical Research*, (1998) **15**, 632.
- [39] Kornfelt, T.; Persson, E.; Palm, L., *Archives of Biochemistry and Biophysics*, (1999) **363**, 43.
- [40] Kim, Y. H.; Berry, A. H.; Spencer, D. S.; Stites, W. E., *Protein Engineering Design and Selection*, (2001) **14**, 343.
- [41] Randhawa, Z. I.; Witkowska, H. E.; Cone, J.; Wilkins, J. A.; Hughes, P.; Yamanishi, K.; Yasuda, S.; Masui, Y.; Arthur, P., *Biochemistry*, (1994) **33**, 4352.

Chapter 5: Targeting Mitochondria with Luminescent Chromophores

5.1 Introduction

As outlined in Chapter 3 the localisation of chromophores within cells has important applications in life science research. After successfully targeting two Ru(II) chromophores to the nucleus with NF- κ B, confirming thereby that the presence of the ruthenium label did not modify the natural distribution of its conjugated peptide sequence, we then aimed to target them to the mitochondria, the organelle to be studied ultimately with the Bid peptides described in chapter 4. Prior to this application, the aim of the present study was to synthesize, purify and characterise mitochondrial targeting peptides conjugated to Ru(II) luminophores and then to carry out preliminary evaluation of their ability to enter and localise in myeloma and bacterial cells lines.

Mitochondrial DNA (mtDNA) located inside mitochondria organelles, exists in multiple copies. Inside mitochondria, reactive oxygen species (ROS) or free radicals, by-products of the constant production of adenosine triphosphate (ATP), create a highly oxidative environment that is known to damage mtDNA.^[1] Targeting the mitochondria with Ru(II) Chromophores has potential for imaging and therapeutic applications. The peptide chosen for supramolecular assembly to target the mitochondria is Magainin 2. Magainin 2 is an antimicrobial peptide (AMP), belonging to a class of short cationic peptides that are strongly membrane active.^[2] Magainin 2 has previously been shown to accumulate fluorescent cargo probes in the mitochondria and nuclei.^[3]

This chapter details the synthesis of ruthenium (II) inorganic metal luminophores conjugated to Magainin 2 (GIGKKLHSAKKFGKAFVGEIMNS-NH₂) and the preliminary cell imaging studies with these conjugates. Conjugation of the chromophores to Magainin 2 allows for their passive entry, without the need for permeabilisation, into living mammalian cells for cellular imaging studies. As previously outlined in Chapter 1, Magainin 2 has antimicrobial properties. It is an amphipathic peptide with potent, broad-spectrum antibiotic activity which has been investigated as a potential novel therapeutic agent for anti-infective but also anticancer applications. Additionally, the intrinsic photophysical properties of these metal complexes, with their triplet excited states can lead to generation of singlet oxygen and other reactive oxygen species which in turn may lead to induced apoptosis in cells, thus, making these dye-peptides potentially valuable in the area of photodynamic therapy. In a

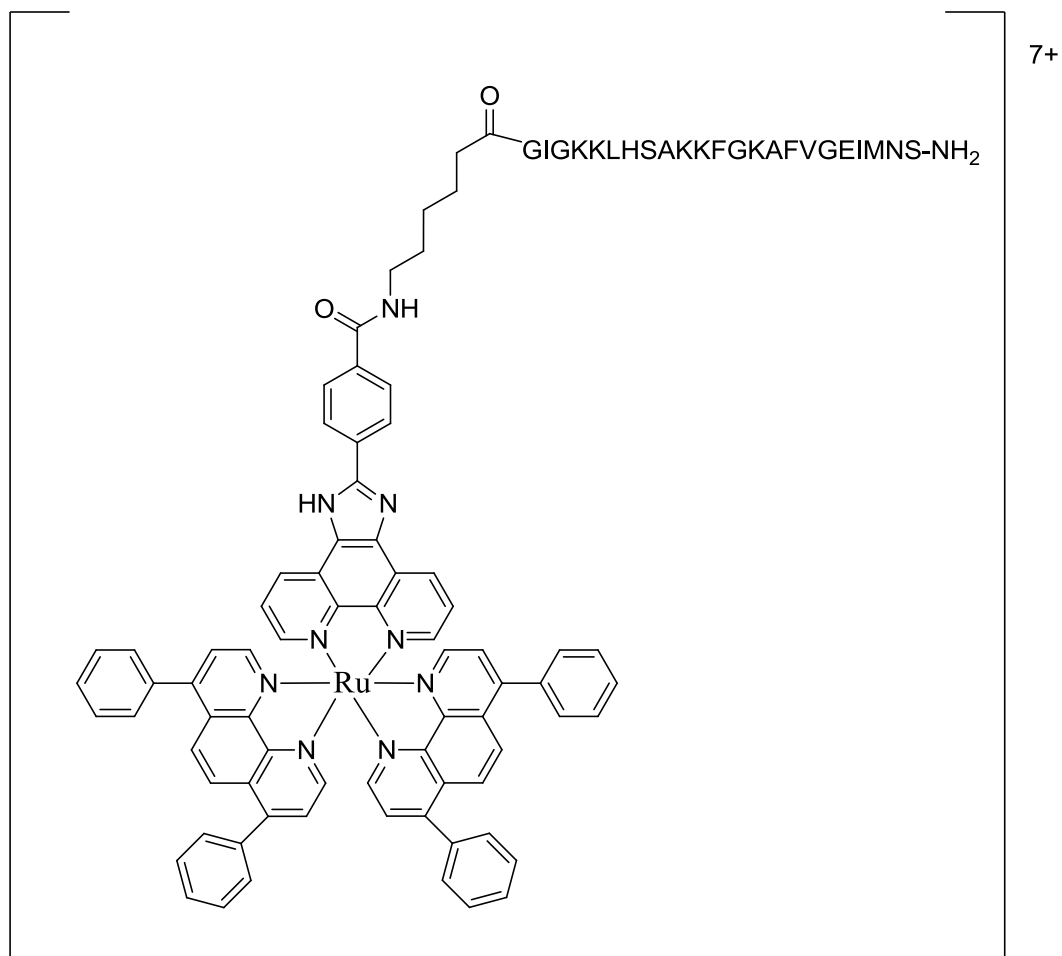
therapeutic context, the peptide and the chromophore may prove to have a very valuable synergistic effect in the detection and treatment of certain diseases.

The supramolecular assemblies synthesized were prepared as described previously in Chapter 3. The peptide, N-terminally modified with a 6-amino-hexanoic acid spacer, was prepared by Merrifield's Solid Phase Peptide Synthesis.^[4] Conjugation of the Ru polypyridal complexes to the peptide occurs through a stable amide bond with the aromatic carboxyl group of the former entity. The coupling reaction was performed on a side-chain protected resin-bound peptide.

5.2 Experimental Details for the Synthesis of targeting peptides-dye conjugates

The conjugates were synthesized according to methods previously reported in Chapter 3. The Ru(II) polypyridal complexes were supplied and characterised by Dr. Ciaran Dolan^[5] and Kellie Adamson (Dublin City University). General experimental details of peptide synthesis itself are outlined in chapter 2 and specific details are outlined below.

5.2.1 Preparation of Ru(dpp)₂PIC- Magainin 2 (Ahx-GIGKKLHSAKKFGKAFVGEIMNS-NH₂) conjugate.



The Magainin 2 (Ahx-GIGKKLHSAKKFGKAFVGEIMNS-NH₂) was assembled from a Rink Amide MBHA Resin (0.1mmol, substitution 0.7mmol/g) by automated synthesis as previously described. Manual coupling of [Ru(dpp)₂PIC] ClO₄ (supplied by DCU) took place by solid phase synthesis, using PyBOP/HOBt (3eq) / DIEA (6eq) coupling chemistry with overnight shaking. The peptide was cleaved by standard methods and then purified by RP-HPLC. Fractions collected on the semi-preparative HPLC were analysed by mass spectrometry.

Purity 84% (Appendix Figure 33)

HRMS m/z: found 3667.68 [M + H]⁺, calculated for C₁₈₈H₂₃₄N₄₀O₃₀RuS 3667.11

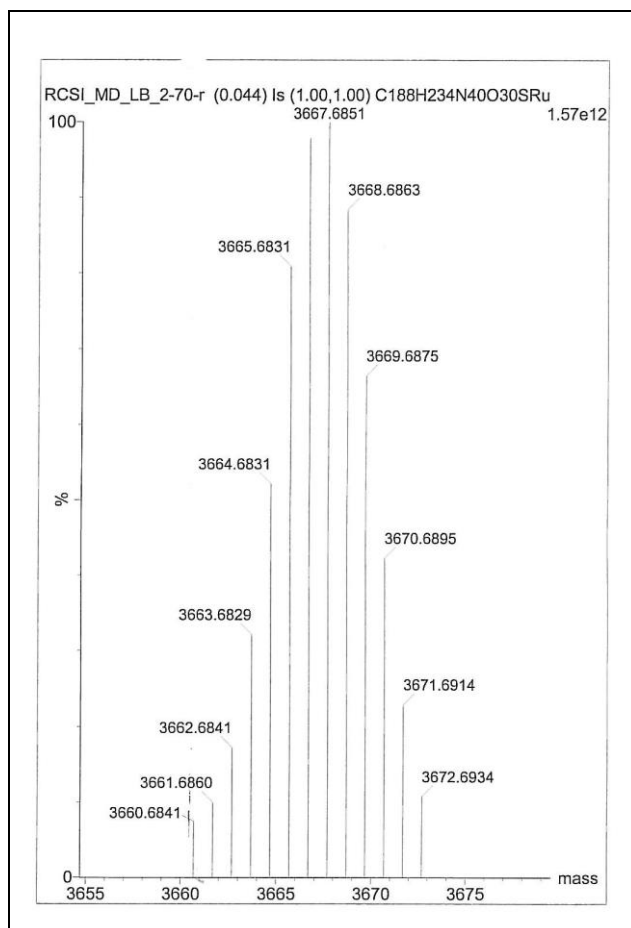
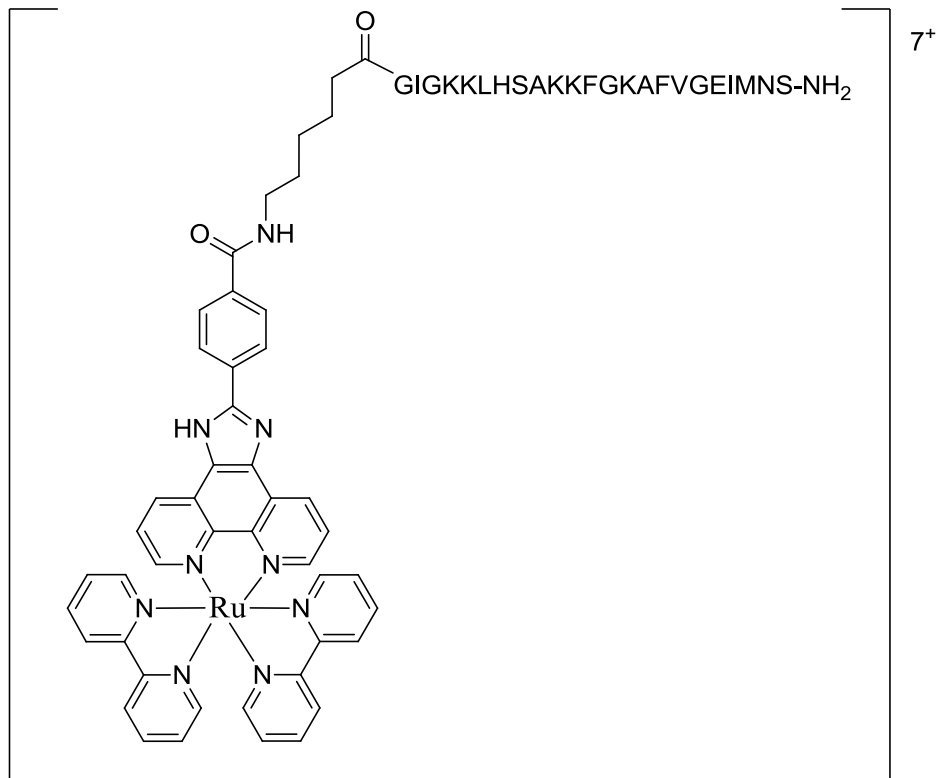


Figure 5. 1 Mass Spectra of Ru(dpp)₂PIC- Magainin 2 (Ahx-GIGKKLHSAKKFGKAFVGEIMNS-NH₂) conjugate

5.2.2 Preparation of Ru(bpy)₂PIC- Magainin 2 (Ahx-GIGKKLHSAKKFGKAFVGEIMNS-NH₂) conjugate.



The Magainin 2 (Ahx-GIGKKLHSAKKFGKAFVGEIMNS-NH₂) was assembled from a Rink Amide MBHA Resin (0.1mmol, substitution 0.7mmol/g) by automated synthesis as previously described. Manual coupling of [Ru(dpp)₂PIC] ClO₄ (supplied by DCU) took place by solid phase synthesis, using PyBOP/HOBt (3eq) / DIEA (6eq) coupling chemistry with overnight shaking. The peptide was cleaved by standard methods and then purified by RP-HPLC. Fractions collected on the semi-preparative HPLC were analysed by mass spectrometry.

Purity 87% (Appendix Figure 34)

MALDI-MS 3315.857 [M+1]⁺ calculated for C₁₆₀H₂₁₈N₄₀O₃₀RuS 3315.25(Figure 5.2)

5.3 Results and Discussion

The synthesis of these two novel Ru(II) polypyridal peptide conjugates was conducted in a similar manner to that outlined in section 3.2. The peptide was synthesized on the Applied Biosystem ABI 433A Synthesizer. The bio-conjugation of chromophore to peptide took place on the resin with PyBOP as the coupling reagent. Cleavage of the Ru(II) polypyridal peptide conjugates from the resin took place in TFA in the presence of scavengers and optimisation of the cleavage was completed as outlined in Section 3.2. Semi-preparative HPLC on reverse phase silica, C₁₈ column was used to achieve purities >83%. A water/ACN gradient with TFA as the acidic ion pairing reagent was used. Monitoring was performed using UV-VIS detector at wavelengths of 214nm and 452nm. The Ru(II) polypyridal peptide conjugates were characterised by mass spectroscopy, with the isotopic distribution pattern of Ru evident in Figure 5.1.

Mass spectrometry and HPLC analysis were used routinely to confirm the purity of these chromophore peptide conjugates. The HPLC chromatograms showed a single peak in both cases and the retention times of these signals are reported in Table 5. 1, using HPLC conditions as set out in the Chapter 2. Again, it is noted that the more hydrophobic Ru(dpp)₂PIC- Magainin 2 conjugate has a retention time which is longer by approximately 8 minutes than the Ru(bpy)₂PIC- Magainin 2 conjugate. This is expected, as in reverse phase HPLC as hydrophobic-hydrophobic interactions are responsible for retention.

The mass spectra of these novel chromophore-peptide conjugates are presented in Table 5.1. As already observed with the NF-κB peptides presented in Chapter 3, oxidation of one residue occurred in the conjugate of the [Ru(bpy)₂PIC]²⁺ complex, as evidenced by the mass spectral results (Figure 5. 2). The correct relative molecular mass of the Ru(bpy)₂PIC- Magainin 2 conjugate is 3315.25 and is seen by the m/z signal in the spectrum. However m/z signal at 3330.55 has an increased mass of 16 and suggests oxidation has occurred. Again, it is believed that this oxidation occurred at the methionine (M) residue in the sequence. The reason why this occurs for [Ru(bpy)₂PIC]²⁺ and not for [Ru(dpp)₂PIC]²⁺ is unclear. The latter is expected to be more electron rich with an oxidation potential which is slightly lower than the bpy analogue. If it is the increased electron density on the dpp complex which is responsible

for oxidation of the M residue, this suggest that there is electronic communication within the assembly which is surprising given the M is so far from the conjugation point. It is more likely to be the time differences of the $[\text{Ru}(\text{bpy})_2\text{PIC}]^{2+}$ peptide conjugate spent in air during the cleave conditions.

Table 5. 1 Synthesised peptide-linker-chromophores with % purities, retention times and experimental mass

Peptide	Linker	Chromophore	Retention Time (mins)	% Purity	Mass (Da)
Magainin 2	Ahx-acid	$[\text{Ru}(\text{bpy})_2\text{PIC}]\text{ClO}_4$	24.2	84	3667.68
Magainin 2	Ahx-acid	$[\text{Ru}(\text{dpp})_2\text{PIC}]\text{ClO}_4$	32.4	87	3315.857

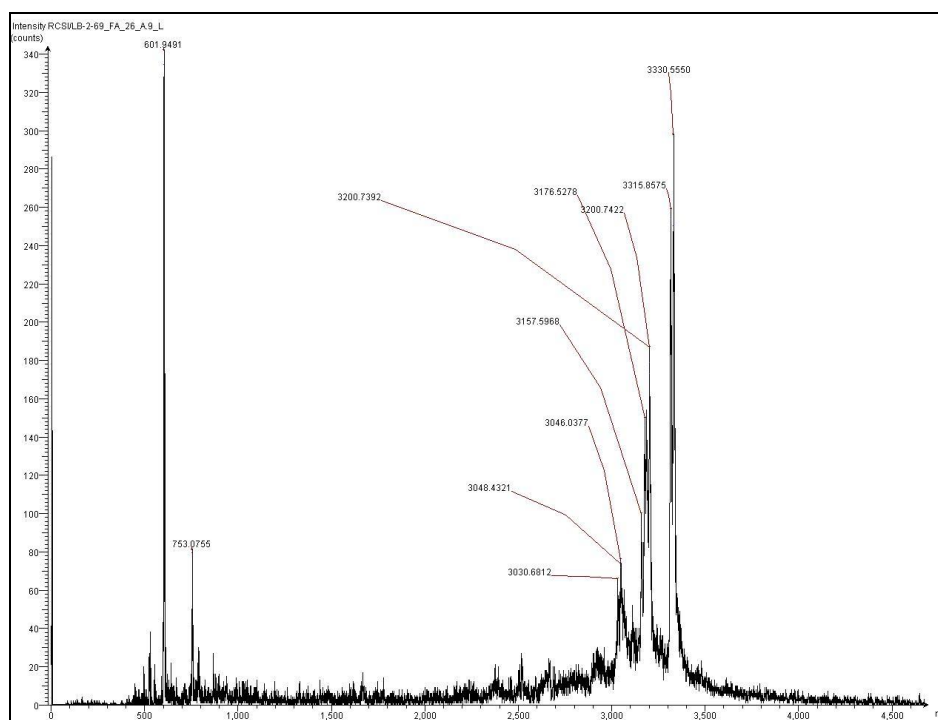


Figure 5. 2 Mass Spectra of $\text{Ru}(\text{bpy})_2\text{PIC}$ - Magainin 2 (Ahx-GIGKKLHSAKKFGKAFVGEIMNS-NH₂) conjugate

5.4 Photophysical Characterisation of the Peptide-Chromophore Conjugates

The spectroscopic and photophysical data of these ruthenium complexes peptides are presented in Table 5.2. Similar to the other peptide conjugates reported in chapter 3, conjugation of the ruthenium (II) dye to the peptide did not cause any significant alterations to the wavelength of absorbance and emission of the conjugate when compared to the parent chromophores. The UV-VIS wavelength is for the MLCT and the emission is the luminescence when excited at this wavelength.

Table 5. 2 The spectroscopic and photophysical data of all ruthenium complexes synthesised

Peptide	Linker	Dye	UV-VIS (nm)	Emission (nm)	Lifetimes Deaerated (μ s)	Lifetimes Aerated (μ s)
Magainin 2	Ahx	[Ru(bpy) ₂ PIC]ClO ₄	455.4	607	0.94 \pm 0.02	0.55 \pm 0.04
Magainin 2	Ahx	[Ru(dpp) ₂ PIC]ClO ₄	456.0	611	3.72 \pm 0.04	0.98 \pm 0.02
Parent	-	[Ru(bpy) ₂ PIC]ClO ₄	455	606	1.02 \pm 0.02	0.16 \pm 0.03
Parent	-	[Ru(dpp) ₂ PIC]ClO ₄	466	614	3.90 \pm 0.03	0.20 \pm 0.04

5.4.1 Absorbance

Figure 5. 1 below shows the overlaid absorbance spectra for the ruthenium (II) peptide (Magainin 2) conjugates synthesised. The UV-VIS spectra of the two Magainin 2 complexes are distinguished by a ruthenium π to ligand π^* MLCT transition at ~460 nm (individual values shown in Table 5.2) Again we can see the further evidence of a MLCT transition within the [Ru(bpy)₂PIC]ClO₄ conjugates at approximately 245nm. The strong absorbance band at approximately 285 nm may be assigned to π - π^* transitions originating within the polypyridal ligands, whereas the shoulder at approximately 330 nm is attributed to the π - π^* transitions of the carboxy-phenylphenanthroline ligands containing the two ionisable protons on the imidazole ring. There is an increase in the absorbance of the conjugates compared to the parent complexes between 270-300nm due to the conjugation to the peptide. The absorbance

profile of these conjugates are almost identical to that of the parent complexes $[\text{Ru}(\text{bpy})_2\text{PIC}]\text{ClO}_4$ and $[\text{Ru}(\text{dpp})_2\text{PIC}]\text{ClO}_4$ seen by our group previously.

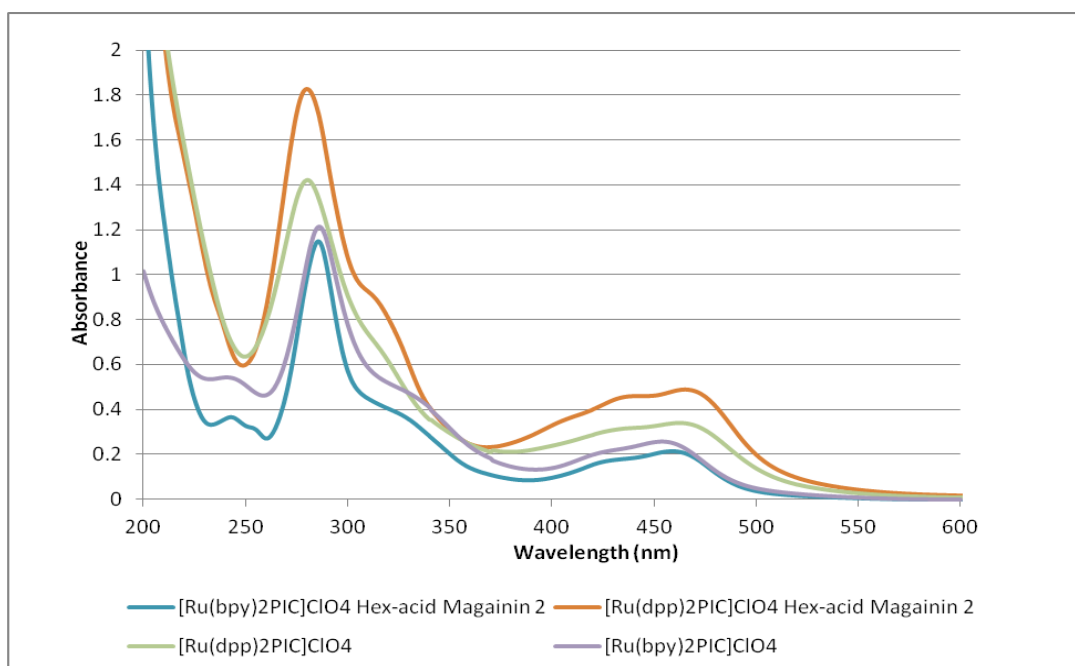


Figure 5. 1 Overlaid absorbance of the synthesised chromophore-peptide conjugates and parent complexes in water

5.4.2 Emission

The emission spectrum of the Ru(II) polypyridal peptide conjugates, Figure 5.2, exhibits a maxima emission at 607nm for $\text{Ru}(\text{bpy})_2\text{PIC}$ - Magainin 2 conjugate and 611nm for $\text{Ru}(\text{dpp})_2\text{PIC}$ - Magainin 2 conjugate when excited into the MLCT absorbance bands outlined in Table 5.2. All emission decays follow monoexponential kinetics with a lifetime in aerated samples shorter than in degassed solutions, as seen with $\text{Ru}(\text{bpy})_2\text{PIC}$ - Magainin 2 the lifetime in aerated is 0.55 μs whereas deaerated is 0.94 μs .

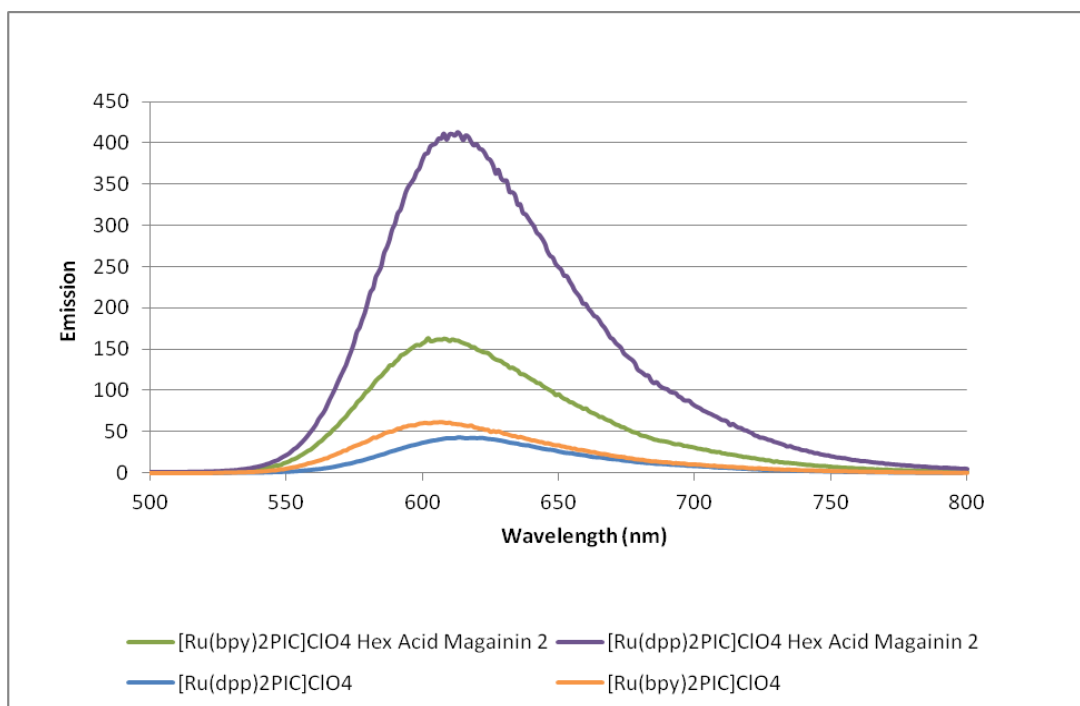


Figure 5.2 Overlaid emission of the synthesised chromophore-peptide conjugates

The emission decays conform to monoexponential kinetics recorded when in aqueous solution at room temperature. The deaerated samples were prepared by bubbling nitrogen through the solution for ~20 minutes before measurements were recorded. The deaerated lifetimes are longer than the aerated as seen in Table 5.2, and as noted that the Ru(dpp)₂PIC- Magainin 2 conjugate lifetime is longer than that of for Ru(bpy)₂PIC- Magainin 2 conjugate due most likely to the greater rigidity of this structure, i.e. reduced non-radiative decay. The increase in lifetime in absence of oxygen is also indication of the triplet MLCT character of the emission.^[6] There is no significant difference in the lifetimes in relation to the length of peptides. The peptides in Chapter 3 contain between 7-10 amino acids whereas the peptide in this chapter is 23 amino acids long. This was actually a little surprising, as we might have expected that the longer peptide residues might offer some protection from O₂, but this was not the case.

5.5 Cellular Uptake of Chromophores-Peptide Conjugates

As Magainin 2 has been known to target the mitochondria and nuclei, cell imaging was performed to investigate if it could direct the Ru polypyridal chromophores to these regions of the cell. In order to assess and compare the ability of the compounds to transport across the cell membrane of CHO cells, the latter were cultured separately on 35 mm glass bottom culture dishes and seeded at 5×10^5 cells in 2 ml media. They were then grown for 24 hours before imaging. Incubation of the ruthenium complexes (40 μ M) was performed at 37 °C overnight. Images were acquired using a Zeiss LSM510 Confocal microscope, 63x oil immersion lens, 458nm laser line for Ru.

Interestingly, no uptake of the Ru(bpy)₂ PIC-Magainin 2 peptide conjugate could be observed from the imaging results, indicating that the Ru(bpy)₂ PIC-Magainin 2 peptide conjugate is unable to cross the cell membrane. This was unexpected for an antimicrobial peptide such as Magainin 2, which was shown to transport across the membrane of CHO-K1 cells in previous studies.^[3] It would seem that the metal complex inhibits uptake, possibly by preventing the formation of a pore required to access the cytoplasm.^[7, 8] The use of the N^α-amino terminus for the conjugation of the complex could also have contributed to this result.^[9-11] As outlined in Chapter 1 Matsuzaki *et al* used TAMRA as their fluorophore and achieved cell penetration in CHO-K1 cells.^[3] TAMRA-Magainin 2 exhibited membrane-permeabilizing activity comparable to that of the parent peptide. TAMRA is also very hydrophobic like the Ru polypyridal complexes and has a molecular weight of 430.45g/mol. The molecular weight of the two Ru polypyridal complexes we used are 753.7g/mol [Ru(bpy)₂PIC]ClO₄ for and 1106.2g/mol for [Ru(bpy)₂PIC]ClO₄.

Interestingly though, on the other hand, the [Ru(dpp)₂ PIC-Magainin 2] peptide conjugate did cross the membrane (Figure 5. 3). Following uptake it was found to be distributed throughout the cell and had concentrated within a section of the nucleus that may be the nucleolus, as seen previously with [Ru(dpp)₂PIC]ClO₄ in Chapter 3. This concentration within the nucleus, we believe to be a feature of the [Ru(dpp)₂PIC]ClO₄ metal complex as opposed to the localisation properties of the peptide it is conjugated to. There also appears to be a lot of cell debris and looks as though the [Ru(dpp)₂ PIC-

Magainin 2] peptide conjugate is killing the cells. This is confirmed by the cytotoxicity results in section 5.6.

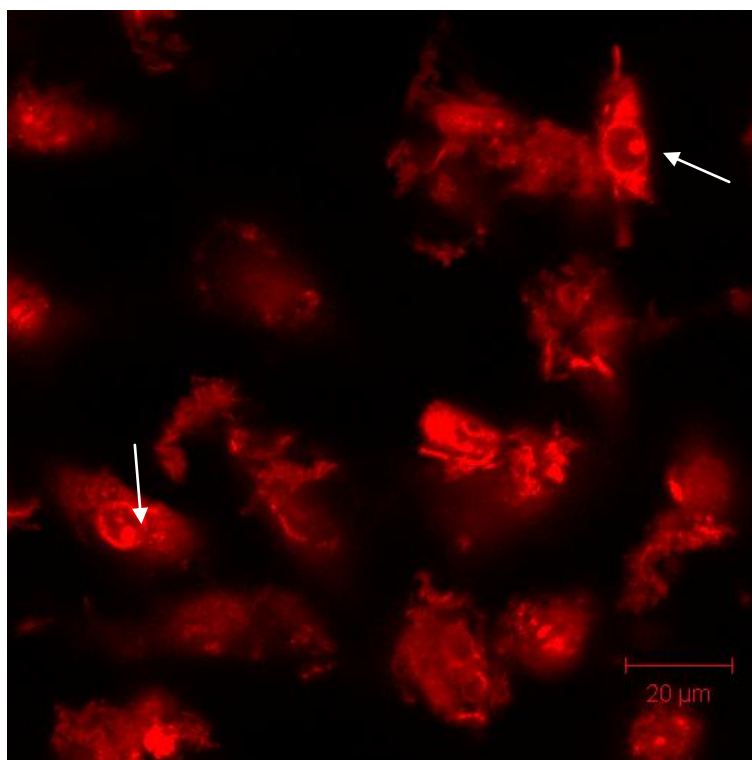


Figure 5. 3 Luminescent confocal images ($\lambda_{ex} = 458\text{nm}$) of live CHO cells incubated with Ru(dpp)₂ PIC-Magainin 2 peptide conjugate overnight in PBS at room temperature. Arrows show concentration within the nucleus. (Image courtesy of Dr. Róisín Moriarty)

5.6 Cytotoxicity

With the evidence of toxic effects following incubation with the [Ru(dpp)₂ PIC] as described in Chapter 3, it was deemed important to assess the potential toxic effects of these chromophore-peptide conjugates complexes on this cell line. The effect of these complexes on the viability of the cells was tested using the alamar blue/resazurin cytotoxicity assay which is explained in detail in section 2.5.14. As seen in Figure 5. 4 it is evident from the results that the Ru(dpp)₂ PIC peptide conjugates are cytotoxic to a degree which is well above that of the Ru(bpy)₂ PIC peptide conjugates. This is confirmed by evidence of cell debris as shown in Figure 5.3. However compared to the Ru(bpy)₂ PIC NLS sequences, the Ru(bpy)₂ PIC Magainin 2 sequence was more toxic.

This is almost certainly a contribution of the cytotoxic characteristics of the peptide itself. As the peptide Magainin 2 alone, interacts with cancer cells at an intracellular target, the mitochondrion. It is therefore not surprising that the Ru(bpy)₂ PIC which cannot penetrate the cytoplasmic membrane, has moderate effects on the viability of CHO cells (% cytotoxicity ~25%) as seen in Figure 5.4.

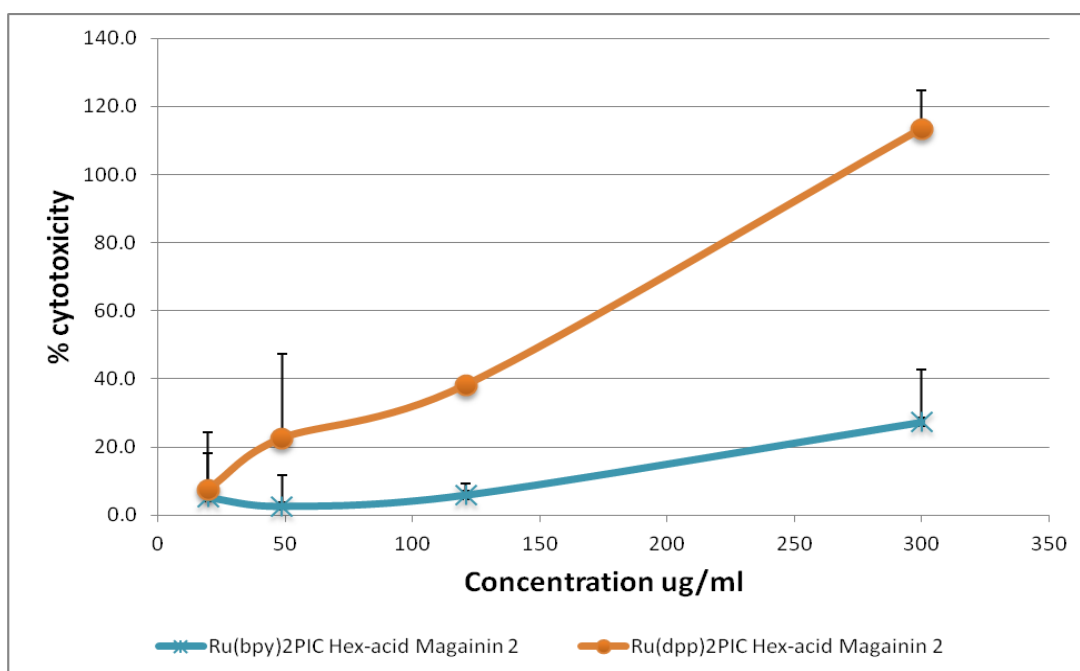


Figure 5. 4 Cytotoxicity assay with CHO cells treated with Chromophore-peptide conjugates
(Data prepared by Dr. Róisín Moriarty)

5.7 Conclusion

This chapter details the conjugation of ruthenium (II) polypyridyl chromophores to a mitochondria targeting peptide, Magainin 2. The synthesis of the chromophore-peptides was completed by standard techniques and proceeded with good yields and purities greater than 85%.

The photophysical results were similar to those obtained with shorter peptide conjugates and were relatively unchanged compared to the parent complexes. As

expected, the luminescent lifetimes for the Ru(dpp)₂PIC polypyridyl peptide conjugates were longer than the corresponding Ru(bpy)₂PIC polypyridyl peptide conjugates and the de-aerated lifetimes were longer for all Ru(II) polypyridyl peptide conjugates than the aerated samples.

Prior to peptide conjugation, neither parent complex exhibited efficient transport across the cell membrane of CHO cells and only the Ru(dpp)₂ PIC complex conjugate crossed the cell membrane of CHO cells after conjugation to the Magainin 2 sequence. In general, this did not lead to localisation of the dyes within the cell's mitochondria, the expected target of the peptide component; however co-localising experiments will be required to confirm this result. The corresponding Ru(bpy)₂ PIC Magainin 2 conjugate did not cross the membrane, which would indicate that there might exist a threshold of hydrophobicity of the cargo controlling the cellular uptake of the conjugate, as both Ru(bpy)₂ PIC and Ru(dpp)₂ PIC complexes should have the same effect on the N-terminal capping of the peptide and its ability to form a transmembrane pore.

The Ru(dpp)₂ PIC peptide conjugates distribute throughout the entire cell. It is possible that it's interaction with the mitochondrial membrane triggers rapid cell death and cannot be imaged. The Ru(dpp)₂ PIC peptide conjugates may be useful in therapeutics as it targets the nucleus and could potentially result in the apoptosis of cancer cells. We believe it to concentrate further within the nucleolus, however further imaging and localising studies must be completed. Also as the Magainin 2 peptide can penetrate bacterial cells, the use of the Ru(II) polypyridyl Magainin 2 conjugate in imaging will be extended to bacterial cells, although the rapid killing mechanism induced by Magainin 2 in prokaryotic cells might make this application challenging.

References

- [1] Cruz, C. M.; Rinna, A.; Forman, H. J.; Ventura, A. L. M.; Persechini, P. M.; Ojcius, D. M., *Journal of Biological Chemistry*, (2007) **282**, 2871.
- [2] Splith, K.; Neundorff, I., *European Biophysics Journal*, (2011) **40**, 387.
- [3] Imura, Y.; Choda, N.; Matsuzaki, K., *Biophysical journal*, (2008) **95**, 5757.
- [4] Merrifield, R. B., *Journal of the American Chemical Society*, (1963) **85**, 2149.
- [5] Dolan, C., Dublin City University Dublin, (2011), p 382.
- [6] Neugebauer, U.; Pellegrin, Y.; Devocelle, M.; Forster, R. J.; Signac, W.; Moran, N.; Keyes, T. E., *Chemical Communications*, (2008), 5307.
- [7] Henriques, S. T., *Journal of Biochemistry*, (2007),
- [8] Takeshima, K., Chikushi, A., Lee, K., Yonehara, S., Matsuzaki, K., *Journal of Biological Chemistry*, (2003) **278**,
- [9] Otvos, L.; de Olivier Inacio, V.; Wade, J. D.; Cudic, P., (2006) Prior Antibacterial Peptide-Mediated Inhibition of Protein Folding in Bacteria Mutes Resistance Enzymes, Vol. 50, 3146.
- [10] Hancock, R. E.; Diamond, G., *Trends Microbiol*, (2000) **8**, 402.
- [11] Juvvadi, P.; Vunnam, S.; Merrifield, R. B., *ChemInform*, (1997) **28**, no.

Chapter 6:

Small molecule Inhibitors of Bcl-2

family proteins

6.1 Introduction

Protein-protein interactions (PPIs) are essential to most biological processes and their modulation can be exploited as targets for human therapeutics. PPIs are a great interest to drug discovery, in particular when they can be disrupted by molecules of low molecular weights which are orally available. However, these small molecule therapeutics can have some drawbacks as potential drug candidates. Small molecule therapeutics that target PPIs can be difficult to manufacture and have poor cell permeability and solubility in water.^[1, 2]

There are challenges associated with finding a suitable small molecule inhibitor (SMI) for protein-protein interactions. One such challenge is to find lead compounds which selectively disrupt interaction surfaces that can be extended and discontinuous. Research into protein-protein interactions is focused on drug discovery through structure-based design, *in silico* screening and fragment based discovery, all of which have led to the identification of small-molecule antagonists of protein -protein interactions.^[3]

Most protein-protein interfaces are large, flat and have a lack of clear pockets, making PPI difficult targets for therapeutic purposes.^[4] The discovery of ‘hot spots’ was a major advance in the progress of small molecule PPI inhibitors.^[5] Small molecules targeting hot spot sites on protein-protein interfaces can disrupt their interaction. Small molecules, shown in Figure 6. 1, targeting these interactions are currently in clinical trials.^[6]

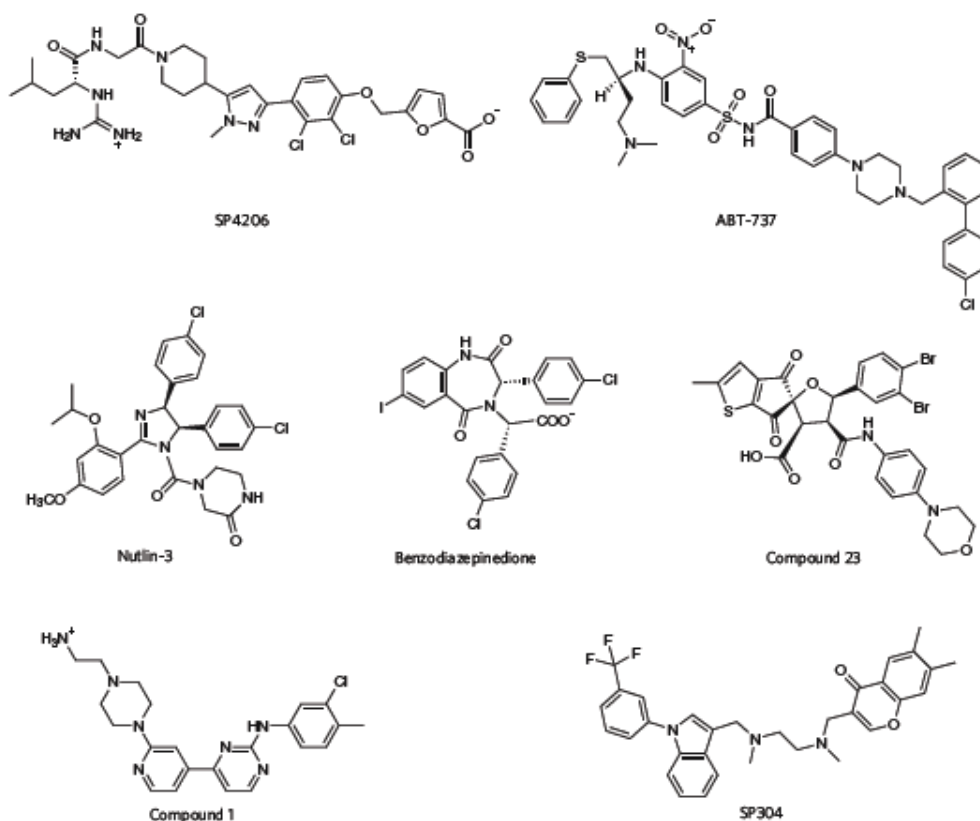


Figure 6. 1 Examples of small molecules that inhibit protein–protein interactions.

6.1.2 Protein interactions between the Bcl-2 family proteins

As previously discussed in Chapter 1, the Bcl-2 family of proteins contain members that are important regulators of cell death. The proteins of this family react with each other, generating pro-apoptotic and anti-apoptotic members. One example of this is the anti-apoptotic protein Bcl-X_L which binds to a 26 residue α -helical section of a pro-apoptotic member BAD and inhibit thereby apoptosis (Figure 6.2).^[6] In Figure 6.2 Bcl-X_L is rendered as a filled surface (grey) with the contact surface shown in green, while the binding protein or peptide is represented as a ribbon diagram (yellow), with selected side-chains shown as sticks (with carbon in yellow, oxygen in red and nitrogen in blue). The small molecule inhibitor of the anti-apoptotic proteins Bcl-2, Bcl-X_L and Bcl-w, ABT-737, is shown in stick format, with the contact surface shown in orange. In the central figure, the small molecule ABT 737 is shown superimposed on the pro-apoptotic protein in the conformation in which it binds to its natural anti-apoptotic protein or peptide partner, and the contact surface (on the target protein) of the natural interaction is shown in green. On the left figure is Bcl-X_L bound to a peptide derived from one of its natural protein partners, BAD.

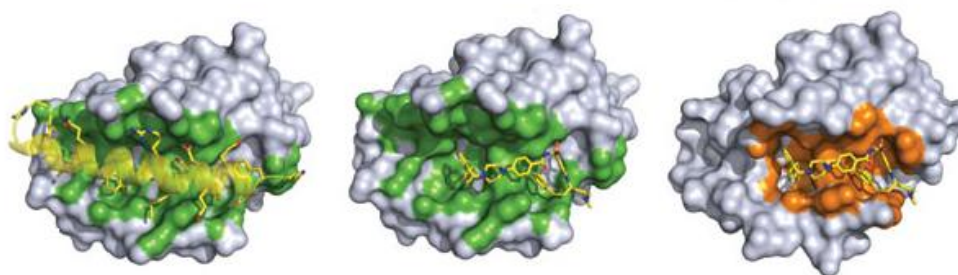


Figure 6. 2 The structures of protein–protein or protein–peptide complexes of pro- and anti-apoptotic proteins. ^[6]

Inhibitors of anti-apoptotic proteins mimicking BAK and BAD are potential drug candidates for the treatment of cancer. Generating small molecule inhibitors that mimic the α -helix residues of BAD has therefore received much attention. ^[7-9] Abbott laboratories in particular developed the BH3 mimetic inhibitor ABT 737, as described in Chapter 1. ^[10] It was discovered using a fragment-based nuclear magnetic resonance (NMR) method known as SAR by NMR and its properties improved by using NMR-structure-guided medicinal chemistry. An orally available derivative of ABT-737, ABT-263, is in phase I/II clinical trials for cancer treatment. ^[11]

6.2 ABT 737 and 263

Major differences are observed in both potency and selectivity of the various small molecule Bcl-2 inhibitors for the different anti-apoptotic Bcl-2 proteins. ^[10, 12-21] By far the most potent small molecule inhibitors described to date are the BAD-like BH3 mimetics, ABT-737 and its orally available analogue ABT-263. ^[22] For this reason they were chosen as low molecular weight candidates to perform localisation studies by cellular imaging with Ru (II) polypyridal probes alongside functional studies. These small molecules bind with very high affinities to Bcl-2, Bcl-XL and Bcl-w but with much lower affinities to Mcl-1 or Bcl2A1. ^[18, 23] Most detailed mechanistic studies on Bcl-2 inhibitors have been carried out using ABT-737 and it is proving to be a very valuable tool for such fundamental studies. ^[24] The development of an orally bioavailable Bcl-2 inhibitor, such as ABT-263, with the ability

to inhibit specifically BH3-Bcl-2 protein-protein interactions at low nanomolar concentrations, potentially marks a significant development in cancer therapy.

The synthetic pathway described in a patent developed by Abbott laboratories was used as a reference for the synthesis of ABT-263^[25] while the synthetic pathway described by Oltersdorf *et al*^[10] was used for ABT-737. The objective of this synthetic work was ultimately to avail, by adapting the original synthetic route(s), if required, of a synthetic method for the preparation of labelled analogues of ABT-263/737. The synthetic strategy adopted to synthesise ABT-737 is shown in the scheme on page 163. It involves a 13 step convergent synthetic route based on three different synthons. The synthesis of ABT-263 was initially investigated according to the scheme presented on page 164. ABT-263 has slight structural variations which improve the oral bioavailability of ABT-737. The structural differences between ABT-737 and ABT-263 are outlined in Figure 6. 3. One of these sites was also proposed as a potential conjugation point for the Ru(II) polypyridal probe. The intermediates synthesised have proton NMRs matching those reported by Oltersdorf and their carbon NMR signals are described for the first time.

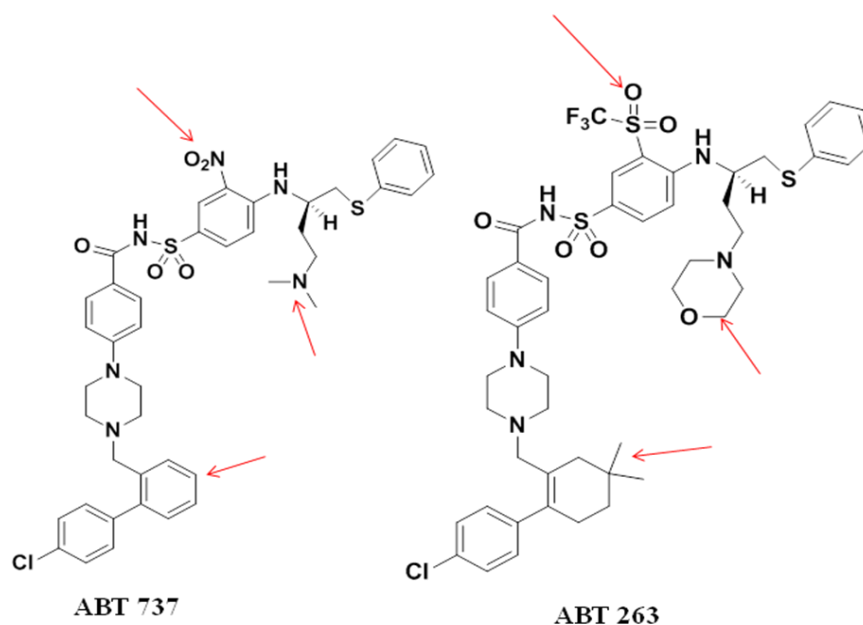
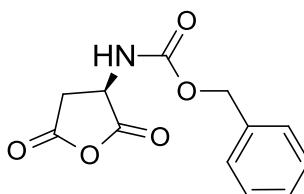


Figure 6. 3 Structures of ABT-737 and ABT-263 with differences pointed out with arrows.

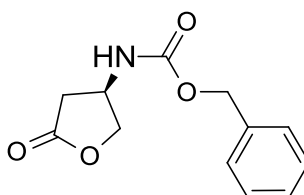
6.3 Synthetic Route 1(red) of ABT 737

6.3.1 Preparation of *N*-benzyloxycarbonyl-D-aspartic acid anhydride



Procedure: *N*-benzyloxycarbonyl-D aspartic acid (5.0328 g, 18.83 mmol) (Merck) and acetic anhydride (11ml, 116 mmol) were placed in a 100 ml round bottom flask and stirred gently overnight under argon . Dry dioxane (12ml) was added to the flask and the solvent mixture was reduced by high vacuum by maintaining the flask in a water bath whose temperature was not allowed to exceed 38°C, until gelation had occurred. This procedure was repeated using dry toluene. (both dioxane and toluene form an azeotrope with acetic acid). The product was dried finally on a freeze-dryer. The solid obtained was used in the next step without purification.

6.3.2 Preparation of (*R*)-benzyl (5-oxotetrahydrofuran-3-yl)carbamate, Compound 1 ABT 737 (Compound 1 ABT 263)



Procedure: To a stirred slurry of sodium borohydride (0.711g, 18.7 mmol) (Sigma) in THF (30 ml) kept at 0°C was added *N*-benzyloxycarbonyl-D-aspartic anhydride, compound 1 (4.65g, 18.7 mmol) in THF (35 ml) over a 3 hours period. After stirring at room temperature for 1 hour, the reaction mixture was acidified to pH 2 using 6M HCl and then concentrated to approximately ¼ the initial volume using a rotary evaporator. The resulting solution was diluted with water and extracted with four portions of ether. The combined organic layers

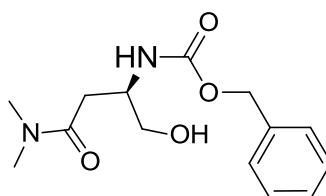
were then concentrated under reduced pressure to a heterogeneous yellow residue. The latter was taken up in toluene (30ml) containing *p*-TsOH (30mg) and water was then azeotropically removed using a Dean-Stark apparatus. After the mixture had refluxed for 5 hours, the toluene was removed by rotary evaporation to afford a viscous orange residue which gave light brown crystals upon trituration with ether. The solid material was collected by vacuum filtration. The filtrate was concentrated under reduced pressure and triturated with ether to afford a second crop of crystals (140mg, 45.7% combined yields).

^1H NMR (DMSO- d_6 , 400MHz) δ 2.38 (dd, J = 18, 4 Hz, 1H), 2.83 (dd, J = 18, 9 Hz, 1H), 4.09 (dd, J = 9, 3 Hz, 1H), 4.30 (m, 1H), 4.41 (dd, J = 9, 6 Hz, 1H), 5.03 (s, 2H), 7.36 (m, 5H), 7.88 (br d, J = 7 Hz, 1H). (Appendix Figure 36)

^{13}C NMR (DMSO- d_6 , 100.6MHz), 33.94, 47.47, 65.52, 72.97, 127.87 136.79 , 155.67, 175.68. (Appendix Figure 37)

HRMS m/z : found 258.075 $[\text{M} + \text{H}]^+$, calculated for $\text{C}_{12}\text{H}_{13}\text{NO}_4\text{Na}$ 258.074 (Appendix Figure 38)

6.3.3 Preparation of (*R*)-benzyl (4-(dimethylamino)-1-hydroxy-4-oxobutan-2-yl)carbamate, Compound 2 ABT 737



Procedure: A solution of 2.0 M *N,N*-dimethylamine in THF was added to compound 2 (500mg, 2.12 mmol) at room temperature until a solution was obtained (~5ml). After stirring at room temp for 14h, the reaction mixture was concentrated to dryness, loaded on a plug of silica and eluted first with 1:1 ethyl acetate:hexanes (fraction discarded) and then with acetone. Concentration of the acetone eluent gave 548 g (91%) of the desired product as thick colourless oil that solidified upon standing.

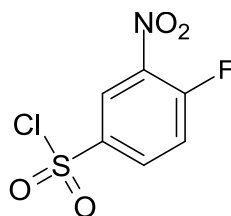
^1H NMR (CDCl_3 , 400MHz) δ 2.43 (dd, Hz, 2H), 2.7 (s, 3H), 2.9 (s, 1H), 3.3 (m, 2H), 3.91 (m, 1H), 5.03 (s, 2H), 7.16 (br d, 1H), 7.32 (m, 5H). (Appendix Figure 39)

^{13}C NMR (CDCl_3 , 100.6MHz), 29.54, 36.74, 50.60, 62.76, 65.11, 128.09 137.25 , 155.55, 171.88. (Appendix Figure 40)

$m/z = 281.52$ (100%, $[\text{M} + \text{H}]^+$) calculated for $\text{C}_{14}\text{H}_{20}\text{N}_2\text{O}_4$ 280.1423(Appendix Figure 41)

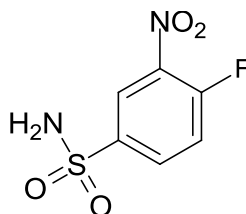
6.4. Synthetic Route 2 (green) of ABT 737

6.4.1 Preparation of 4-fluoro-3-nitrobenzene-1-sulfonyl chloride, Compound 6 ABT 737



Procedure: A solution of 1-fluoro-2-nitrobenzene (1.0 g, 5.7 mmol) in chlorosulfonic acid (4 mL) was heated at 80 °C overnight and poured onto crushed ice. The mixture was diluted with ethyl acetate, and the layers were separated. The aqueous layer was extracted with ethyl acetate ($\times 2$), and the combined organic layers were dried over MgSO_4 , filtered, and concentrated to give a crude product (1.4 g, 93%), which was used in the next step without further purification.

6.4.2 Preparation of 4-fluoro-3-nitrobenzenesulfonamide, Compound 7 ABT 737



Procedure: To a solution of the sulfonyl chloride, Compound 6 (1.4 g, 5.3 mmol) in 20 mL of THF-MeOH (1:1) cooled to -50 °C was added ammonium hydroxide (28% aqueous solution, 1.8 mL, 26.5 mmol). The reaction mixture was allowed to warm to 0 °C, and the

solvent was removed in vacuo. The residue was purified by chromatography (SiO₂, 20% ethyl acetate in hexanes) to give a yellow powder (704 mg, 60.4% over two steps).

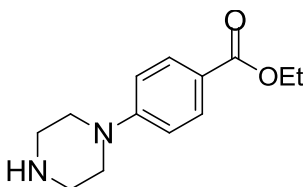
¹H NMR (DMSO-*d*₆, 400MHz) δ 7.75 (s, 2H), 7.81 (dd, *J* = 8.72, 10.9 Hz, 1H), 8.20 (ddd, *J* = 2.4, 4.06, 8.84 Hz, 2H), 8.52 (dd, *J* = 2.2, 6.9 Hz, 2H) (Appendix Figure 42)

¹³C NMR (DMSO-*d*₆, 400MHz) δ 158.7, 140.86, 133.46, 133.36, 124.02, 120.00 (Appendix Figure 43)

HRMS *m/z*: found 218.9873 [M-H]⁺, calculated for C₆H₅FN₂O₄S 219.9954 (Appendix Figure 44)

6.5 Synthetic Route 3 (blue) of ABT 737

6.5.1 Preparation of ethyl 4-(piperazin-1-yl)benzoate, Compound 8 ABT 737 (Compound 8 ABT 263)



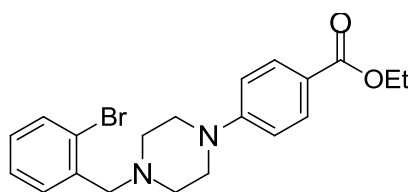
Procedure: DMSO (10ml) was added to piperazine (5.2g, 60mmol) to prepare a suspension to which ethyl-4-fluorobenzoate (2.5g, 0.015 mmol) was added at room temperature. The reaction mixture was stirred at 120°C for 20hrs. After this time the reaction mixture was taken up in DCM (~250ml) and washed 3 times with saturated NaHCO₃ (x3) and once with saturated NaCl and water. The organic layer was concentrated under reduced pressure to yield a cream solid. (2.774g, 78.9%).

¹H NMR (CDCl₃, 400MHz) δ : 1.36 (t, *J* = 7.05 Hz, 3H), 3.04 (m, 4H), 3.27 (m, 4H), 4.31(q, *J* = 7.02Hz, 2H), 6.86 (d, *J* = 9.07 Hz, 2H), 7.92 (d, *J* = 8.99 Hz, 2H) (Appendix Figure 45)

^{13}C NMR (CDCl_3 , 400MHz) δ : 14.46, 45.87, 48.68, 60.37, 113.67, 120.17, 131.14, 154.51, 166.70. (Appendix Figure 46)

HRMS m/z : found 235.1451 $[\text{M} + \text{H}]^+$, calculated for $\text{C}_{13}\text{H}_{18}\text{N}_2\text{O}_2$ 234.1368 (Appendix Figure 47)

6.5.2 Preparation of ethyl 4-(4-(2-bromobenzyl)piperazin-1-yl)benzoate, Compound 9 ABT 737



Procedure: To Compound 8 (58.06 mg, 0.248 mmol) in acetonitrile (20 ml) was added 2-bromobenzylbromide (92.97mg, 0.372 mmol) and DIEA (65 μl , 0.372 mmol). and the resulting mixture was allowed to stir at room temperature overnight. The product was isolated as a white powder by filtration. (41 mg, 41%)

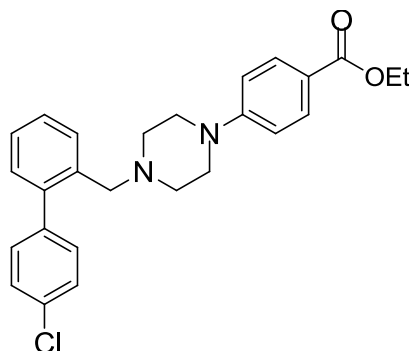
^1H NMR (CDCl_3 , 400MHz) δ : 1.36 (t, $J = 7.05$ Hz, 3H), 2.68 (m, 4H), 3.35 (m, 4H), 3.67 (s, 2H), 4.32 (q, $J = 7.02$ Hz, 2H), 6.86 (d, $J = 9.07$ Hz, 2H), 7.15 (t, $J = 8.15$ Hz, 1H) 7.30 (t, $J = 7.02$ Hz, 1H) 7.49(d, $J = 7.80$ Hz, 1H) 7.57 (d, $J = 8.15$ Hz, 1H) 7.92 (d, $J = 8.99$ Hz, 2H) (Appendix Figure 48)

^{13}C NMR (CDCl_3 , 400MHz) δ :14.09, 47.81, 52.97, 60.53, 61.74, 113.63, 120.04, 124.72, 127.49, 128.59, 130.47, 131.44, 133.17, 137.27, 154.18, 166.70. (Appendix Figure 49)

HRMS m/z : found 403.1036 $[\text{M} + \text{H}]^+$, calculated for $\text{C}_{20}\text{H}_{23}\text{BrN}_2\text{O}_2$ 402.0943 (Appendix Figure 50)

CHN: Theoretical C 59.56%, H 5.75%, N 6.95% Experimental C 59.56%, H 5.73%, N 6.91% (Appendix Figure 51)

6.5.3 Preparation of ethyl 4-((4'-(4-chlorobiphenyl-2-yl)methyl)piperazin-1-yl)benzoate, Compound 10 ABT 737



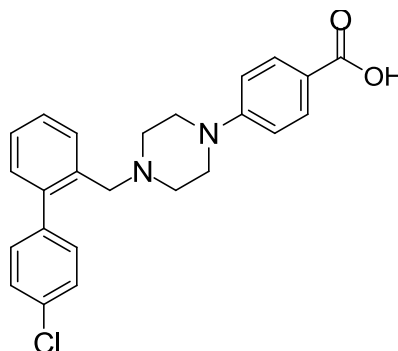
Procedure: To a suspension of compound 9 (0.812 g, 2 mmol), 4-chlorophenylboronic acid (0.375 g, 2.4 mmol) and aqueous sodium carbonate (2M, 2.5 mL, 2.4 mmol) in DME-H₂O-EtOH (7 mL-3 mL-2 mL) was added PdCl₂(PPh₃)₂ (56 mg, 0.8 mmol). The mixture was heated at 85 °C for 3 h under nitrogen atmosphere and filtered through a pad of Celite. The filter cake was washed with ethyl acetate and the combined filtrates were concentrated. The crude product was crystallised from MeOH to yield white crystals. (1.77 g, 89%).

¹H NMR (CDCl₃, 400MHz) δ : 1.32 (t, J = 7.05Hz, 3H), 2.39 (m, 4H), 3.24 (m, 4H), 3.39 (s, 2H), 4.23 (q, J = 7.02Hz, 2H), 6.89 (d, J = 9.07Hz, 2H), 7.15 (t, J = 8.15Hz, 1H), 7.30 (t, J = 7.02Hz, 1H), 7.49 (d, J = 7.80Hz, 1H), 7.57 (d, J = 8.15Hz, 1H), 7.39 (d, J = 8.99Hz, 2H) (Appendix Figure 52)

¹³C NMR (CDCl₃, 400MHz) δ : 14.27, 46.70, 51.38, 59.24, 59.83, 113.67, 118.39, 127.20, 127.46, 127.92, 129.68, 130.03, 130.61, 131.06, 131.86, 135.12, 139.68, 153.81, 165.62. (Appendix Figure 53)

HRMS m/z: found 435.1818 [M + H]⁺, calculated for C₂₆H₂₇ClN₂O₂ 434.1761 (Appendix Figure 54)

6.5.4 Preparation of 4-(4-((4'-chloro-[1,1'-biphenyl]-2-yl)methyl)piperazin-1-yl)benzoic acid, Compound 11 ABT 737



Procedure: A suspension of compound 10 (945 mg, 2.17 mmol) and LiOH (41.96 mg, 8.68 mmol) in water (7ml) and dioxane (45ml) was heated at 100°C for 18 hours. The dioxane was removed by evaporation and the resulting solution was diluted with water and heated to reflux for 1 hour. The solution was neutralized with 2M HCl and the resulting white solid collected by filtration and dried to yield the desired product, (796 mg, 87%).

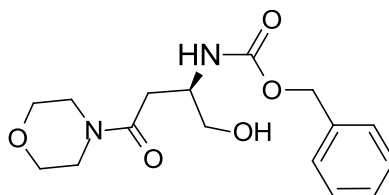
¹H NMR (CDCl₃, 400MHz) δ: 2.39 (m, 4H), 3.24 (m, 4H), 3.39 (s, 2H), 6.90 (d, J= 9.07 Hz, 2H), 7.15 (t, J= 8.15 Hz, 1H), 7.30 (t, J= 7.02Hz, 1H), 7.49(d, J= 7.80 Hz, 1H), 7.52 (s, 4H), 7.57 (d, J= 8.15Hz, 1H), 7.41 (d, J= 8.99 Hz, 2H). (Appendix Figure 55)

¹³C NMR (CDCl₃, 400MHz) δ: 46.02, 52.01, 113.30, 120.17, 131.14, 153.65, 167.23(Appendix Figure 56)

HRMS m/z: found 407.1543 [M + H]⁺, calculated for C₂₄H₂₃ClN₂O₂ 406.1448 (Appendix Figure 57)

6.6 Synthetic procedures of ABT 263

6.6.1 Preparation of (R)-benzyl (1-hydroxy-4-morpholino-4-oxobutan-2-yl)carbamate, Compound 2 ABT 263



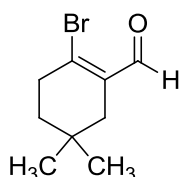
Procedure: (R)-benzyl (5-oxotetrahydrofuran-3-yl)carbamate (1.459 g, 6.2 mmol) and morpholine were added to a microwave vial (15 ml vial) filled to the required volume using dioxane. Using the microwave synthesizer, Biotage Initiator 2.5, the reaction was run for 4.5 hrs at 90°C with pre-stirring of 1min, adsorption level normal and fixed hold time on. After this time the solution was concentrated yielding a clear gel. The product was purified by column chromatography on silica gel using 10% MeOH and ethyl acetate. Yield 73%, 1.462g.

^1H NMR (CDCl_3 , 400MHz) δ : 2.71 (dd, $J=5.8\text{Hz}$, 2H), 3.66 (m, 11H), 3.97 (m, 1H), 5.09 (s, 2H), 7.35 (m, 5H) (Appendix Figure 58)

^{13}C NMR (CDCl_3 , 100.6MHz) 34.4, 46.0, 50.0, 63.8, 66.8, 67.5, 128.0, 128.2, 128.50, 136.3, 156.3, 169.9. (Appendix Figure 59)

$m/z=325.63$ (100%, $[\text{M} + \text{H}]^+$) calculated for $\text{C}_{16}\text{H}_{22}\text{N}_2\text{O}_5$ 323.1529 (Appendix Figure 60)

6.6.2 Preparation of 1-bromo-4,4dimethylcyclohex-1-ene-carbaldehyde, Compound 9 ABT 263



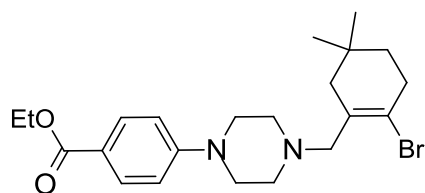
Procedure: A magnetically stirred solution of DMF (18.2 mmol, 1.411 ml) in anhydrous chloroform (10 ml) at 3°C was carefully treated with phosphorus tribromide (18.2 mmol, 4.93 g). The resulting pale yellow liquid was warmed to room temperature and was allowed to stir for an additional 20 min.

A solution of 4, 4-dimethyl cyclohexanone (4.5 mmol, 574 mg) in anhydrous chloroform (9ml) was added dropwise to the reaction mixture. It was then heated to 60°C for 1hr resulting in a red/orange solution. The solution was then poured into ice and neutralised with solid sodium bicarbonate. The product was extracted with ether which was washed with brine twice, dried using MgSO_4 and evaporated to yield a yellow oil. Yield: 38% 380mg

^1H NMR (CDCl_3 , 400MHz) δ : 0.88 (s, 6H), 1.45 (t, J = 6.54 Hz, 2H), 2.01 (s, 2H), 2.69 (m, 2H), 9.96 (s, 1H). (Appendix Figure 61)

^{13}C NMR (CDCl_3 , 400MHz) δ : 27.62, 28.48, 36.76, 38.29, 50.92, 134.02, 142.77, 194.00. (Appendix Figure 62)

6.6.3 Preparation of ethyl 4-(4-((2-bromo-5,5-dimethylcyclohex-1-en-1-yl)methyl)piperazin-1-yl)benzoate, Compound 10 ABT 263



Procedure: 1 bromo-4,4-dimethyl cyclohexene carbaldehyde (0.737 g, 3.4 mmol) and ethyl 4-(piperazin-1-yl)benzoate (0.830 g, 3.5 mmol) in MeOH (~40ml) was treated with sodium cyanoborohydride (0.440 g, 7.1 mmol) adjusted to pH 5 with acetic acid and stirred for 18hrs. After this time the solution was concentrated to yield a cream solid. Yield 73%, 1.077g

^1H NMR (CDCl_3 , 400MHz) δ : 0.924 (s, 6H), 1.36 (t, J =7.34 Hz, 3H), 1.43 (t, J =6.69 Hz, 2H), 1.99 (s, 2H), 2.49 (t, 2H), 3.40 (m, 4H), 3.57 (m, 4H), 4.20 (s, 2H), 4.32 (q, J =7.3 Hz, 2H), 6.88 (d, J =8.39, 2H), 7.95 (d, J =8.39 2H) (Appendix Figure 63)

^{13}C NMR (CDCl_3 , 400MHz) δ : 14.38, 27.77, 29.18, 34.47, 37.13, 42.82, 43.69, 45.28, 60.74, 66.34, 114.96, 120.23, 131.37, 133.93, 152.81(Appendix Figure 64)

m/z =435.57 (100%, $[\text{M} + \text{H}]^+$) calculated for $\text{C}_{22}\text{H}_{31}\text{BrN}_2\text{O}_2$ 434.1569 (Appendix Figure 65)

The reaction scheme illustrates the synthesis of a Ru(II) complex. The scheme is divided into two main parts: the synthesis of a chiral diamine ligand (1) and the synthesis of a chiral sulfonamide ligand (5).

Synthesis of Chiral Diamine Ligand (1):

- Starting materials: 4-fluorobenzenesulfonamide (2) and 4-nitrophenylamine (3).
- Reaction 1: 2 + 3 → 4 (Intermediate: 4-(4-nitrophenyl)-N-(4-fluorophenyl)propan-1-amine).
- Reaction 2: 4 → 1 (Intermediate: 4-(4-nitrophenyl)-N-(4-fluorophenyl)-2-methylpropan-1-amine).

Synthesis of Chiral Sulfonamide Ligand (5):

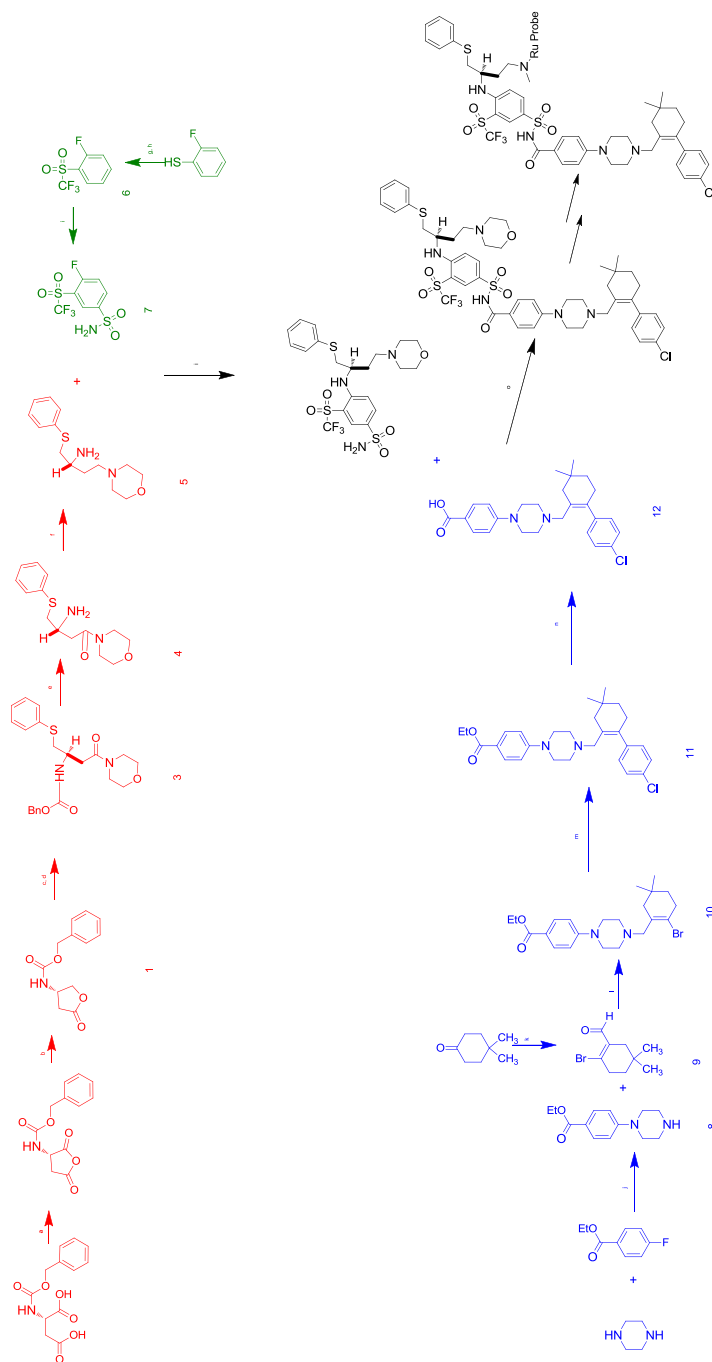
- Starting materials: 4-fluorobenzenesulfonamide (2) and 4-nitrophenylamine (3).
- Reaction 3: 2 + 3 → 6 (Intermediate: 4-(4-nitrophenyl)-N-(4-fluorophenyl)-2-methylpropan-1-amine).
- Reaction 4: 6 → 5 (Intermediate: 4-(4-nitrophenyl)-N-(4-fluorophenyl)-2-methylpropan-1-amine).

Synthesis of Ru(II) Complex:

- Starting materials: Chiral diamine ligand (1), Chiral sulfonamide ligand (5), and Ru(II) precursor (7).
- Reaction 5: 1 + 5 + 7 → Ru(II) complex (Final product: Ru(II) complex with chiral diamine and chiral sulfonamide ligands).

163

Synthesis of Ru Probe-ABT-263



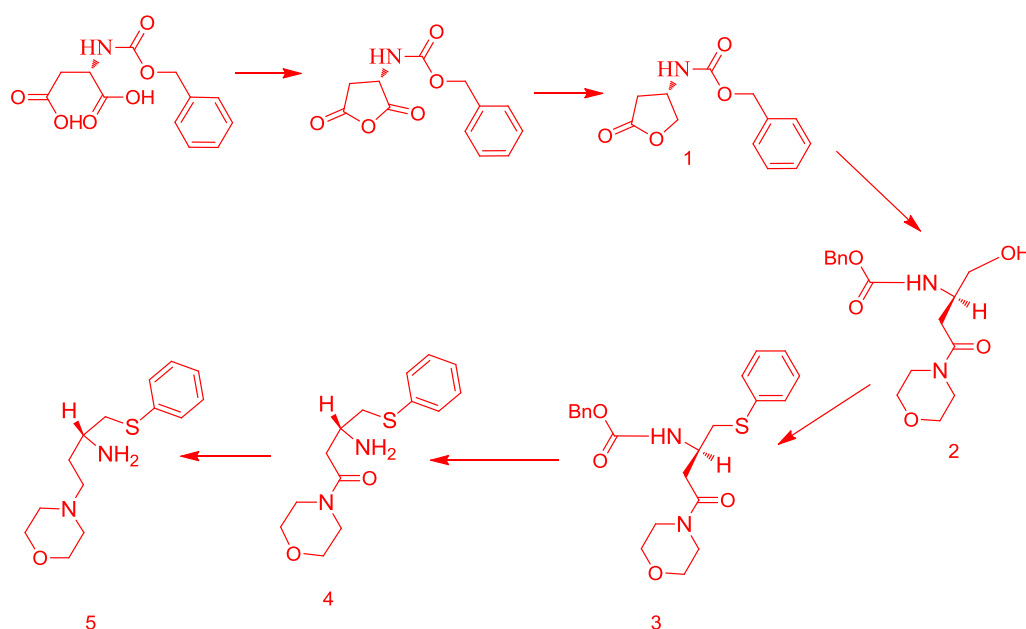
a. EtOAc, rt; **b.** NaBH₄, THF, rt, HCl; **c.** morpholine, dioxane 65°C; **d.** (PhS)₂, Bu₃P, toluene, 80°C; **e.** 30% HBr/HOAc, rt; **f.** BH₃-THF, THF, rt, MeOH, HCl (conc); **g.** methyl viologen hydrochloride, DMF CF₃I, TEA 25°C; **h.** NaIO₄, RuCl₃·H₂O, 25°C, DCM; **i.** THF, DIEA 50°C; **j.** DMSO, 120°C; **k.** CHCl₃/PBr₃, DMF, 25°C; **l.** MeOH, NaBH₃(CN), CH₃COOH; **m.** 4-chlorophenylboronic acid, Pd(PPh₃)₂Cl₂/DME, EtOH 2m aq. Na₂CO₃; **n.** LiOH-H₂O, dioxane 100°C; **o.** DMAP, EDCI, CH₂Cl₂, rt.

6.7 Results and Discussion

6.7.1 ABT 263

The synthetic routes for ABT 263 and ABT 737 are similar. ABT 263 was initially selected as it belongs to a newer generation of BH3 mimetic inhibitors, orally available and which has progressed to clinical trials.^[11] The literature available for the synthesis of this candidate is limited to a patent to Abbott laboratories, which was used as a reference for the synthetic procedures. Limited details of the synthetic protocols and characterisation data were disclosed in this document.

6.7.1.1 Route 1 ABT 263



Scheme 6. 1 Route 1 of ABT 263: Synthesis of 4-morpholino-1-(phenylthio)butan-2-amine (5)

Route 1 was investigated separately originally, but to benefit of the advantages of a convergent synthesis, the preparation of the 3 main synthons was in due course performed in parallel. The required *N*-benzyloxycarbonyl-D aspartic acid anhydride (1) was prepared through the reaction of *N*-benzyloxycarbonyl-D-aspartic acid with acetic anhydride by the method of Lutz and co-workers^[26] as this step was not described in the patent. This dehydration reaction involves the conversion of the carboxylic acids to an acid anhydride. The starting material, *N*-benzyloxycarbonyl -D-aspartic acid, is protected by the Bergmann-Zervas benzyloxycarbonyl group. The electron withdrawing nature of the carbonyl group exerted on the nitrogen's lone pair of electrons, is reduced by the donation of a lone pair of electrons from the oxygen, which also renders the carbonyl carbon less susceptible to

nucleophiles. Liberation of the amino group will occur upon completion of route 1 by treatment with hydrobromic acid (HBr) of the labile carbon-oxygen bond. This can also be achieved cleanly by catalytic hydrogenation producing carbon dioxide and toluene as side products. Due to the sensitivity of the anhydride to hydrolysis, it was used directly in the next step after freeze-drying without purification. This step consistently produced low yield (~40%) of materials and was very time consuming as the removal of the azeotropic solvents could not be performed above 38°C and could take up to 3 weeks on the high vacuum line. Alternative methods were therefore investigated.

An alternative reaction for the formation of the acid anhydride used thionyl chloride. Thionyl chloride would convert the carboxylic acid to the acyl chloride, followed by addition-elimination mechanism in which the chloride anion is the leaving group. In the initial reaction step, the carboxyl oxygen reacts by nucleophilic attack with the considerably electrophilic acyl halide's carbonyl carbon. As a result, a tetrahedral intermediate is formed. In the second reaction step, a chloride - a good leaving group - is eliminated from the tetrahedral intermediate resulting in the closed ring structure. This reaction gave us similar low yields and due to the harmful properties of thionyl chloride, the first reaction option was maintained.

The next step required the selective reduction of the anhydride to form the 3-(*R*) carboxybenzyl-amino-butyrolactone (1). As described in the patent this was achieved by treatment with sodium borohydride (NaBH₄) and resulted in the regiospecific reduction of the anhydride to obtain the desired product (1). Sodium borohydride is a common reducing agent for carbonyl compounds. It is a simple, safe, inexpensive reagent and reduction can be achieved within 3-4hrs. Operational simplicity makes this procedure generally attractive. It does not require anhydrous conditions and avoids the use of an inert atmosphere, unlike the powerful reducing agent lithium aluminum hydride. The regioselectivity of this approach has been shown by McGarvey *et al.* [27] These two combined steps to form 3-(*R*)-*N*-benzyloxycarbonyl -amino-butyrolactone (1) gave yields up to 50%.

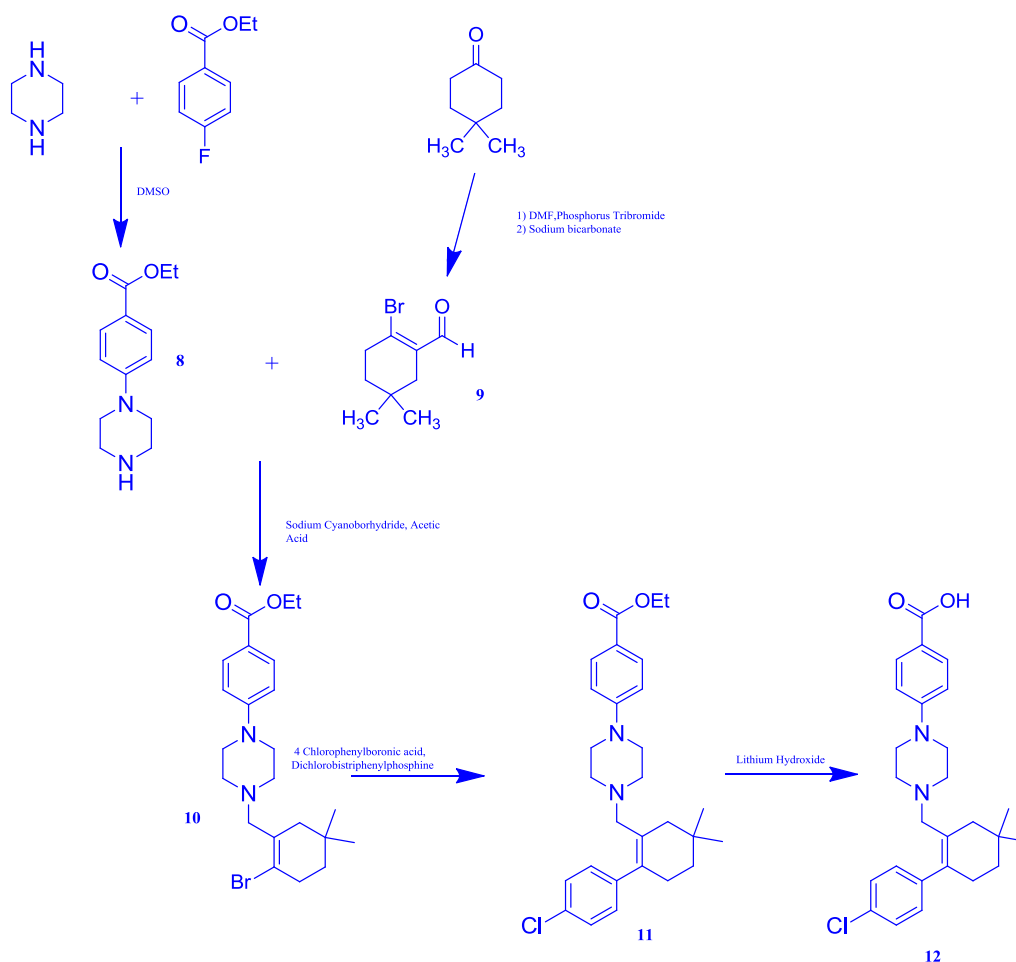
The next step required the nucleophilic reaction of the morpholine ring with the lactone group of 3-(*R*)-*N*-benzyloxycarbonyl-amino-butyrolactone (1) to form (R)-benzyl (1-hydroxy-4-morpholino-4-oxobutan-2-yl)carbamate (2). This was first attempted by the method reported in the patent and involved the reaction of 3-(*R*)-*N*-benzyloxycarbonyl-amino-butyrolactone (1) in the presence of 2 molar equivalence of morpholine in dioxane stirred for 24 hours at 65°C. On the first attempt the reaction did not go to completion and a significant amount of starting material remained, resulting in yields as low as 16%. The

reaction was repeated and monitored by TLC, using a total of 16 molar equivalents of morpholine, added over 60hrs. The reaction failed again to go to completion. Several attempts to alter the reaction conditions all remained unsuccessful and microwave activation was then considered.^[28]

There are numerous reports in the literature showing that microwave heating can intensely reduce reaction times, increase product purities and improve product yields by decreasing unwanted side-reactions when compared to conventional heating methods.^[29, 30] In principle, any chemical reaction that involves heat can be achieved under microwave conditions has been largely accepted as a fact by the scientific community.^[31] The short reaction times provided by microwave synthesis make it ideal for rapid reaction scouting and optimization of reaction conditions. Having had success with microwave-assisted peptide synthesis, this reaction was first attempted on a small scale (2-5ml vial).

The reaction took place in the Biotage Initiator 2.5 microwave synthesizer. A reaction time of 4.5hrs, with a fix hold time, which means that the time of the reaction does not start until the reaction reaches the target temperature, were selected, according to the manufacturer's guidelines. Pre-stirring was set to 1 minute and dioxane was used as the solvent, as its boiling point is 101°C, while the reaction was conducted at 90°C. After purification this small scale reaction gave a yield of 63%. This increase in yield and reduction in reaction time was consistent with previous reports on microwave-assisted organic synthesis. When conducted on a larger scale the yield was further increased to 73%. This is as far as Route 1 ABT 263 proceeded. Multiple attempts performed to convert the hydroxyl into a phenylthio group consistently failed.

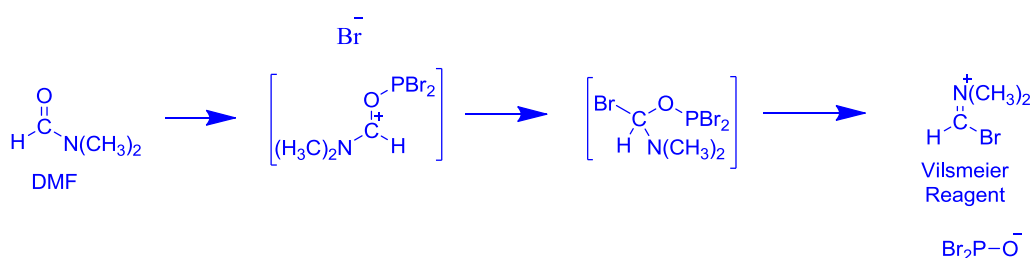
6.7.1.2 Route 3 ABT 263



Scheme 6. 2 Synthesis of 4-(4-((4'-chloro-4,4-dimethyl-3,4,5,6-tetrahydro-[1,1'-biphenyl]-2-yl)methyl)piperazin-1-yl)benzoic acid (12)

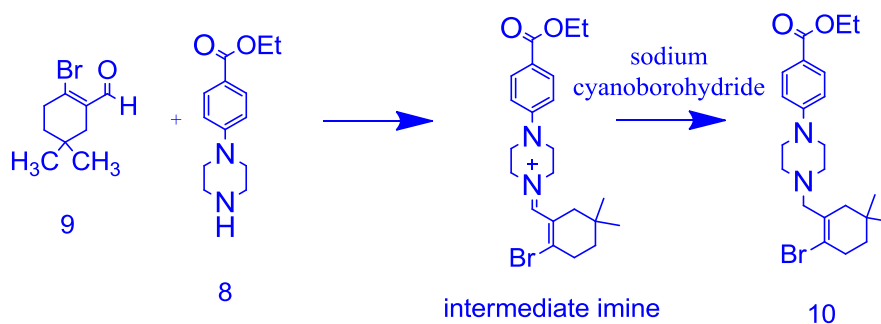
4-Piperazin-1-ylbenzoic acid ethyl ester (8) was directly performed as the starting material of this synthetic route by Abbott laboratories in their patent. However, the cost of this material proved to be prohibitive for our studies and as this starting material can be conveniently prepared in a single step from readily available reagents, it was decided to synthesise this intermediate. The simple aromatic substitution reaction was carried out according to Kubota *et al.* and isolated yields up to 79% were obtained.^[32] The product and impurities were first taken up in DCM and washed with a mild base, sodium bicarbonate, resulting in deprotonation of the amine resulting in the product 4-piperazin-1-ylbenzoic acid ethyl ester (8). After a wash with brine the product was isolated by rotary evaporation. The reaction gave no noticeable side-products and therefore produced an intermediate used in the next step without purification.

The first attempt to synthesise 1-bromo-4,4-dimethylcyclohexane-carbaldehyde (9) was performed according to the method reported in the patent. A crude yield of 32% was obtained and NMR analysis showed evidences of a large amount of starting material remaining in this crude product. This was confirmed by the low yield for the purified product (5%). This reaction proceeds by first forming the Vilsmeier reagent from DMF in the presence of phosphorus tri-bromide (Scheme 6.4) ^[33, 34]. The Vilsmeier reagent is utilized to form both the intermediate and the final product. This reaction cannot be monitored by TLC as the final product is made during the work-up. The reaction conditions described in the patent consisted in stirring the preformed Vilsmeier reagent with 4,4 dimethyl-cyclohexanone at room temperature for 18 hours. However, as reported by Xiang *et al.*, when the reaction was conducted at higher temperatures (60°C) the reaction time was reduced (1 hour) and the yield increased (38%).^[35] The product was also obtained with a good purity, as shown by NMR analysis, and could proceed to the next synthetic step without purification.



Scheme 6. 3 Formation of the Vilsmeier reagent

4-[4-(2-Bromo-5,5-dimethyl-cyclohex-1-enylmethyl)-piperazin-1-yl]-benzoic acid ethyl ester (10) is formed by reductive amination (Scheme 6.5). This involves the conversion of the carbonyl group of 1-bromo-4,4-dimethylcyclohexane-carbaldehyde (9) to an amine via an intermediate imine. The amine source is 4-piperazin-1-ylbenzoic acid ethyl ester (8). This reaction was carried out by a one-pot procedure, with the imine formation and reduction occurring consecutively. In this case sodium cyanoborohydride (NaBH_3CN) was chosen as the reducing agent. Good yields of crude materials (93%) were obtained for this step. These materials were relatively pure with residual acetic acid being the main impurity.



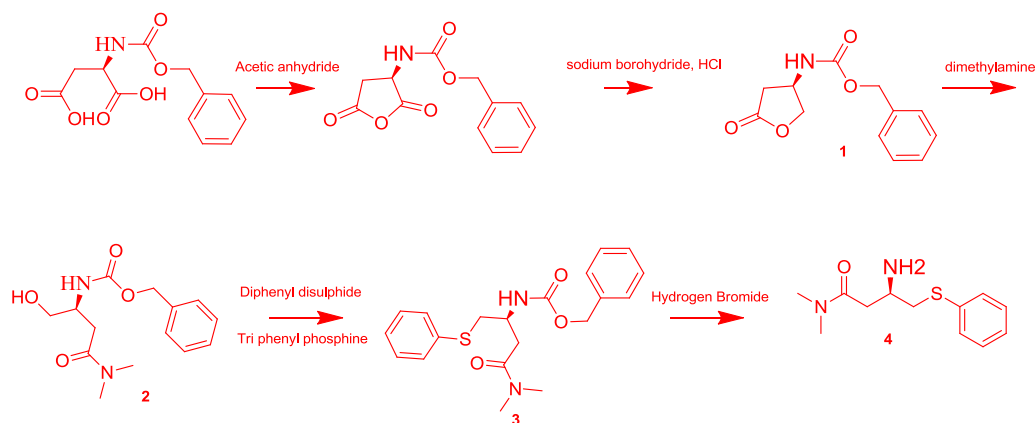
Scheme 6. 4 Formation of the 4-[4-(2-Bromo-5,5-dimethyl-cyclohex-1-enylmethyl)-piperazin-1-yl]-benzoic acid ethyl ester by reductive amination.

This is as far as the synthesis of ABT 263 was attempted. Independent difficulties occurring in the preparation of another synthon, attempted according to Route 2 of the overall synthetic scheme for ABT 263 shown in green on page 164. The synthesis of 4-fluoro-3-trifluoromethanesulfonyl-benzenesulfonamide requires the use of trifluoromethyl iodide, a gas that ultimately couldn't be handled safely. Considering also the potential formation of hydrogen fluoride from this reagent and the high cost of another starting material for this synthetic route 2 of ABT 263 (2-fluorothiophenol), the 4-fluoro-3-trifluoromethanesulfonyl-benzenesulfonamide synthon was replaced by 4-fluoro-3-nitrobenzenesulfonamide. This involves the synthesis of ABT 737 in place of ABT 263, but as the other 2 synthons in their synthetic route are similar, most of the work completed to this point could be transferred to the new synthetic route. In term of their ultimate application, ABT 737 and ABT 263 differ by their oral bioavailability, a factor that doesn't impact on the investigation of the localisation and function of a BH3 mimetic inhibitor labelled with a ruthenium probe in cell culture studies.

6.7.2 ABT 737

The synthesis of ABT 737 proceeded as described by Oltersdorf *et al*^[10] with a few changes as outlined below. Route 1 had been partly investigated previously for the synthesis of ABT 263, but could not be progressed further due to time constraints. Route 2 and 3 were prioritised and completed.

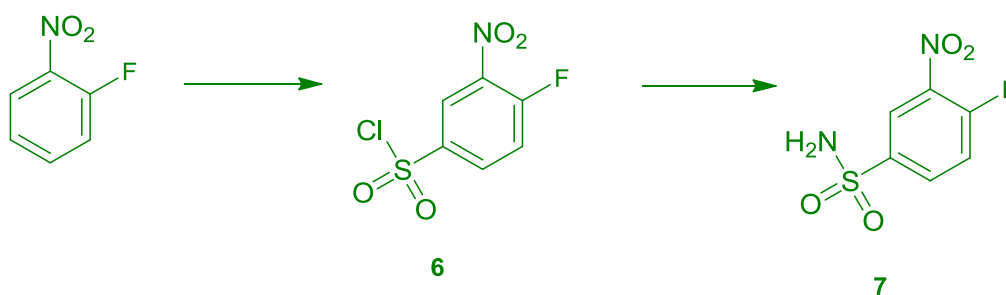
6.7.2.1 Route 1 ABT 737



Scheme 6.6 Route 1: Synthesis of (R)-3-amino-N,N-dimethyl-4-(phenylthio)butanamide

Route 1 of ABT 737 is identical to Route 1 of ABT 263 as far as intermediate 1. This has been described previously in section 6.7. The next step of route 1 for ABT 737 involved the nucleophilic substitution by reaction of *N,N*-dimethylamine with 3-(*R*)-*N*-benzyloxycarbonyl-amino-butyrolactone (1) to form (*R*)-benzyl-(4-(dimethylamino)-1-hydroxy-4-oxobutan-2-yl) carbamate. Oltersdorf's procedure^[10] involved bubbling gaseous dimethylamine into a solution of 3-(*R*)-*N*-benzyloxycarbonyl-amino-butyrolactone (1), however the use of a dimethylamine solution was favoured to meet health and safety standards with the equipment available in the laboratory. Yields up to 91 % were obtained in these conditions, but the next step could not be investigated due to a lack of time.

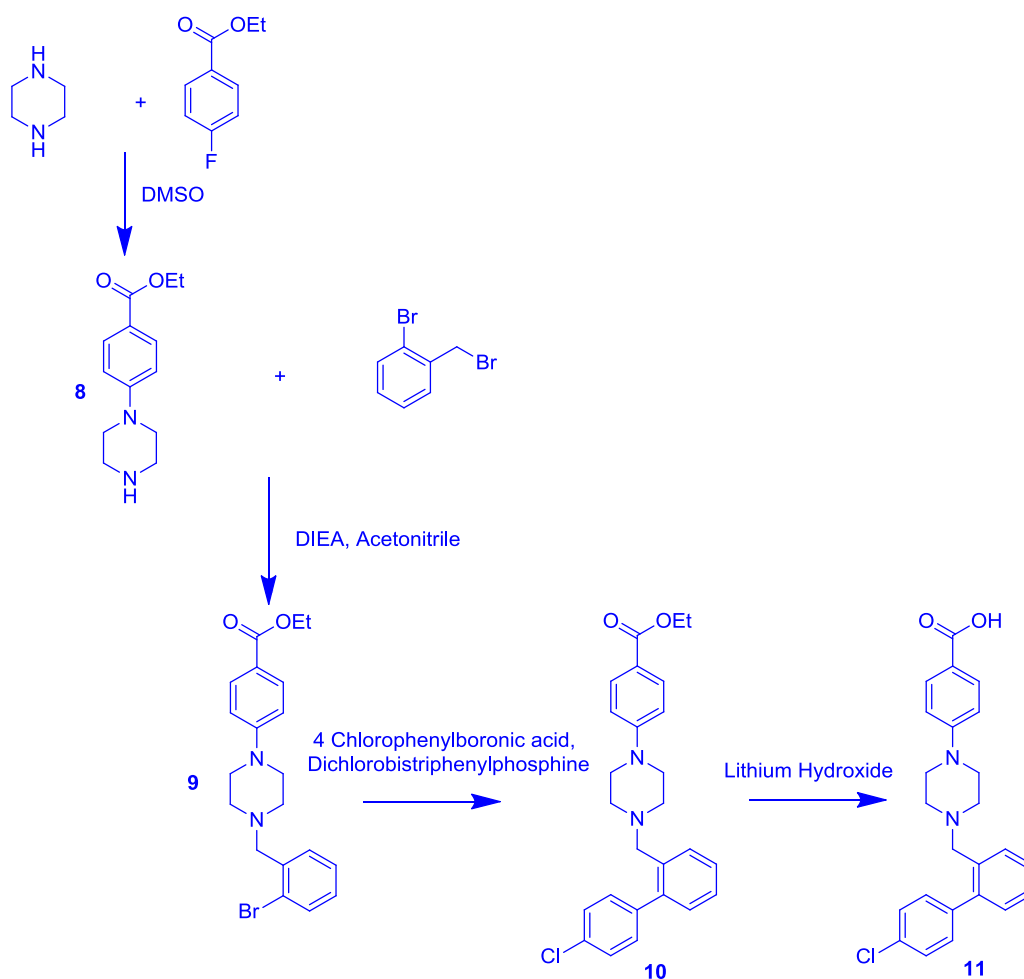
6.7.2.2 Route 2 ABT 737



Scheme 6.7 Route 2 Synthesis of 4-fluoro-3-nitrobenzenesulfonamide

The shortest of the three converging routes, route 2 begins with 1-fluoro-2-nitrobenzene. The nitro groups meta directing effects forms the sulfonic acid intermediate 4-fluoro-3-nitrobenzene-1-sulfonyl chloride (6). This compound reacts in the next step with ammonium hydroxide to form the corresponding sulphonamide (7). This route 2 for ABT 737 proceeded to completion and gave yields of 60% over the two steps.

6.7.2.3 Route 3 ABT 737



Scheme 6. 8 Synthesis of 4-(4-((4'-chloro-[1,1'-biphenyl]-2-yl)methyl)piperazin-1-yl)benzoic acid.

In route 3 of ABT 737, ethyl 4-(piperazin-1-yl)-benzoate intermediate (8) is the same as the previously described in Route 3 of ABT 263. The next step in the synthesis of ABT 737 involves an amine alkylation. The alkyl halide in this case is 1-bromo-2-bromomethylbenzene. This nucleophilic aliphatic substitution reaction forms the higher substituted amine. *N,N*-Diisopropylethylamine was added as a base to assist the deprotonation of the amine. As a tertiary amine is formed the reaction does not require as much control as if the desired product was to be a primary or secondary amine and therefore equal molar equivalents of the amine to the halide is added to form the desired product ethyl 4-(4-(2-bromobenzyl)piperazin-1-yl)benzoate (9).

Suzuki coupling is used to form the next intermediate, ethyl 4-(4-((4'-chloro-[1,1'-biphenyl]-2-yl)methyl)piperazin-1-yl)benzoate (10). The first step in the Suzuki reaction is the oxidative addition of the palladium, $\text{PdCl}_2(\text{PPh}_3)_2$ to the previous intermediate ethyl 4-(4-

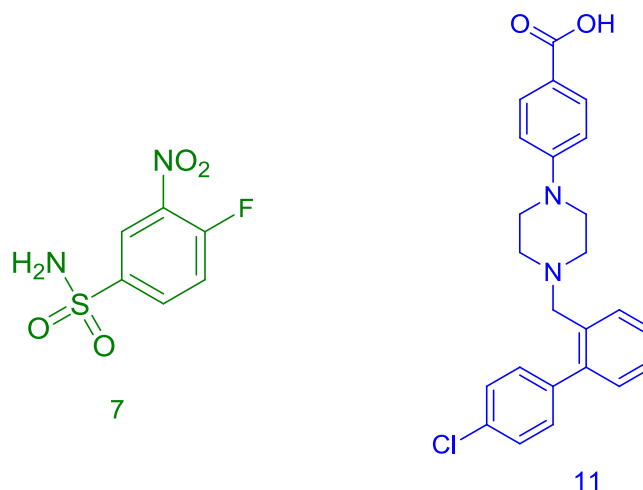
(2-bromobenzyl)piperazin-1-yl)benzoate (9). This forms an organopalladium species which reacts with the base, sodium carbonate forms another organopalladium species, via transmetalation with the chlorophenylboronic acid. This is then reduced, reforming the palladium catalyst and the desired product ethyl 4-(4-((4'-chloro-[1,1'-biphenyl]-2-yl)methyl)piperazin-1-yl)benzoate (10).

The final step of this route is the deprotection of the ethyl ester in (10) to form the corresponding carboxylic acid, 4-(4-((4'-chloro-[1,1'-biphenyl]-2-yl)methyl)piperazin-1-yl)benzoic acid (11). This is achieved by using LiOH-promoted hydrolysis to form the carboxylate. The free carboxylic acid (11) is formed by acidification with HCl, giving yields for (11) of 87%.

6.8 Photophysical Results

The use of the ABT 263 molecule was initially intended for cellular localisation and function studies, by modifying the morpholino substituent by a ruthenium label conjugated through a linker by an amide bond, once the synthetic procedures for the parent BH3 mimetic inhibitor had been optimised. The intention was also to apply this approach to the ABT 737 candidate, by replacement of the dimethylamino group. However the structure of the ABT 737 molecule itself led us to believe that the molecule may be capable of fluorescence. Therefore the photophysics was explored with two of the fully assembled synthons. The final intermediate of Route 3 for ABT 737, 4-(4-((4'-chloro-[1,1'-biphenyl]-2-yl)methyl)piperazin-1-yl)benzoic acid (11) contained biphenyl rings and had therefore a promising structure as a ridged molecule with an extended π system, that might be capable of absorbing light resulting in a π - π^* transition.

The final intermediates in Route 2 and Route 3 of ABT 737, were investigated for their photophysical properties, the compounds are shown in Scheme 6.9. 4-Fluoro-3-nitrobenzenesulfonamide (7) from route 2 used in a 2.3 mM aqueous solution presented a UV-VIS spectra distinguished by a signal at 248 nm and a shoulder at 296 nm, likely to originate from π - π^* and nitro based transitions respectively. On the other hand, it did not emit in aqueous solution. The material was incubated with CHO cells and confocal imaging attempted, but as expected resulted in no compound visible within the cells.



Scheme 6.9 ABT 737 Route 2 Final molecule 7 and Route 3 Final molecule 11

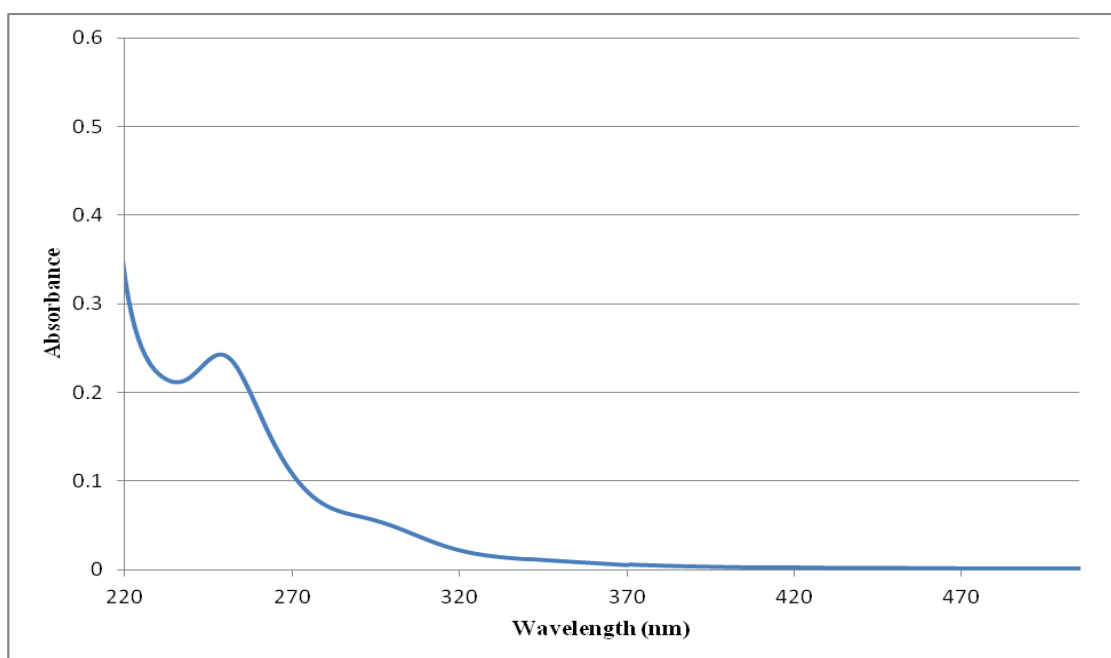


Figure 6. 1 UV-VIS spectrum of ABT 737, 4-fluoro-3-nitrobenzenesulfonamide (7) (2.3mM)

The UV-VIS spectra of (11) is distinguished by a signal at 289 nm. Interestingly, when the molecule was excited at this wavelength it gave a dual emission at 363 nm and 704

nm, to our knowledge, the emission of ABT derivatives has not been reported previously. Both emissions are genuine as confirmed by excitation studies. The dual emission was very interesting and we believed it had potential for direct cellular imaging for localisation and functional studies, without conjugation to a chromophore. However, as cell testing was conducted the emission was found not to be sufficiently strong to be distinguished from the background. Therefore conjugation to a chromophore is required for future work involving confocal imaging.

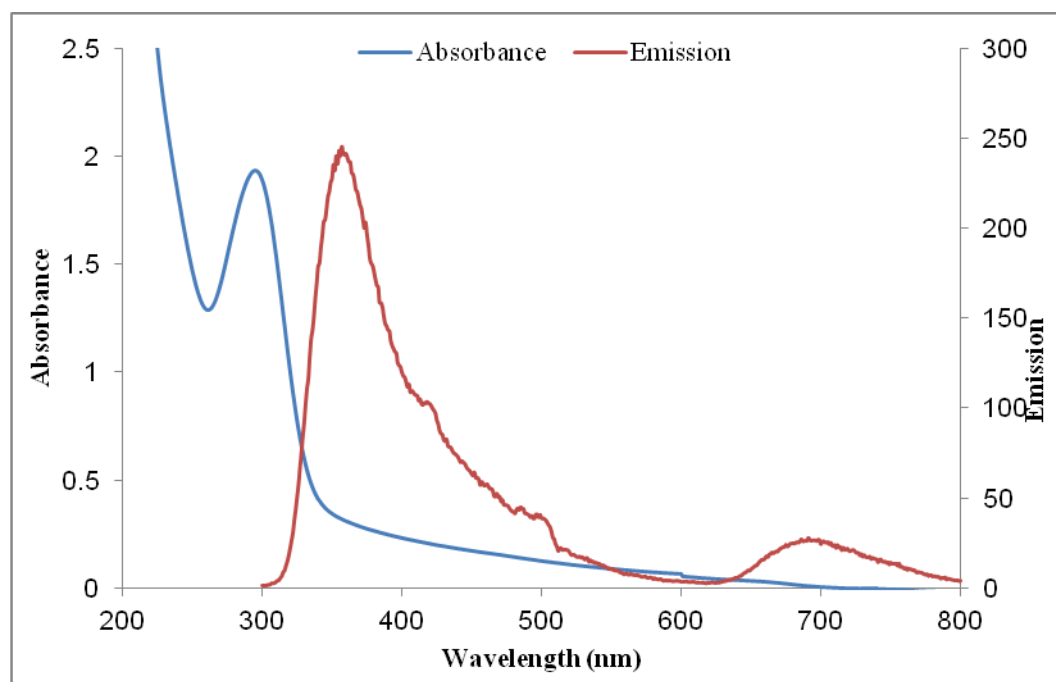


Figure 6.3 UV-VIS spectrum emission of spectrum of ABT 737 Route 3 Final Molecule in aqueous solvent.

6.9 Cytotoxicity

Preliminary cytotoxicity was conducted for the final molecules in Route 2 (7) and Route 3 (11) of ABT 737 as outlined in Chapter 3. Synthon (11) proved to be non toxic whereas synthon (7) proved to be very toxic. Synthon (7) of ABT 737 induces cellular toxicity (in CHO cells) at concentrations above 10 μ M when incubated overnight at 37°C. Further studies to investigate if cell death is occurring through apoptosis or necrosis are currently conducted.

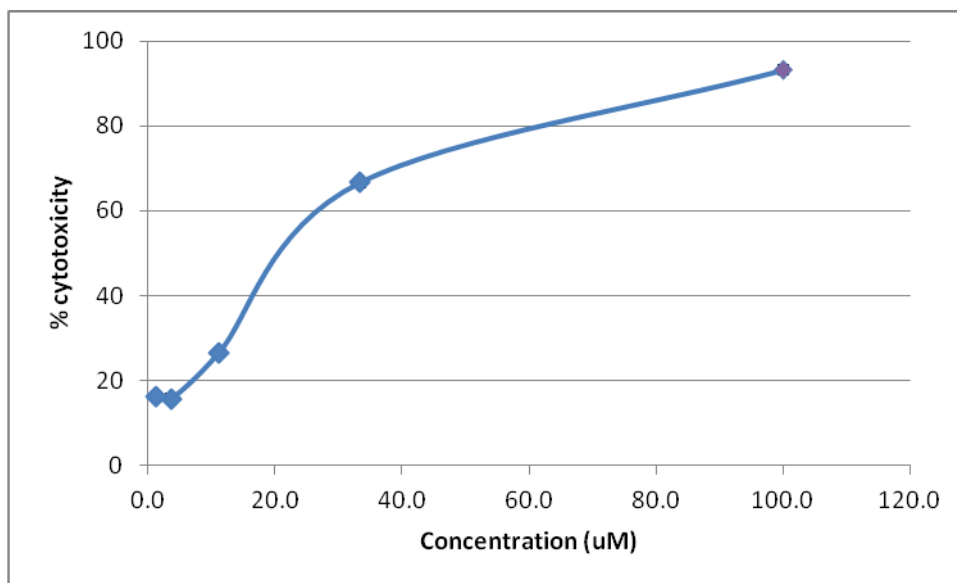


Figure 6. 4 Cytotoxicity assay with CHO cells treated with Route 2 Final molecule (7) (Data collected by Dr. Róisín Moriarty)

6.10 Conclusions

This work was commenced in order to investigate the location and functional of ABT 263 by confocal microscopy. Originally the ABT 263 molecule was chosen for investigation. This seemed to be an ideal small molecular inhibitor to select for investigation as it is in stage 3 clinical trials, however due to difficulties in its synthesis, the close analogue ABT 737 was selected for synthetic and labelling feasibility studies. Using the information disclosed in a patent proved to be challenging due to the absence of some synthetic details in the protocols implemented and of some analytical data. ABT 737 has the same target and therefore cellular localisation as ABT 263 and therefore could be used for the same purpose in term of cellular imaging. There have been many difficulties to be addressed to complete the assembly of 2 of the 3 synthons of ABT 737, leading to the inability to complete the synthesis the final molecule. One major hurdle remainig in the synthesis of ABT 737 is to initiate Route 1. Its first intermediate (1) proved to be a very unstable molecule to be isolated through a long and low yielding work-up.

Due to the growing cost of the synthesis, it was decided to discontinue the synthesis of these BH3 mimetic inhibitors and to focus on the inherent potential photophysical properties of the molecule ABT 737. We aimed to achieve our original goal of cellular imaging with the synthesised fragments obtained from the completed routes 2 and 3. Although the synthon from the latter gave promising photophysical results, this intermediate

failed to give a strong dual emission with two peaks an intense emission around 380 nm and a weaker transition, which at 700 nm. Unfortunately, the requirement for UV excitation to generate these emissions meant it was still unsuitable for applications in cell imaging. Route 2 final intermediate (7) molecule had poor photophysical results and proved moreover to be very toxic to CHO cells.

References

- [1] Blazer, L. L.; Neubig, R. R., *Neuropsychopharmacology*, (2008) **34**, 126.
- [2] Arkin, M. R.; Wells, J. A., *Nat Rev Drug Discov*, (2004) **3**, 301.
- [3] Berg, T., *Angewandte Chemie International Edition*, (2003) **42**, 2462.
- [4] Chakrabarti, P.; Janin, J., *Proteins: Structure, Function, and Bioinformatics*, (2002) **47**, 334.
- [5] Fernández-Recio, J., *Wiley Interdisciplinary Reviews: Computational Molecular Science*, (2011) **1**, 680.
- [6] Wells, J. A.; McClendon, C. L., *Nature*, (2007) **450**, 1001.
- [7] Sadowsky, J. D.; Fairlie, W. D.; Hadley, E. B.; Lee, H.-S.; Umezawa, N.; Nikolovska-Coleska, Z.; Wang, S.; Huang, D. C. S.; Tomita, Y.; Gellman, S. H., *Journal of the American Chemical Society*, (2006) **129**, 139.
- [8] Sadowsky, J. D.; Murray, J. K.; Tomita, Y.; Gellman, S. H., *ChemBioChem*, (2007) **8**, 903.
- [9] Yin, X.-M.; Wang, K.; Gross, A.; Zhao, Y.; Zinkel, S.; Klocke, B.; Roth, K. A.; Korsmeyer, S. J., *Nature*, (1999) **400**, 886.
- [10] Oltersdorf, T.; Elmore, S. W.; Shoemaker, A. R.; Armstrong, R. C.; Augeri, D. J.; Belli, B. A.; Bruncko, M.; Deckwerth, T. L.; Dinges, J.; Hajduk, P. J.; Joseph, M. K.; Kitada, S.; Korsmeyer, S. J.; Kunzer, A. R.; Letai, A.; Li, C.; Mitten, M. J.; Nettesheim, D. G.; Ng, S.; Nimmer, P. M.; O'Connor, J. M.; Oleksijew, A.; Petros, A. M.; Reed, J. C.; Shen, W.; Tahir, S. K.; Thompson, C. B.; Tomaselli, K. J.; Wang, B.; Wendt, M. D.; Zhang, H.; Fesik, S. W.; Rosenberg, S. H., *Nature*, (2005) **435**, 677.
- [11] Petros, A. M.; Dinges, J.; Augeri, D. J.; Baumeister, S. A.; Betebenner, D. A.; Bures, M. G.; Elmore, S. W.; Hajduk, P. J.; Joseph, M. K.; Landis, S. K.; Nettesheim, D. G.; Rosenberg, S. H.; Shen, W.; Thomas, S.; Wang, X.; Zanze, I.; Zhang, H.; Fesik, S. W., *J Med Chem*, (2006) **49**, 656.
- [12] Chan, S. L.; Lee, M. C.; Tan, K. O.; Yang, L. K.; Lee, A. S.; Flotow, H.; Fu, N. Y.; Butler, M. S.; Soejarto, D. D.; Buss, A. D.; Yu, V. C., *J Biol Chem*, (2003) **278**, 20453.
- [13] Becattini, B.; Kitada, S.; Leone, M.; Monosov, E.; Chandler, S.; Zhai, D.; Kipps, T. J.; Reed, J. C.; Pellecchia, M., *Chem Biol*, (2004) **11**, 389.
- [14] Degterev, A.; Lugovskoy, A.; Cardone, M.; Mulley, B.; Wagner, G.; Mitchison, T.; Yuan, J., *Nat Cell Biol*, (2001) **3**, 173.
- [15] Kitada, S.; Leone, M.; Sareth, S.; Zhai, D.; Reed, J. C.; Pellecchia, M., *J Med Chem*, (2003) **46**, 4259.
- [16] Mohammad, R.; Giri, A.; Goustin, A. S., *Recent Pat Anticancer Drug Discov*, (2008) **3**, 20.

- [17] Nguyen, M.; Marcellus, R. C.; Roulston, A.; Watson, M.; Serfass, L.; Murthy Madiraju, S. R.; Goulet, D.; Viallet, J.; Belec, L.; Billot, X.; Acoca, S.; Purisima, E.; Wiegmanns, A.; Cluse, L.; Johnstone, R. W.; Beauparlant, P.; Shore, G. C., *Proc Natl Acad Sci U S A*, (2007) **104**, 19512.
- [18] Tse, C.; Shoemaker, A. R.; Adickes, J.; Anderson, M. G.; Chen, J.; Jin, S.; Johnson, E. F.; Marsh, K. C.; Mitten, M. J.; Nimmer, P.; Roberts, L.; Tahir, S. K.; Xiao, Y.; Yang, X.; Zhang, H.; Fesik, S.; Rosenberg, S. H.; Elmore, S. W., *Cancer Res*, (2008) **68**, 3421.
- [19] Tang, G.; Yang, C. Y.; Nikolovska-Coleska, Z.; Guo, J.; Qiu, S.; Wang, R.; Gao, W.; Wang, G.; Stuckey, J.; Krajewski, K.; Jiang, S.; Roller, P. P.; Wang, S., *J Med Chem*, (2007) **50**, 1723.
- [20] Tzung, S. P.; Kim, K. M.; Basanez, G.; Giedt, C. D.; Simon, J.; Zimmerberg, J.; Zhang, K. Y.; Hockenbery, D. M., *Nat Cell Biol*, (2001) **3**, 183.
- [21] Wang, G.; Nikolovska-Coleska, Z.; Yang, C. Y.; Wang, R.; Tang, G.; Guo, J.; Shangary, S.; Qiu, S.; Gao, W.; Yang, D.; Meagher, J.; Stuckey, J.; Krajewski, K.; Jiang, S.; Roller, P. P.; Abaan, H. O.; Tomita, Y.; Wang, S., *J Med Chem*, (2006) **49**, 6139.
- [22] Zhang, L.; Ming, L.; Yu, J., *Drug Resist Updat*, (2007) **10**, 207.
- [23] Zhai, D.; Jin, C.; Satterthwait, A. C.; Reed, J. C., *Cell Death Differ*, (2006) **13**, 1419.
- [24] Vogler, M.; Dinsdale, D.; Dyer, M. J.; Cohen, G. M., *Cell Death Differ*, (2009) **16**, 360.
- [25] Bruncko, M.; Hong, D.; Elmore, S. W.; Kunzer, A. R.; Lynch, C.; McCellan, W.; Park, C. M.; Song, X.; Wang, X., Apoptosis Promoters, WO 2007/040650 A3, (2007).
- [26] Lutz, W. B.; Ressler, C.; Nettleton, D. E.; Du Vigneaud, V., (1959),
- [27] McGarvey, G. J.; Williams, J. M.; Hiner, R. N.; Matsubara, Y.; Oh, T., *Journal of the American Chemical Society*, (1986) **108**, 4943.
- [28] Genta, M. T.; Villa, C.; Mariani, E.; Loupy, A.; Petit, A.; Rizzetto, R.; Mascarotti, A.; Morini, F.; Ferro, M., *Int J Pharm*, (2002) **231**, 11.
- [29] Galema, S. A., *Chemical Society Reviews*, (1997) **26**, 233.
- [30] Lidstrom, P.; Tierney, J.; Wathey, B.; Westman, J., *Tetrahedron*, (2001) **57**, 9225.
- [31] Chighine, A.; Sechi, G.; Bradley, M., *Drug Discov Today*, (2007) **12**, 459.
- [32] Kubota, D.; Ishikawa, M.; Yamamoto, M.; Murakami, S.; Hachisu, M.; Katano, K.; Ajito, K., *Bioorg Med Chem*, (2006) **14**, 2089.
- [33] Lilienkampf, A.; Johansson, M. P.; Wahala, K., *Org Lett*, (2003) **5**, 3387.
- [34] Liu, Y.; Dong, D.; Liu, Q.; Qi, Y.; Wang, Z., *Org Biomol Chem*, (2004) **2**, 28.
- [35] Xiang, D.; Yang, Y.; Zhang, R.; Liang, Y.; Pan, W.; Huang, J.; Dong, D., *J Org Chem*, (2007) **72**, 8593.

Chapter 7:

Conclusions and Future Work

7.0 Conclusions and Future Work

Peptide labelled metal complex luminophores for imaging and exploring the environment of living cells is a relatively new topic of research. It is driven by the many advantages such complexes have over conventional imaging dyes, including Stoke-shifts tuneable emission and environmental sensitivity. This thesis is part of on-going research by our group that focussed on the development of ruthenium (II) polypyridyl –peptide conjugates for cellular imaging. This thesis focusses on the synthesis, characterisation and identification of novel ruthenium complex-peptide bioconjugates suitable for applications in cellular imaging and the investigation of their sub-cellular targeting and localisation. The compounds can be considered supramolecular dyads, A-L-B containing, A, the photoactive sensing unit, L, in this case a benign linker and B the targeting and/or transport peptide.

Chapter 1 overviewed the assembly of supramolecular bioconjugates of metal complexes for application in targeted cellular imaging. Chapter 2, outlined the experimental methods used. Chapter 3 detailed the synthesis and a detailed comparative study of the preparation of nuclear localisation peptides, NF- κ B and SV-40, and their conjugation to ruthenium (II) polypyridyl chromophores. The desire to direct Ru(II) to the nucleus was driven by the extensively reported interactions of such complexes with DNA. Many Ru(II) polypyridyl complexes bind strongly to DNA through electrostatic and intercalative interactions and have been demonstrated, in solution, to photocleave DNA. Therapeutic exploitation of these interactions requires that the complex can be directed to the cell nucleus.

Six novel Ru II polypyridyl peptide conjugates were synthesised by standard SPPS. Assembly of the peptide sequence and elongation with a (2 or 5 carbon) linker was performed by automated synthesis, with final N-terminal deprotection. The Ru II polypyridal complex was conjugated by manual coupling. Cleavage of the Ru (II) polypyridal peptide conjugates from the resin took place by treatment with TFA in the presence of scavengers. Semi-preparative HPLC on a reverse phase polymeric support was used to achieve purities of the metal conjugates >85%. The Ru (II) polypyridal peptide conjugates were characterised by mass spectroscopy. The effect of the identity of the linker between the metal complex and the peptide was also investigated with β -alanine, a 2 carbon linker and 6-amino-hexanoic acid, a 5 carbon linker compared. Photophysical studies showed that the

emission characteristics of the conjugates were comparable to those of the parent chromophores.

Prior to peptide conjugation, neither parent complex exhibited efficient transport across the cell membrane of CHO cells. Both Ru(II) chromophores coupled to the NF- κ B sequence underwent diffusion across the cell membrane of CHO cells and their uptake was not affected by the length of the linker. In general, this led to the localisation of the dyes within the cells' nucleus. Not all NLS peptides are able to promote the cellular uptake of ruthenium (II) polypyridyl chromophores. The Ru(bpy)₂ PIC-SV-40 conjugate for example did not exhibit efficient transport across the cell membrane. On the other hand, the Ru(dpp)₂ PIC-SV-40 conjugate did penetrate the cell membrane however we believe that this occurred through its disruption of the cell membrane, eventually leading to cell death. This is supported by preliminary cytotoxicity studies which showed Ru(dpp)₂PIC polypyridyl peptide conjugates have a higher cytotoxicity than the corresponding Ru(bpy)₂PIC polypyridyl peptide conjugates.

The Ru(bpy)₂PIC polypyridyl peptide conjugates show promise as imaging agents. They also exhibit efficient nuclear localisation and low cytotoxicity. The Ru(dpp)₂PIC polypyridyl peptide conjugates do not appear to be as efficient as imaging agents as the Ru(bpy)₂PIC polypyridyl peptide conjugates due to their higher toxicity. The Ru(dpp)₂PIC polypyridyl peptide conjugates also remain mainly associated with the cell membrane. This suggests that the toxic nature of the dye occurs through its higher hydrophobicity and interaction with the cell membrane. The ability of its conjugates to impart nuclear localization is affected by the nature of the cargo, with larger and more positively charged ruthenium complex being more difficult to direct than smaller ones. The Ru(dpp)₂ PIC peptide conjugates may be useful as therapeutics if their effects on the cell membrane could be alleviated by conjugation to alternative peptide sequence or use of another delivery technique such as liposomes or polymeric vectors and if their accumulation in the nucleus result in the apoptosis of cancer cells. This work will continue with detailed studies on the ability of both conjugates to induced photo-stimulated cell death in living cells.

Chapter 4 described the synthesis of 11 overlapping BID peptide sequences spanning the complete protein (tBid). Most of these peptides could not be prepared by routine techniques. This stepwise elongation was successful for 2 sequences, BID 155-177 and BID 78-101. For the other 9 BID sequences with a higher content of hydrophobic residues this method failed. For these 9 BID sequences, the peptide was assembled on the synthesiser up to the longest stretch of hydrophobic amino acids and then transferred to a syringe for completion by manual synthesis. This method allowed the use of longer reaction

times and higher equivalents of amino acids and coupling reagents to force the reaction to completion. Both the coupling and deprotection reactions were monitored by Kaiser test. When this elongation of the peptide sequence became difficult, as shown by mixed results from a Kaiser test, coupling and deprotection reactions were completed in the Biotage Initiator 2.5 microwave synthesizer. This was carried out for BID 175-195, residue 176 (N) and BID137-157, residue 143 (E). The 11 BID sequences coupled to biotin were successfully synthesised, purified and characterised and available for protein binding studies which will be conducted through an independent collaborative project.

Two of the BID sequences, BID 137-157 and BID 155-177, were chosen for conjugation with $[\text{Ru}(\text{dppz})_2\text{PIC}]\text{ClO}_4$ on the basis of their high hydrophobic amino acid contents. The synthesis and purification of these proved to be more difficult than the biotin-labelled analogues, requiring a change in the coupling chemistry to overcome the low reactivity of the carboxyl group from the ruthenium complex. The optimal conditions for $[\text{Ru}(\text{dppz})_2\text{PIC}]\text{ClO}_4$ conjugation were identified and should be successfully applied to any of the other BID sequences which would show promising results from the protein binding studies. These studies addressed in particular the choice of the linker between the label and the peptide to ensure sufficient solubility in aqueous media of the conjugates. Photophysical and imaging studies were conducted with BID 155-177 and showed that the properties of the parent complex are not significantly modified by the conjugation to the peptide sequence. Unlike its unconjugated complex, $\text{Ru}(\text{dppz})_2\text{PIC}$ BID 155-177 underwent diffusion across the cell membrane of Kelly neuroblastoma cells, with no accumulation in the nucleus, but also showed significant toxicity which could result from its interaction with the cell membrane and/or uptake in the cytoplasm.

This work will continue with protein binding studies with the 11 BID-Biotin peptide conjugates will be performed by the group Prof. Jochen Prehn in the Department of Physiology and Medical Physics at the Royal College of Surgeons in Ireland. Further studies with $\text{Ru}(\text{dppz})_2\text{PIC}$ -BID 155-177 by confocal microscopy, to determine its sub-cellular localisation, and by the cytotoxicity assay, to elucidate the chronology of the uptake and toxicity events are currently being performed.

Chapter 5 detailed the conjugation of the hydrophilic and hydrophobic ruthenium (II) polypyridyl chromophores to a cationic antimicrobial peptide with mitochondria targeting ability, Magainin 2. The peptide was synthesized on the Applied Biosystem ABI 433A Synthesizer and the bio-conjugation of chromophore to peptide took place on the resin with PyBOP as the coupling reagent. Cleavage of the Ru(II) polypyridal peptide conjugates

from the resin took place in TFA in the presence of scavengers. Semi-preparative HPLC was used to achieve purities >83%. The Ru(II) polypyridal peptide conjugates were characterised by mass spectroscopy.

As these complexes are O₂ and pH sensitive, it is important to be able to target them to organelles where such measurements will be of benefit in cell metabolic studies. The photophysical results showed the complexes did not change significantly on peptide conjugation, compared with the parent complexes. Prior to peptide conjugation, neither parent complex exhibited efficient transport across the cell membrane of CHO cells and only the [Ru(dpp)₂ PIC]²⁺ complex conjugate crossed the cell membrane of CHO cells after conjugation to the Magainin 2 sequence. In general, this did not lead to localisation of the dyes within the cell's mitochondria, the expected target of the peptide component; however co-localising experiments will be required to confirm this result. The corresponding Ru(bpy)₂ PIC Magainin 2 conjugate did not cross the membrane, which would indicate that there might exist a threshold of hydrophobicity of the cargo that controls the cellular uptake of the conjugate, as both [Ru(bpy)₂ PIC]²⁺ and [Ru(dpp)₂ PIC]²⁺ complexes should have the same effect on the N-terminal capping of the peptide and its ability to form a transmembrane pore.

The [Ru(dpp)₂ PIC]²⁺ peptide conjugates remains associated with the entire cell membrane. It is possible that it's interaction with the mitochondrial membrane triggers rapid cell death and cannot be imaged. The parent complex was also successful in passing through the cell membrane. The [Ru(dpp)₂ PIC]²⁺ peptide conjugate may be useful in therapeutic applications as it targets the nucleus and could potentially result in the apoptosis of cancer cells. We believe it to concentrate further within the nucleolus, however further imaging and localising studies must be completed. Also as the Magainin 2 peptide can penetrate bacterial cells, the use of the Ru(II) polypyridyl Magainin 2 conjugate in imaging will be extended to bacterial cells, although the rapid killing mechanism induced by Magainin 2 in prokaryotic cells might make this application challenging.

Chapter 6 examined the synthesis of small molecule inhibitors of the Bcl-2 family proteins. Originally the ABT 263 molecule was selected for investigation, with the objective of applying an imaging agent to it to follow its localisation. This seemed to be an ideal small molecular inhibitor as it is in stage 3 clinical trials, however due to difficulties in its synthesis, the close analogue ABT 737 was selected for synthetic and labelling feasibility studies. This was again a very challenging synthesis work to date and has led to the assembly of 2 of the 3 synthons of ABT 737, however the synthesis of the final molecule was not achieved. One major hurdle remaining in the synthesis of ABT 737 is to initiate the

preparation of the (R)-3-amino-N,N-dimethyl-4-(phenylthio)butanamide synthon. Its first intermediate N-benzyloxycarbonyl-D aspartic acid anhydride proved to be a very unstable molecule to be isolated through a long and low yielding work-up.

Due to time and resource limitations, it was decided to discontinue the synthesis of these BH3 mimetic inhibitors and to focus on the inherent potential photophysical properties of the molecule ABT 737. We aimed to achieve our original goal of cellular imaging with the 4-fluoro-3-nitrobenzenesulfonamide (7) and 4-[4-(4'-Chloro-biphenyl-2-ylmethyl)-piperazin-1-yl]-benzoic acid (11) synthons produced. Although the latter synthon gave promising photophysical results, this intermediate failed to give an emission which could be excited with the visible wavelengths conventionally used in confocal imaging. Route 2 final intermediate (7) molecule did not emit, but interestingly proved to be very toxic to CHO cells.

The supramolecular synthetic strategies attempted in this thesis have shown that coordination compound peptide labelled probes can be readily made using solid state peptide synthesis. The conjugates synthesised in Chapter 3 show promise as nuclear imaging agents, with particularly in the case of the NLS peptides, the ability to target the complexes to specific organelles. Although the work described in Chapter 4 is still awaiting protein-binding studies, we have developed the synthetic approach to identify the functional motifs of a protein. Chapter 5 has investigated a mitochondria targeting peptide with Ru(II) complexes. These conjugates require further imaging before a conclusive statement can be made on their application. Chapter 6 outline how difficult it was to achieve a probe conjugated to a small molecule inhibitor and unfortunately this had to be abandoned. In conclusion, this thesis detailed the ongoing intense efforts to develop imaging probes for cell imaging, to aid biochemical understanding of cellular processes and medical diagnostics and described potential molecular probes capable of making advances in these areas.

Appendix 1: NMR, HPLC and Mass Spectrometry Results

Chapter 3: Luminescent Chromophores for Cellular Imaging

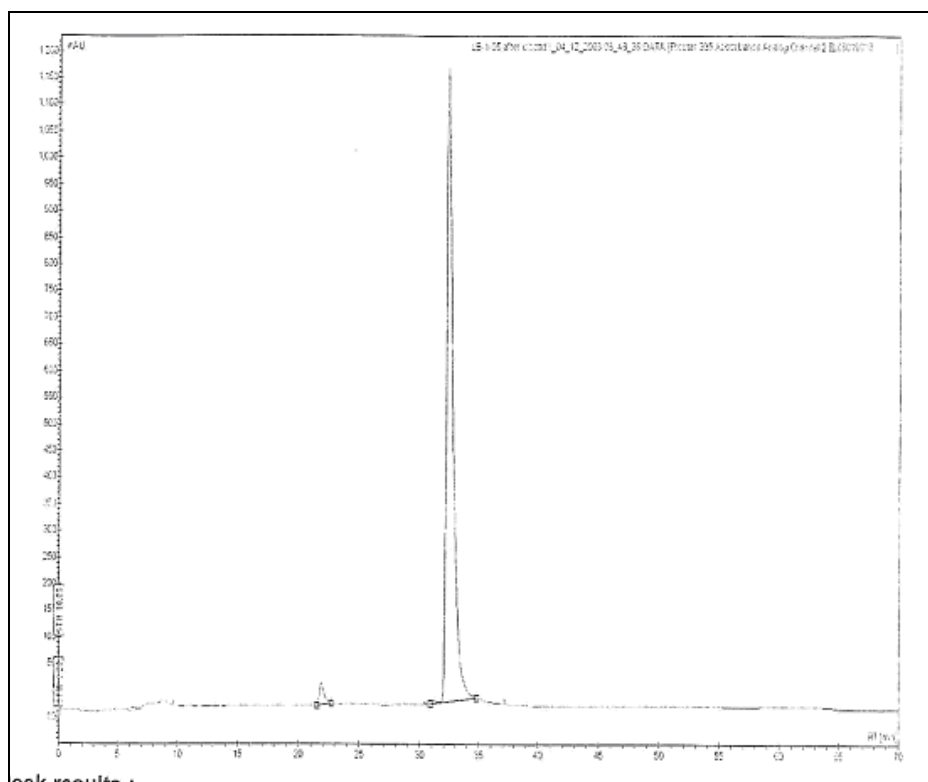


Figure 1: Purity of NF- κ B (β A-VQRKRQKLMP-NH₂) [Ru(dpp)₂PIC] conjugate

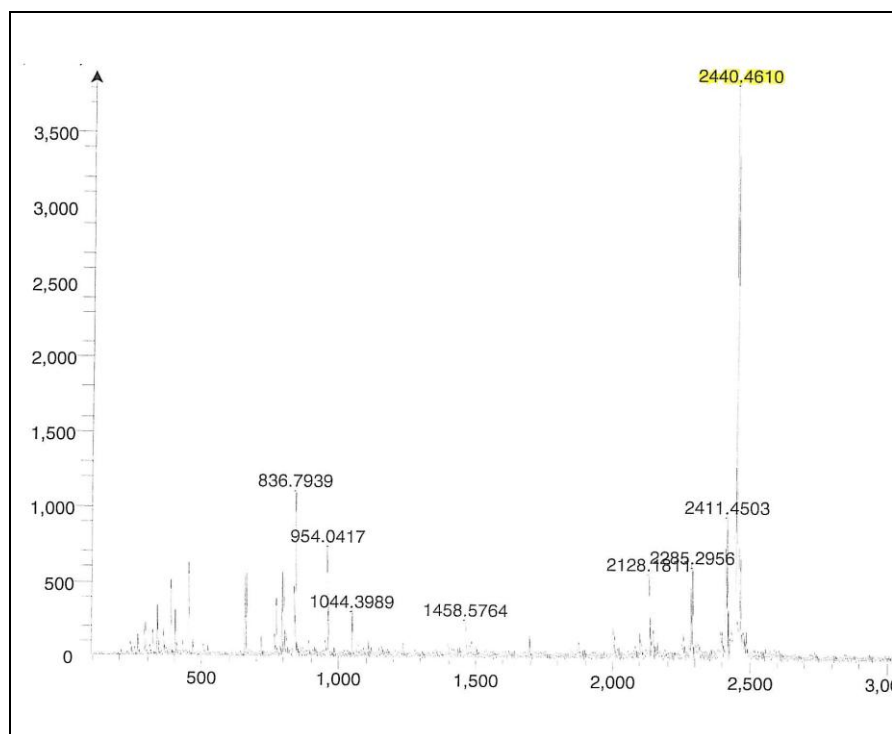


Figure 2: MALDI-TOF of NF- κ B (β A-VQRKRQKLMP-NH₂) [Ru(dpp)₂PIC] conjugate using α -cyano-4-hydroxycinnamic acid matrix

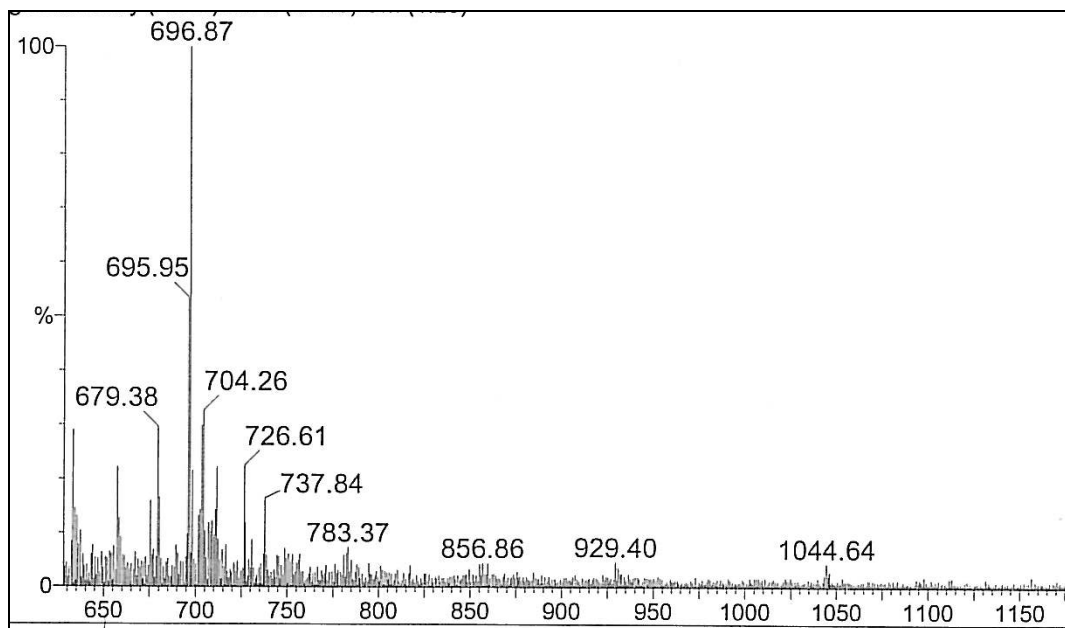


Figure 3: Mass Spectrum of NF-κB (βA-VQRKRQKLMP-NH₂) [Ru(bpy)₂PIC] conjugate

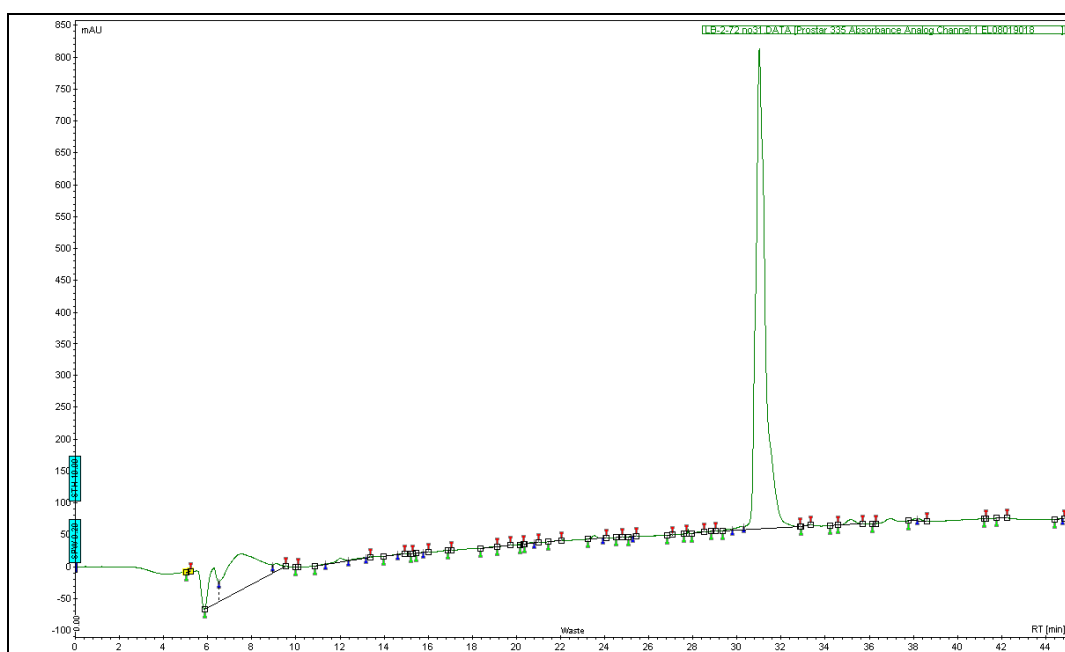


Figure 4: Purity of NF-κB (Ahx-VQRKRQKLMP-NH₂) [Ru(dpp)₂PIC] conjugate

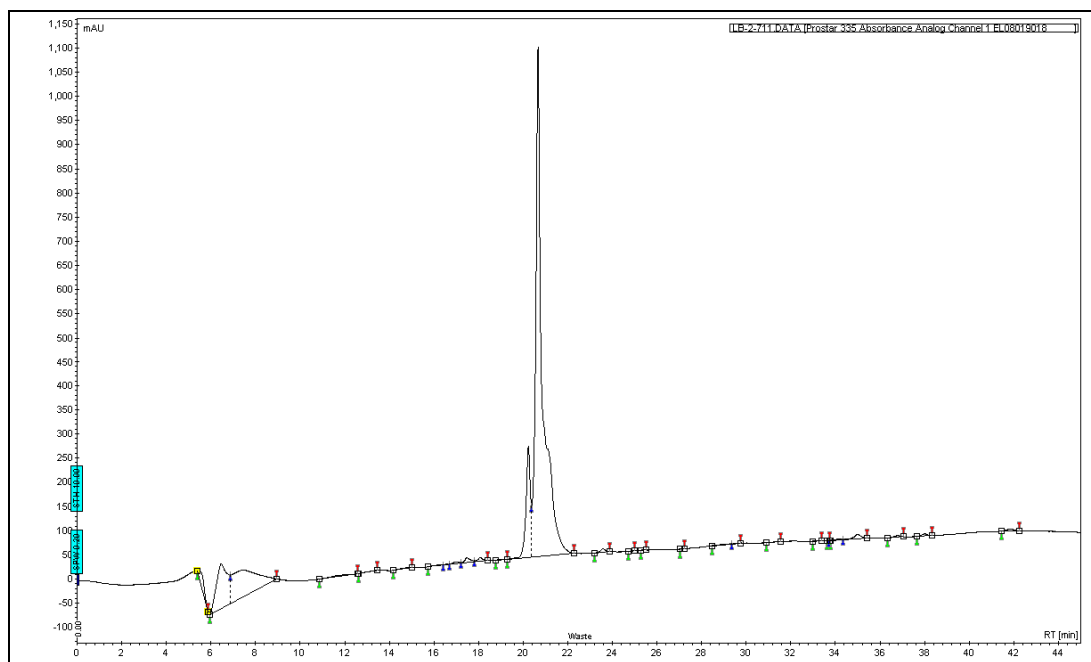


Figure 5: Purity of NF-κB (Ahx-VQRKRQKLMP-NH₂) [Ru(bpy)₂PIC] conjugate

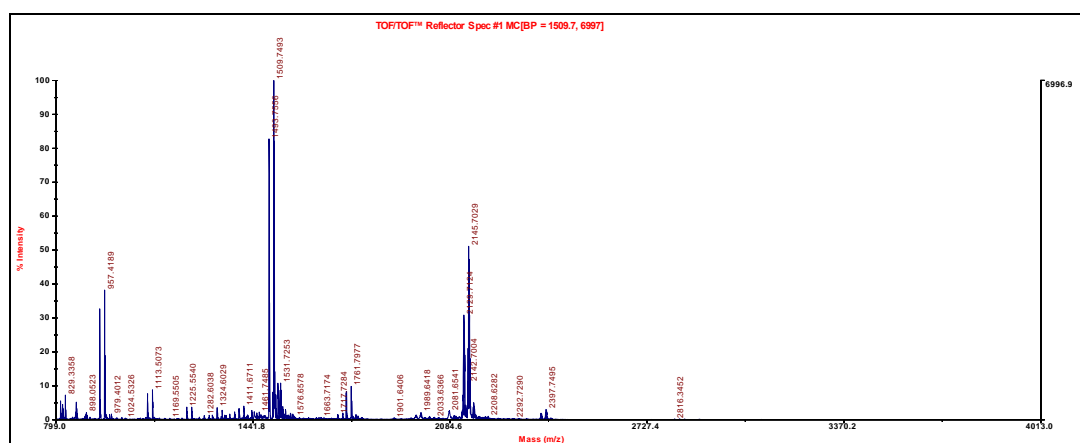


Figure 6: Mass Spectra of NF-κB (Ahx-VQRKRQKLMP-NH₂) [Ru(bpy)₂PIC] conjugate

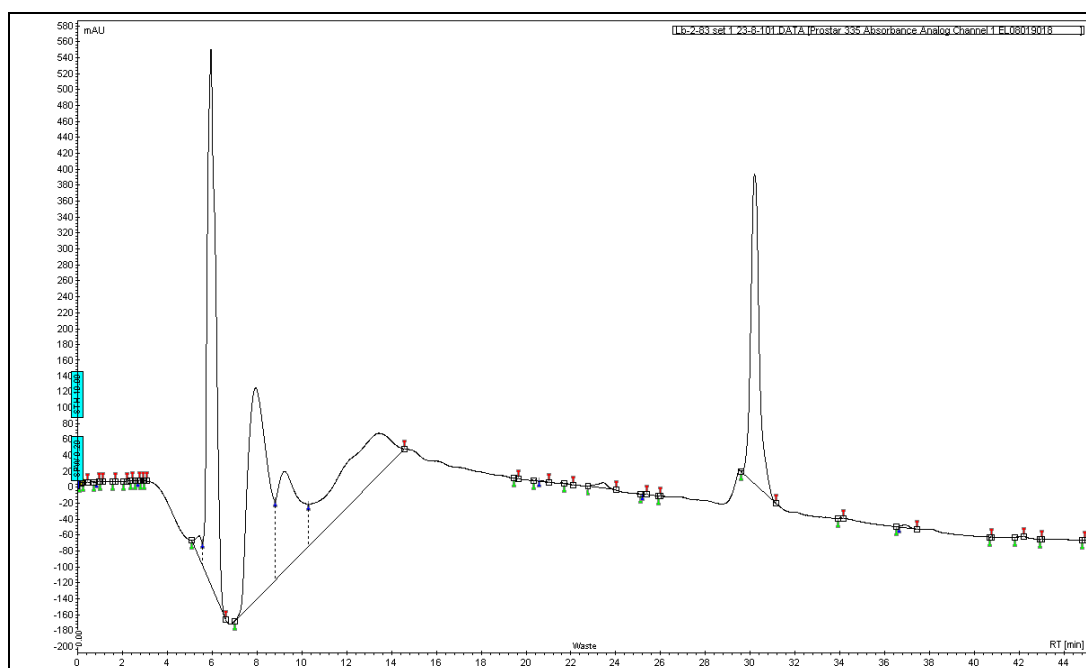


Figure 7: Purity of SV-40[Ru(dpp)₂PIC]ClO₄

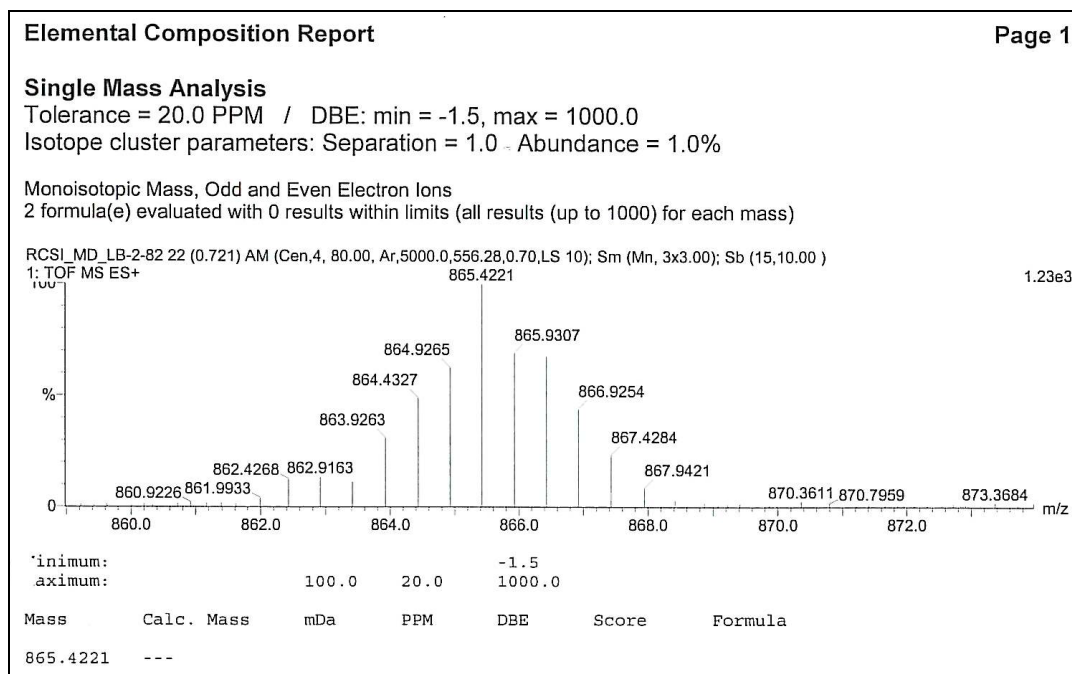


Figure 8: Mass Spectra of Sv-40 (Ahx-PKKKRV-NH₂) [Ru(bpy)₂PIC] conjugate

Chapter 4: BH3 Interacting Domain Death Agonist

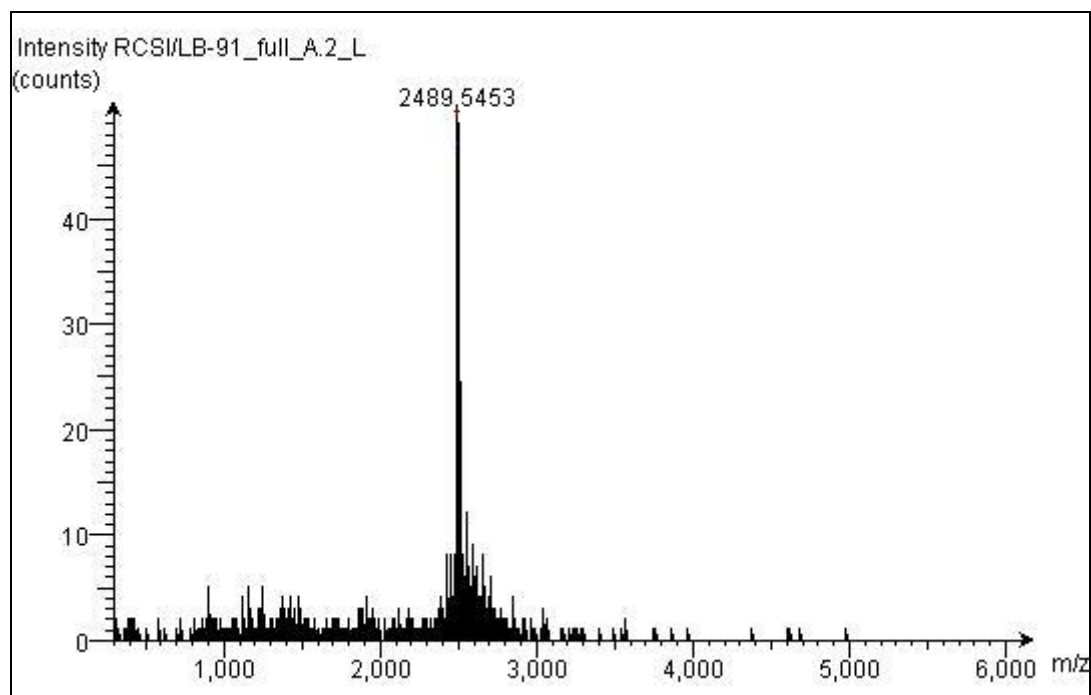


Figure 9: MALDI-TOF of biotinylated BID 1-20 using α -cyano-4-hydroxycinnamic acid matrix

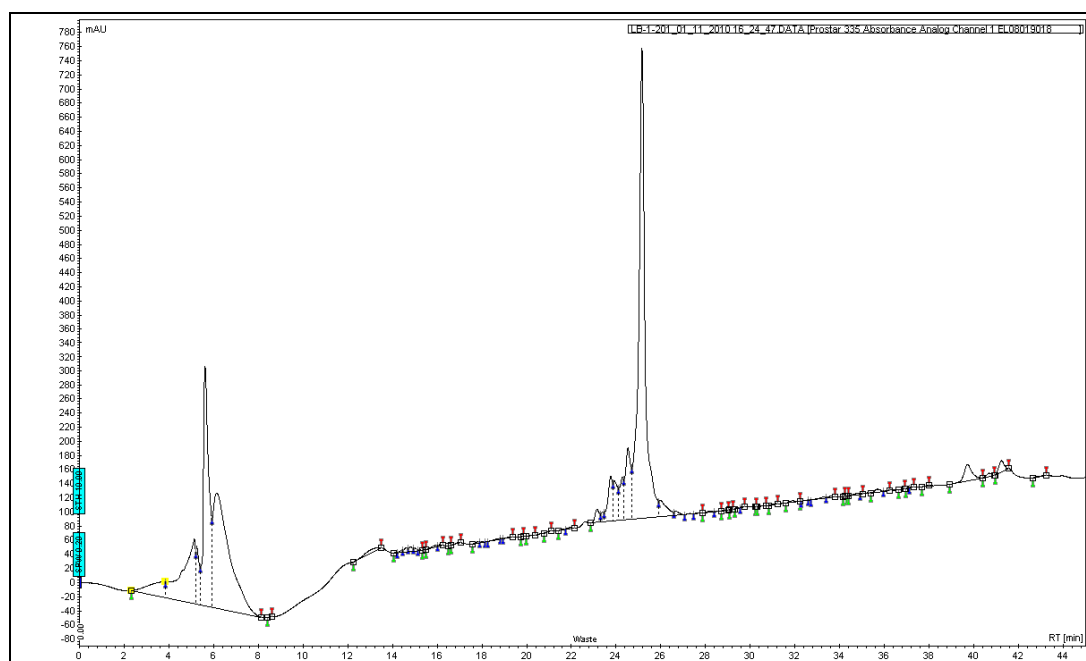


Figure 10: HPLC of biotinylated BID 1-20

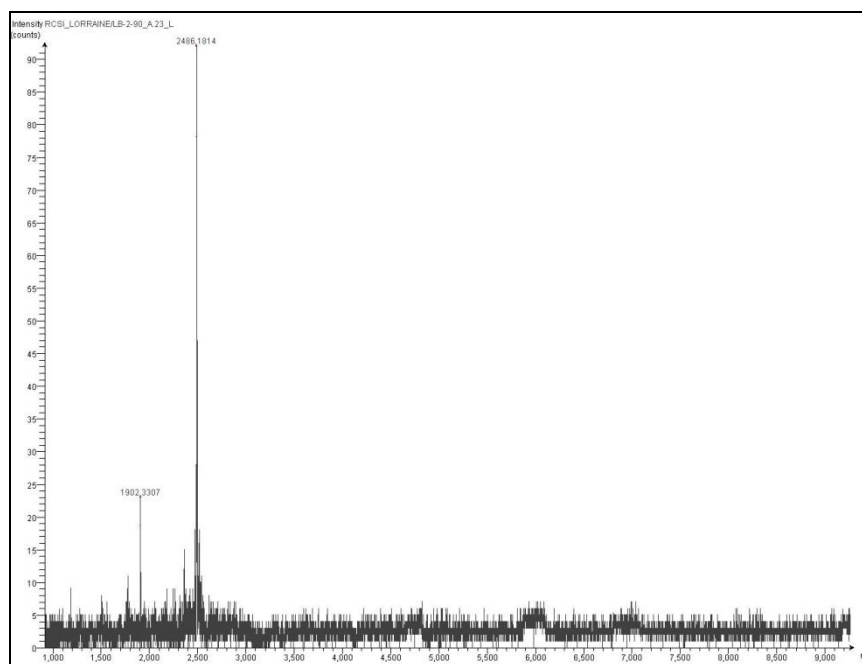


Figure 11: MALDI-TOF of biotinylated BID 18-36 using α -cyano-4-hydroxycinnamic acid matrix

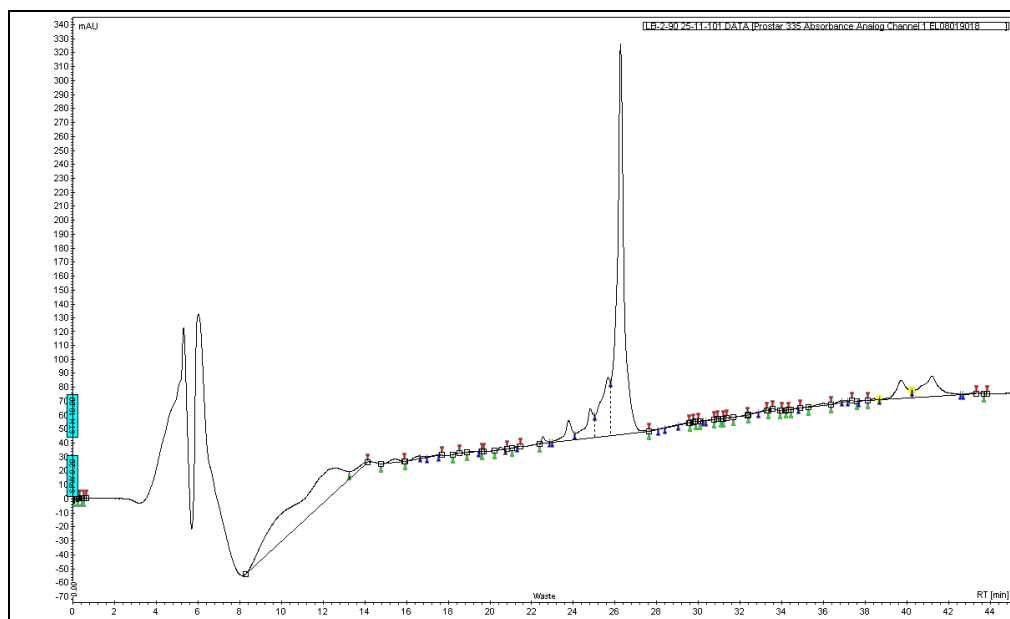


Figure 12: HPLC of biotinylated BID 18-36

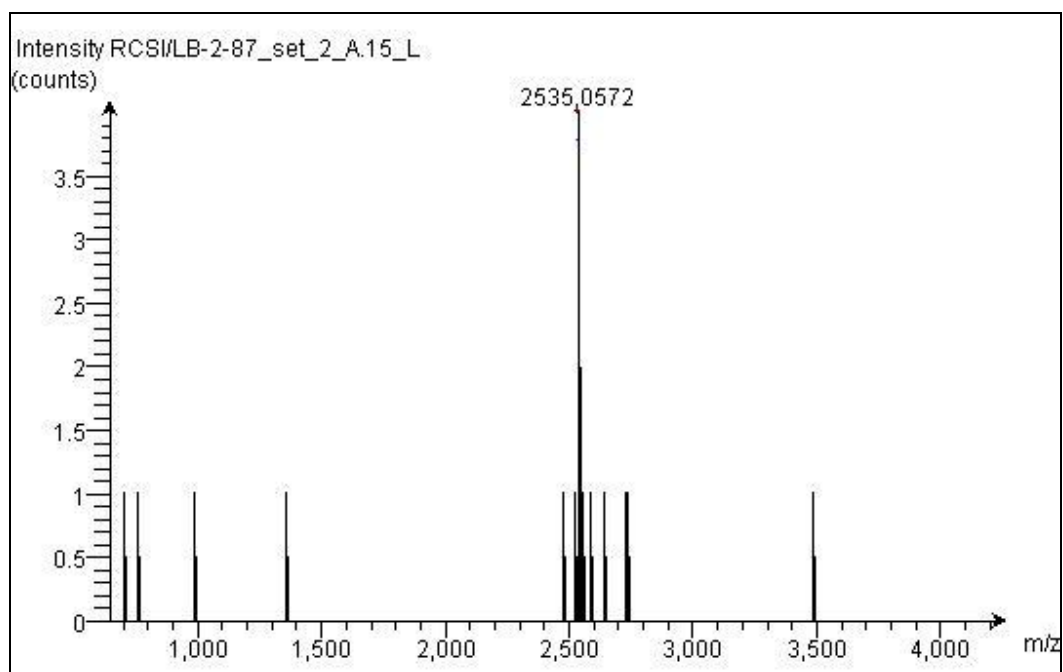


Figure 13: MALDI-TOF of biotinylated BID 29-48 using α -cyano-4-hydrxycinnamic acid matrix

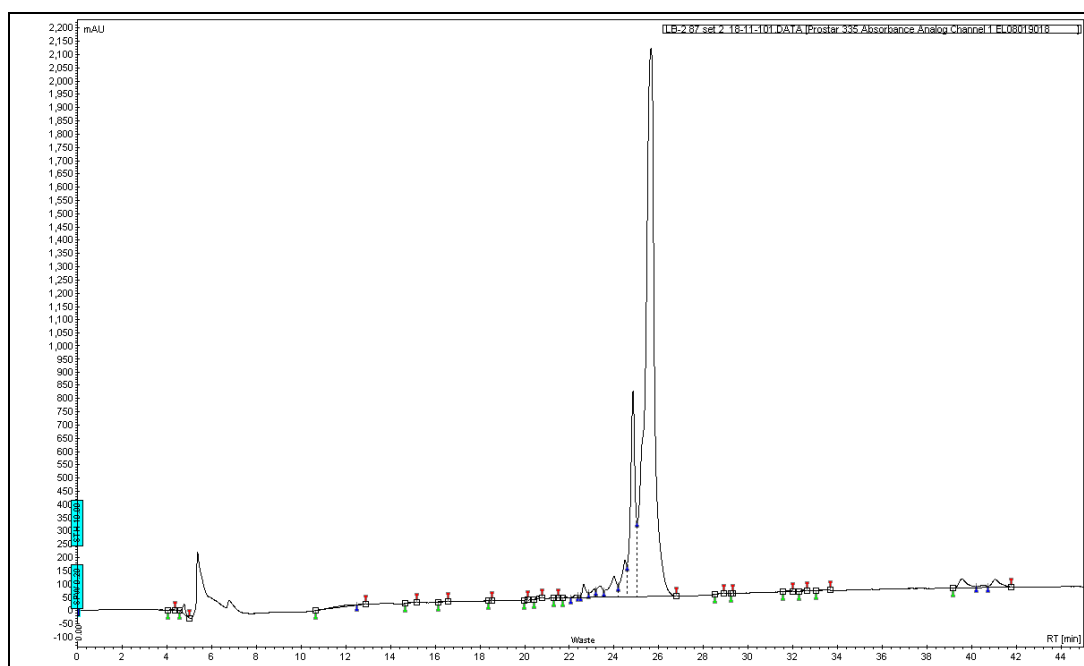


Figure 14: HPLC of biotinylated BID 29-48

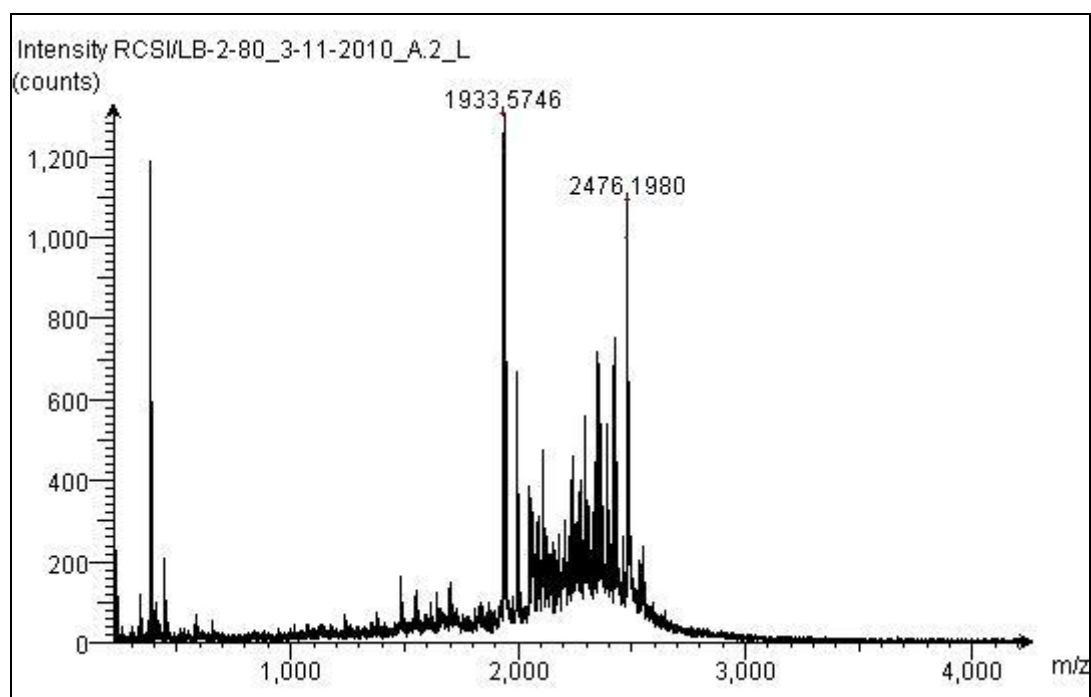


Figure 15: MALDI-TOF of biotinylated BID 46-64 using α -cyano-4-hydroxycinnamic acid matrix

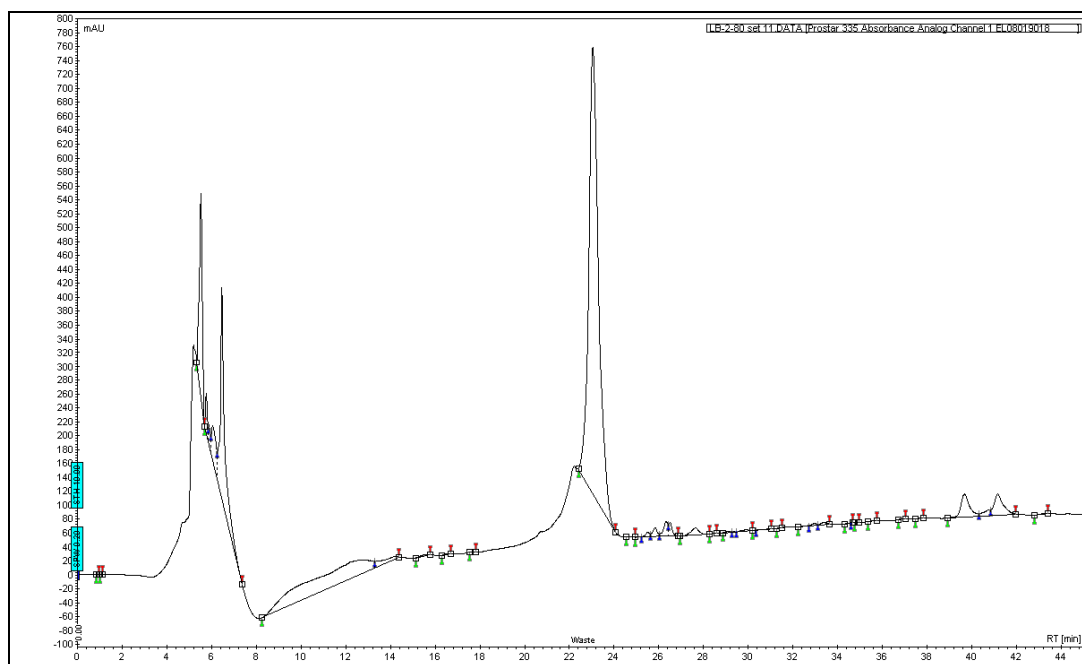


Figure 16: HPLC of BID biotinylated 46-64

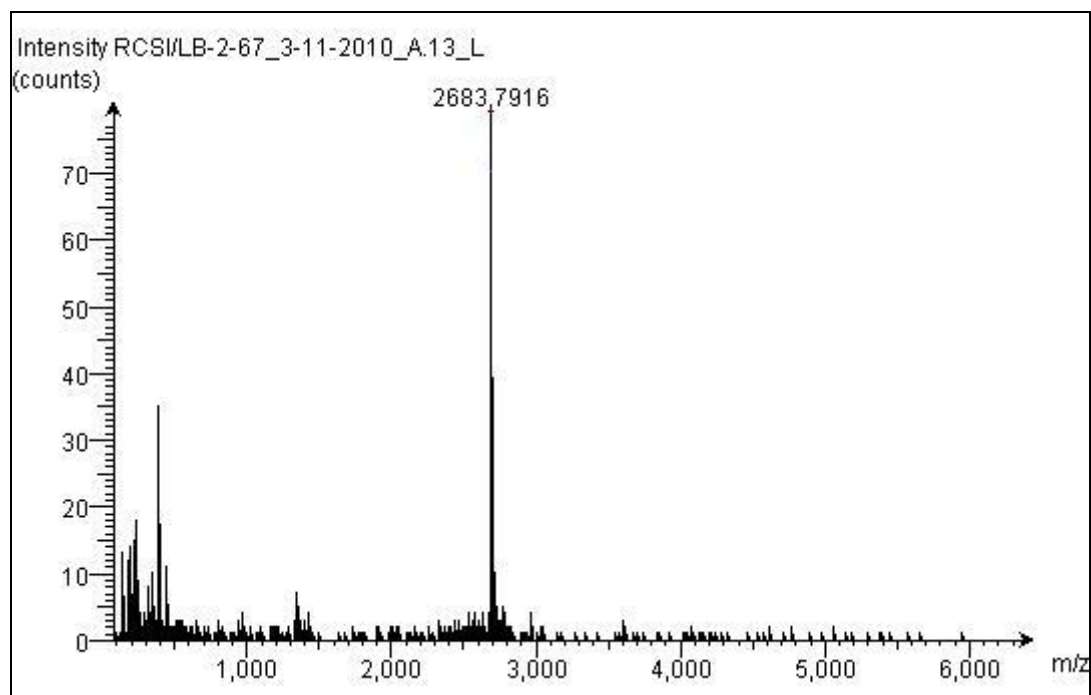


Figure 17: MALDI-TOF of biotinylated BID 62-82 using α -cyano-4-hydroxycinnamic acid matrix

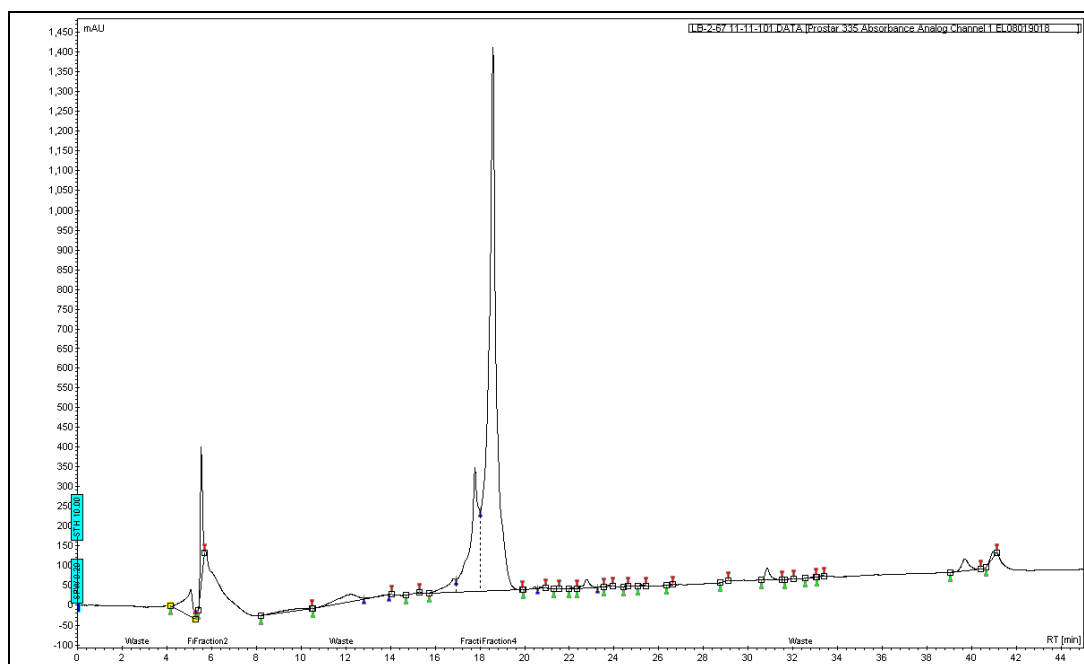


Figure 18: HPLC of biotinylated BID 62-82

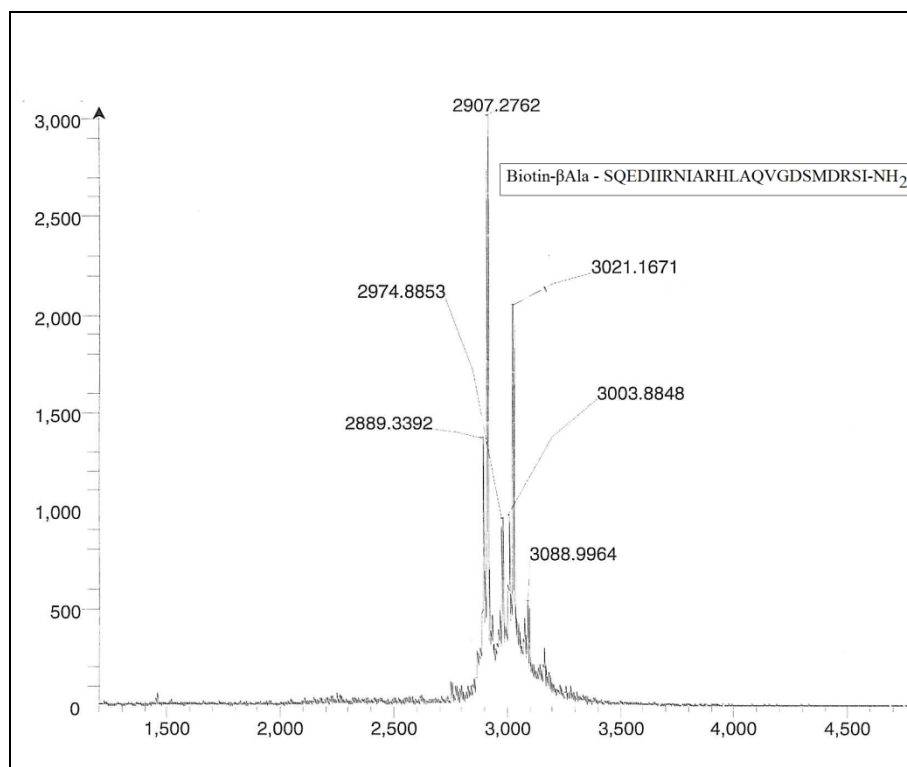


Figure 19: MALDI-TOF of biotinylated BID 78-101 using α -cyano-4-hydroxycinnamic acid matrix

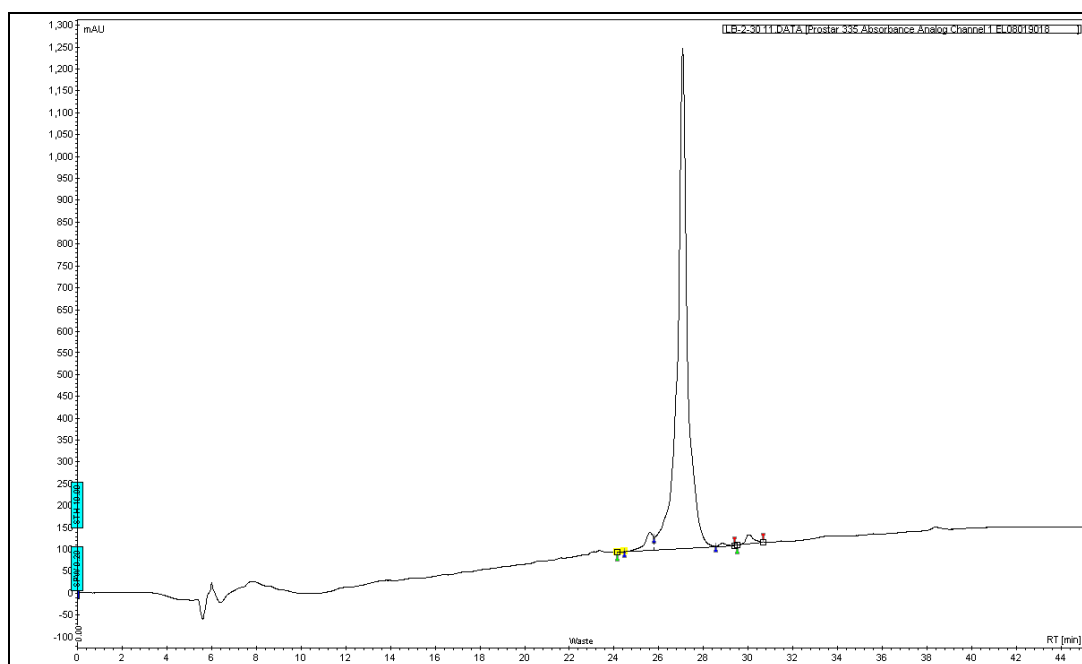


Figure 20: HPLC of biotinylated BID 78-101

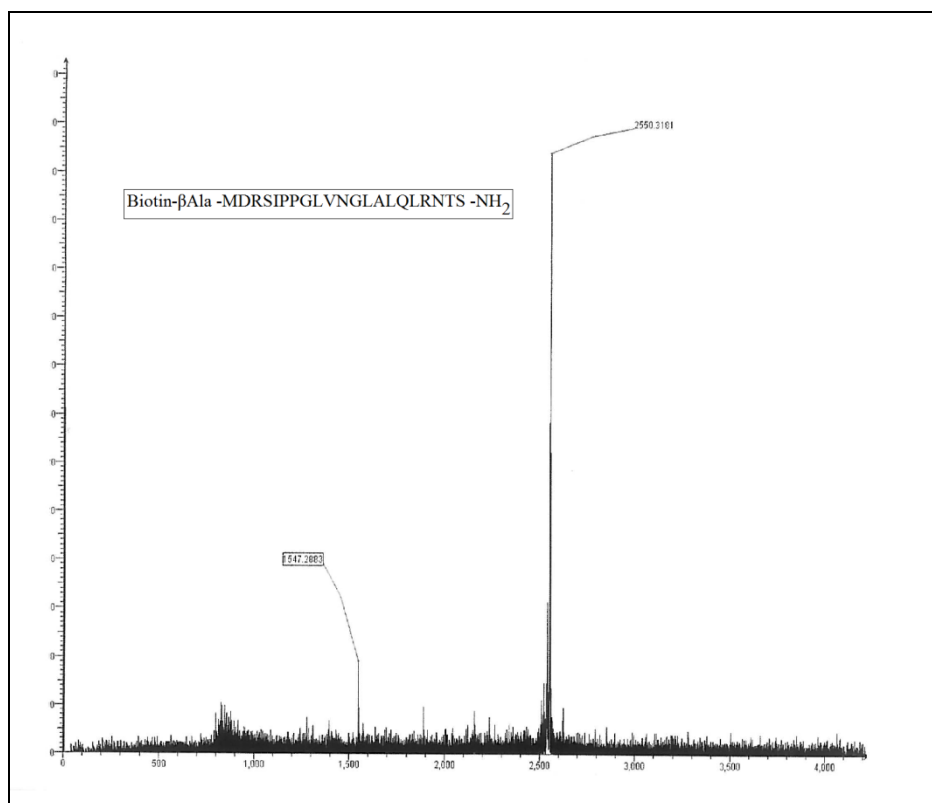


Figure 21: MALDI-TOF of biotinylated BID 97-117 using α -cyano-4-hydroxycinnamic acid matrix

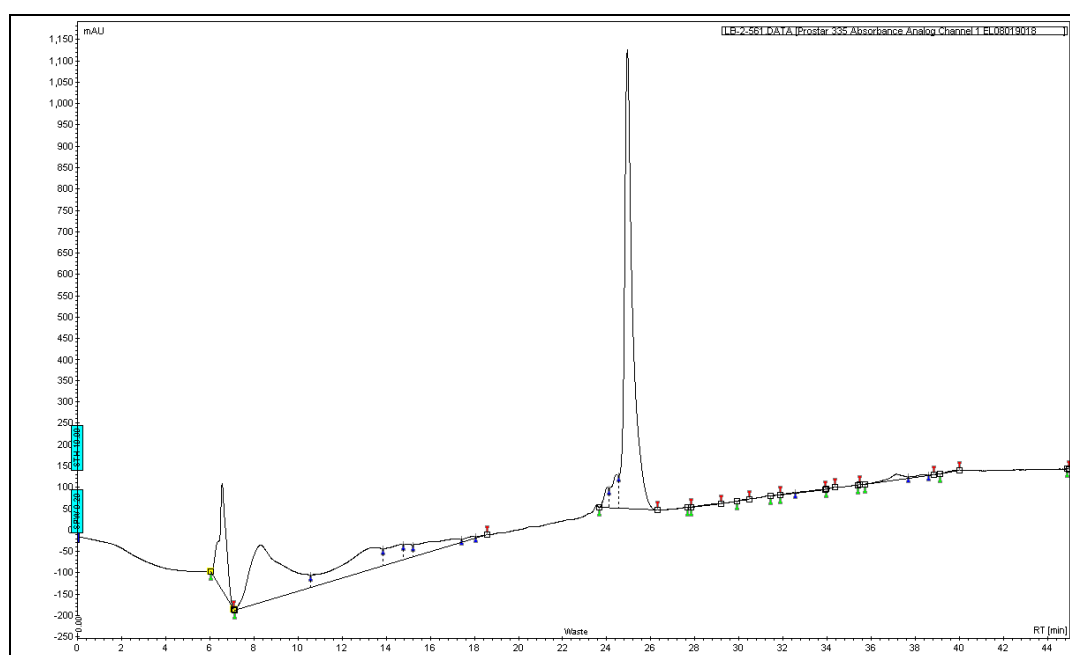


Figure 22: HPLC of biotinylated BID 97-117

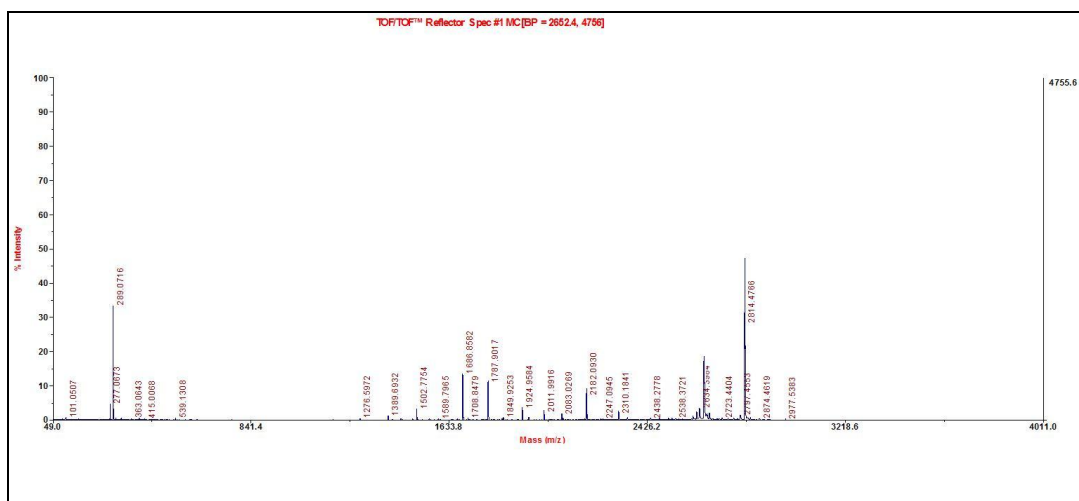


Figure 23: MALDI-TOF of biotinylated BID 116-137 using α -cyano-4-hydroxycinnamic acid matrix

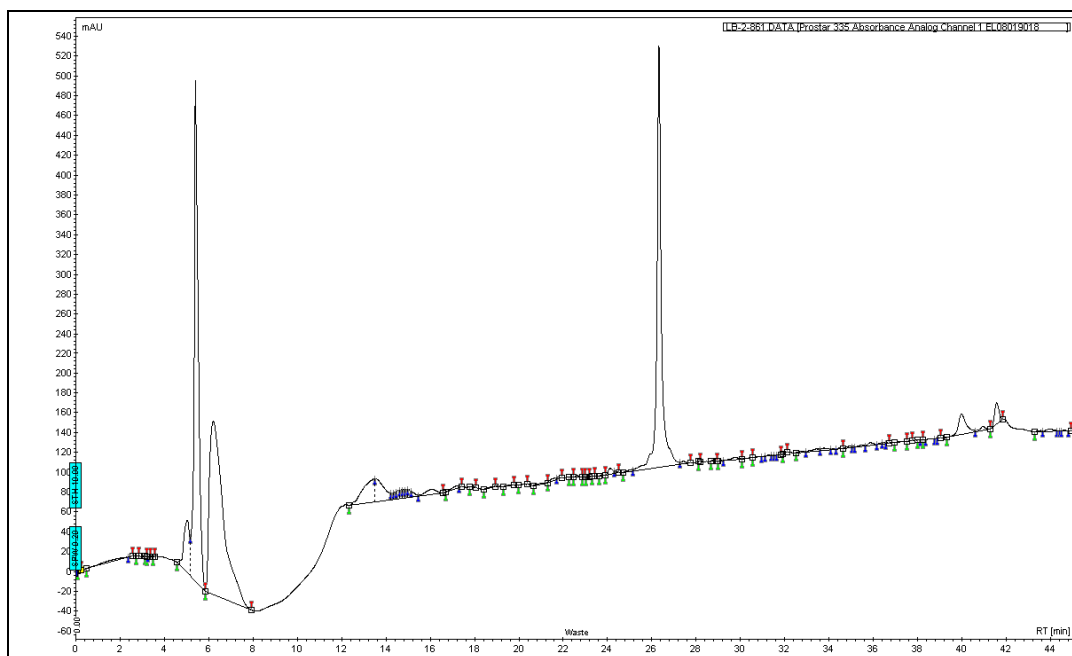


Figure 24: HPLC of biotinylated BID 116-137

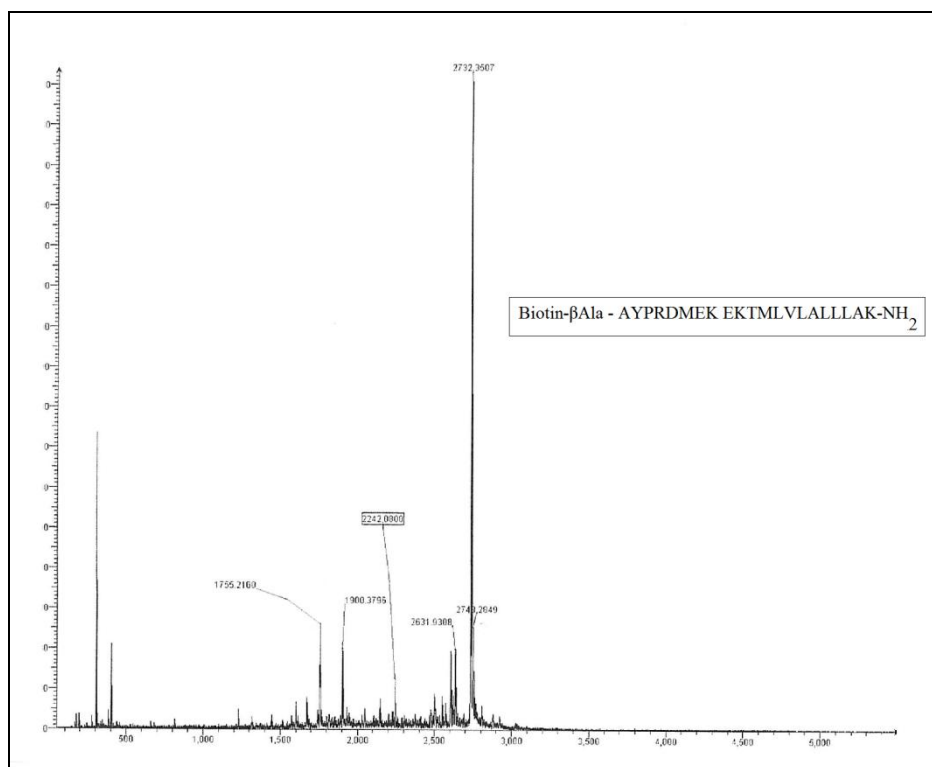


Figure 25: MALDI-TOF of biotinylated BID 137-157 using α -cyano-4-hydroxycinnamic acid matrix

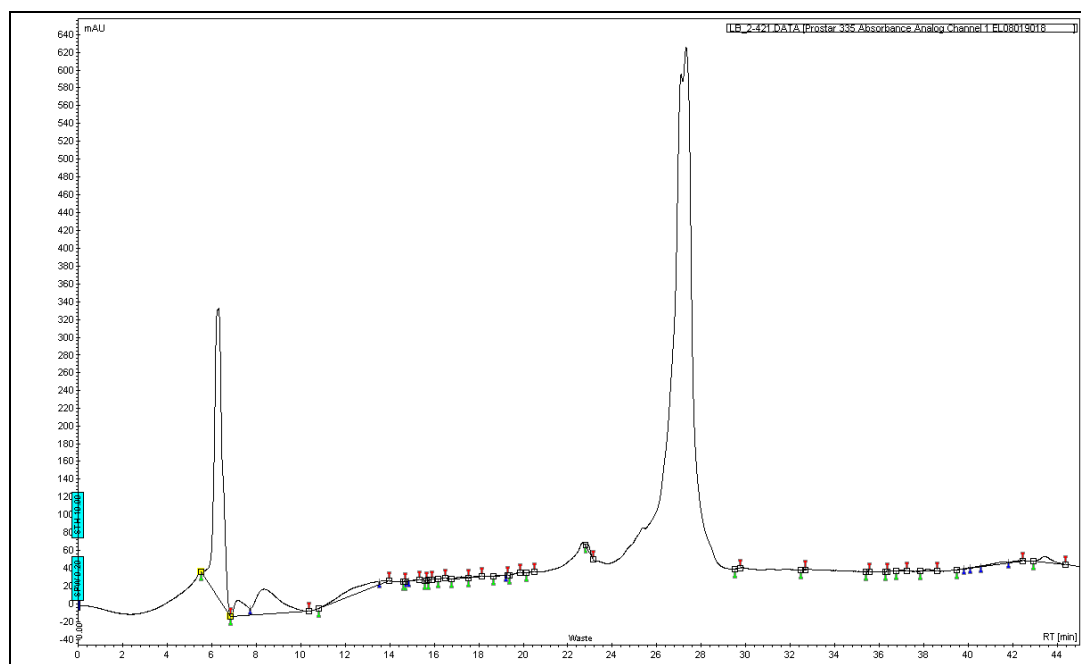


Figure 26: HPLC of biotinylated BID 137-157

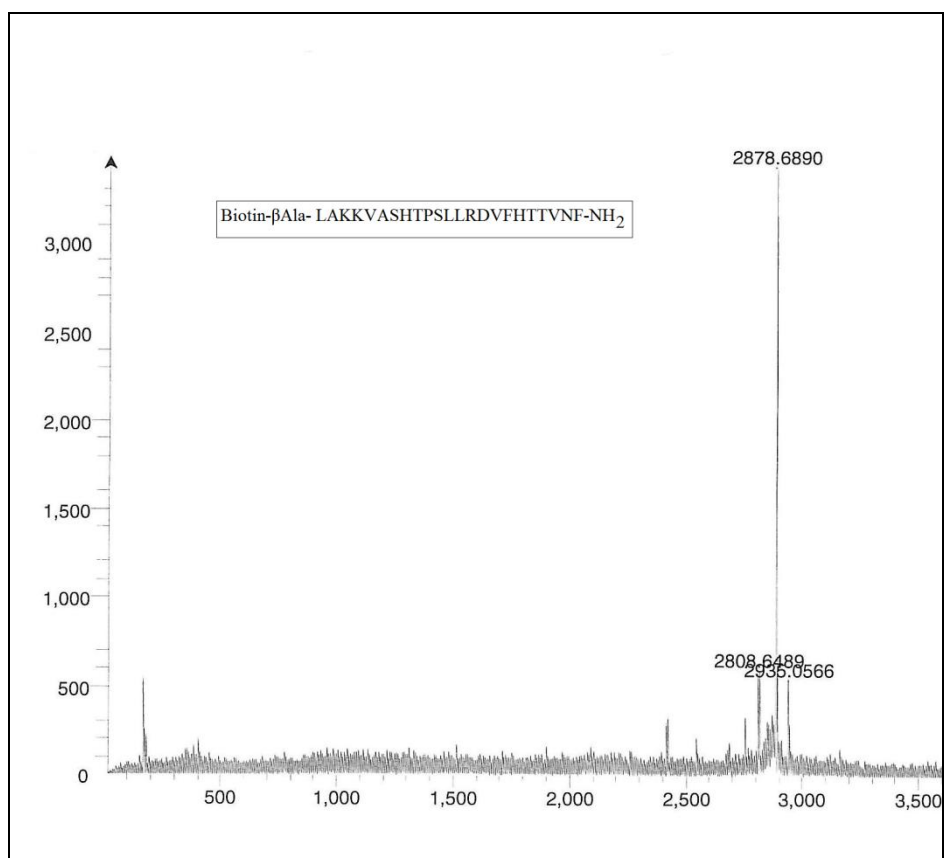


Figure 27: MALDI-TOF of biotinylated BID155-177 using α -cyano-4-hydroxycinnamic acid matrix

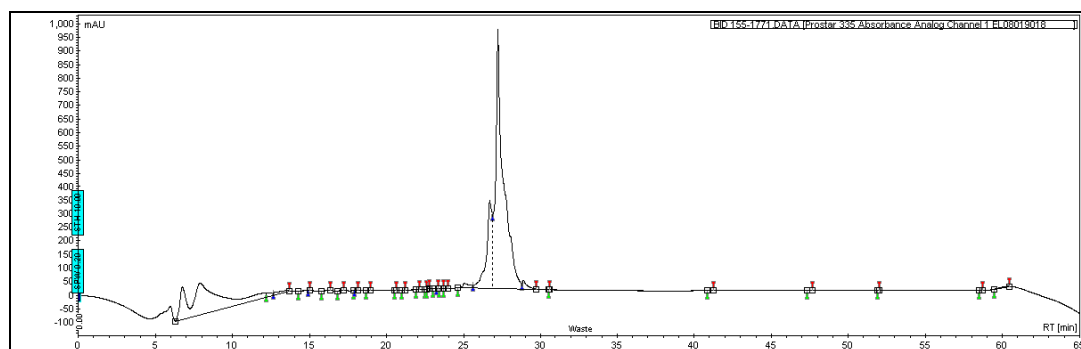


Figure 28: HPLC of biotinylated BID 155-177

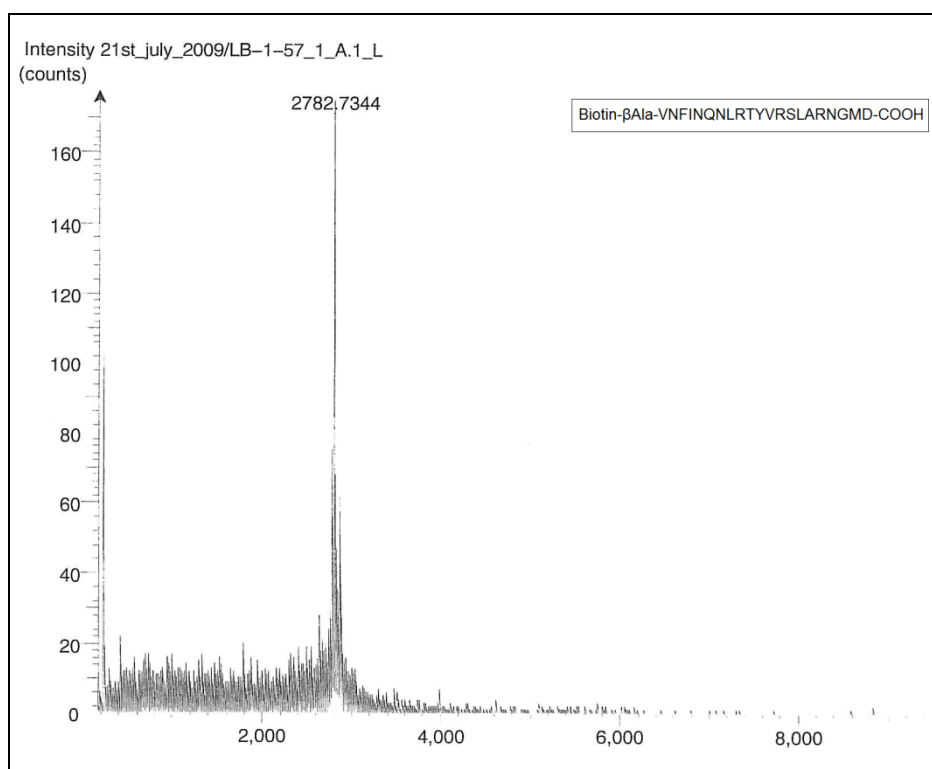


Figure 29: MALDI-TOF of biotinylated BID 175-195 using α -cyano-4-hydroxycinnamic acid matrix

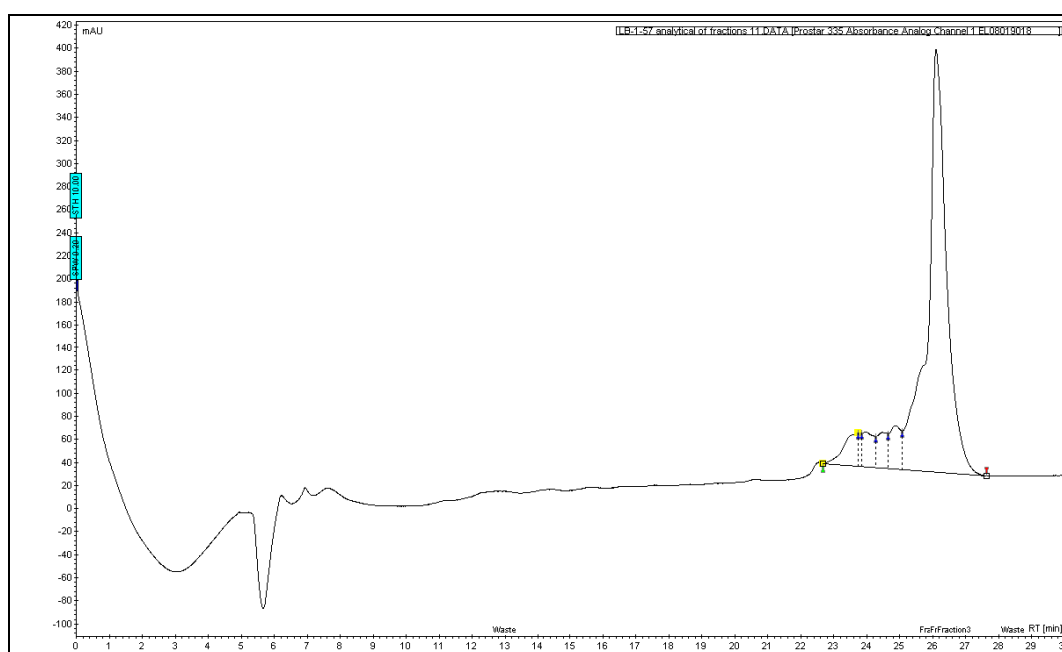


Figure 30: HPLC of biotinylated BID 175-195

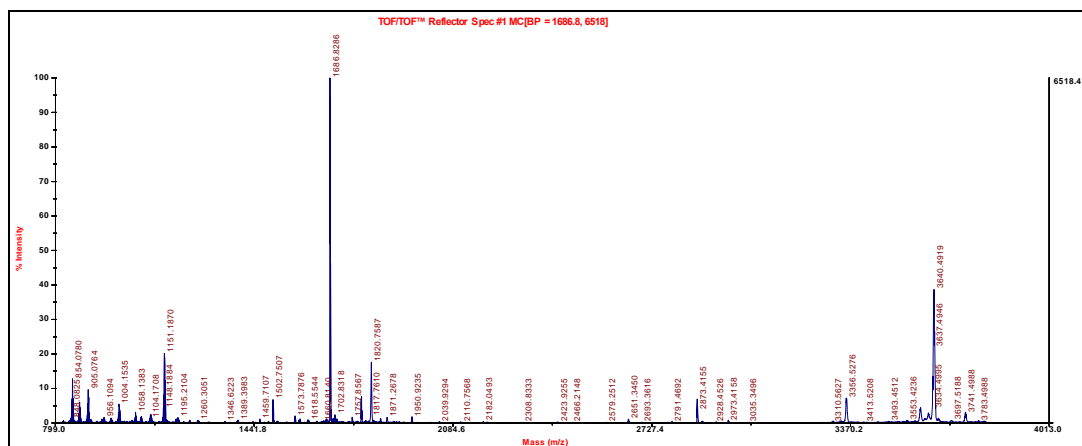


Figure 31: MALDI-TOF of BID 155-177 coupled to Ru(dppz)₂PIC using α -cyano-4-hydroxycinnamic acid matrix

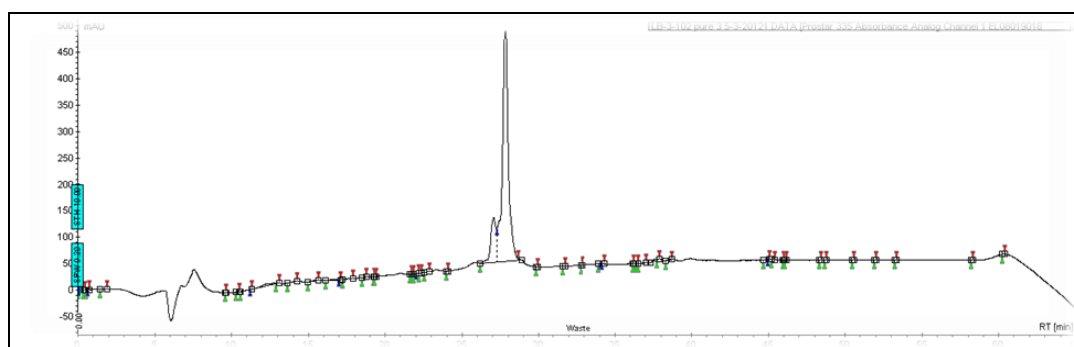


Figure 32: HPLC of BID 155-177 coupled to Ru(dppz)₂PIC

Chapter 5: Targeting Mitochondria with Luminescent Chromophores

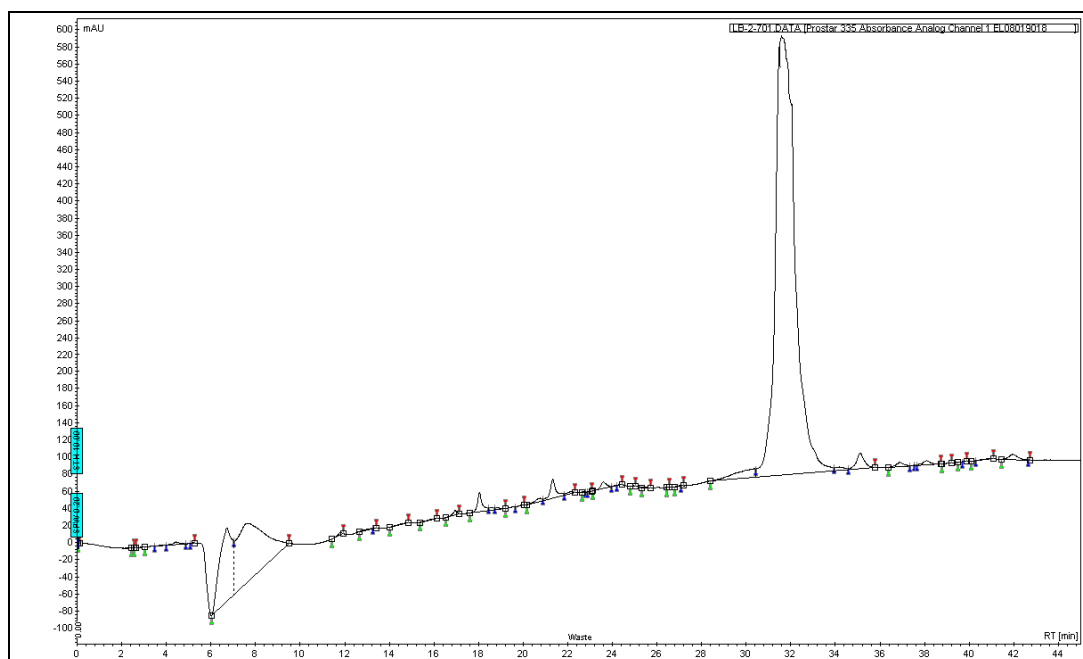


Figure 33: Purity of Magainin 2 (Ahx-GIGKKLHSAKKFGKAFVGEIMNS-NH₂)

[Ru(dpp)₂PIC] conjugate

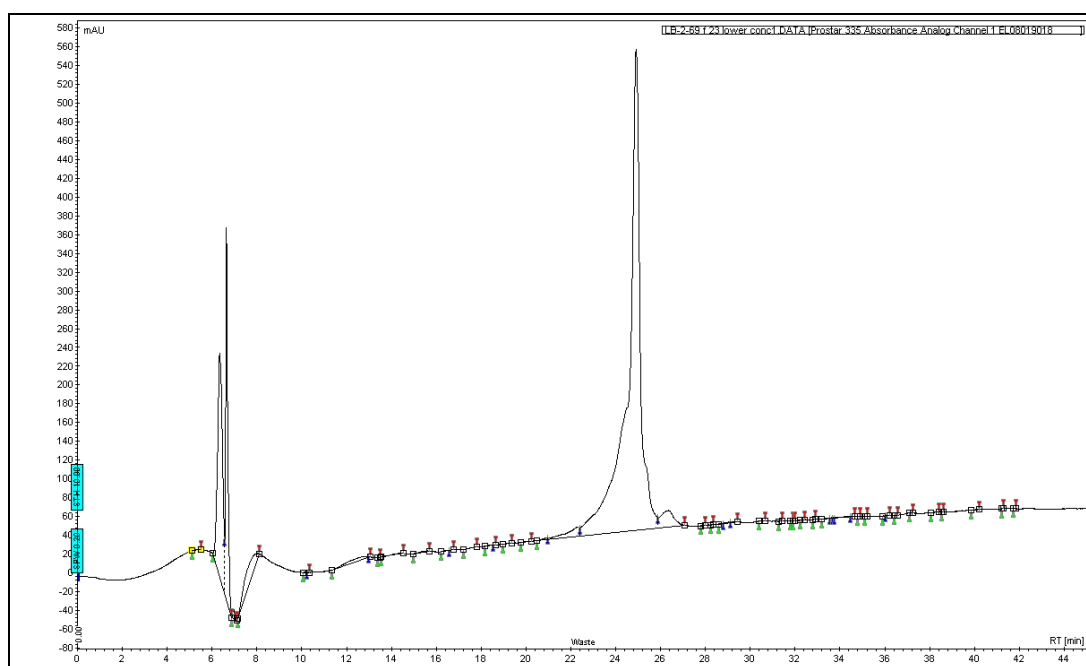
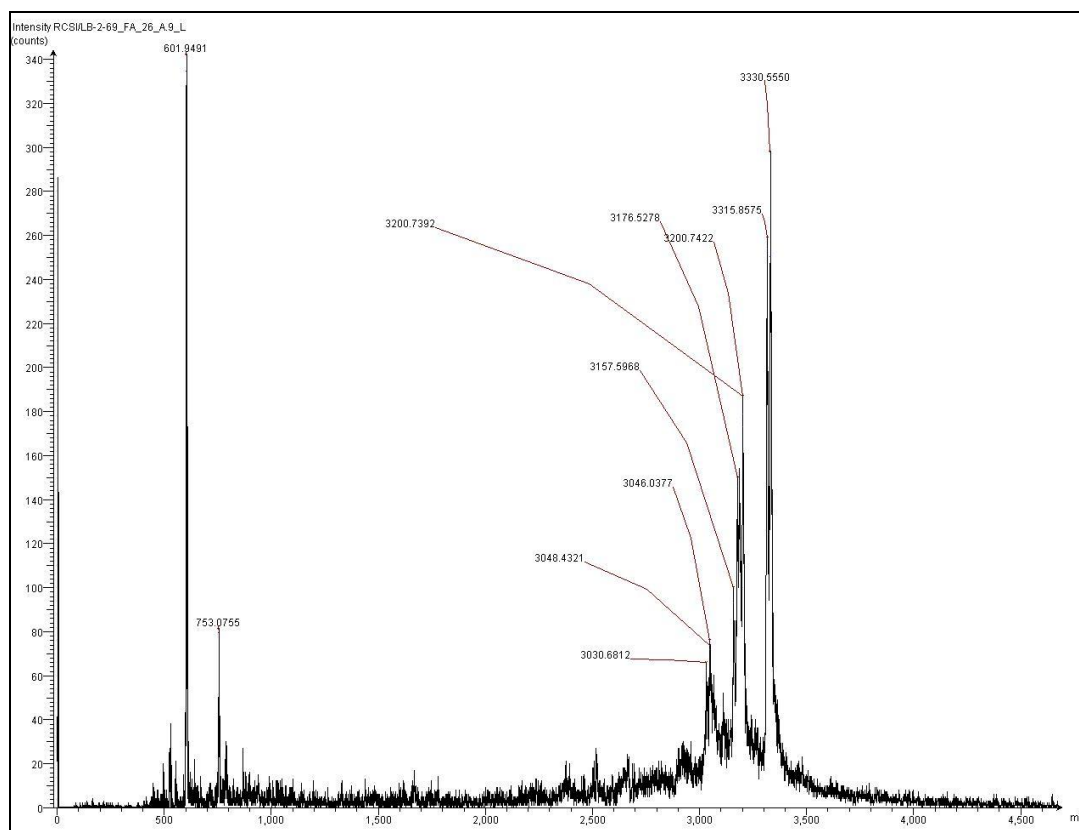


Figure 34: Purity of Magainin 2 (Ahx-GIGKKLHSAKKFGKAFVGEIMNS-NH₂)

[Ru(bpy)₂PIC] conjugate



**Figure 35: Mass Spectra of Magainin 2 (Ahx-GIGKKLHSAKKFGKAFVGEIMNS-NH₂)
[Ru(bpy)₂PIC] conjugate**

Chapter 6: Small molecule Inhibitors of Bcl-2 family proteins

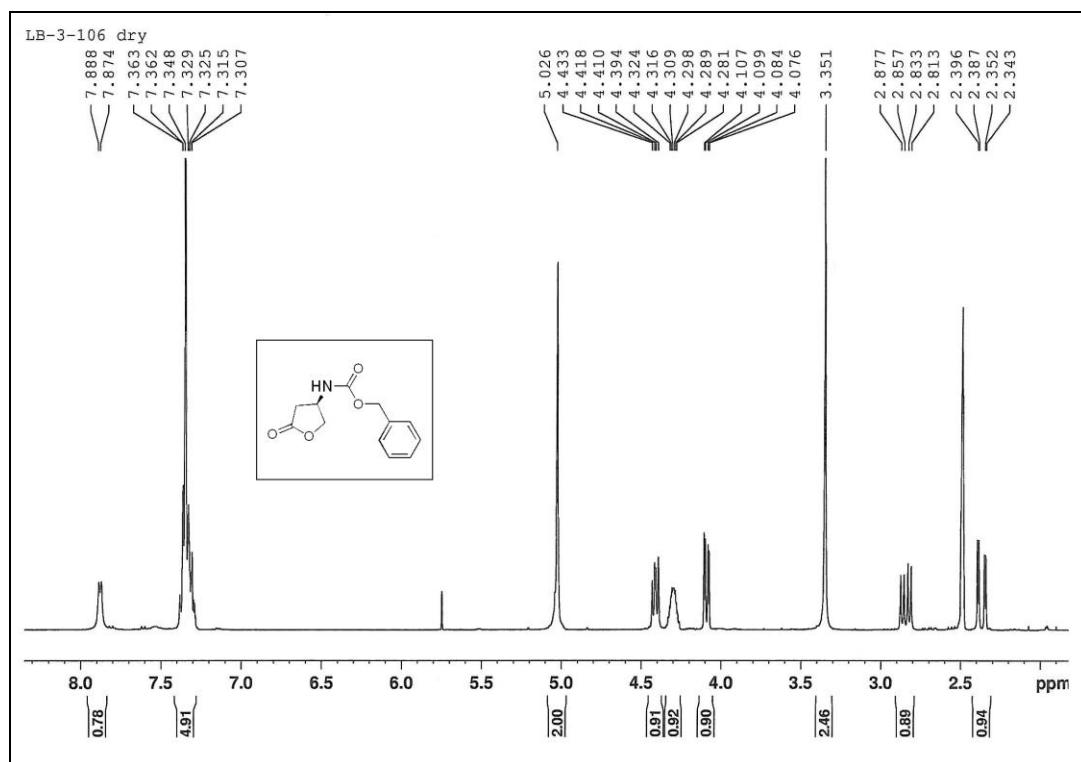


Figure 36: Proton NMR of (R)-benzyl (5-oxotetrahydrofuran-3-yl)carbamate in DMSO-d₆

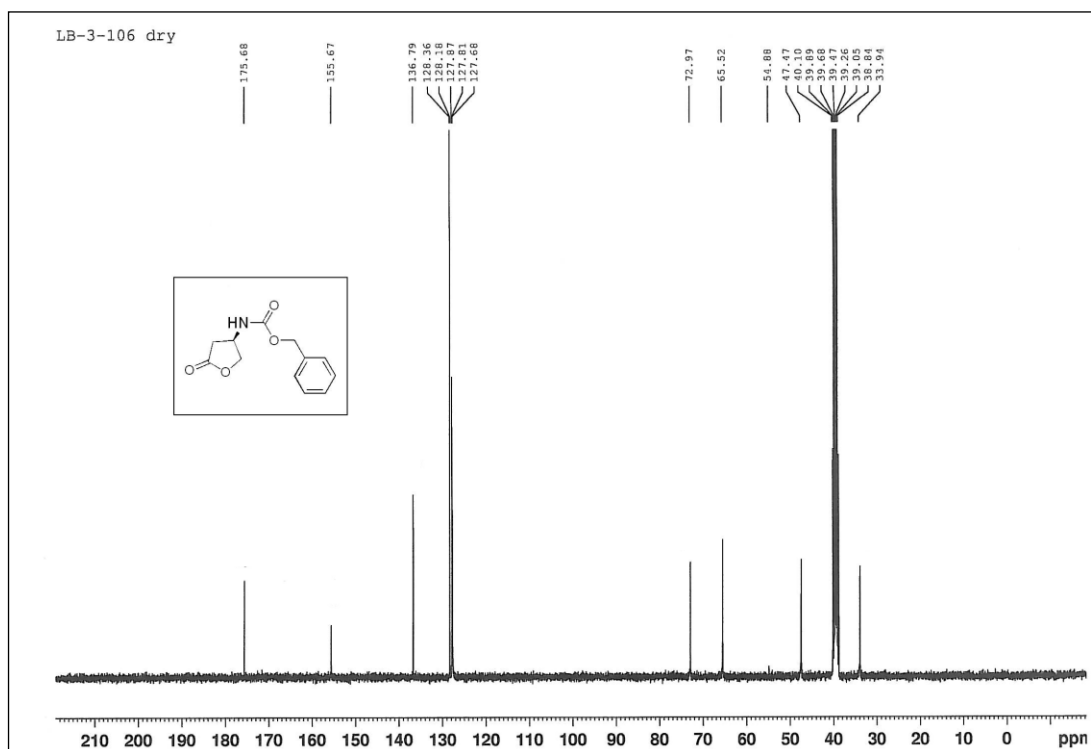


Figure 37: Carbon NMR of (R)-benzyl (5-oxotetrahydrofuran-3-yl)carbamate in DMSO-d₆

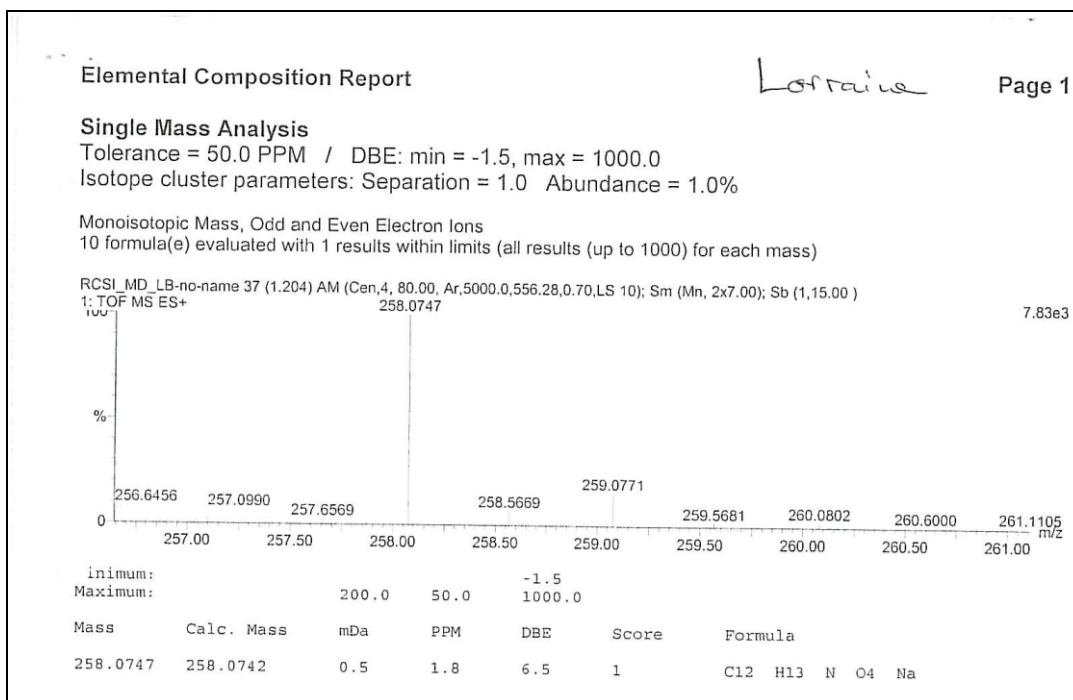


Figure 38: Mass Spectra of (R)-benzyl (5-oxotetrahydrofuran-3-yl)carbamate

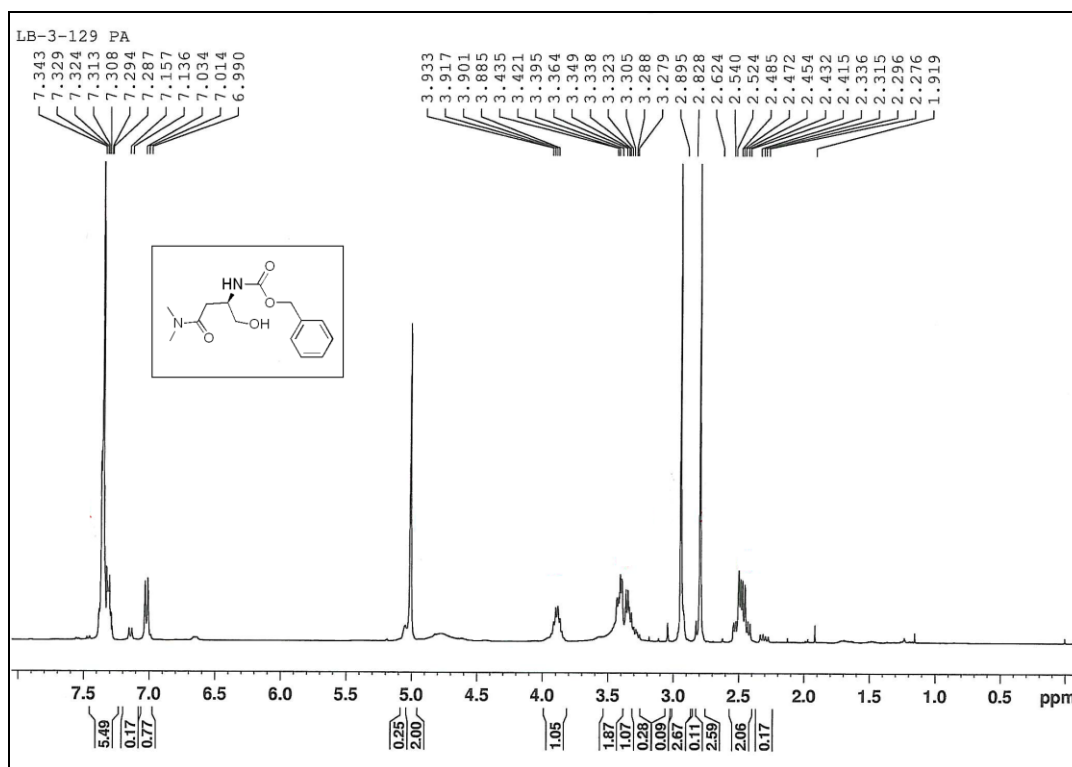


Figure 39: Proton NMR of (R)-benzyl (4-(dimethylamino)-1-hydroxy-4-oxobutan-2-yl)carbamate in CDCl_3

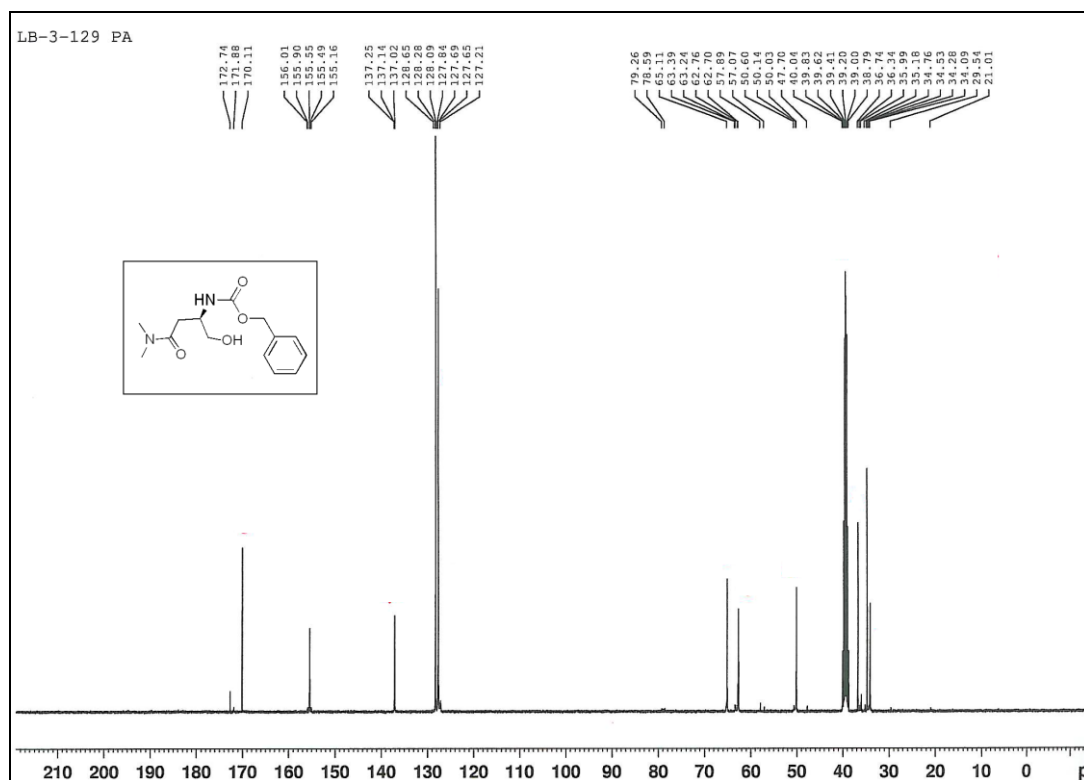


Figure 40: Carbon NMR of (R)-benzyl (4-(dimethylamino)-1-hydroxy-4-oxobutan-2-yl)carbamate in CDCl₃

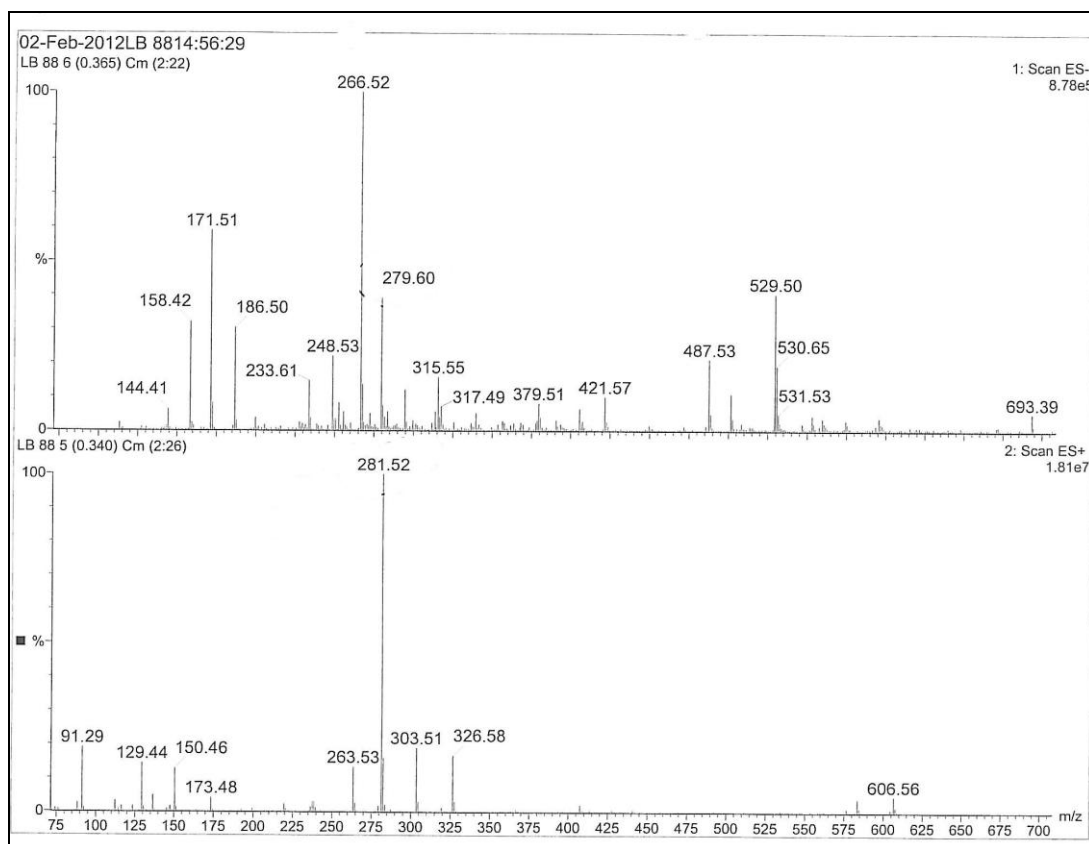


Figure 41: Mass Spectra of (R)-benzyl (4-(dimethylamino)-1-hydroxy-4-oxobutan-2-yl)carbamate

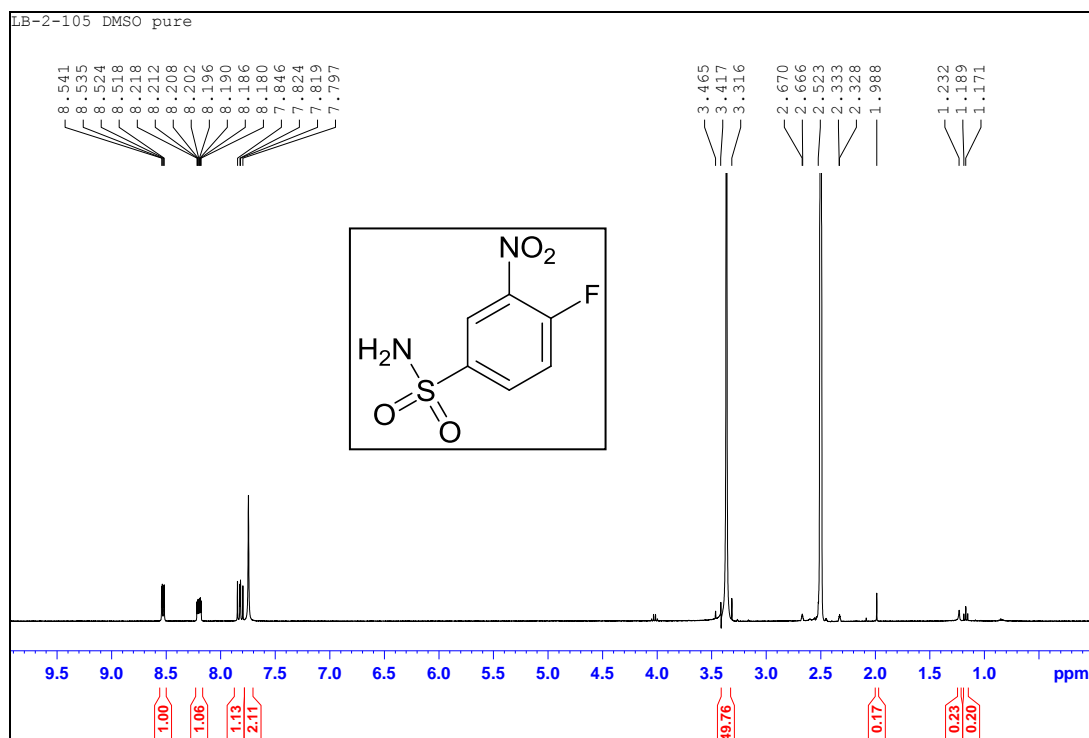


Figure 42: 4-fluoro-3-nitrobenzenesulfonamide proton NMR in DMSO-d₆

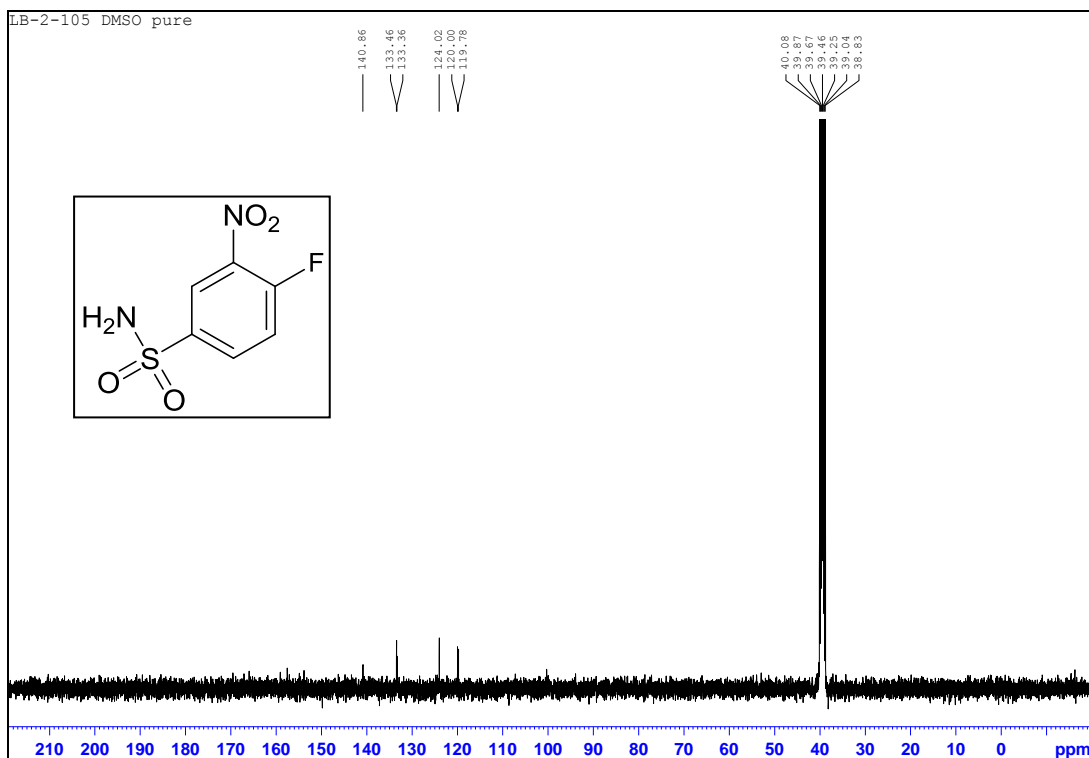


Figure 43: 4-fluoro-3-nitrobenzenesulfonamide carbon NMR in DMSO-d₆

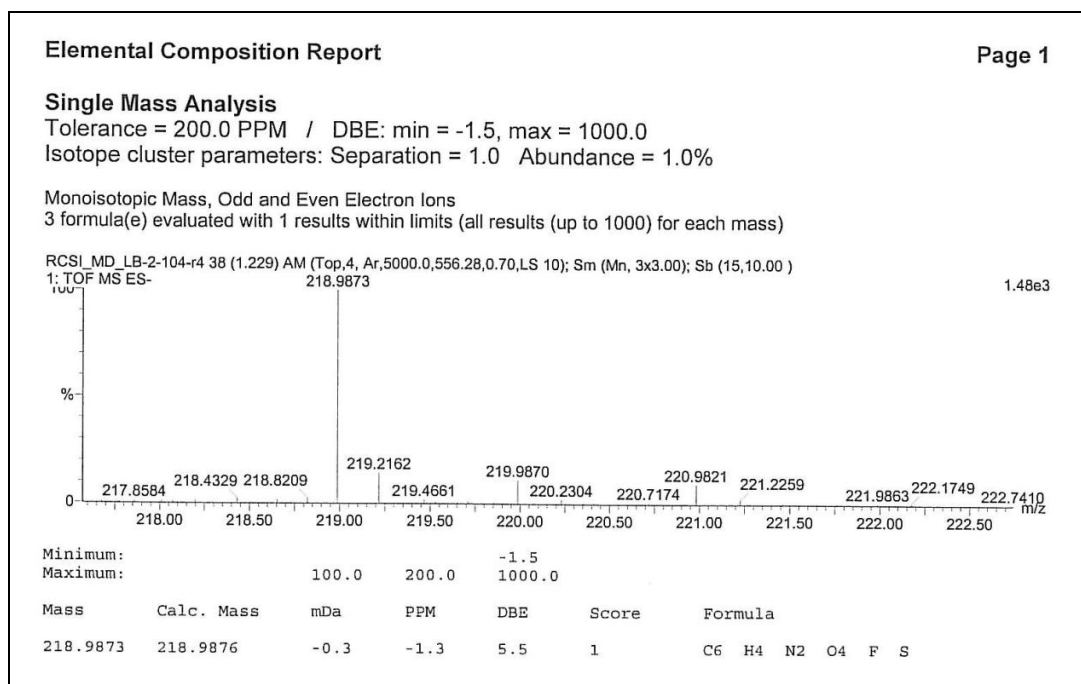


Figure 44: Mass Spectra of 4-fluoro-3-nitrobenzenesulfonamide

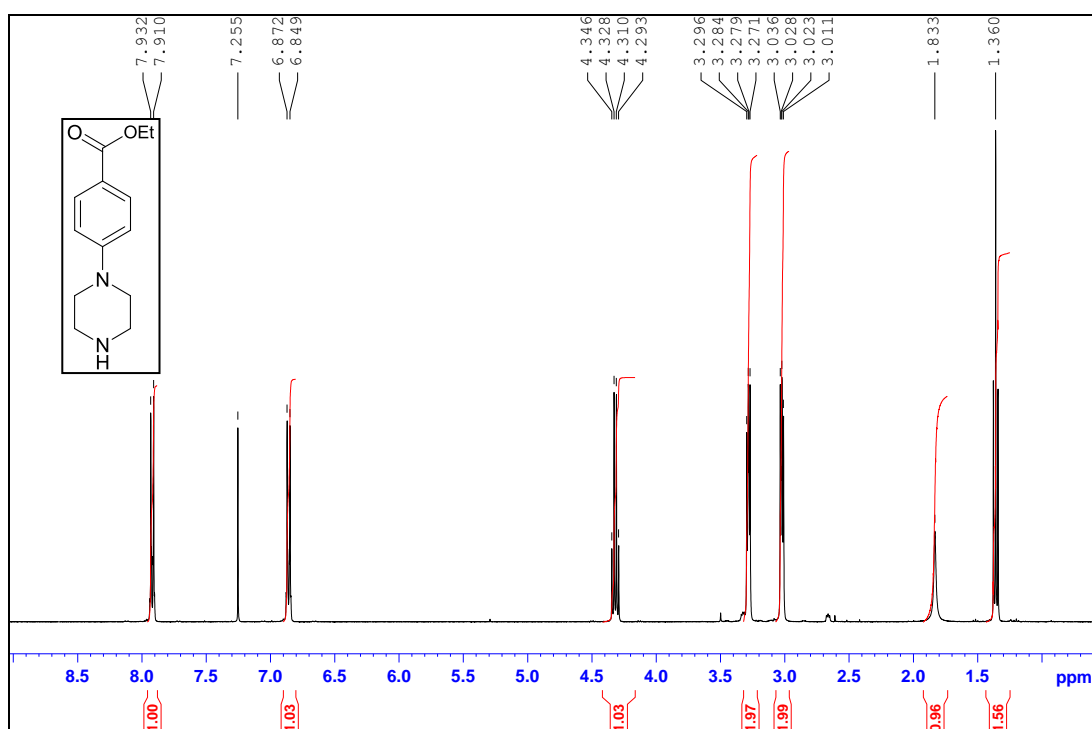


Figure 45: ethyl 4-(piperazin-1-yl)benzoate proton NMR in CDCl₃

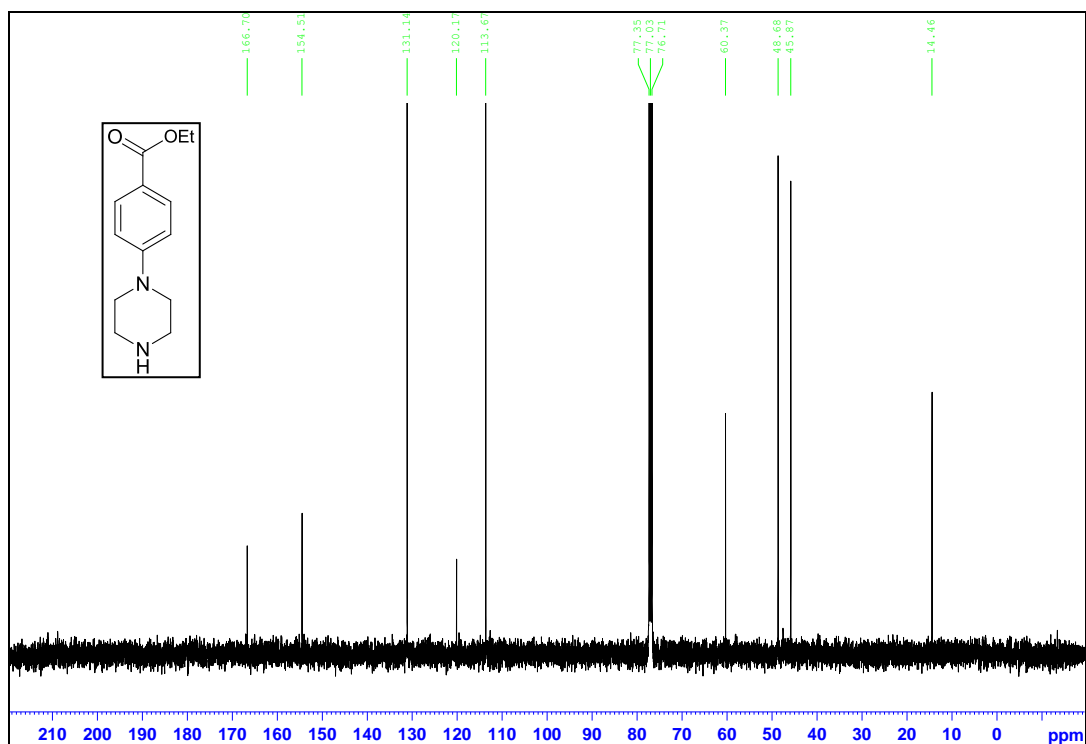


Figure 46: ethyl 4-(piperazin-1-yl)benzoate carbon NMR in CDCl_3

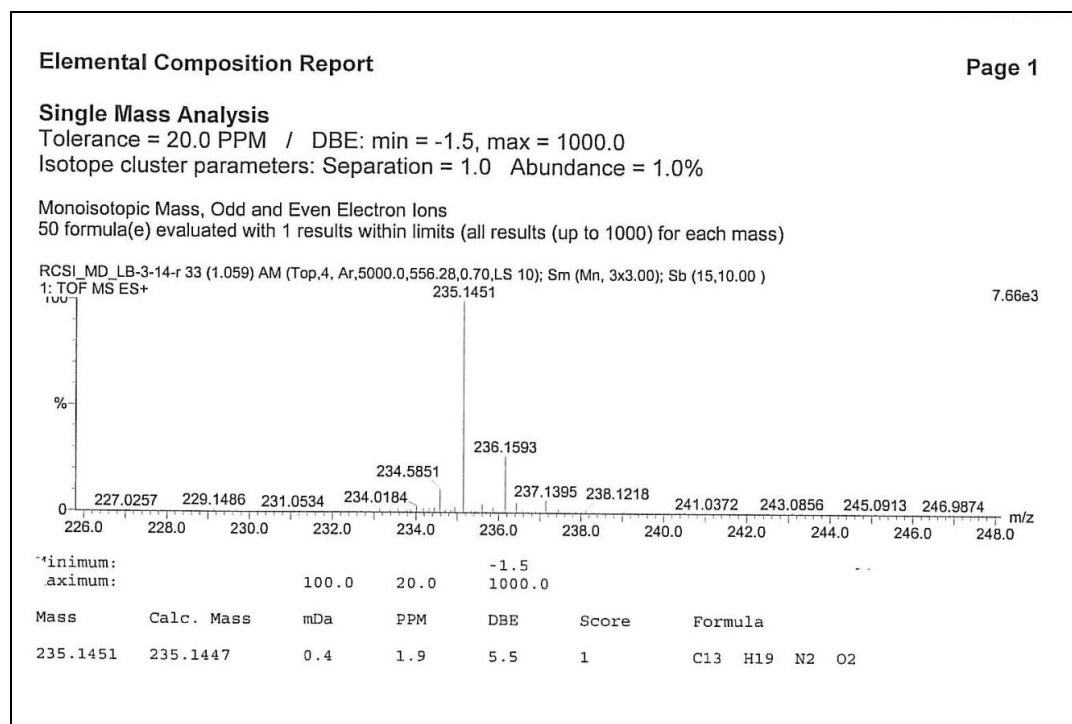


Figure 47: Mass spectra of ethyl 4-(piperazin-1-yl)benzoate

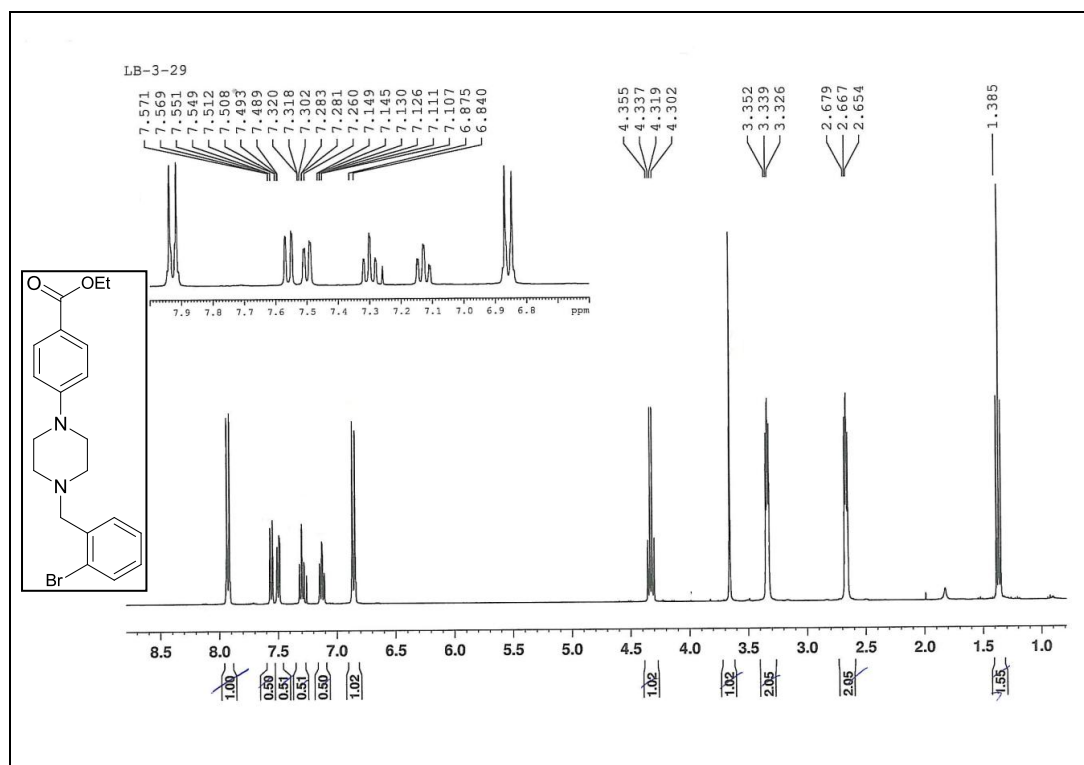


Figure 48: Proton NMR of 4-(4-(2-bromobenzyl)piperazin-1-yl)benzoate in DMSO-d₆

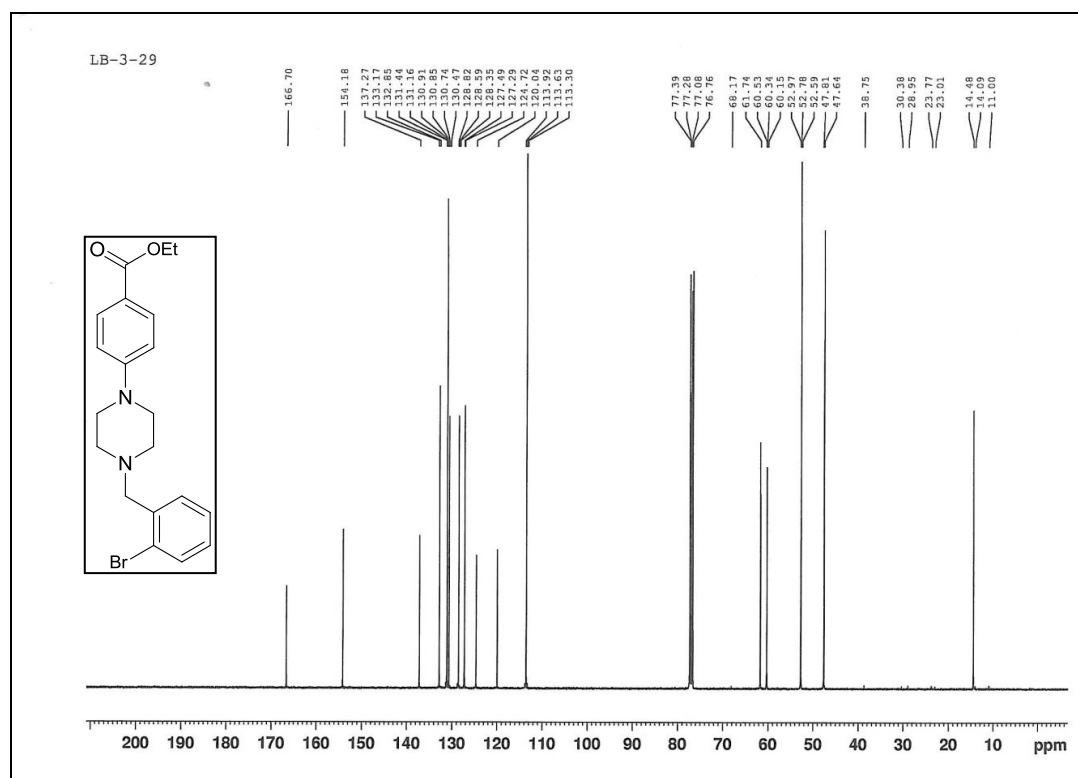


Figure 49: Carbon NMR 4-(4-(2-bromobenzyl)piperazin-1-yl)benzoate in DMSO-d₆

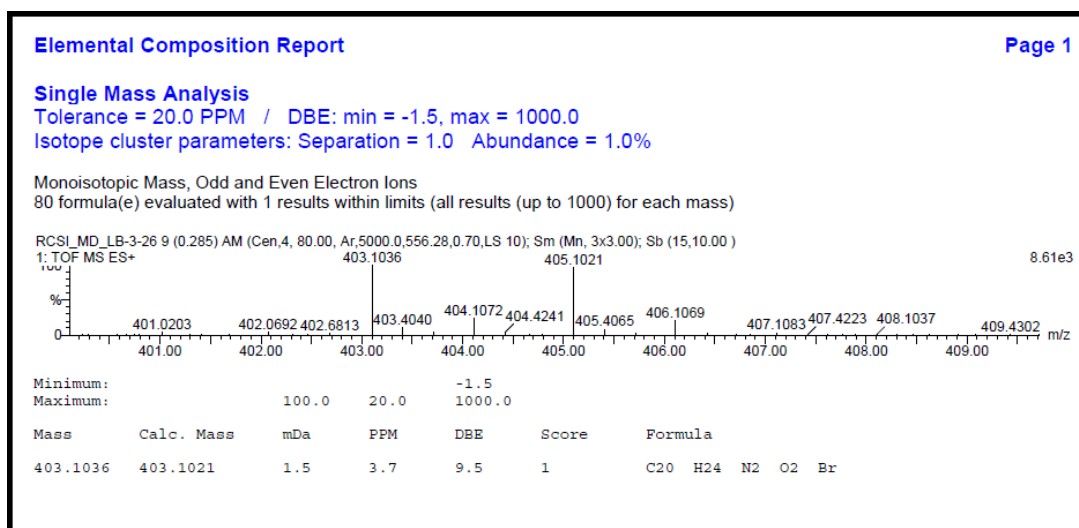


Figure 50: Mass Spectra of 4-(4-(2-bromobenzyl)piperazin-1-yl)benzoate

Wednesday, July 20, 2011 12:24:04 PM					
Run Type	SHA	ID=	LB-3-29	Wt=	1688.9 ug
Counter#	1557	Run#	9	Sealed=	No
PT=	60	CT=	60	FT=	50
BC=	259	BH=	1275	BN=	70
KC=	22.240	KH=	69.009	KN=	8.010
CR	=27152	HR=	13401	NR=	5806
CZ	= 4524	HZ=	5448	NZ=	4801

R-Z=	22628	R-Z=	7953	R-Z=	1005
Sample was recalculated					
Date - 20 Jul 2011					
Time - 2:14:00					
Recalculation Number - 79					

Figure 51 : Elemental Analysis of 4-(4-(2-bromobenzyl)piperazin-1-yl)benzoate

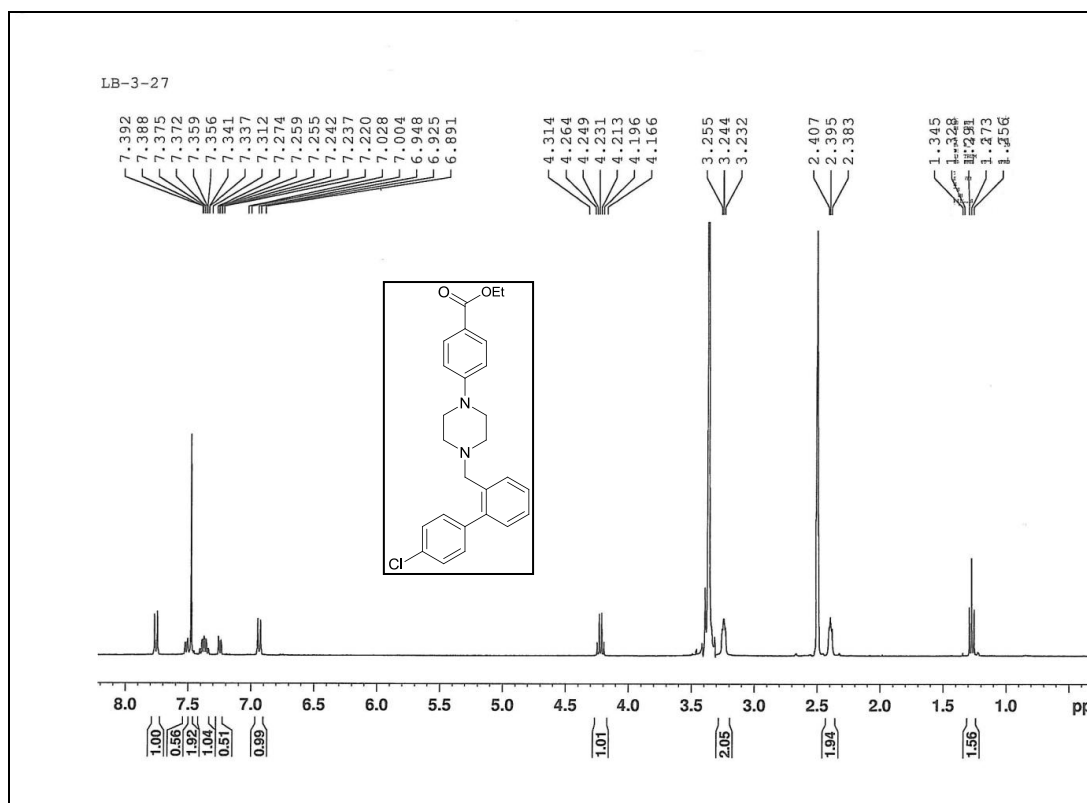


Figure 52 : Proton NMR 4-((4'-chlorobiphenyl-2-yl)methyl)piperazin-1-yl)benzoate in DMSO-d₆

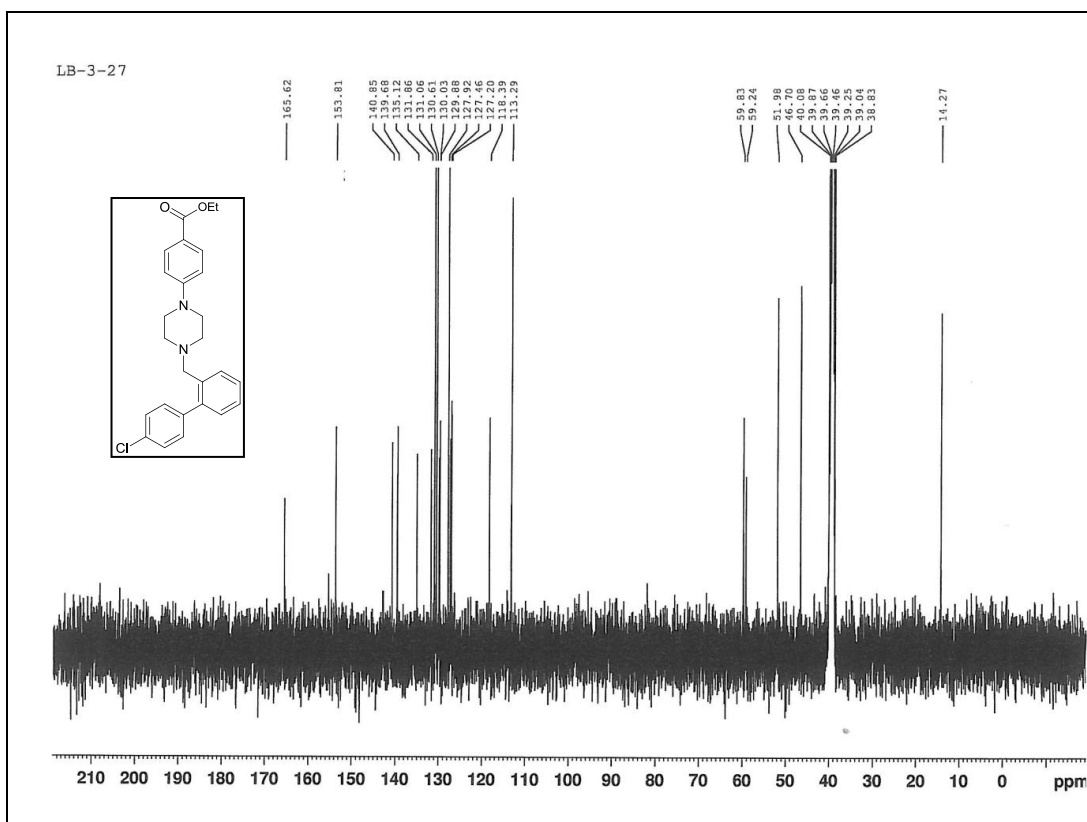


Figure 53: Carbon NMR 4-((4'-chlorobiphenyl-2-yl)methyl)piperazin-1-yl)benzoate in DMSO-d₆

Single Mass Analysis

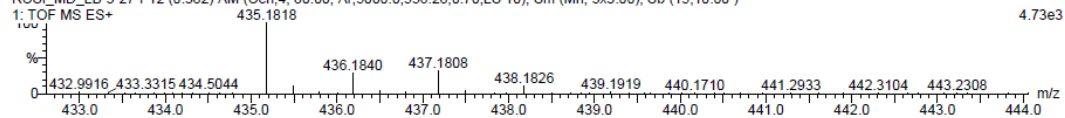
Tolerance = 20.0 PPM / DBE: min = -1.5, max = 1000.0

Isotope cluster parameters: Separation = 1.0 Abundance = 1.0%

Monoisotopic Mass, Odd and Even Electron Ions

78 formula(e) evaluated with 1 results within limits (all results (up to 1000) for each mass)

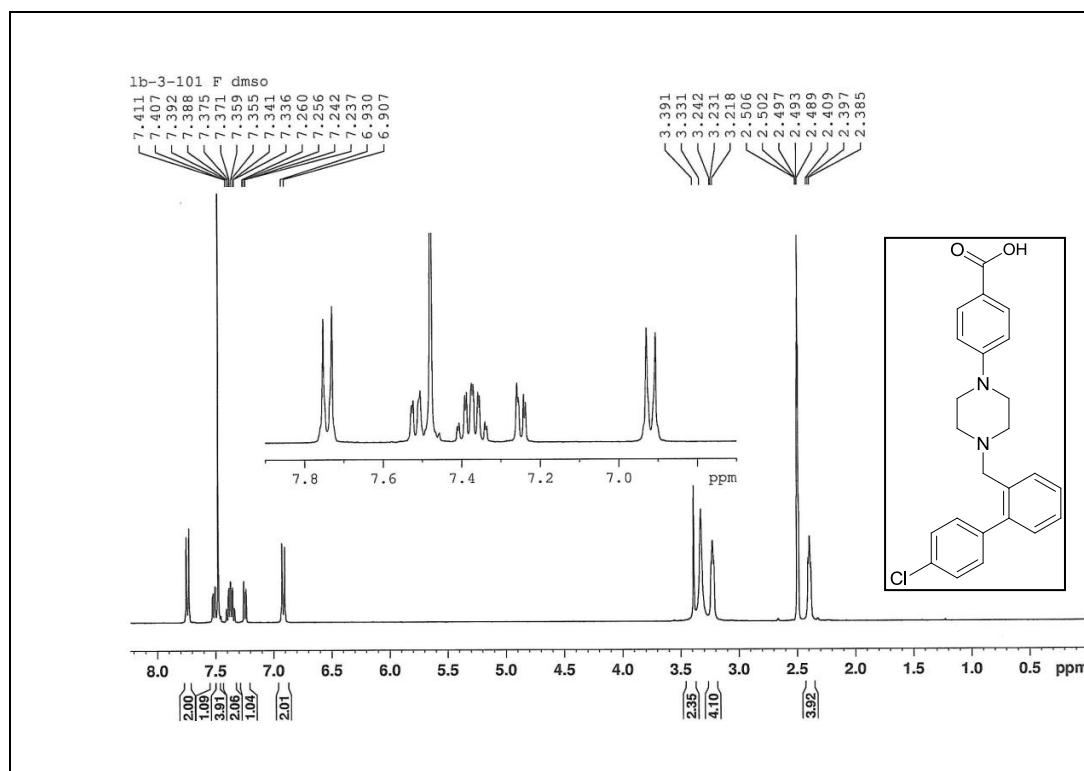
RCSI_MD_LB-3-27-r 12 (0.382) AM (Cen,4, 80.00, Ar,5000.0,556.28,0.70,LS 10); Sm (Mn, 3x3.00); Sb (15,10.00)



Minimum: -1.5
Maximum: 1000.0

Mass	Calc. Mass	mDa	PPM	DBE	Score	Formula
435.1818	435.1839	-2.1	-4.9	13.5	1	C26 H28 N2 O2 Cl

Figure 54: Mass spectra of 4-(4-((4'-chlorobiphenyl-2-yl)methyl)piperazin-1-yl)benzoate

Figure 55: Proton NMR of 4-(4-((4'-chloro-[1,1'-biphenyl]-2-yl)methyl)piperazin-1-yl)benzoic acid in DMSO-d₆

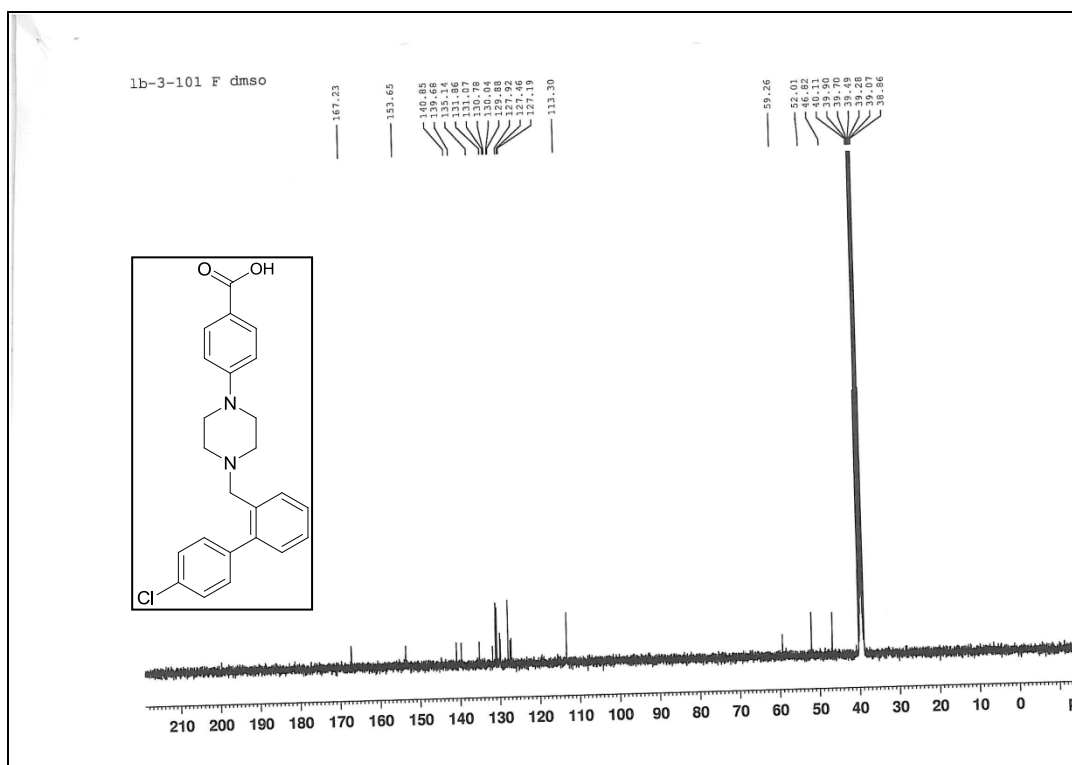


Figure 56: Carbon NMR 4-(4-((4'-chloro-[1,1'-biphenyl]-2-yl)methyl)piperazin-1-yl)benzoic acid in DMSO-d₆

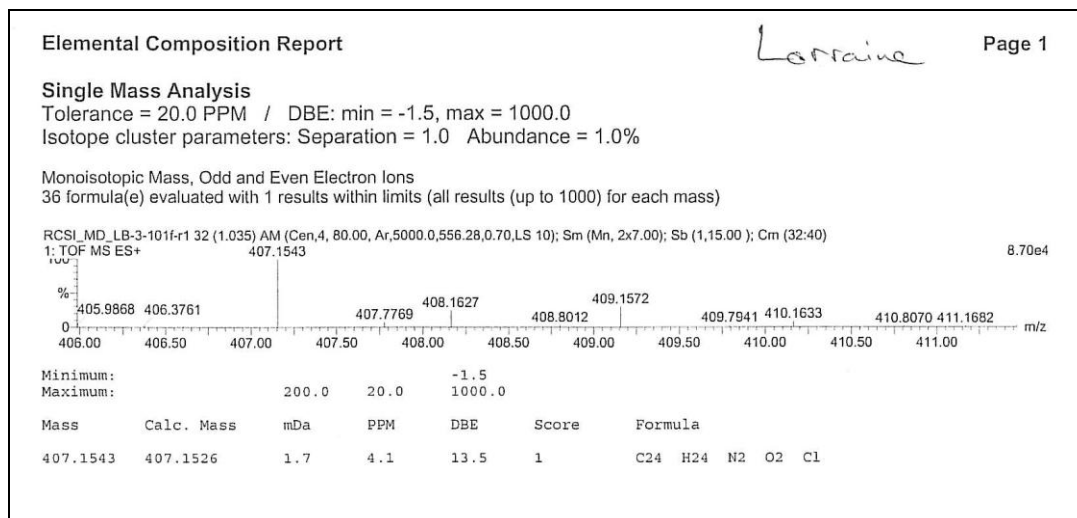


Figure 57: Mass spectra of 4-(4-((4'-chloro-[1,1'-biphenyl]-2-yl)methyl)piperazin-1-yl)benzoic acid

ABT 263

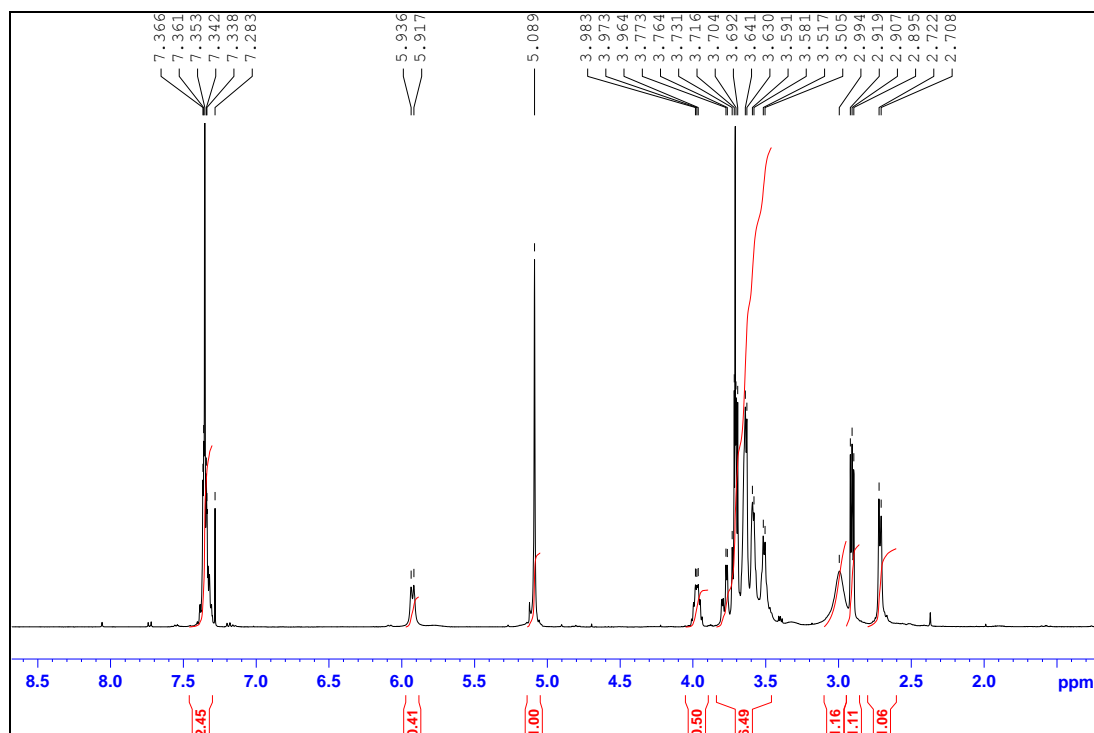


Figure 58: Proton NMR of (R)-benzyl (1-hydroxy-4-morpholino-4-oxobutan-2-yl)carbamate in CDCl₃

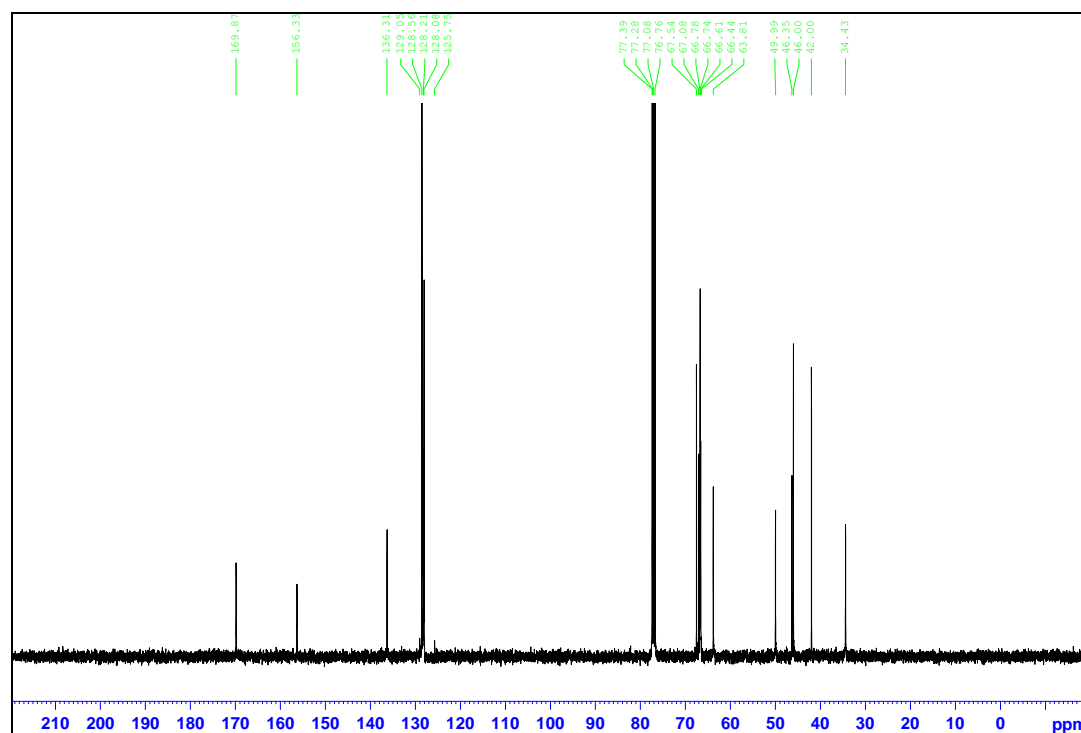


Figure 59: Carbon NMR of (R)-benzyl (1-hydroxy-4-morpholino-4-oxobutan-2-yl)carbamate in CDCl_3

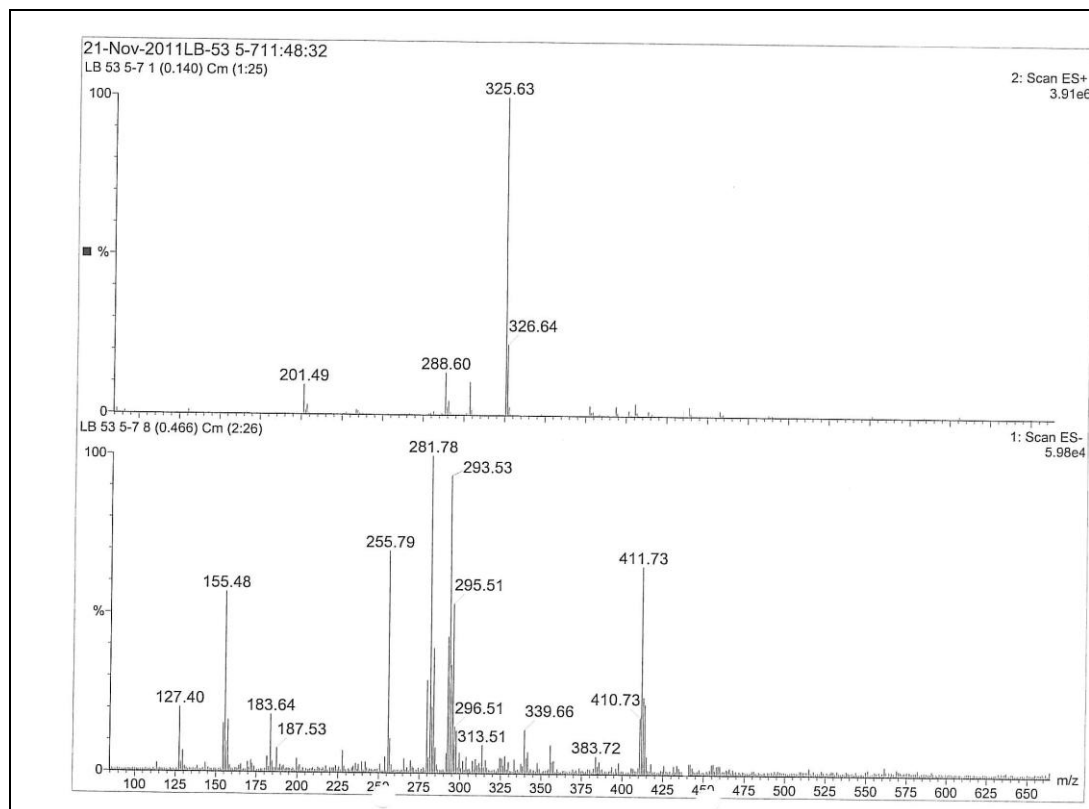


Figure 60: Mass spectra of (R)-benzyl (1-hydroxy-4-morpholino-4-oxobutan-2-yl)carbamate

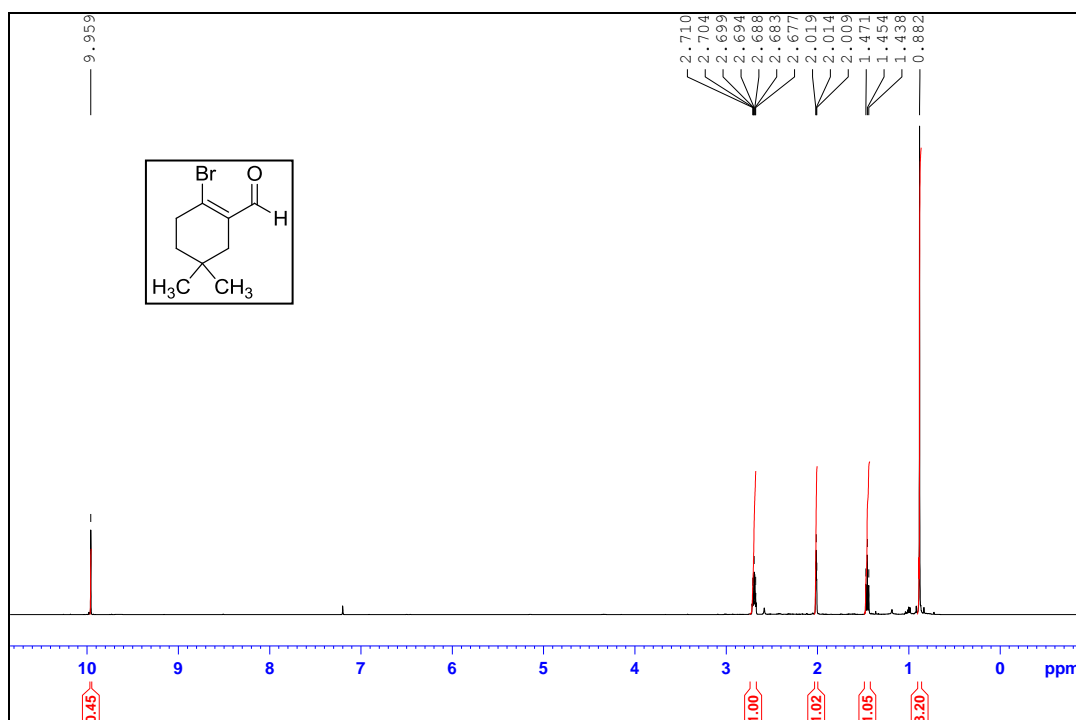


Figure 61: Proton NMR 1-bromo-4,4-dimethylcyclohexane-carbaldehyde in CDCl_3

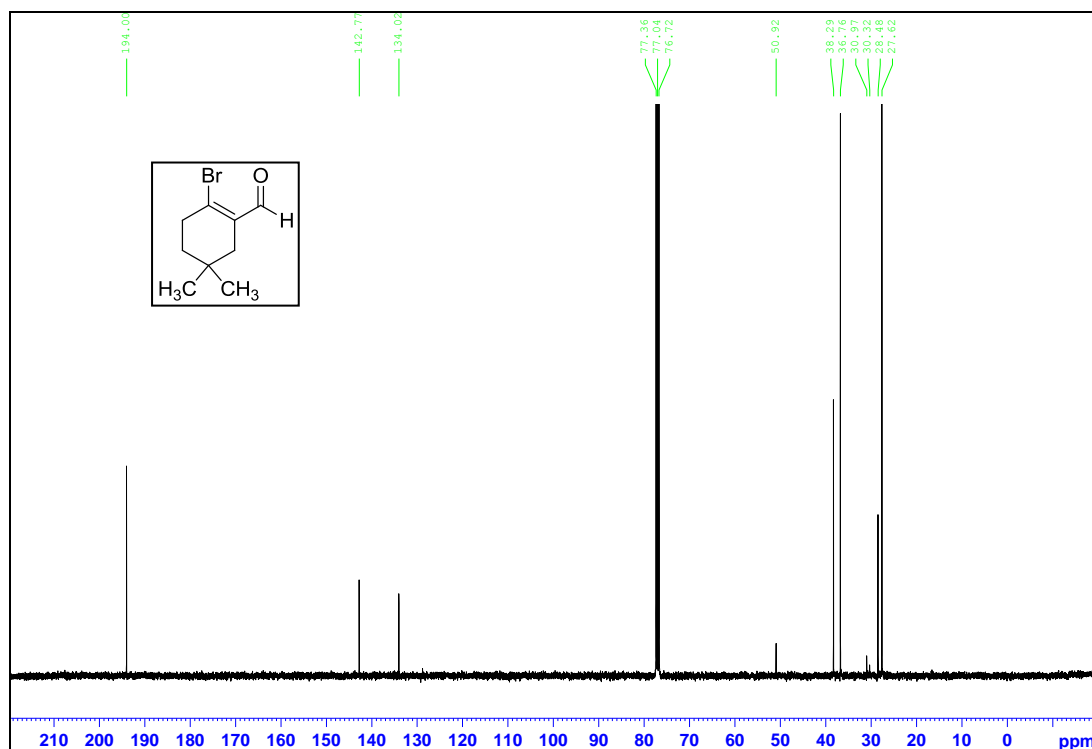


Figure 62: Carbon NMR 1-bromo-4,4dimethylcyclohexane-carbaldehyde in CDCl_3

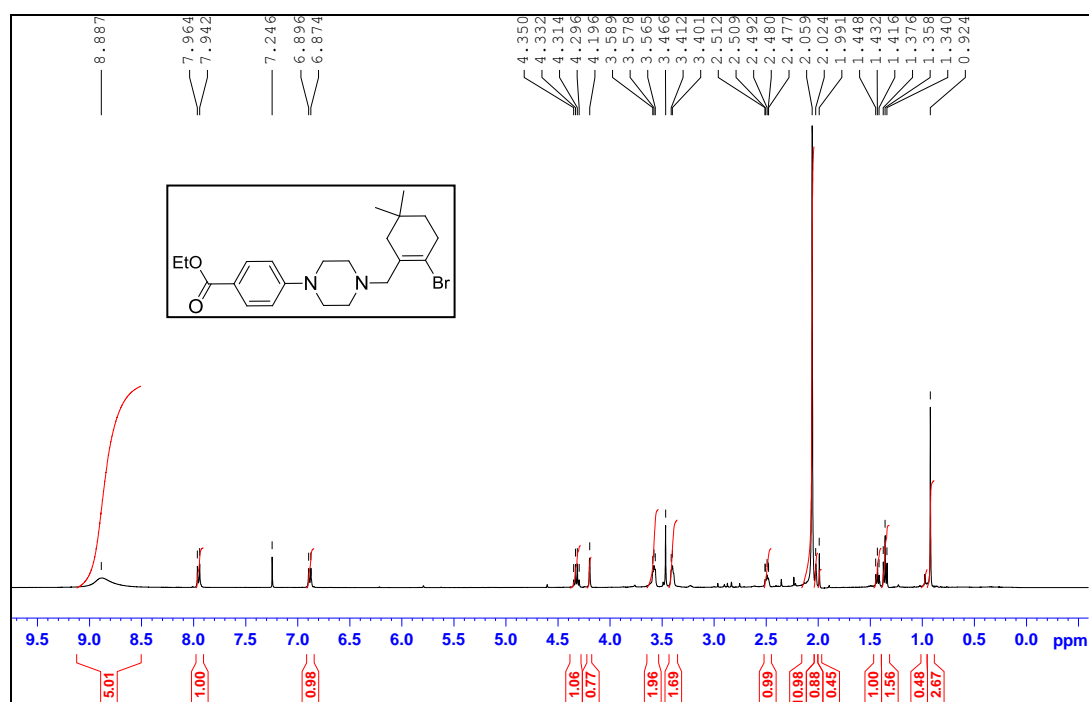


Figure 63: Proton NMR ethyl 4-(4-((2-bromo-5,5-dimethylcyclohex-1-en-1-yl)methyl)piperazin-1-yl)benzoate in CDCl_3

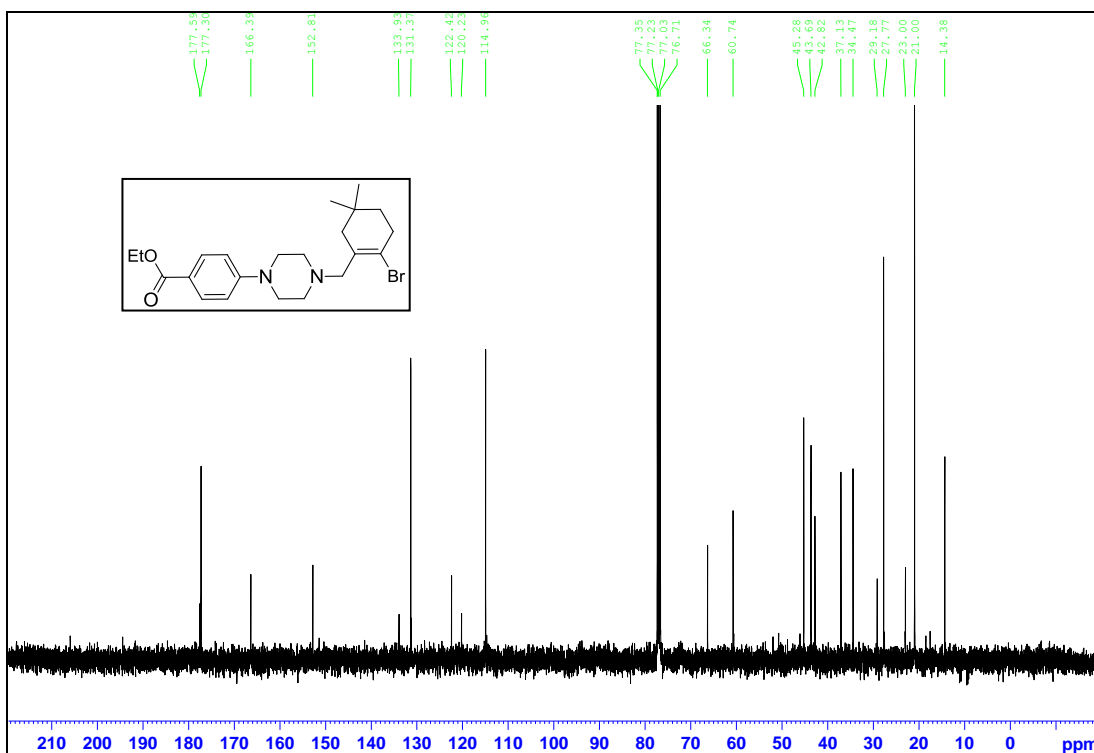


Figure 64: Carbon NMR ethyl 4-((2-bromo-5,5-dimethylcyclohex-1-en-1-yl)methyl)piperazin-1-yl)benzoate in CDCl_3

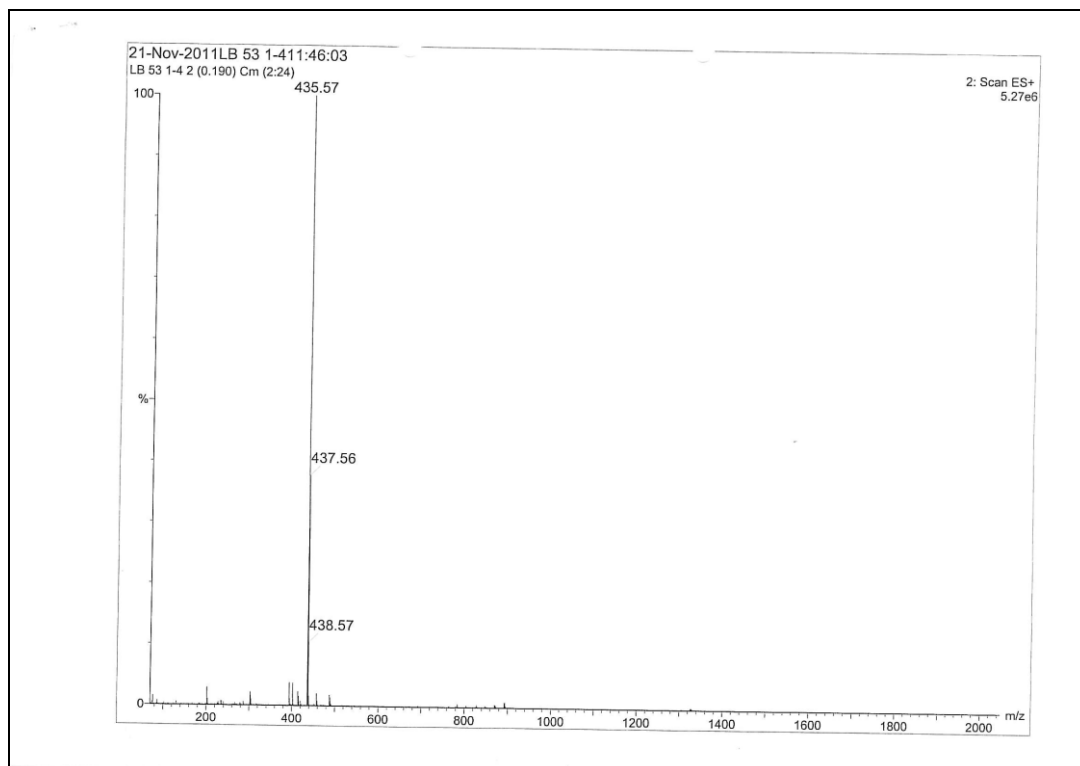


Figure 65: Mass spectra of ethyl 4-((2-bromo-5,5-dimethylcyclohex-1-en-1-yl)methyl)piperazin-1-yl)benzoate

Publications and Posters

- Inaugural National Biophotonics and Imaging Platform of Ireland Conference (2009) (Poster)
- Centre for Synthesis & Chemical Biology Symposium 2009 (Poster)
- Royal College of Surgeons in Ireland Research Day 2010 (Poster)
- 62nd Irish Universities Chemical Research Colloquium 2010 (Poster)
- Inaugural Peptide Workshop 2010(Poster)
- UNSCR Symposium 2010 (Poster)
- BioPic 2010 (Poster)
- 5th International Peptide Symposium 2010 Japan (Poster)
- Centre for Synthesis & Chemical Biology Symposium 2010 (Poster)
- *Conference Proceeding*: Blackmore, L., Dolan, C., Cosgrave, L., Forster, R.J., Keyes, T.E., Devocelle, M. ‘Targeting Environmentally Sensitive Phosphors within Cells’, (2010) Peptide Science, 5th International Peptide Symposium
- Royal College of Surgeons in Ireland Research Day 2011 (Poster)
- 33rd School of Pharmacy Research Seminar 2011 (Oral Presentation)
- 63rd Irish Universities Chemical Research Colloquium 2011 (Poster)
- COST D39 Final Whole Action Meeting, Metallo-Drug Design and Action 2011 (Poster & Oral) (2nd Place Poster Blitz Prize)
- 4th annual meeting of the Irish institute of metal based drugs 2011 (Oral)
- Centre for Synthesis & Chemical Biology Symposium 2011 (Poster)
- Royal College of Surgeons in Ireland Research Day 2012 (Poster)
- 64th Irish Universities Chemical Research Colloquium 2012 (Oral)
- *Publication in Preparation*: Blackmore, L., Dolan, C., Moriarty, R., Forster, R.J., Keyes, T.E. and Devocelle, M. ‘Molecular Dyes for Imaging the Sub-cellular Localization of Peptides’, submitted to JACS.